THE UNIVERSITY OF SHEFFIELD
Department of Chemical & Biological Engineering

Movement of a secondary immiscible liquid within a suspension of hydrophilic particles in a continuous hydrophobic phase

SYED F. ISLAM

Thesis submitted in partial fulfilment of the requirements for the degree of “Doctor of Philosophy”

January 2017

Abstract

Numerous food products are suspensions of hydrophilic particles dispersed in a continuous fat phase, examples being peanut butter, chocolate spread, chocolate, praline and various confectionary fillings. The uptake of moisture by such materials and its interaction with the suspension can profoundly affect their qualities of texture, taste, appearance and conservation. The moisture could be transferred between different components of a product or from the environment, provided there is a gradient of water activity between the two regions, or perhaps introduced directly. Therefore, an understanding of the mechanisms (e.g. gravity, capillary and diffusion) responsible for moisture migration is needed to design better products and optimise the distribution chain.

The aim of this study is to understand the changes which occur, when model suspensions (sugar and sunflower oil) interact with a secondary immiscible liquid (water, sugar solutions and glycerol), via both direct addition and atmospheric exposure (varying humidity), during both short (seconds to minutes) and long (hours to days) term storage. A novel methodology developed using non-destructive dynamic X-ray computer tomography (CT), proved successful in tracking the secondary liquid and the effects of moisture migration from atmospheric exposure.

Upon direct addition of a secondary liquid droplet to a suspension, following gravitational effects as the liquid encounters the surface of the suspension, surface penetration was assumed to be driven by capillary effects, dominated by the viscosity and contact angle of the liquid with the sugar particles. Subsequent penetration of the liquid within the suspension was driven by the capacity of the liquid droplet to absorb solid sugar from the bulk suspension. The movement of particles into the liquid was against gravity as the droplet progressed into the suspension. Final transport of the liquid was believed to be driven by diffusion into the bulk suspension. This was based on microscale observations using high resolution X-ray CT, with the continued movement of the liquid being ascribed to

the thermodynamically favoured wetting properties leading to a network formation between solid sucrose particles.

A model was developed for the stage in which solid sucrose moves into the secondary liquid based on the flux of sucrose from the bulk suspension. It was found that the penetration of the liquid into the suspension was dominated by the capacity of the liquid to take up sucrose, with density and gravitational effects playing a minimal role in driving the kinetics.

For atmospheric exposure of the suspension to water, it was shown that if the humidity level was above the critical deliquescence relative humidity (DRH) point of sucrose, a contraction of the volume occupied by the solids occurred due to liquid bridge formation causing an inward pulling force. The moisture migration travelled as a uniform front through the cross sectional area of the suspension sample.

Finally, the findings from this research provide valuable insight useful to optimise product design and processing and realise improved stability over shelf-life for a key class of food materials. They lead to a better understanding of issues which need to be considered during product development. Focus is on the prevailing crystalline solid used – sucrose – but also considers the interactions between ingredients in influencing the overall properties of the final product. This would be particularly useful for assuring product quality in global market places where high humidity prevails, through tailoring the product to resist undesirable changes.

Acknowledgments

First of all, I would like to express my greatest gratitude to God, for making this possible. Next, I would like to direct my thanks and appreciation to my academic supervisors Professor Agba Salman, in guiding me throughout this journey and offering assistance as needed, and Professor Michael Hounslow in helping develop the models.

I would also like to extend my thanks to my industrial supervisors Dr Steve Whitehouse, Dr Ramana Sundara, Dr Tim Althaus and Professor Stefan Palzer for their continuous support and feedback throughout my PhD.

A big thanks goes to the members of the PPG group, who have made the journey more enjoyable and created great memories throughout. Chalak, Menan, Riyadh and William with whom this journey started and will soon end. Special mention must go out to Mohammed, with whom this journey started in 2009 during our undergraduate career and may our journey together continue for many years. Also to Dr Robert Mitchell and Dr Alessandra Negreiros, who helped me in the early parts of my PhD which proved pivotal in laying the foundations for this journey, as well as, Dr Ranjit Dhenge and Dr Kimiaki Washino for their continued support and guidance throughout.

I would like to extend my thanks to Carine Meyer (NRC) for allowing to conduct my first of many scans using X-ray CT, Prof. Duncan Bell from Fisherideas for loaning me the brass chucks and sample holders to conduct X-ray CT trials, Dr Pete Laity & Dr Maryam Dadkhah for letting me conduct trails scans at Huddersfield University and Magdeburg University respectively, Dr Alan Ruddell and EPSRC for the loan of the SkyScan system and training, Dr Lucia Mancini for assisting in trials at the Elettra synchrotron facility, Dr Tomasz Wysokinski & Dr George Belev for assisting in trails at the CLS synchrotron facility and Dr Xianghui Xiao for assisting in trials at the APS synchrotron facility.

I am also thankful to the workshop technicians (Andy, Steve, Adrian, Stuart, Usman, Oz, Mark & Keith) in carrying out the manufacturing for sample holders and other technical services which were fundamental for my studies.

Also, I would like to thank Dr Martin Pitt for his guidance and support during my undergraduate as a lecturer and his ideas and experience which continued throughout my postgraduate.

Finally and most importantly my parents for their unconditional love, support and guidance throughout my life. For without this, for sure I wouldn't be able to achieve any of this. Thanks to my elder brothers Iqbal, Aklak, Amlak, Imran and Ekramul who have enabled me to pursue further education by removing some of the household responsibilities.

"Aspire to inspire, before you expire."

List of Publications and Presentations

Movement of a secondary immiscible liquid in a suspension using a non-invasive technique, S. F. Islam, R. V. Sundara, S. Whitehouse, T. O. Althaus, S. Palzer, M. J. Hounslow, A. D. Salman. **Chemical Engineering Research and Design,** 110, 160-170. (doi; dx.doi.org/10.1016/j.cherd.2016.02.023).

Dynamic studies of model suspensions using high resolution synchrotron X-ray microtomography, S. F. Islam, L. Mancini, R. V. Sundara, S. Whitehouse, S. Palzer, M. J. Hounslow, A. D. Salman. **Chemical Engineering Research and Design,** 117, 756-772. (doi; dx.doi.org/10.1016/j.cherd.2016.11.034).

Monitoring the segregation of an oil and sucrose suspension at different humidity conditions, S. F. Islam, R. V. Sundara, S. Whitehouse, T. O. Althaus, S. Palzer, M. J. Hounslow, A. D. Salman. (Submitted to **Food Packaging and Shelf Life**).

Non-invasive techniques to track storage life of confectionary products, Oral presentation, Nestle PhD Student Symposium, York, U.K. 10^{th}-11^{th} September 2015.

Kinetics for a secondary immiscible liquid within a suspension, Oral presentation, 7^{th} International Granulation Workshop, Sheffield, U.K. Paper no. 12. 1^{st}-3^{rd} July 2015.

Dynamics of a secondary immiscible liquid within a suspension, Poster presentation, Chem Eng Day, Sheffield, U.K. 8^{th}-9^{th} April 2015.

Movement of a secondary immiscible liquid within a suspension, Oral presentation, Nestle PhD Student Symposium, York, U.K. 2^{nd}-3^{rd} September 2013.

Kinetics of a secondary immiscible liquid in a suspension, Poster presentation, 6^{th} International Granulation Workshop, Sheffield, U.K. 26^{th}-28^{th} June 2013.

Notation

Greek symbols

Symbol	Meaning	Unit
γ	Surface Tension	[mN m^{-1}]
φ	Sphericity of Particles	[-]
ε	Porosity	[-]
θ	Contact Angle	[°]
α	Angle between Capillary and Reference Plane	[°]
μ	Dynamic Viscosity	[N s m^{-2}]
τ_{CDA}	Penetration Time for Constant Drawing Area	[s]
τ_{DDA}	Penetration Time for Decreasing Drawing Area	[s]
π	3.14…	[-]
ρ	Density	[kg m^{-3}]

Acronyms

Acronym	Meaning
CDA	Constant Drawing Area
DDA	Decreasing Drawing Area
DRH	Deliquescence Relative Humidity
MRI	Magnetic Resonance Imaging
PKO	Palm Kernel Oil
RH	Relative Humidity
SEM	Scanning Electron Microscopy
X-ray CT	X-ray Computer Tomography

Latin symbols

Symbol	Meaning	Unit
a	Surface area	[m^2]
a_w	Water activity	[-]
c	Material Constant	[-]
d	Droplet diameter	[m]
d_{32}	Sauter Mean Diameter	[m]
$D_{10,3}$	Volume-based Size which 10% of the Particle Size Distribution lies below	[m]
$D_{50,3}$	Volume-based Size which 50% of the Particle Size Distribution lies below	[m]
$D_{90,3}$	Volume-based Size which 90% of the Particle Size Distribution lies below	[m]
D_{eff}	Unsteady State Diffusivity	[$cm^2\ s^{-1}$]
D_f	Fundamental Diffusion Coefficient	[$cm^2\ s^{-1}$]
e	Sample Thickness	[m]
g	Gravitational Acceleration	[9.81 m s^{-2}]
h	Height Drawn up Capillary	[m]
J	Flux Movement of Solid Sucrose	[$m^3\ m^{-2}\ s^{-1}$]
J_i	Molar Diffusion Flux of Migrating Molecules	[mol $cm^{-2}\ s^{-1}$]
k	Kappa	[-]
l	Film Thickness	[m]
m	Mass	[kg]
p	Partial Vapour Pressure of Sample	[N m^{-2}]
P_c	Laplace Capillary Suction Pressure	[N m^{-2}]
p_0	Standard State Vapour Pressure of Pure Water	[N m^{-2}]
r_c	Capillary Radius	[m]
r_d	Drawing Radius	[m]
R_{pore}	Characteristic Pore Size of Bed	[m]
t	Time	[s]
t_{lag}	Lag Time	[s]
V_0	Droplet Volume	[m^3]

X^*	Average Moisture Content	[g g^{-1} dry basis]
X_0	Initial Moisture Content	[g g^{-1} dry basis]
X_∞	Equilibrium Moisture Content	[g g^{-1} dry basis]

Table of Contents

Chapter 1 Introduction & Aim

Several food produce are comprised of suspensions in which a solid phase (hydrophilic or hydrophobic particles) is dispersed throughout a continuous phase (hydrophobic). Examples of these include chocolate and peanut butter spread. When a secondary immiscible liquid (such as water or glycerol) is added to a suspension of this kind, the behaviour of the mixture can change quite vividly in terms of the rheological properties, physical appearance and texture (Koos and Willenbacher, 2011).

Though, how the secondary liquid propagates initially and then redistributes after longer timescales, throughout stagnant and non-stagnant conditions is not fully understood. Furthermore, the dominant mechanisms for the transportation taking place, such as capillary, diffusion and gravitational effects have yet to be identified.

In addition to this, when suspension based products are exposed to environments with a high humidity either during manufacturing or after, this can also result in exterior and interior changes to the sample. This in turn will affect the properties and potentially the shelf life of the product. Some of the undesired effects can be microbial growth and chemical reactions within the product which will ultimately lead to substantial produce wastage (Ghosh et al., 2004). Therefore, it is anticipated by understanding what changes occur within the product and how they affect the product, steps can be taken either to mitigate or eradicate the effect in the final product and thus, help reduce wastage and consumer complaints.

The transition from a fluid-like to gel-like structure for suspensions was demonstrated for suspensions with the addition of 0.2 wt. % water as the secondary immiscible liquid (Koos and Willenbacher, 2011). This transition was attributed to the formation of pendular bridges between the solid particles causing agglomeration. This phenomenon is similar to that seen when sandcastles are made. With dry sand, it is not possible to make sandcastles, however with the addition of water it is (at least up until a certain point). Here the water enables liquid bridges to form between particles which results in capillary attraction between sand particles, allowing the structure to remain stable. As well as the

visual effects of adding small amounts of secondary liquids to suspensions, it has been shown that the rheological properties such as the yield stress and viscosity can increase several fold (Koos et al., 2012, Yucel and Coupland, 2011).

The movement of the secondary liquid will continue to occur, as long as there is a concentration gradient present between the different regions. The moisture content of the domains will determine the movement direction of the liquid, and this can be very important when considering the preservation of food produce and the behaviour occurring during storage. For example if a product during manufacturing is suddenly exposed to a new environment with a higher RH, then the material in direct contact with the vapour may have a higher moisture content than the bulk, and as a result of this, migration of moisture from regions of higher moisture to regions of lower moisture will occur.

Present work in the literature has mainly focused on the assumption of diffusion being the dominant mechanism for moisture movement within such systems. Models have been presented based on apparent/effective diffusivities within suspensions to simplify the mechanisms taking place (Yuan et al., 2009, Yuan et al., 2012). However, it is understood that it is more plausible that a combination of transport mechanisms are taking place, which are responsible for the movement of the secondary, liquid such as gravity, capillary and diffusion (Ghosh et al., 2004). From the studies mentioned, it is challenging to follow the localised mass transfer on the microscale of moisture/water within the system. These studies focused on the bulk mass transfers on the macroscale based on weight changes of samples. Thus, the presented mass transfers were as an overall average of the sample and did not represent the kinetics of movement taking place locally within the sample on the microscale.

At present, there is limited work within the literature which has been able to follow the localised movement of a secondary immiscible liquid within a suspension and qualitatively track the interactions and structural changes taking place on a microscale, affecting macroscale properties. A non-invasive investigative approach, to observe such local interactions would allow for the characterisation of

mass transfer responsible for the change in rheological behaviour to be appreciated visually.

1.1 Objectives of Thesis

The objective of this study is to elucidate the movement taking place when a secondary immiscible liquid is either exposed (water vapour) to or applied directly to the surface of a suspension (containing hydrophilic particles suspended in a continuous fat phase). This work will examine the movement taking place during both short term (minutes to hours) and long term storage (days to weeks), in order to observe the mechanisms of movement taking place, and how the most dominant mechanisms differ over time. This will encompass looking at the bulk macroscale and localised microscale movement for the secondary liquid within the suspension. Experiments are performed using a combination of both invasive and non-invasive methods.

The experimental work conducted will focus on two methods of secondary immiscible liquid addition. The first is where the secondary liquid will be directly deposited onto the surface of the suspension (as a bulk), allowing the liquid to progress while monitoring it progress into the sample, as is shown schematically in Figure 1-1.

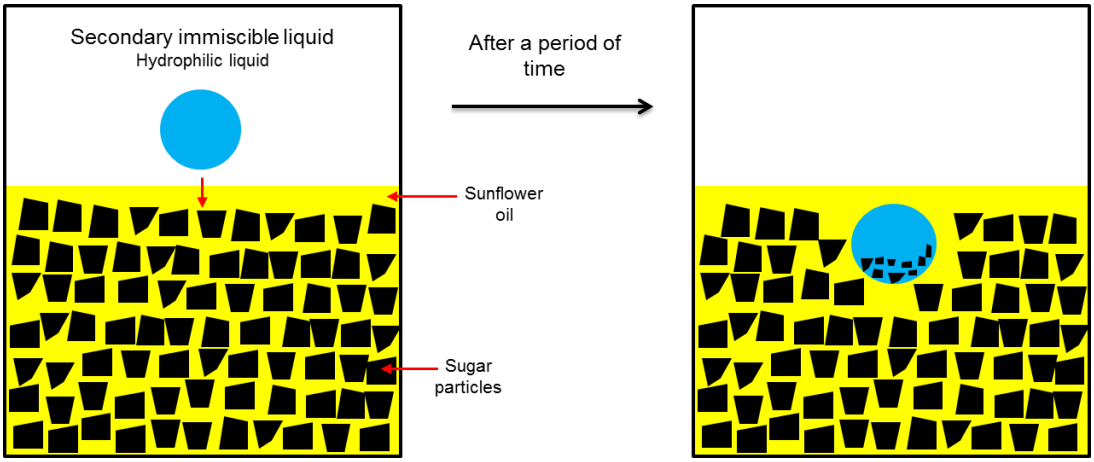

Figure 1-1. Hypothesized movement of secondary liquid once applied to suspension surface.

The second is exposing the sample to an environment of high humidity, in which the secondary immiscible liquid (water) is present within the surrounding atmosphere, as shown schematically in Figure 1-2.

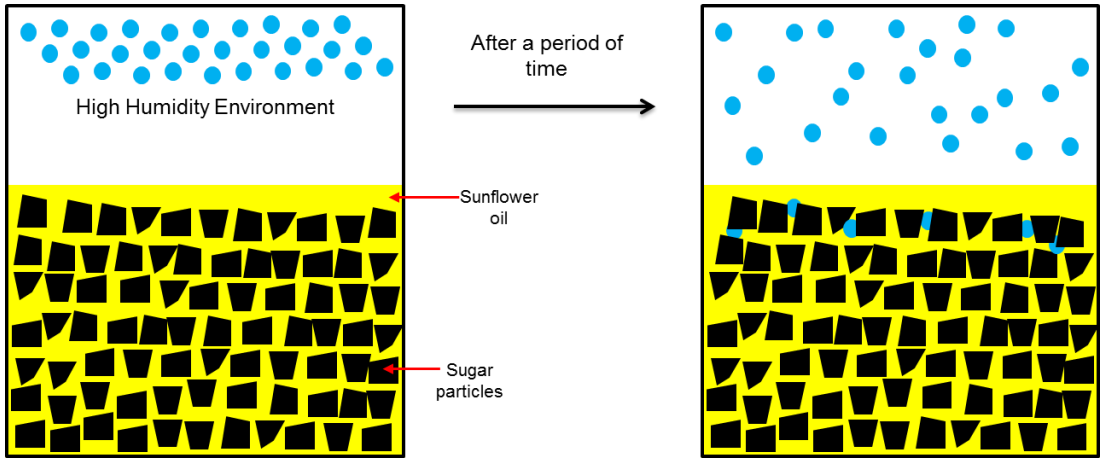

Figure 1-2. Hypothesized movement of secondary liquid when exposed to a high humidity environment.

It is hypothesized that the mechanisms responsible for both the short term and long term movement differ and will encompass a combination of mechanisms.

Once an experimental approach was developed to allow the movement of the secondary liquid to be tracked and thus quantified, efforts were then focused on changing the process parameters to see the effect this had upon the migration of the secondary liquid. The process parameters include:

- Quantity of secondary liquid;
- Type of secondary liquid (distilled water/glycerol/range of sugar solutions);
- Solid particle type and quantity (sucrose or fructose or mixtures of both).

The research conducted during this thesis; aim to give an insight into the mechanisms responsible for the migration of secondary immiscible liquids within suspensions of hydrophilic particles suspended throughout a continuous hydrophobic phase. The secondary liquid addition was either in a liquid phase (as a bulk) or vapour phase (in the surrounding atmosphere at high relative humidity) to see how this affects the induced migration mechanism.

The intentions for the research conducted within this thesis are as follows:

- Identify a non-invasive method to qualitatively monitor the movement of a secondary immiscible liquid within a suspension;
- Experimentally measure the movement of a secondary liquid when added to a suspension to explore the kinetics of the responsible mechanisms;
- Study the effect of exposing suspensions to high humidity environments to understand which mechanisms are dominant for the mass transfer taking place;
- Apply models based on different mechanisms to correlate with experimental data.

1.2 Thesis Outline

The fundamental transport mechanisms, responsible following the addition of a secondary immiscible liquid to model suspensions are investigated on both the microscale and macroscale using a range of qualitative and quantitative methods. The format of this thesis is as follows:

- In chapter 2 of this thesis, existing literature and methodologies relating to suspensions, in particular moisture and fat migration are reviewed. Also, the methods used to achieve this are highlighted.
- In chapter 3, the materials used and the experimental methodologies employed are described in detail.
- In chapters 4 to 8 the results obtained and discussions for the work conducted are displayed.
- In chapter 4, efforts are focused on monitoring the rate/speed of movement of the secondary liquid during the early stages from addition. A combination of optical and a non-invasive method using benchtop X-ray tomography are employed. The effect of varying the volume of the secondary liquid (water) is investigated upon the kinetics taking place.
- In chapter 5, high resolution scans conducted at the Synchrotron facility are presented. It is shown how the movement of the sucrose particles from the bulk phase into the water droplet could be tracked and quantified from the X-ray scans.

- In chapter 6, the effect of changing the type of secondary liquid is investigated, by varying the viscosity, density and the dissolved sucrose concentration within the secondary liquid. It is shown how the sucrose solubility plays a key factor in driving the movement of the secondary liquid within the suspension and the microscale detail between individual sucrose particles.
- In chapter 7, the consequence of changing the environmental conditions at which the suspensions are stored is investigated. The conditions are above the critical deliquescence relative humidity (DRH) point of sucrose (86 % RH) and fructose (62 % RH). Also, efforts were taken to show how the effect of environmental conditions could be temporarily retarded by using the sorption properties of sucrose for a suspension of fructose and sunflower oil, which is more susceptible to moisture gain.
- In chapter 8, models are presented to show the different mechanisms responsible for the moisture movement seen. Early stage capillary action as well as flux of solid sucrose from the bulk suspension into the water droplet is modelled.
- Finally, in chapter 9 of this thesis, conclusions drawn from the present work are summarised showing some of the similarities in behaviour seen between direct addition of the secondary liquid and environmental storage of the suspension samples. Recommendations of how the present work could be pursued further and developed upon are also given.

Chapter 2 Literature Review

This chapter will take into account the previous work from the literature related to suspensions and the agglomeration of particles within these suspensions. In addition to this, background into techniques used to measure the effects of the addition of a secondary liquid within a suspension will also be looked into. This will include the wettability of particles, the rheological properties and mass transfer both qualitatively and quantitatively in tracking moisture or oil migration.

2.1 Interfacial Properties

The contact angle is a measure of the wettability of a solid surface. It indicates the relation between the different interfacial forces such as the adhesive forces between the liquid and solid and the cohesive forces within the liquid. It is a key parameter when looking at the relationship between a liquid phase and solid phase.

The contact angle (θ) is the angle measured between the solid surface and the liquid/vapour or liquid/liquid interface (Figure 2-1). It specifies if a surface is wetting or non-wetting, where 90° is the cut off. For contact angles with a value lower than 90°, the fluid will spread over a considerable area of the solid surface. For contact angles with a value greater than 90°, the fluid will spread over a minimal area of the solid surface to reduce the area of contact between the liquid and solid. If the liquid being used is water, for a contact angle lower than 90° the solid substrate would be termed hydrophilic, whereas, for a contact angle greater than 90°, the solid substrate would be termed hydrophobic (Gomes et al., 2013). Examples of both cases can be seen in Figure 2-2.

The wetting is related to the cohesive and adhesive forces between the different phases present. If the adhesive force between the solid/liquid interfaces is stronger than the solid/gas adhesive force and the liquid cohesive force, wetting will occur. If the adhesive force between the solid/liquid interface is weaker than the solid/gas adhesive force and the liquid cohesive force, wetting will not occur (Lazghab et al., 2005, Lam et al., 2002).

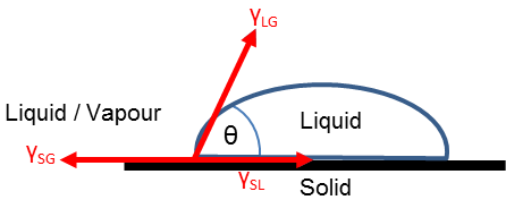

Figure 2-1. Contact angle for a liquid on solid surface, θ is the contact angle between the interface of the solid surface and liquid phase, γ_{SG} is the interfacial tension between the solid and gas, γ_{SL} is the interfacial tension between the solid and liquid and γ_{LG} is the interfacial tension between the liquid and gas.

The contact angle is related to the surface energies by the following Young equation (Lazghab et al., 2005):

$$\cos\theta = \frac{\gamma_{SG} - \gamma_{SL}}{\gamma_{LG}} \qquad \text{Equation 2-1}$$

Generally, if the droplet size is small the gravitational effects are neglected. If the droplet of liquid spreads easily over the solid surface, it is said that the liquid molecules are strongly attracted to the solid molecules.

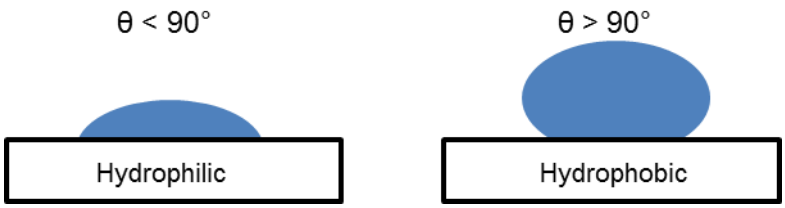

Figure 2-2. Liquid spreading on a hydrophilic or hydrophobic solid surface.

Consideration must be taken when the solid surface is not smooth (for example if it is rough or irregular). It may be that the contact angle being measured is not the actual true contact angle, and therefore adjustments need to be made to compensate for this when calculating the contact angle.

There are numerous methods which can be used for measuring the contact angle between a solid and liquid interface. Depending on the type of solid/liquid materials being used, and the size of the particles, the best suited and most appropriate method is chosen. The method chosen should allow reproducible results to be obtained, and for comparison purposes, the same specific chosen method should be followed when comparing contact angle values for different solid surfaces or liquids.

2.1.1 Sessile Drop Method

The sessile drop method is a simple technique for measuring the contact angle. It works by using a syringe positioned vertically above the sample surface being measured. A fixed volume of liquid is then injected on top of the solid surface (Lazghab et al., 2005). A high resolution camera is used to take images which are then analysed to calculate the contact angle between the liquid and sample surface.

2.1.2 Washburn Method

Another frequently used technique is the Washburn method. This comprises of filling a cylindrical tube with the powder being tested, with the bottom of the cylinder being permeable to the liquid. This is then suspended from a microbalance above the liquid and these are brought into contact. The change in mass during the liquid uptake is recorded, which can then be used to calculate the contact angle in the following equation (Lazghab et al., 2005):

$$\cos\theta = \frac{\mu}{c \cdot \rho_{\mathrm{L}}^2 \cdot \gamma_{\mathrm{LG}}} \frac{m^2}{t} \qquad \text{Equation 2-2}$$

where μ is the viscosity of the liquid, m is the mass of liquid absorbed, c is a material constant which is related to the particle arrangement and the packing within the cylinder, ρ_{L} is the density of the liquid, γ_{LG} is the interfacial tension between the liquid and gas (air) and t is the time at which the mass recording was taken.

The material constant needs to be determined first, by conducting an experiment with a known liquid which fully wets the powder ($\cos\theta$=1). Once the material constant has been determined, further experiments can be performed, with the same packed arrangement of the powder to calculate the contact angle of different liquids. From Equation 2-2, a plot of the mass squared of the liquid uptake against the time will allow for the contact angle to be determined (Galet et al., 2010).

Due to the requirement of initially determining the material constant with a fully wetting liquid in the Washburn method, which can prove difficult, the sessile drop method is more commonly used.

2.2 Mass Transfer in Suspensions

The movement of water into, within or out of some food related suspension products (such as chocolate or peanut butter spread) can be due to several mechanisms. These may include: capillary forces, diffusion, gravity and differences in pressure (Edmondson et al., 2005). The difficulty when attempting to experimentally measure these mechanisms arises when trying to isolate the contribution of each one individually. Knowing the role of individual mechanisms is important when attempting to model the movement, to correlate experimental results with modelled data.

A study by Yuan et al. (2009) looked at vapour and liquid moisture migration in palm kernel oil (PKO) films. The unsteady state diffusivity (D_{eff}) was calculated from a plot of the weight loss of the film, with time using the following equation:

$$D_{\text{eff}} = \frac{l^2}{6t_{\text{lag}}} \qquad \text{Equation 2-3}$$

where l is the thickness of the film and t_{lag} is the lag time. An example for the plot of weight loss vs time can be seen in Figure 2-3, with the linear portion line extended to calculate the lag time.

Also, it was noted depending on the water activity gradient, the diffusion path would change. If the water activity gradient was low (below the deliquescence point of sucrose, 0.85 a_w), the diffusion path would be around the sucrose particles, as the particles were in a solid state. If the water activity gradient was high (above the deliquescence point of sucrose), the diffusion path would be through the sucrose particles, due to the phase change from solid to liquid.

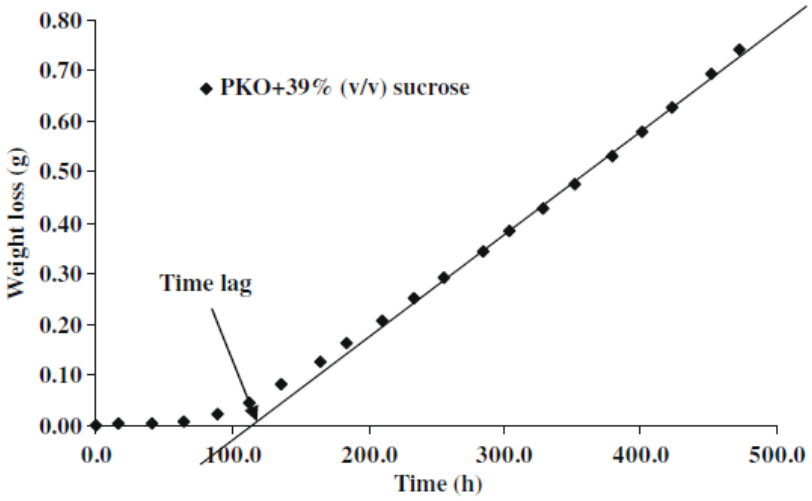

Figure 2-3. Plot of weight loss vs time, to calculate lag time needed for calculating unsteady state effective diffusivity (D_{eff}) (Yuan et al., 2009).

A plot of the calculated diffusivity for different volume fractions of sucrose in PKO films under vapour and liquid induced conditions can be seen in Figure 2-4. The calculated diffusivity is the average diffusivity along the thickness of the film. Initially, as the moisture passes through the film, there will be different diffusivity rates along the thickness of the film. Thus, this gives an overall average and does not correspond to the localised diffusivity taking place along the thickness, within the PKO film.

Also, it is known there are other mechanisms of movement which were unaccounted for such as gravitational and capillary, which was noted during the study.

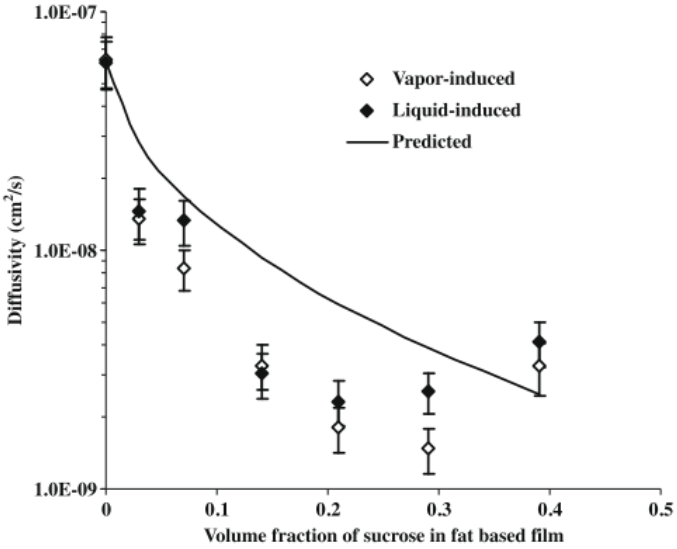

Figure 2-4. Experimental and modelled unsteady state diffusivity under vapour and liquid water activity gradients of 1.0 (Yuan et al., 2009).

Furthermore, Yuan et al. (2012) indicated that the components which make up the suspensions influences the transport mechanisms. The moisture sorption properties of the components within food products (either hydrophilic or lipophilic) may either progress or retard moisture migration depending upon the affinity they have towards water.

For fat migration related to fat bloom in chocolate, both diffusion and capillary pressure have been suggested and modelled to better understand the phenomena taking place (Ziegler, 2009). Though, as of yet no conclusive work has been demonstrated which fits models of diffusion or capillary pressure completely with the experimental data. This suggests that the actual movement taking place is more complex and is most likely to be a combination of several mechanisms (Motwani et al., 2011).

2.2.1 Capillary Forces

Capillary forces result from a pressure difference (Laplace pressure) resulting from a curved surface. The surface in turn is related to the wettability effects of the liquid of the sides of a capillary. If the pores are small enough, then the curvature will be quite significant, and therefore the force will cause the inward penetration of the liquid. Visually this can be appreciated when a straw is placed in a beaker

containing water. The cohesive forces within the liquid and the adhesive forces between the liquid and the straw draw the water up to a higher level in comparison to that in the beaker. The smaller the diameter of the straw, the higher the water is drawn up the straw.

Capillary forces amongst particles can be of significant importance when looking at the rheological properties of suspensions. McCulfor et al. (2011) showed the substantial increase in viscosity when a small amount of water was added to a suspension of glass and mineral oil. The increase in viscosity was ascribed to the formation of liquid bridges between particles, which resulted in the formation of a solid-like structure. This was due to adsorption of water by the hydrophilic particles within the suspension, which in turn resulted in the formation of liquid bridges (Johansson and Bergenståhl, 1992).

Koos and Willenbacher (2011) demonstrated the dramatic visual changes for when suspensions of calcium carbonate in silicone oil were mixed with a secondary immiscible liquid (water). The graphical changes observed in the physical appearance can be seen in Figure 2-5. The transition from a fluid-like arrangement to a gel-like structure is clearly visible with the addition of 0.2 wt. % water, which is a moderately small amount of water.

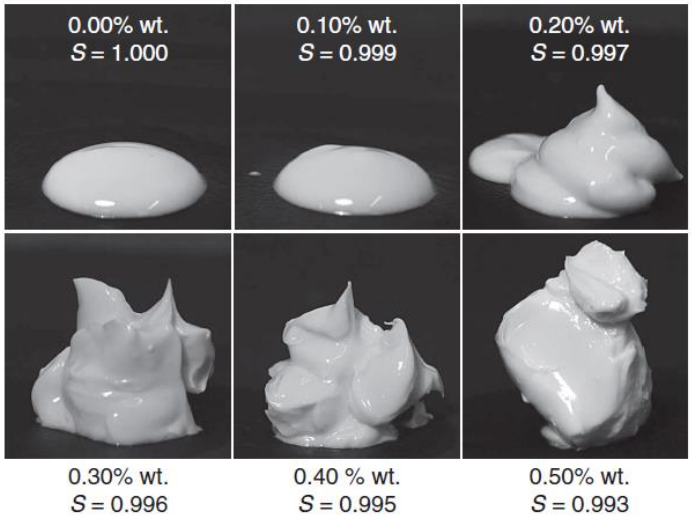

Figure 2-5. Transition from a fluid-like to gel-like structure to suspensions of calcium carbonate suspended in silicone oil with the addition of small amounts of water. *S* is the percentage of the total liquid volume occupied by the continuous phase (Koos and Willenbacher, 2011).

Comparable results were found for suspensions of sucrose/glass spheres and vegetable oil, to which water was added as the secondary liquid (Negreiros et al., 2015). This is of significant importance to several industries, as it illustrates that with the addition of minor amounts of water, which may be added or present inadvertently from the moisture in the air, the rheological properties of the suspension can change profoundly.

In model suspensions of sucrose and soybean oil, it was shown how a sugar skeleton network, could resist elevated temperatures (upwards of 50°C) through the addition of water. The incorporation of water either directly or indirectly through an emulsion mixture allowed the sample to maintain its structure for longer periods at elevated temperatures, in comparison to samples without any water addition (Killian and Coupland, 2012).

Similar behaviour was achieved for water based suspensions of cocoa particles, in which this time the secondary immiscible liquid was oleic acid (Wollgarten et al., 2016). The liquid bridge formation was from a combination of the cocoa butter within the cocoa particles as well as the added oleic acid. However, for this system the temperature dependence of viscosity was important. If the temperature was set sufficiently high to melt the cocoa butter, the network formation was destroyed due to the phase change from solid to liquid for the secondary immiscible liquid.

The main goal for incorporation of water into suspensions is to create chocolates which are heat resistant and more stable at temperatures experienced nearer to the equator. Patents have shown promising results through the integration of secondary immiscible liquids (water or glycerol) to create a three-dimensional network matrix, which can achieve this desired goal. However, how the network initially forms and how secondary liquid redistributes itself throughout the system is not fully understood (Whitehouse, 2013, Althaus et al., 2013, Hoffmann et al., 2014).

2.2.1.1 Droplet Penetration

When a liquid penetrates into a porous bed, this is due to the Laplace capillary suction pressure (P_c). The equation to calculate the Laplace capillary suction pressure (P_c) is (Charles-Williams et al., 2011):

$$P_c = \frac{2\gamma_{LG}\cos\theta}{R_{\text{pore}}} \qquad \text{Equation 2-4}$$

where γ_{LG} is the interfacial tension between the liquid and gas, θ is the contact angle, and R_{pore} is the characteristic pore size of the bed.

The calculation for R_{pore} is (Hapgood et al., 2002):

$$R_{\text{pore}} = \frac{\varphi d_{32}}{3}\frac{\varepsilon}{(1-\varepsilon)} \qquad \text{Equation 2-5}$$

where φ is the sphericity of the particles, d_{32} is the Sauter mean diameter (i.e. the diameter of a sphere which has the same volume/surface area ratio in relation to the particle of interest), and ε is porosity.

The penetration of a liquid into a porous bed has two limiting cases, in terms of the fastest and slowest penetration time based on the area of contact between the liquid and the porous bed. These are described by Hapgood et al. (2002) as the constant drawing area (CDA) and decreasing drawing area (DDA), which can be seen in Figure 2-6.

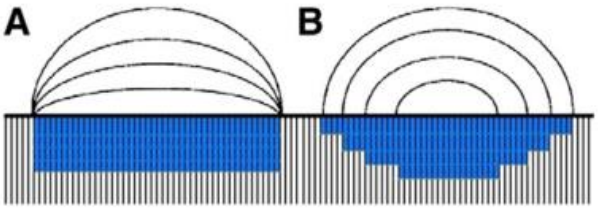

Figure 2-6. Liquid penetration into porous bed A) CDA, B) DDA (Charles-Williams et al., 2011).

In the case of CDA, the contact angle decreases as penetration occurs, whereas in DDA the contact angle remains constant but the penetration is slower. For the case of CDA, as the area of contact is maintained and therefore, the penetration time the quickest. For DDA, the area of contact decreases progressively, therefore, the

penetration time is the slowest. Generally, for experimental purposes it is found the penetration time is between the two limiting cases (CDA and DDA).

The predicted time for liquid penetration (τ) based on the CDA and DDA is (Hapgood et al., 2002):

$$\tau_{\mathrm{CDA}} = 1.35 \frac{V_o^{2/3}}{\varepsilon^2 R_{\mathrm{pore}}} \frac{\mu}{\gamma_{\mathrm{LG}} \cos\theta} \qquad \text{Equation 2-6}$$

$$\tau_{\mathrm{DDA}} = 9\tau_{\mathrm{CDA}} \qquad \text{Equation 2-7}$$

where μ is the viscosity of the liquid and V_0 is the drop volume. It can be seen that the penetration time for DDA is 9 times greater than CDA.

The equations mentioned so far only deal with the penetration of liquid into powder bed after complete penetration. When trying to understand the kinetics, the penetration with time is important to help correlate modelled data with experimental data. The volume of liquid penetrating into a powder bed can be calculated from Equation 2-8, which assumes CDA (Denesuk et al., 1993):

$$V_{\mathrm{p}}(t) = k \int_0^t \frac{r_{\mathrm{d}}^2(t')}{\sqrt{t'}}\, dt' \qquad \text{Equation 2-8}$$

where:

$$k = \pi\, \varepsilon \sqrt{\frac{\gamma_{\mathrm{LG}}\, R_{\mathrm{pore}} \cos\theta}{2\mu}} \qquad \text{Equation 2-9}$$

where $V_{\mathrm{p}}(t)$ is the volume of liquid penetrated into the powder bed at time t, and r_{d} is the drawing radius. Therefore, at any time t', the volume of liquid penetrated can be calculated. It should be noted Equation 2-8 is based on the CDA approach, which as previously mentioned is the quickest in terms of time taken for penetration.

A study was conducted by Nguyen et al. (2009) looking at the penetration time of water into powder bed mixtures, containing hydrophilic and hydrophobic materials (lactose and salicylic acid, respectively). This was based on the CDA approach

(Equation 2-6) and it was seen that the experimental penetration time varied greatly in comparison to the modelled penetration time. It was noted, that the modelled times are based on the assumption that the penetration time is for completely hydrophilic powder beds, and the dissolution of the lactose will affect the viscosity and surface tension during penetration which is not accounted for within the model.

2.2.2 Diffusion

Diffusion occurs when there is a concentration gradient present between two regions. The movement of molecular species is in the direction from an area of high concentration to an area of low concentration. This will proceed until the two regions are in equilibrium. This movement is related to the chemical potential, though more often the term concentration is used for ease, divided by the resistance to movement encountered by these molecules. A typical equation based on Fick's law of diffusion is (Ghosh et al., 2002):

$$J_{\mathrm{i}} = D_{\mathrm{f}} \frac{\partial_{\mu \mathrm{i}}}{\partial_{\mathrm{xi}}} \qquad \text{Equation 2-10}$$

where J_{i} is the molar diffusion flux of the migrating molecules, D_{f} is the diffusion coefficient, X_i is the diffusion length and μ_i is the chemical potential of the species.

Edmondson et al. (2005) studied the mass transfer of water (due to drying) in chocolate crumbs (mixture of sugar, milk and cocoa solids) of irregular shape. The crumbs used were of two size classes (either 10 mm or 100 mm in mean diameter). The crumbs passed in a counter-current flow, in relation to the hot air over a distance of 4 metres (in a spray dryer). The initial moisture content for both size crumbs was 4 %. For the larger crumbs (100 mm), only a small portion of moisture was removed (0.18%), whereas, for the smaller crumbs (10 mm), almost half of the moisture present was removed (1.99%). This highlighted the effect of having a larger surface area to volume ratio. The area of contact between the hot air and the smaller crumbs was greater in comparison to the larger crumbs, and thus resulted in a greater mass transfer of moisture. Furthermore, the distance the moisture has to travel from the centre of the body to the surface in contact with the

air, in the smaller size class crumbs is less, and therefore, the resistance to internal diffusion is less significant in comparison to larger crumbs when drying.

2.2.2.1 Fat Migration

One of the major problems for chocolate based products, post production is fat blooming. This is visually observed as a whitish coating on the surface of chocolate and can also result in sensory defects of the product, which is undesired (Ghosh et al., 2002, Beckett, 2009). The main causes of fat blooming are due to improper tempering (correct tempering ensures removal of unwanted crystals) during production and storage conditions of the product after production. The reason of blooming is due to the different types of triglycerides present within chocolate. These triglycerides are polymorphic (6 crystal forms exist) and can undergo polymorphism, which in turn changes the melting point. The triglycerides with lower melting points can begin to melt at temperatures experienced during storage or transportation. These melted triglycerides are then squeezed (capillary and diffusion forces driving the movement of the oil) to the surface via the air pockets present within the chocolate. Once the surface of the chocolate has been reached, these triglycerides then recrystallize (Aguilera et al., 2004, Dahlenborg et al., 2015, Reinke et al., 2016, Ziegler, 2009).

A study conducted by Guiheneuf et al. (1997) looked at how oil migration is affected by temperature from a hazelnut oil layer to a chocolate layer using magnetic resonance imaging (MRI). The methodology applied allowed this to be measured non-invasively, which ensured that the movement was not influenced and could be tracked over a long term storage period. The migration of the oil to the chocolate layer was successfully tracked, and it was shown that storage temperature plays an influential part upon the migration rate. For samples stored at 19°C, the oil migration was very limited over the storage period of 40 days, whereas, for samples stored at 28°C the migration rate dramatically increased. The difference in oil migration was ascribed to the temperature dependence of diffusion and due to the partial melting of the fats, which allows for faster diffusion.

Miquel and Hall (2002) also used MRI to monitor the migration of fat during storage of chocolates at various temperatures. The cream centre filling can be seen to be moving to the surface as the level of whiteness increases near the surface (from the arrows in image b and c in Figure 2-7). This is further confirmed by the brighter spots shown on the MRI scan, where the brighter regions are associated with the presence of fat. It can be seen that as the chocolate is stored for a longer duration of time, the movement of lipids from the centre filling (white line) is moving towards the outside of the chocolate.

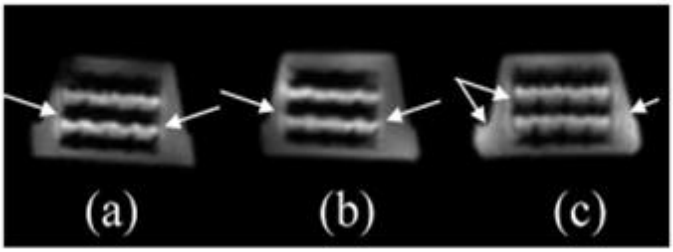

Figure 2-7. The migration of lipids after storage at 23°C for (a) 1 week, (b) 3 weeks and (c) 2 months (Miquel and Hall, 2002).

Further research conducted by Altimiras et al. (2007), studied the effect of solid particle size upon oil migration rate. Model chocolate bars were prepared with cocoa butter mixed with sand particles (as model particles) of three different size classes. Mass change of the bars was documented by measuring the mass increase of filter paper situated on the bar, which correlated to the cocoa butter migration. In Figure 2-8 over the first four days for bars stored at the same temperature (30°C), the quickest migration of cocoa butter was observed for chocolate bars with the smallest particles. After 4 days up until 22 days, the rate of migration slowed down dramatically. This indicates that the solid particle size has a significant affect upon the oil migration rate.

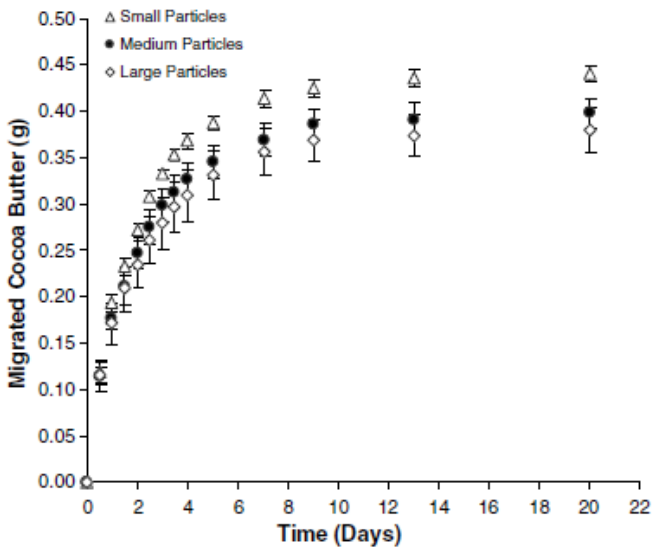

Figure 2-8. The migration of cocoa butter for different size particles in chocolate bars (Altimiras et al., 2007).

The data from Figure 2-8 was compared to modelled data using the following equation based on capillary theory:

$$\frac{2}{r_c}\gamma\cos\theta = \frac{8}{r_c^2}\mu h\frac{dh}{dt} \pm \rho_L g h\cos\alpha \qquad \text{Equation 2-11}$$

where, r_c is the radius of the capillary, γ is the surface tension of the fluid, θ is the contact angle between the fluid and the capillary wall, μ and ρ_L are the viscosity and density of the liquid, h is the height the liquid has been drawn up the capillary, g is the acceleration due to gravity and α is the angle between the capillary and a reference horizontal plane.

The results from Equation 2-5 showed that fastest liquid migration is obtained for bars containing larger particles (which contain bigger capillaries) as can be seen in Figure 2-9. This is in contrast to the results shown, as liquid migration for the smaller particles was quicker. Also, the magnitude of capillary movement is on the order of seconds, whereas, results show movement after days signifying a combination of mechanisms or other mechanisms being present (Altimiras et al., 2007).

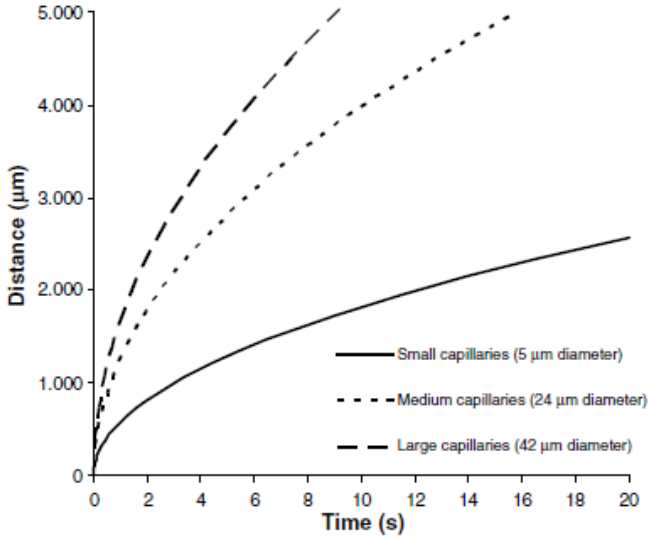

Figure 2-9. Migration rate of oil based on capillary for different size capillary diameters (Altimiras et al., 2007).

This illustrates that liquid migration can arise quite rapidly at a moderate temperature of 30°C. This temperature is below the average temperatures experienced in some countries located on or nearby the equator. Thus, unless the chocolate is stored and transported under controlled temperatures, liquid migration would take place, with the consequences of this phenomenon present before the product reaches the consumer. Therefore, by better understanding the mechanisms responsible for the oil migration, steps can be taken to reduce/mitigate the effects.

Altan et al. (2011) and Lee et al. (2010) conducted a comparable study using MRI to look at the oil migration from almond products and peanut oil/butter paste which were in contact with a chocolate layer. Comparable scans were taken similar to those by Miquel and Hall (2002) on chocolate bars, which were then quantified based on the change in signal intensity. The presence of oil resulted in the highest signal intensity for the MRI scan. It was revealed that the oil was migrating from the almond layer to the chocolate layer, and the speed of migration was proportional to the storage temperature. This highlights the significance of storing filling based chocolates at appropriate environmental conditions, and the importance of product formulation in assisting to control liquid migration from multi-layered products

(McCarthy and McCarthy, 2008, Rumsey and McCarthy, 2012, Motwani et al., 2011, Smith et al., 2007).

It is theorised that it would be possible to track the migration of water using MRI as a non-invasive approach, as the change in signal due to the water replacing the continuous phase of fat can be observed. Thus, by following the change in signal intensity, which could then be correlated to a change in water content and allowing the migration of moisture into the suspension to be tracked. This could be achieved qualitatively by conducting regular scans and from the resulting images, quantitatively analysing the signal intensity of grey scale within the images. The approach would be comparable to that demonstrated by Miquel et al. (2001), as can be seen in Figure 2-10 for liquid migration from the hazelnut filling to a chocolate layer. The main constraint in this approach is the resolution of the scan, which is inadequate to visually see the primary particles or the internal structure of the sample.

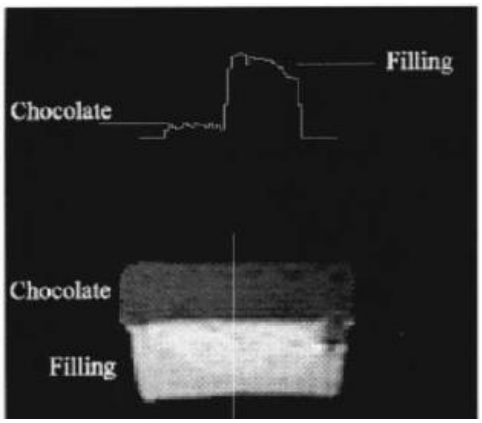

Figure 2-10. Liquid migration between composite layers. White signal indicates high oil content (Miquel et al., 2001).

Svanberg et al. (2012) studied fat migration by monitoring the swelling (height profile using confocal chromatic displacement sensor (CCDS) using polychromatic white light) and mass gain of dark chocolate samples, which were placed in contact with an oil layer. It was shown how initially, even with the migration of oil over the first 21 days, visually the sample displayed very little change (though the mass uptake was significant) as can be seen in Figure 2-11. However, after longer periods of storage (21+ days), the swelling became more evident due to the uptake

of fat and could be visually tracked. This highlights the limitations in certain optical methods and measuring the weight change with time, in tracking the actual liquid migration within the sample.

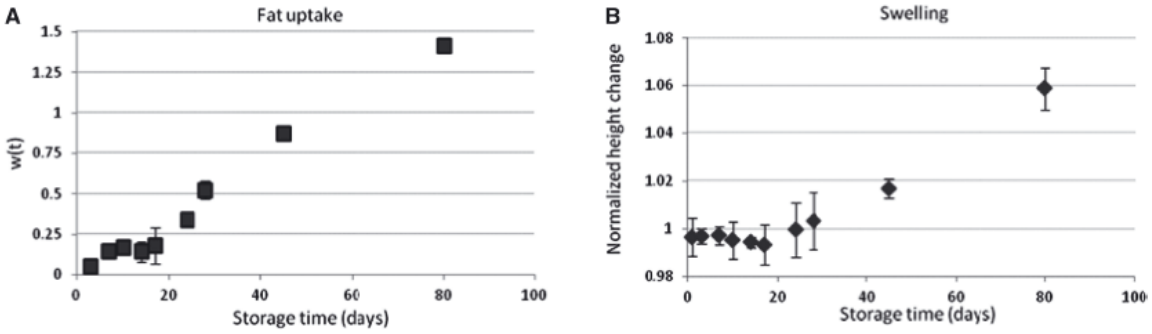

Figure 2-11. Effect of oil migration on chocolate samples, (a) change in mass with time, (b) change in height with time (Svanberg et al., 2012).

2.2.2.2 Water Migration

An additional major issue encountered by confectionary manufacturers is the migration of water from neighbouring layers within products (i.e. a wafer layer in KitKat chocolate). This is due to a water activity gradient between the layers and can lead to permanent texture loss (Guillard et al., 2003b). One important parameter when considering the migration of water is the physical state of the secondary liquid (vapour or liquid) and thus needs to be accounted for when attempting to model the kinetics taking place (Yuan et al., 2009, Morillon et al., 1999). One common approach used within the literature has been to monitor the change in weight of the sample with time within a controlled and sealed environment, known as the gravimetric cup method (ASTM-E96, 2016). This enables the bulk movement of moisture to be tracked in a quantitative method, though does not allow the localised movement of moisture within the sample to be tracked.

Guillard et al. (2003b) conducted an experiment for a sample containing a layer of sponge cake (water activity 0.84) in contact with an agar gel (water activity 0.999). The moisture content within the sponge cake was observed after different periods of storage, to examine the effect of moisture transfer with time. The sponge cake layer was positioned on top of the agar gel. After different periods of storage,

samples of the sponge cake were sliced into 2 mm portions, to measure the moisture content to track the moisture profile within the sample. From Figure 2-12 it can be seen that as the duration of storage is prolonged, the moisture content within the sponge cake rises. This signifies that moisture is migrating from the agar gel to the sponge cake.

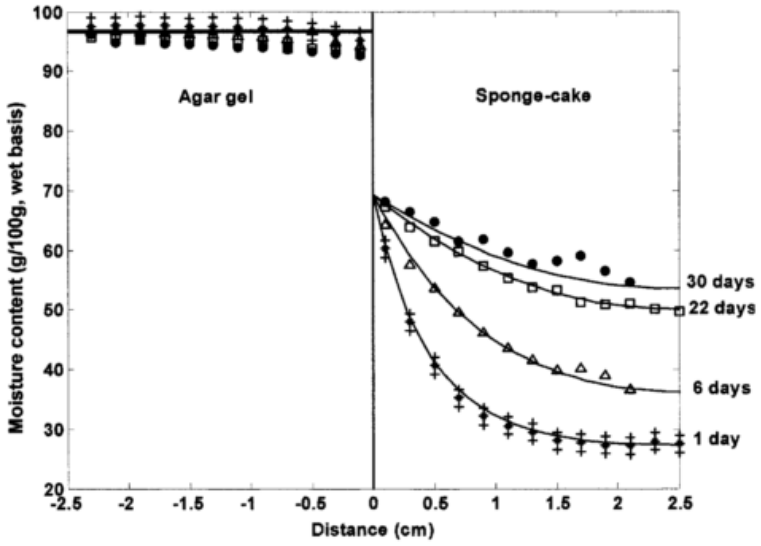

Figure 2-12. Moisture content of sponge cake after various days when placed above agar gel (Guillard et al., 2003a).

The data points signify the experimental data after different storage periods in Figure 2-12. The general trend which can be seen is that as the storage period increases from 1 to 30 days, the moisture content within the sponge cake layer increases which the agar gel remains fairly constant. It can also be seen that there is a moisture content gradient within the sponge cake, with the highest value for the region in contact with the agar gel and lower near the area furthest from the agar gel. This shows the direction of movement of the moisture within the sponge cake and that even after 30 days equilibrium has not been reached between the 2 layers.

It is presumed that as soon as the monolayer of the sponge cake which is in contact with the agar gel is saturated, diffusion would then occur predominantly through the vapour phase due to the high porosity (air pockets) present within the sponge cake structure. Complete saturation results in a reduction in porosity of the

sponge cake, leading to a secondary mechanism stage of liquid diffusion, which is now the dominating mechanism of water movement. Vapour diffusion is faster in comparison to liquid diffusion. The effective water diffusivity decreased as the moisture content of the sponge cake increases. This agrees with Figure 2-12, as with time the rate of increase in moisture content gain of the sponge cake is slower (Guillard et al., 2003b).

A similar experiment was carried out on a dry biscuit in contact with agar gel. It was established that the water transfer rate from the agar gel to the biscuit could be delayed by positioning an edible film (acetylated monoglyceride) between the agar gel and the biscuit (Guillard et al., 2004). The rise in moisture content of the biscuit was delayed over the first three days as edible film adsorbed the moisture initially, in comparison to when the edible film was not used. However, once the barrier became saturated with moisture, it was no longer able to restrict moisture movement and passed on the moisture onto the biscuit layer. This highlights the potential of using a film as a potential barrier, though, proving only successful in reducing the moisture transfer rate for a short time period (3 days for a film with 316 µm thickness) when considering the shelf-life of confectionary products.

Yuan et al. (2012) demonstrated how the rate of diffusivity is affected by the presence/absence of different components within films of palm kernel oil with sucrose, cellulose and lecithin, using the gravimetric cup method (monitoring change in mass within sealed a environment). This change was ascribed to the different sorption properties of the materials present, which can be seen in Figure 2-13.

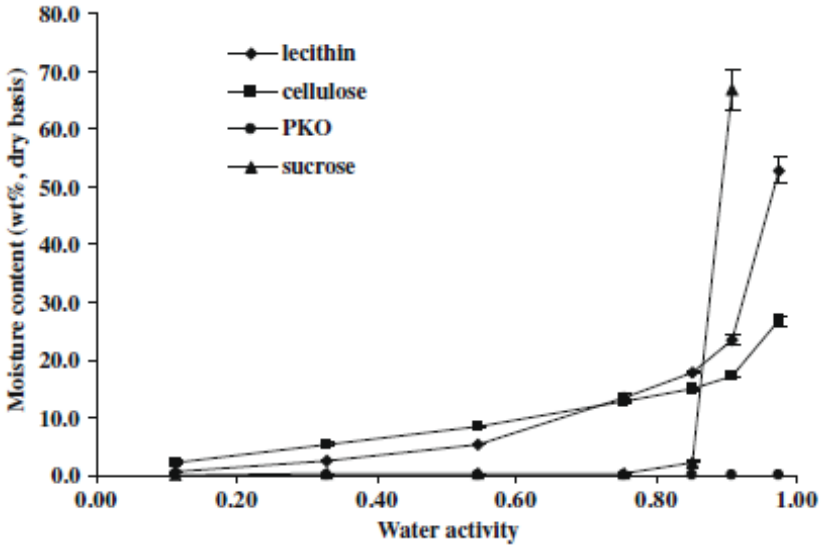

Figure 2-13. Sorption isotherms for sucrose, lecithin, cellulose and PKO at 25ºC (Yuan et al., 2009).

From Figure 2-13 it can be seen that when the water activity is increased above 0.85, the moisture content of sucrose rises substantially as this is now above the deliquescence point of sucrose. The general trend seen is for a crystalline material in which at lower water activities there is very minimal moisture gain, then after reaching and exceeding the deliquescence point the water uptake is substantial and now the sucrose is in a liquid state.

Ghosh et al. (2004) stated that the physical state of sucrose, will influence the diffusion path taken by water. For a water activity environment below 0.85, moisture will migrate around the sucrose particles. This is slower due to the tortuosity (path taken by water), as the water activity is lower than the deliquescence point of sucrose and therefore the sucrose is in a solid state, in comparison to a higher water activity, in which the sucrose particles will have dissolved. Thus, less resistance will exist as the water migrates. Other components such as cocoa powder, cellulose and lecithin have different effects upon moisture migration, due to the varying structure and sorption capacity of the materials (Lee et al., 2010, Ghosh et al., 2005).

Morillon et al. (1999) showed the importance of the continuous phase component (hydrophilic or hydrophobic) within a film upon the rate of moisture migration. This is for both vapour and liquid water exposure. This was displayed for cellophane

films (hydrophilic in nature), which had a considerably higher permeability of water in comparison to polyethylene films (hydrophobic in nature). The significance of the physical state of the water (vapour or liquid) is important only when the continuous phase is water sensitive. When the continuous phase is hydrophobic, the moisture migration is affected by the difference in vapour pressure between the surrounding atmosphere and the film.

Guillard et al. (2003b) modelled the moisture transfer from an agar gel to a sponge cake using several diffusivity laws (linear, exponential, polynomial and power law). The power law (Equation 2-12 based on Fick's second law) was the most suitable model when trying to fit the experimental data with a theoretical curve for experimental moisture content profiles from the sorption kinetics as can be seen in Figure 2-14.

$$\frac{X^* - X_0}{X_\infty - X_0} = 1 - \sum_{n=0}^{\infty} \frac{8}{(2n+1)^2\pi^2} \exp\left\{\frac{D_{eff}(2n+1)^2\pi^2 t}{4e^2}\right\} \qquad \text{Equation 2-12}$$

where X^* is the average moisture content (g g^{-1} dry basis), X_0 is the initial moisture content (g g^{-1} dry basis), X_∞ is the equilibrium moisture content (g g^{-1} dry basis) and e is the thickness of the sample (m).

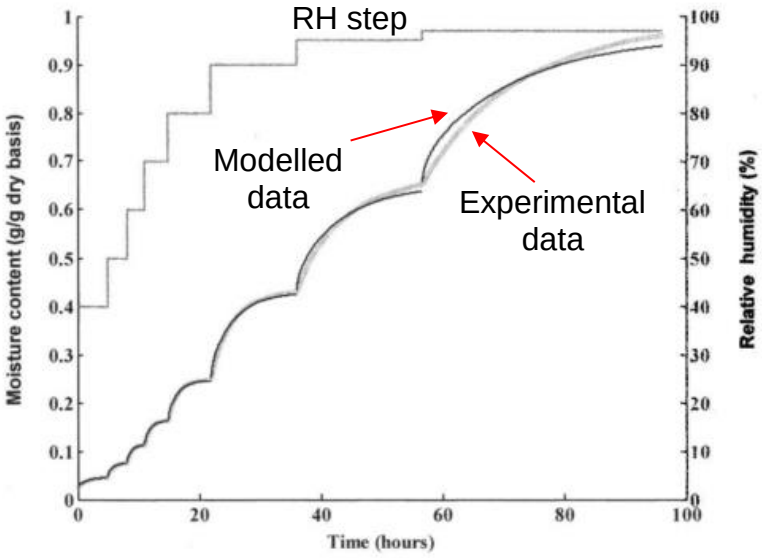

Figure 2-14. Kinetic data for water adsorption of sponge cake. The grey curve represents experimental data, whereas the black curve is for modelled data. The solid grey line represents the relative humidity condition (Guillard et al., 2003b).

The experimental and modelled data fit in Figure 2-14 is in agreement (black curve and grey curve represent modelled and experimental data respectively). This, therefore, highlighted the possibility in using such models to be used for varying water activity gradients to predict moisture transfer in food products from the surrounding atmosphere.

Paluri et al. (2015) used a similar method to that mentioned in Section 2.2.2.1 this time using MRI to track moisture migration from an agar gel to a cocoa/palm kernel oil lipid layer. The signal intensity from the grey scale image was used to track the movement of moisture. The method proved successful to track the bulk movement of moisture, but was unsuccessful in identifying and tracking microscale localised movement of moisture within the sample.

Svanberg et al. (2012) looked at both fat and moisture migration with chocolate samples (when placed in direct contact with water and oil). It was shown that the migration rate for the moisture was significantly quicker in comparison to the fat migration, based on the mass gain with time (14 hours for moisture, 45 days for oil for comparable mass increase). This indicates that potentially different mechanisms are responsible for the kinetics taking place.

2.3 Non-invasive Methods to Monitor Liquid Migration

One of the concerns with the methodology of monitoring mass change discussed is that only bulk transfer is being monitored. The localised mass transfer taking place cannot be tracked using weight measurements alone. Also the visual movement of how and where the liquid is migrating to and from within a multi-layered product cannot be seen, which is of extreme importance when attempting to understand the movement kinetics responsible for liquid migration.

Of the several visual techniques available, the two most common non-invasive methods include Magnetic Resonance Imaging (MRI) and X-ray computer tomography (CT). Although, as of yet, no work could be found in the literature on suspension based products to monitor the localised mass transfer of water with time. The novelty of the work conducted in this study is using dynamic X-ray CT to track the movement of a secondary immiscible liquid within a suspension based

system. The main advantage of using this non-invasive approach is that it enables the liquid migration within a suspension system to be seen within its natural state. Also, as the technique is non-destructive, dynamic studies can take place over long storage periods. This is of paramount importance when trying to understand the shelf-life of food products and gaining a better understanding of the underlying mass transport mechanisms taking place.

X-ray CT has been successfully and effectively used to analyse rocks, metals and granules to determine the porosity and binder distribution (Dadkhah et al., 2012). It has also been used extensively to examine the internal structure of food products such as aerated chocolate bars and mousses (Lim and Barigou, 2004). Numerous studies have been conducted on food based products using this approach to look at liquid migration and water content distribution in oil fillings, apples and mayonnaise to name a few (Guiheneuf et al., 1997, Altan et al., 2011, Lee et al., 2010, McCarthy and McCarthy, 2008, Miquel and Hall, 2002, Rumsey and McCarthy, 2012, Laverse et al., 2012, Herremans et al., 2014, Lim and Barigou, 2004). Due to the high signal intensity it was possible to track the liquid phase location and movement using X-ray scans. Therefore, X-ray CT is a viable technique which can be applied to better understand the mechanisms of migration responsible for the movement of a secondary immiscible liquid within a suspension.

2.3.1 Magnetic Resonance Imaging (MRI)

Magnetic resonance imaging (MRI) is a common imaging technique used for medical purposes. However, recently it has been utilised in other fields of research such as pharmaceutical industry as well as food industry.

Its principle is based on the atomic nuclei absorbing and emitting different radio frequencies when placed within an external magnetic field. Most commonly, the hydrogen atoms within samples are tracked due to the high occurrence within samples.

It was demonstrated how MRI could be used to track tablet swelling, after positioning tablets in a aqueous media and scanning using a benchtop MRI system

(Laity et al., 2010). The echo intensity allowed the water migration into the tablet to be tracked, as can be seen from Figure 2-15. The dry tablet core had a low intensity reading, while the outer surface of the tablet in contact with the liquid medium had a high intensity reading.

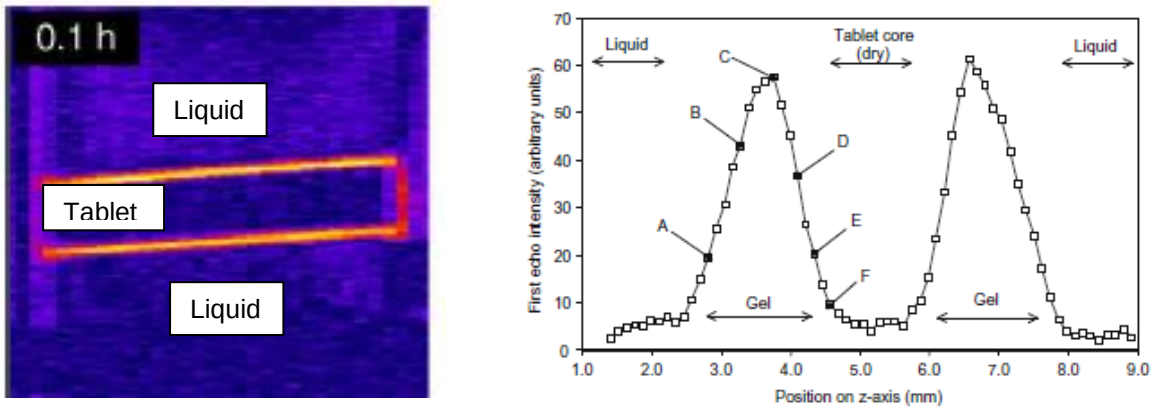

Figure 2-15. Image from MRI and signal intensity in relation to tablet swelling.

Van Duynhoven et al. (2009) demonstrated how MRI could successfully be used to monitor bulk movement and study food products on the macroscopic level. Though, the limitations of this technique did not allow the microscopic level detail to be studied.

2.3.2 X-ray Computer Tomography (CT)

Transmission X-ray computer tomography (CT) is a non-destructive technique based on the mapping of the linear attenuation coefficient of X-rays crossing the studied sample and allowing the internal 3D microstructure of a sample to be visualized and analysed. This is achieved by taking a series of projections, as the sample is rotated between the X-ray source and detector. These projections are then reconstructed using an algorithm which allows the 3D internal structure at the micron spatial resolution to be seen.

Historically, it has been successful for medical applications; however, recently it has been used in other fields of research including food science. Its principle is based on the different absorption properties of different materials. In conventional lab based CT systems, X-rays are generated by accelerating a charged particle

from a filament (cathode) towards a target (normally a metal material, anode), which in turn produces X-ray radiation and a large amount of heat (Stock, 2009).

Depending on the molecular mass of a material, different amount of radiation are absorbed, while the remaining radiation is transmitted onto a scintillator screen, which is then converted into a shadow image. Projections are taken while the sample is rotated over 180° or 360°, in specified increments. These projections results in a stack of 2D images which are then, reconstructed using the algorithm within the user software, which produces a 3D internal structure of the sample under study to be seen along the different planes (axial, coronal and sagittal).

A schematic for the typical setup for the X-ray source, sample and detector within conventional lab based CT systems can be seen in Figure 2-16. The majority of lab based X-ray CT systems have a cone and beam arrangement. Other arrangements are possible such as parallel beam configuration which is common for synchrotron setups. A typical arrangement for a parallel beam configuration can be seen in Figure 2-17. The main advantage of synchrotron based X-ray CT over lab based systems is the higher resolution images with greater details in comparison to lab based systems, though accessing synchrotron facilities can be challenging (Stock, 2009).

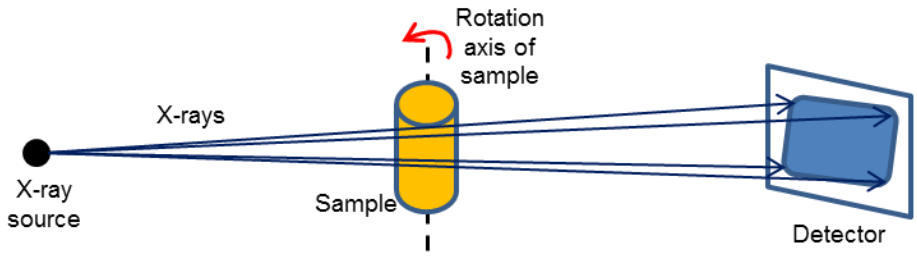

Figure 2-16. Schematic view of the experimental set up used for bench top X-ray CT.

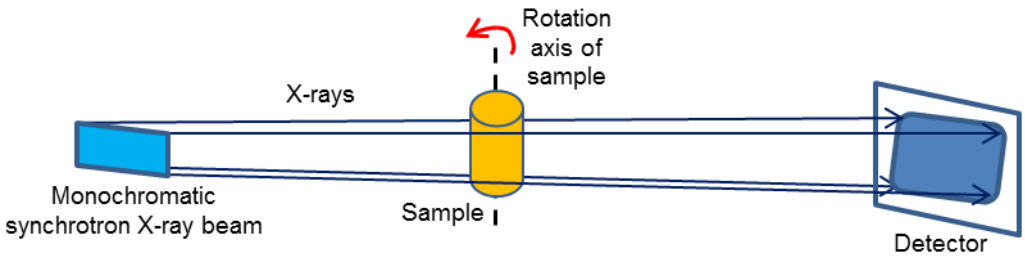

Figure 2-17. Schematic view of the experimental set up used for synchrotron beamline X-ray CT.

Performing synchrotron X-ray CT experiments at a third-generation synchrotron source, such as Elettra or Canadian Light Source (CLS), highly improves the image quality when compared to conventional laboratory X-ray sources. Synchrotron X-ray beam features properties that significantly increase the data quality, in terms of contrast and spatial resolution, which extend the imaging possibilities. These properties are due to the beam monochromaticity, its high intensity, high spatial coherence and nearly-parallel geometry. A monochromatic and highly-intense X-ray beam leads to reconstructed slices free of beam hardening effects (Baruchel et al., 2000) and with a high signal-to-noise ratio.

The key advantage of X-ray CT over other experimental lab based methods is that it is possible to see the internal structure of the sample being studied, in its natural state under standard conditions, without having any destructive effects. Also it allows for the possibility of multiple scans to be performed on the sample, to study the dynamics of a system (Lim and Barigou, 2004, Laverse et al., 2012).

The reconstructed file after a scan, results in a stack of images with different grey values for the sample, which is related to the different components/densities within the sample. X-ray CT has been successfully used to study the swelling of tablets, as well as the ingress of a solution into a dry tablet powder. This is important for controlled drug dosage release, after consumption to ensure a consistent absorption into the blood stream (Laity et al., 2010). This highlights the prospective and capabilities of using this non-invasive approach to monitor the ingress of liquid to better understand the dynamics. Also, it has been used to study oil recovery using model samples of glass suspended in oil, which is then injected with contrast

water. This showed how more than 2 phases could be isolated and identified for complex systems (Marques and Appoloni, 2015).

To date, the author is not aware of any research which has been conducted utilising X-ray CT, to study the dynamics of water within a suspension through a time lapse of scans. It is foreseen this approach will allow the displacement of the continuous phase of oil by a secondary immiscible liquid, such as water within a suspension to be observed.

Chapter 3 Materials & Methods

Generally food products are very complex systems, composed of various components/ingredients. This in turn makes it difficult when studying to identify and isolating the responsible component/ingredient for the behaviour observed. It has been shown that materials have their own affinity towards water, which in turn will affect the migration and dynamics of the system. This necessitates simplification of the system to help isolate and reduce the effect of numerous components; thus, a model system will be used for the experimental approach. This will allow the focus to be placed upon understanding the key physical kinetics taking place, and help to identify and isolate the mechanisms of movement taking place for the secondary liquid as well as how the storage conditions effect the system dynamics.

The model system employed in this study was hydrophilic particles (sucrose / fructose) suspended in a continuous hydrophobic phase (high oleic sunflower oil). The secondary immiscible liquids used throughout this study were distilled water, glycerol, sucrose solutions, saturated sucrose solution and saturated fructose solution.

3.1 Materials

3.1.1 Hydrophilic Particles

Sucrose ($C_{12}H_{22}O_{11}$) (density 1588 kg/m^3, ZMR Zuckermühle Rupperswil AG, Germany) is a disaccharide composed of the monosaccharides fructose and glucose. Sucrose is key ingredient found in chocolate (approximately 50 % wt.) and it is known for its high purity level (>99.9%) (Bucke, 1995, Beckett, 2009).

Fructose ($C_6H_{12}O_6$) (Danisco, Copenhagen, Denmark) is a monosaccharide. One of the main advantages it has over sucrose and other naturally occurring sugars is its higher sweetness index (Danisco, 2003, Beckett, 2011). Also, unlike sucrose it does not raise the blood sugar level significantly when consumed and thus can be found in special chocolates for diabetic people (Beckett, 2009). However, it is very hygroscopic (more than sucrose) and thus care needs to be taken to ensure appropriate storage conditions (Beckett, 2009).

One of the issues when using sugars as the hydrophilic particles within the suspension is that when the secondary liquid (water) is added, there will be both the migration of the secondary liquid as well as the dissolution of the sugar. Both sugars are very soluble in water. This will, therefore, affect the rheological properties and the rate of migration of water. Also, the solubility of sugars increases with temperature, as can be seen in Figure 3-1.

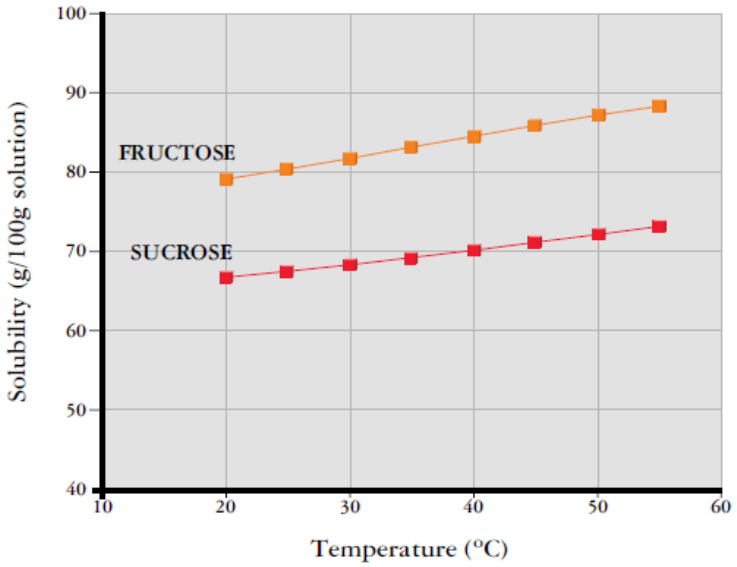

Figure 3-1. Sugar solubility with temperature (Danisco, 2003).

Therefore, in order to overcome this issue, experiments were conducted using a secondary liquid in which sucrose has low solubility such as glycerol. This will eliminate the dissolution problem and allow emphasis to be placed on the movement and of the secondary liquid, as glycerol will remain more constant as it is not affected by solubility of sucrose. The sugars were used as received for experimental purposes.

3.1.2 Hydrophobic Continuous Phase

The continuous fat phase used for this study was sunflower oil supplied by Nestlé (Sofinol Oils, Switzerland, Surface tension 35.5 mN/m, Viscosity 49 mPa·s, measured at 25°C). The density is 891.9 kg/m^3 (measured using a 10 ml pycnometer), measured at 25°C. It contained by mass, 23% mono-unsaturated fatty acids, 65% polyunsaturated fatty acids and 12% saturated fatty acids. Sunflower oil is composed of mainly triglycerides (TGA), which have a glycerol

group attached to three fatty acids. Saturated fatty acids contain no double bonds between carbon molecules. Generally, unsaturated fatty acids have a lower melting point in comparison to saturated fatty acids (O'Brien, 2004).

Sunflower oil was chosen as the continuous phase as opposed to cocoa butter or palm kernel oil, due to being in a liquid phase at room temperature.

3.1.3 Secondary Immiscible Liquid

The secondary immiscible liquids used during this study were distilled water, sucrose solutions (10 % wt., 30 % wt., 40 % wt. and 67 % wt. 25°C, Sigma-Aldrich, UK), saturated fructose solution (81 % wt. fructose at 25°C, Danisco, Denmark) and glycerol (Sigma Aldrich, UK, density 1258 kg/m^3 (Perry, 1997)).

Sucrose solutions were prepared by mixing the relevant mass fraction of sucrose particles and distilled water, to achieve the desired solution concentration. Saturated solutions of sucrose and fructose were prepared by dissolving (mixing) the relevant amount of sucrose or fructose crystals in deionised water until complete dissolution at room temperature (25°C, (Bucke, 1995, Danisco, 2003)).

Glycerol was chosen as a secondary immiscible liquid as it is a common component found in food products and its low solubility of sucrose.

3.2 Methods

3.2.1 Particle Size Distribution

Many methods are available which can be used to measure the particle size distribution, such as sieving, optical methods and laser diffraction. The various methods available have their different advantages and disadvantages. Depending on the material being measured, some methods may be more suitable than others.

Particle sizes were measured using the Camsizer XT (Retsch Technology GmbH, Germany). The principle is based on image analysis with a dual camera set-up. The first camera (basic) is for larger particles and the second camera (zoom) is for capturing the smaller class size particles. The set-up allows for 3 different dispersion units, which are the X-fall for free flowing powder, X-jet which uses compressed air to assist in the dispersion of the powder (ideal for small and

cohesive powders) and the X-flow for measuring particles suspended within a liquid medium. For the primary particles used in this work, the most appropriate unit was the X-jet due to the small primary particle size being used and the cohesiveness experienced for the sugar particles.

Table 3-1. Primary particle size distribution (± standard deviation).

	Sucrose (µm)	Fructose (µm)
$D_{10,3}$	8.45 ± 0.07	12.25 ± 5.3
$D_{50,3}$	30.9 ± 1.98	35.25 ± 9.40
$D_{90,3}$	82.65 ± 7.70	63.4 ± 1.84

3.2.2 Interfacial Tension

Interfacial tension measurements were carried out using the pendant drop method with the FTA 125 machine at 25°C. At equilibrium, the shape of the droplet when suspended from a needle is a balance between the interfacial tension, and the external forces being exerted on the liquid. The droplet can be suspended in air or within a secondary immiscible liquid to create either a liquid/air or liquid/liquid interface. An example of this can be seen in Figure 3-2.

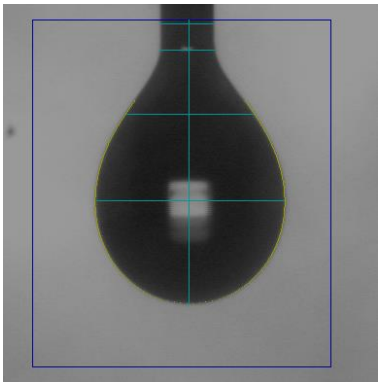

Figure 3-2. Example of interfacial tension measurement using pendant drop method (FTA 125).

Surface tension measurements of different secondary liquids which were used for experimental purposes were measured using a 20 gauge needle (outer diameter 0.9081 mm, inner diameter 0.603 mm).

3.2.3 Contact Angle

The contact angle for the different secondary liquids were measured on large sucrose crystals (Figure 3-3, diameter 1 to 2 mm), either in air or coated in sunflower oil using the FTA 125. A drop of the secondary liquid was deposited using a 26 gauge needle (outer diameter 0.4636 mm, inner diameter 0.159 mm) onto the sucrose surface and then the contact angle with time was measured, an example for which can be seen in Figure 3-4.

Figure 3-3. Large sucrose crystals used for contact angle measurements.

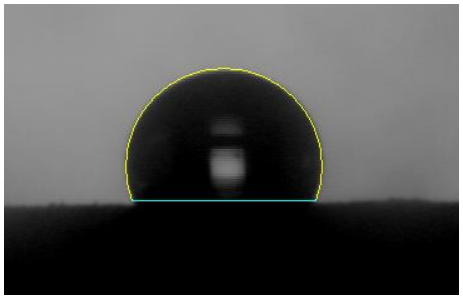

Figure 3-4. Example of contact angle measurement (FTA 125).

3.2.4 Rheological Properties

The rheological properties were conducted using a rotational rheometer (Kinexus Lab+, Malvern, UK). For liquid samples a cone & plate geometry (Figure 3-5) was used (1/50, with a 1° angle and 50 mm diameter). This ensures a constant shear rate application along the sample. For suspension samples a serrated parallel geometry (Figure 3-6) was used (diameter of upper and lower plate of 40 mm, 1 mm gap). The serrated plate geometry was used to prevent slippage of the sample, as the bulk solid can settle creating layer oil on the surface.

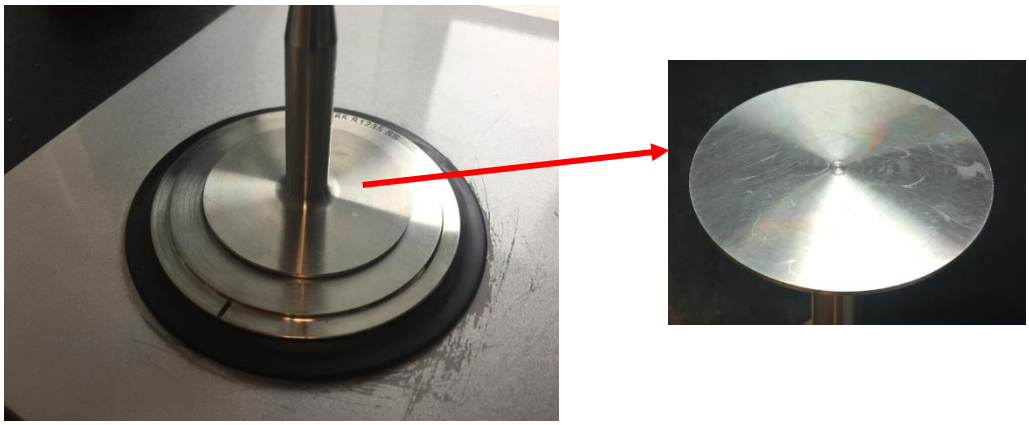

Figure 3-5. Geometry for cone and plate, with magnified image showing upper plate.

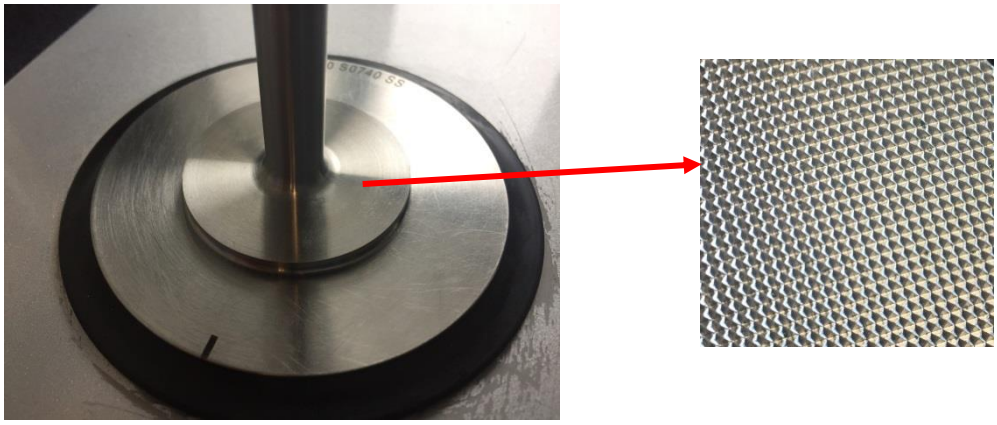

Figure 3-6. Geometry for serrated plate, with magnified image showing serration.

Measurements were conducted using a shear rate ramp between the range of 10 – 1000 s^{-1}, ensuring steady state had been reached at each step before proceeding to the next set shear rate. All experiments were conducted at room temperature of 25°C.

3.2.5 Tablet Production

Tablets of sucrose were produced using the Instron testing machine (Instron 3367,USA) for penetration tests. The tablet force used was 6250 N, mass of powder used was 5.0 g and die of diameter of 30 mm (die height 20 mm, punch speed 1 mm/min and 1 second dwell time). This ensured the production of tablets which were sufficiently strong to be handled for experimental purposes.

3.2.6 High Speed Camera

Penetration tests were conducted on sucrose tablets with and without oil to see the initial capillary suction. High speed camera (Photron, 100KC) images were taken (1000 frames per second), to capture the droplet penetration into the tablet. A fixed volume of liquid (water was dyed with erythrosine B, for ease of identification) was deposited onto the surface of the tablet and the penetration of the droplet was recorded. The experimental set-up can be seen in Figure 3-7.

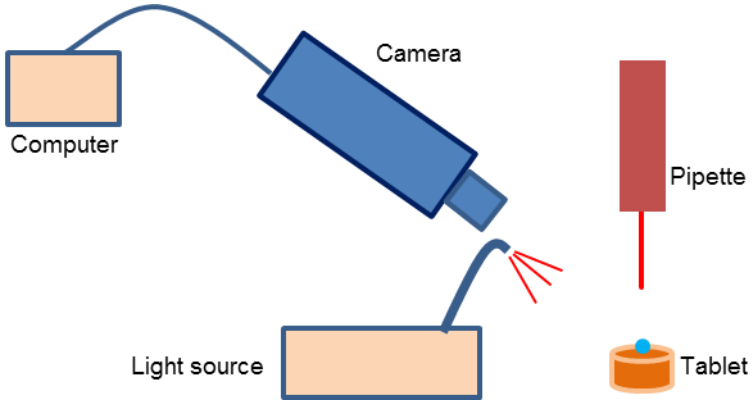

Figure 3-7. Schematic of setup for penetration test.

3.2.7 Water Activity

The water activity (a_w) of a sample, is defined as the partial vapour pressure of the sample/substance (p), divided by the standard state vapour pressure of pure water (p_0) (Reid, 2008):

$$a_w = \frac{p}{p_0}$$ Equation 3-1

Water activity measurements were conducted using the Rotronic Hygrolab (HW4, Switzerland). Its principle is based on measuring the relative humidity of the headspace above the sample, once the sample and headspace have reached equilibrium. It is an indirect method to measure the water activity of the sample.

3.2.8 Scanning Electron Microscopy (SEM)

Images were taken using scanning electron microscope (SEM) (JOEL, JSM-6010LA) to visually observe both primary particles, as well as, the mixture of water/sucrose droplet after removal from the sucrose and sunflower oil suspension.

Images were taken to visualise the surface topography of the sample after an initial gold coating which is needed for obtaining an image after applying a focused beam of electrons. Scans were conducted at a moderate energy level of 20 kV, which was found to be appropriate after trialling various energy levels for the samples being scanned.

3.2.9 Suspension Preparation

Suspensions of sucrose/fructose and sunflower oil were mixed by using an overhead stirrer (IKA, RW16, U.K.) with a marine impeller (A100, Lightnin UK) at 650 rpm for 10 minutes. The mass fractions of the solid and liquid phases were 50 % wt. for both. This was chosen based on the particle size of the sugars; ensuring sufficient sunflower oil is present to completely coat all particles, while minimising the effect of settling of the solid particles.

Once the suspensions were prepared, they were mixed manually with a glass rod for a further 30 seconds and then transferred into cellulose straws (9 or 5.75 mm diameter, Fishers Ideas UK) which were glued (to prevent leaking of sample) to a plastic chuck specifically designed for the X-ray CT experiments using a disposable pipette. A specifically prepared lid with a hole in the centre to fit the pipette tip was then placed on top, which ensured that the addition of the secondary liquid to the centre of the suspension. The secondary liquid was added to the surface of the suspension using an electronic pipette (Eppendorf Xplorer, UK), locating the tip of the pipette close to the surface of the suspension, though not actually touching the surface. A schematic of this can be seen in Figure 3-8. The distance between the surface of the suspension and the pipette tip was approximately 5 mm. Once the secondary liquid was added, another lid was placed which contained no hole, to prevent the evaporation of the secondary liquid, during the experiment.

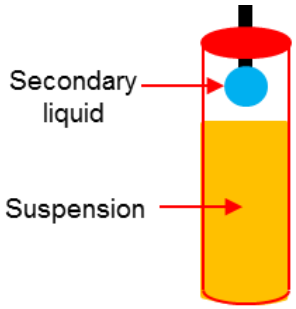

Figure 3-8. Schematic for delivery of secondary liquid to surface of suspension.

The amount of the secondary liquid added or the environmental conditions (Relative Humidity) the sample was exposed to varied throughout the experiments. The actual conditions will be given for each experiment when presented in the appropriate chapters. All experiments were conducted at 25ºC.

3.2.10 Experimental Set-up for Changing Humidity

A square box of 10 cm in length (1 cm thick acrylic plastic), with an air inlet feed and outlet exit was made to store the samples at specified conditions. The box was connected to a humidity generator (GenRH-A, London, UK) which fed humid air (at a set RH) at a flowrate of 0.5 L/min. A schematic set-up of this can be seen in Figure 3-9. The room temperature was set to 25°C. An external humidity probe was used to measure the humidity (Rotronic, HL-1D) within the box. The humidity reading within the box was approximately 1% lower than the air being fed into the box.

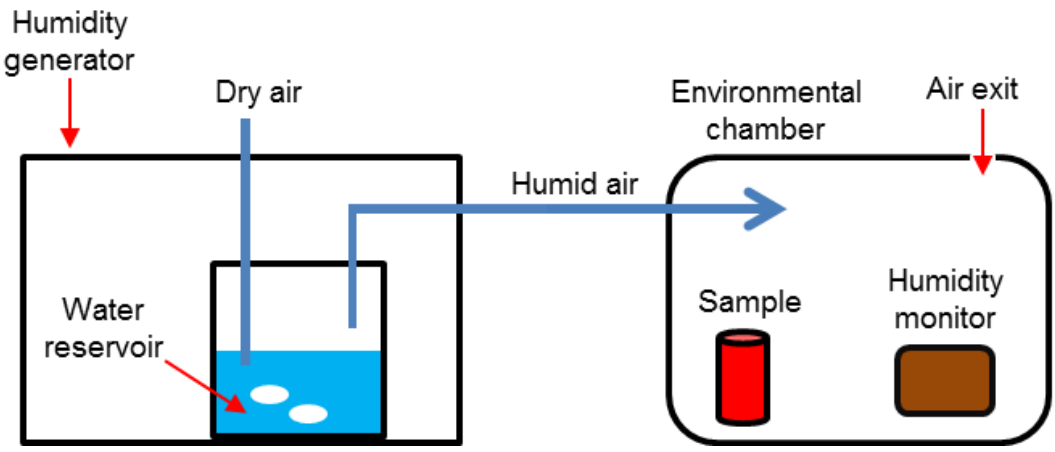

Figure 3-9. Schematic drawing for experimental setup for sample suspensions.

A photograph of the actual experimental set-up used to study the effect of humidity can be seen in Figure 3-10.

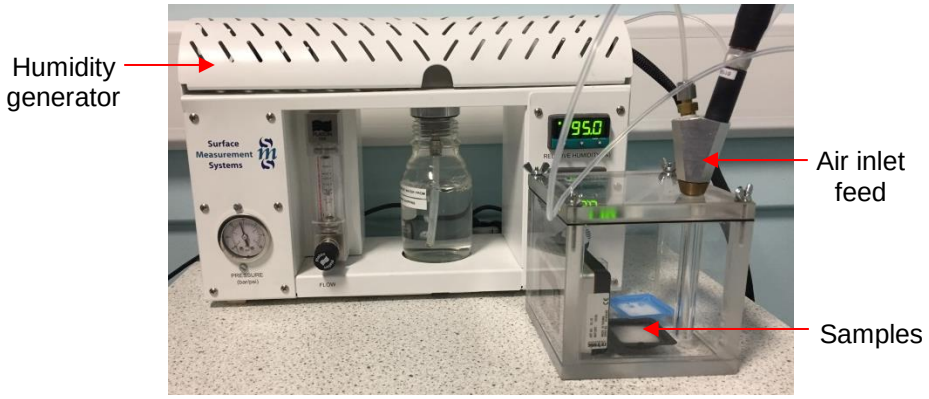

Figure 3-10. Experimental set-up used to study effect of humidity.

In addition to the set-up shown in Figure 3-10, some experiments were conducted on single layer suspensions and crystals of sugar. This was achieved using an inverted microscope with a bio-cell, connected to a controlled humidity air feed (Wetsys Humidity Generator, Setaram, France) with a flow rate of 50 mL/min. The set-up for this can be seen in Figure 3-11.

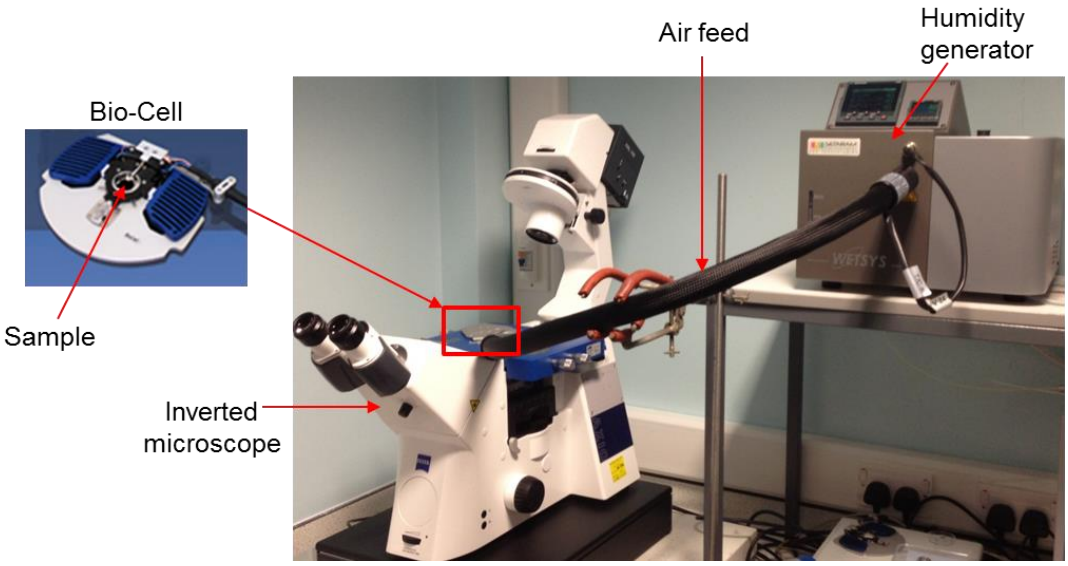

Figure 3-11. Set up for the inverted microscope, with controlled humidity air feed to the bio-cell.

In addition to this, some experiments were conducted in a climatic chamber (Binder KMF 240, Germany) for larger samples.

3.2.11 X-ray CT

Non-invasive methods, using X-ray computed tomography (X-ray CT), were employed to observe the migration of the secondary liquid in a suspension. The main advantage these have over conventional methods such as optical techniques is they offer a non-destructive approach and allow the internal structure to be seen to allow the tracking of the secondary liquid. Also, dynamic scans of the sample can be taken, to monitor the progress for a set period of time.

X-ray CT uses the different densities of material to allow a 3D structure of the sample to be constructed. This is achieved by placing a sample between an X-ray source and a detector. This sample is then rotated axially during which an X-ray beam is passed through the sample and a shadow received by the detector. The sample is rotated to obtain a series of 2D projection images, which are reconstructed using an back projection algorithm to obtain a 3D volume of the sample. Different material densities result in different absorption which correlates to different grey scale values seen in images taken by the detector.

3.2.11.1 Benchtop Systems

X-ray CT scans were performed on two different bench top systems. The X-ray CT machines used for scans were the Scanco µCT35 (Scanco, Switzerland) and SkyScan 1174 (Bruker microCT, Belgium) which can both be seen in Figure 3-12.

Initially the SkyScan 1174 system was loaned from the Engineering amd Physical Sciences Research Council (EPSRC) loan pool for 6 months. After successful trial scans proving the viability of employing this technique for the study being undertaken, the Scanco µCT35 was purchased within the group for further studies.

(a) Scanco µCT35 (b) Skyscan 1174

Figure 3-12. Benchtop X-ray CT systems used.

Initial trial scans were conducted on samples to find the optimum parameters in terms of voltage, current, exposure time and degree of rotations. The parameters chosen were changed to find a compromise between a relatively quick scans with sufficient resolution to capture the dynamics of the system taking place. This information was then used to engineer a plan for long term scans to investigate the dynamics taking place. Longer duration scans with higher resolution was possible, but due to the samples being scanned, this was not suitable as the dynamics taking place would be missed and the reconstructed image would not be clear due to too much sample movement. Ideally when scanning a sample using X-ray CT, the sample should remain completely stationary.

For the samples scanned using the SkyScan 1174, the spatial resolution of the scans was set to 11.4 µm. The system was operated at 50 keV, 800 µA with an exposure time of 1600 ms. Samples were rotated 180° in increments of 0.5° with one frame was taken at each step. The total scan time for each sample was approximately 10 mins. This ensured the scan duration was fast enough to capture the dynamics taking place and of sufficient quality to distinguish the different components within the sample.

All scans were reconstructed using the back projection algorithm provided with NRecon software (Bruker microCT, Kontich, Belgium). All reconstructed 3D datasets contained 1004 slices and a voxel size of 11.4 μm^3.

For the samples scanned using the Scanco µCT35, the spatial resolution of the scans was set to 12 µm. The system was operated at 45 keV, 177 µA 8W with an exposure time of 400 ms. Samples were rotated 360° with one frame taken at each step. The total scan time for each sample was approximately 20 minutes.

3.2.11.2 Synchrotron Facilities

Additional scans were conducted at the synchrotron facilities globally. Proposals were submitted using results from the benchtop systems. The synchrotron facilities used were the SYRMEP (Elettra, Italy, Trieste) and the Biomedical Imaging and Therapy (CLS, Canada, Saskatoon). Proposals were submitted for requesting beam time, and these were the successful applications.

For the samples scanned at the Elettra facility, the X-ray energy used was 17 keV. For each sample 900 projections were acquired with equiangular steps over a range of 180°, with a regular angular step of 0.2°. The projections were recorded with a 12 bit, water-cooled, Photonic Science XDI-VHR CCD camera, consisting of a full frame CCD imager. The camera has a 4008 × 2672 pixel chip. The effective pixel size of the detector is 4.5 µm. For the experiments, the pixel size was fixed to 9.0 µm, applying a 2 × 2 binning, thus yielding a field of view of 18 mm (horizontal) × 12 mm (vertical). The total scan time for each sample was 24 minutes.

For the samples scanned at the CLS facility, the X-ray energy used was 25 keV. For each sample 750 projections were acquired with equiangular steps over a range of 360°, with a regular angular step of 0.24°. The effective pixel size of the detector is 3.2 µm. For the experiments, the pixel size was fixed to 6.4 µm, applying a 2 × 2 binning. The total scan time for each sample was 12 minutes.

The main advantages of synchrotron facilities over conventional X-ray systems are the higher resolution images, greater contrast between different phases and quicker scan times offered. The reason for this is the parallel beam layout of the system along with the better quality camera system which enables quicker scans as explained earlier. Benchtop systems require longer acquisition times due to low X-ray flux, whereas synchrotron facilities offer high X-ray fluxes, therefore, the acquisition time is reduced dramatically.

3.2.11.3 Image Analysis

Reconstructed slices from the X-ray scans were processed using the software Image J. The images were converted to 16 bit images (grey range of 0-65535, where 0 is black and 65535 is white and in between are shades of grey), which were then analysed to track the change in grey value of the droplet with time from the sequence of scans. The slice chosen for the analysis corresponded to when the secondary liquid is largest in terms of diameter along the x-axis. A schematic for the axis being mentioned can be seen in Figure 3-13.

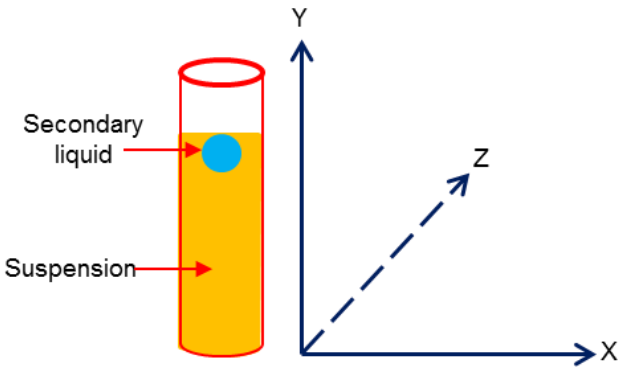

Figure 3-13. Schematic of axis in relation to sample and scans.

Images of the 3D visualization are presented which were obtained through a volume rendering procedure, which was achieved using the commercial software VGStudio MAX 2.0 (Volume Graphics, Germany). From the stack of the 2D slices, a raw 3D file was created in Image J, which could then be opened in the VGStudio MAX. This was then processed by adjusting the relevant greyscale threshold to highlight and isolate the region of interest.

Chapter 4 Early stages of secondary immiscible liquid movement

4.1 Introduction

Many food products are composed of suspensions of hydrophilic particles being suspended within a continuous fat phase. One of the issues with these products is the behaviour once exposed to a secondary immiscible liquid/vapour such as water and the effect of the moisture migration taking place (Ghosh et al., 2004).

Experiments were conducted to help elucidate the mechanisms taking place to better understand the behaviours observed from previous studies. Initial experiments involved observations optically to track the early stages of penetration of distilled water (as secondary immiscible liquid) on samples of:

1. Sunflower oil;
2. Dry sucrose tablet;
3. Sucrose tablet immersed in sunflower oil;
4. Suspension of sucrose and sunflower oil.

This was then followed up by using X-ray CT to track the movement into the suspension, to study the movement after the initial surface penetration.

4.2 Materials & Methods

Tablets of sucrose were produced to using the Instron machine using the methodology in Section 3.2.5.

Suspensions were prepared as mentioned in Section 3.2.9 for sucrose and sunflower oil suspensions. The mass fraction for both components of sucrose and sunflower oil was 50 % wt. The secondary immiscible liquid used was water of different volumes. The diameter of the sample holder used was 9 mm. The scan duration was approximately 10 minutes. All X-ray scans in this chapter were conducted of the benchtop SkyScan system mentioned in Section 3.2.11.1. An SEM image for the primary sucrose particles used can be seen in Figure 4-1, showing the irregular shape of the primary particles used.

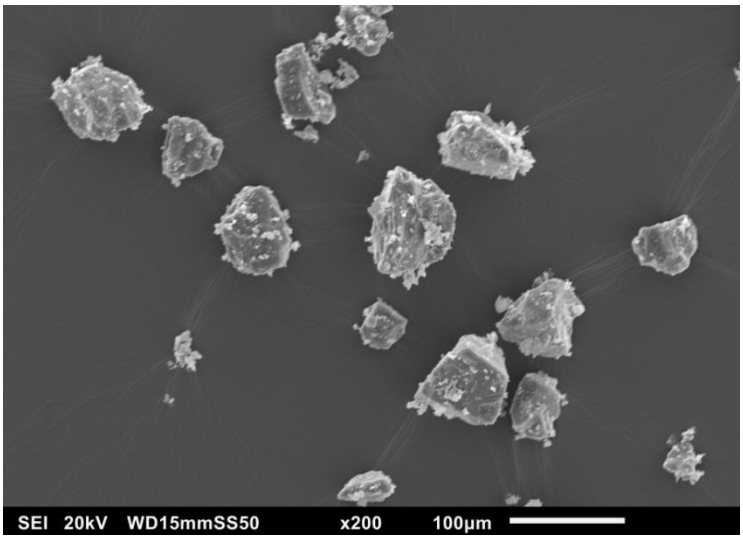

Figure 4-1. SEM image of primary sucrose particles.

4.3 Results & Discussions

4.3.1 Penetration Experiments

Penetration tests of water were conducted on different sample surfaces, to see how this affects the penetration rate. These include:

1. Sunflower oil;
2. Dry sucrose tablet;
3. Sucrose tablet immersed in sunflower oil;
4. Suspension of sucrose and sunflower oil.

The distilled water was coloured with red erythrosine B dye, for ease of identification during the experiments. A high speed camera (500 fps) was used for which the set-up was described in Section 3.2.6 (experimental set-up used can be seen in Figure 3-7).

4.3.1.1 Sunflower Oil

The starting image (after initial contact with the surface) and final image after complete penetration (breaking the surface tension and being fully immersed and covered by sunflower oil) of a 5 µl water droplet on sunflower oil can be seen in Figure 4-2. The surface penetration was achieved in approximately 0.014 seconds and it can be seen, the water droplet holds its spherical shape (due to camera

angle shape does not appear completely spherical) due to the hydrophilic/hydrophobic and immiscible nature of the water and oil.

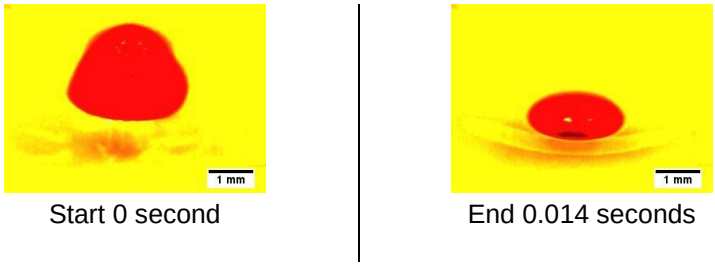

Figure 4-2. Water penetration of a 5 µl droplet on sunflower oil.

A schematic of the end being referred to in Figure 4-2 can be seen in Figure 4-3 for better understanding.

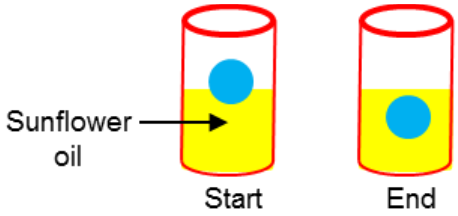

Figure 4-3. Schematic of water penetration from Figure 4-2.

4.3.1.2 Dry Sucrose Tablet

It was not possible to track the penetration of water onto a loose sucrose powder bed easily, due to the surface roughness. Therefore sucrose tablets were prepared to enable a smoother surface and conditions which could be replicated. The penetration of a 5 µl water droplet when deposited onto the sucrose tablet can be seen in Figure 4-4. The starting image, after the droplet came into complete contact with the surface of the tablet, is shown along with the end image, once the droplet is no longer visible on the surface and has fully penetrated.

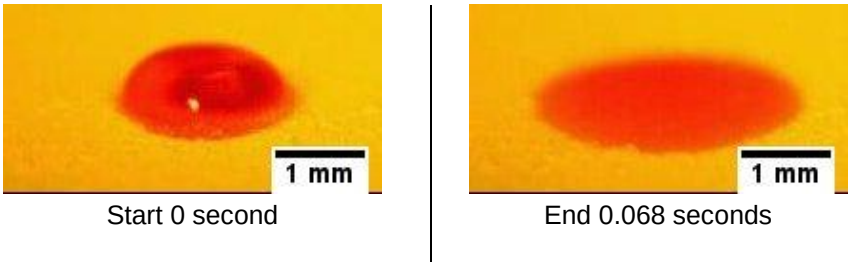

Figure 4-4. Water penetration of 5 µl droplet on a sucrose tablet.

An image was taken from above (along the Y-axis in Figure 3-13) after complete penetration of the 5 µl water droplet using a microscope (Keyence, VHX-2000), which can be seen in Figure 4-5. The original image can be seen in Figure 4-5a, while Figure 4-5b is after applying a filter to enhance the water location (enhancing contrast based on colour threshold). In Figure 4-5b, the complete point of contact upon impact can be seen, which had an approximate diameter of 5 mm. After complete penetration the diameter of contact increased to 7 mm due to axial spreading during penetration.

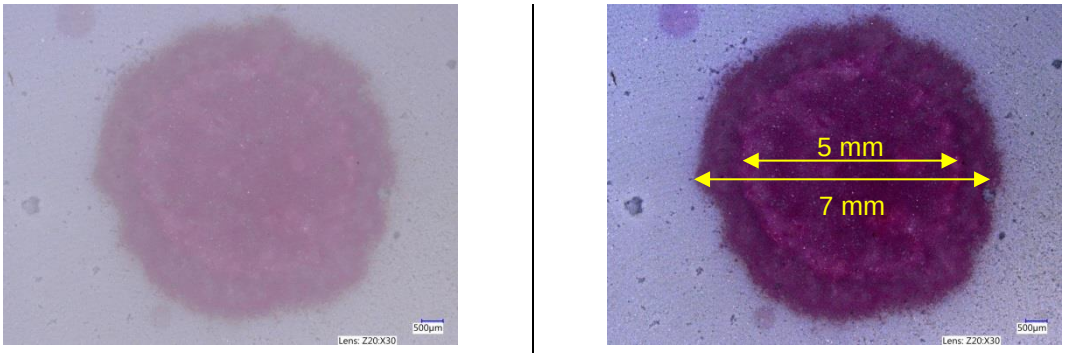

(a) Standard image (b) After applying filter

Figure 4-5. Image from above, showing region of contact for the 5 µl water droplet on a sucrose tablet. Scale on bottom right of the image is 500 µm.

4.3.1.3 Sucrose Tablet Immersed in Sunflower Oil

Similar experiments were conducted on sucrose tablets which were covered in sunflower oil and left for a few hours to allow the oil to fully penetrate the pores of the tablet. After this, the penetration of a 5 µl water droplet was observed for which images can be seen in Figure 4-6. The shape of the droplet on the tablet surface in Figure 4-4 at the beginning is similar to that seen in Figure 4-6 at the start after complete contact. After approximately 0.068 seconds which was the time required for complete penetration of the water droplet on the dry sucrose tablet, it can be seen for the tablet immersed in sunflower oil, a large portion of the water droplet remains on the surface.

For the dry sucrose tablet in Section 4.3.1.2, without the oil present, the water faces very little resistance from the air within the dry tablet and therefore can penetrate relatively quickly. When the tablet and the pores of the tablet are covered in oil, the water has to displace the oil to proceed into the tablet, and this is the

reason for the slower penetration time. It can be seen after 16 seconds in Figure 4-6, the droplet has not completely penetrated the tablet and there is some axial spreading occurring. This shows with the introduction of oil into the system, the time for capillary penetration of the droplet from the surface into the tablet is significantly increased.

It should be noted that during the experiment, the water droplet will not only penetrate the tablet, but will also dissolve some sucrose as it penetrates the sucrose tablet. This will in turn increase the volume of the water droplet due to the dissolution of sucrose and thus, change the viscosity and density of the droplet.

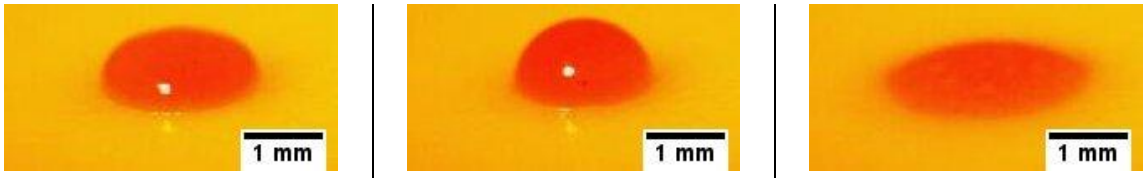

Start 0 second | After 0.068 seconds | After 16 seconds

Figure 4-6. Water penetration of 5 µl droplet into sucrose tablet covered with sunflower oil.

4.3.1.4 Suspension of Sucrose and Sunflower Oil

A similar penetration test was conducted on a suspension of sucrose and sunflower oil (50 % wt. for both) which can be seen in Figure 4-7. After the same 0.014 second period which was needed for complete surface penetration of the water droplet into a layer of sunflower oil as shown in Figure 4-2, it can be seen for the case of the sucrose and sunflower oil suspension, it has not yet completely penetrated. This is due to the resistance offered by sucrose, which needs to either be displaced or absorbed before the water droplet can penetrate in. After approximately 0.5 seconds, the water droplet did completely penetrate the surface of the suspension and is now surrounded by sunflower oil and sugar.

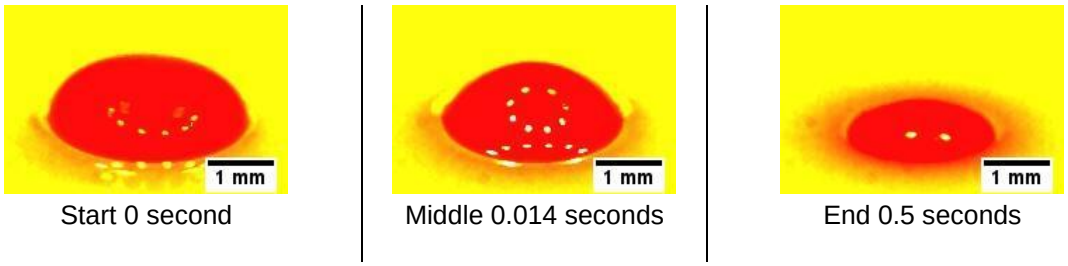

Figure 4-7. Water penetration of 5 µl droplet on of sucrose and sunflower oil suspension.

A schematic of the penetration being referred to in Figure 4-7 can be seen in Figure 4-8, highlighting the end after the complete immersion of the water droplet into the suspension.

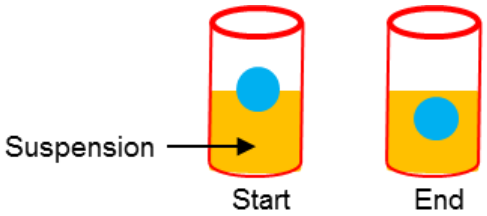

Figure 4-8. Schematic of water penetration from Figure 4-7.

Similar experiments were conducted for a larger volume of water (10 µl, double the volume of water) for all the four conditions used (sunflower oil only, dry sucrose tablet, sucrose tablet immersed in sunflower oil and a suspension of sucrose and sunflower oil). The time required for penetration was comparable to the 5 µl volume and similar trends were seen in terms of the sunflower oil alone being the quickest.

4.3.2 Benchtop X-ray CT

In Section 4.3.1, the surface penetration when water was added to the surface of sucrose was investigated. To take this one step further of how the droplet moves within a suspension, alternative methods were required as optically it is not possible to see the penetration within a suspension. After several attempts, it was found X-ray CT offered a suitable solution for this.

X-ray scans were conducted on suspensions of sucrose and oil (50 % wt. for both). Suspensions were transferred to the sample holder immediately after mixing. Scans were conducted every 30 minutes from 0 – 240 minutes (0 minute refers to when the first X-ray scan was taken, 9 scans in total on each sample). Some

further scans were taken after longer periods of storage to study long term dynamics. The secondary liquid was applied to the surface of the suspension using a pipette (drop height approximately 5 mm), after which a lid was used to cover the top of the sample and seal it from the surrounding environment. The time taken from adding the secondary liquid to beginning the X-ray scans was approximately 40 seconds.

Image slices from the scans were processed using the software Image J, to analyse the scans and calculate the penetration distance of the secondary liquid and the change in dimensions of the secondary liquid with time, which corresponds to the spreading of the secondary liquid. The image slice chosen from the stack of images is when the secondary liquid is largest in terms of diameter along the X-axis in relation to Figure 3-13.

The effect of changing the volume of secondary liquid applied to the surface of suspension was investigated. In total 4 different volumes of secondary liquid were used which were 5 µl, 15 µl, 20 µl and 25 µl. A time lapse of images for the 5 µl, 15 µl, 20 µl and 25 µl water droplets can be seen in Figure 4-9, Figure 4-10, Figure 4-11 and Figure 4-12 respectively. It can be seen when comparing the first image from the first scan for all the volumes, the secondary liquid droplet is progressively getting larger, which is expected, as a greater volume of secondary liquid is being used.

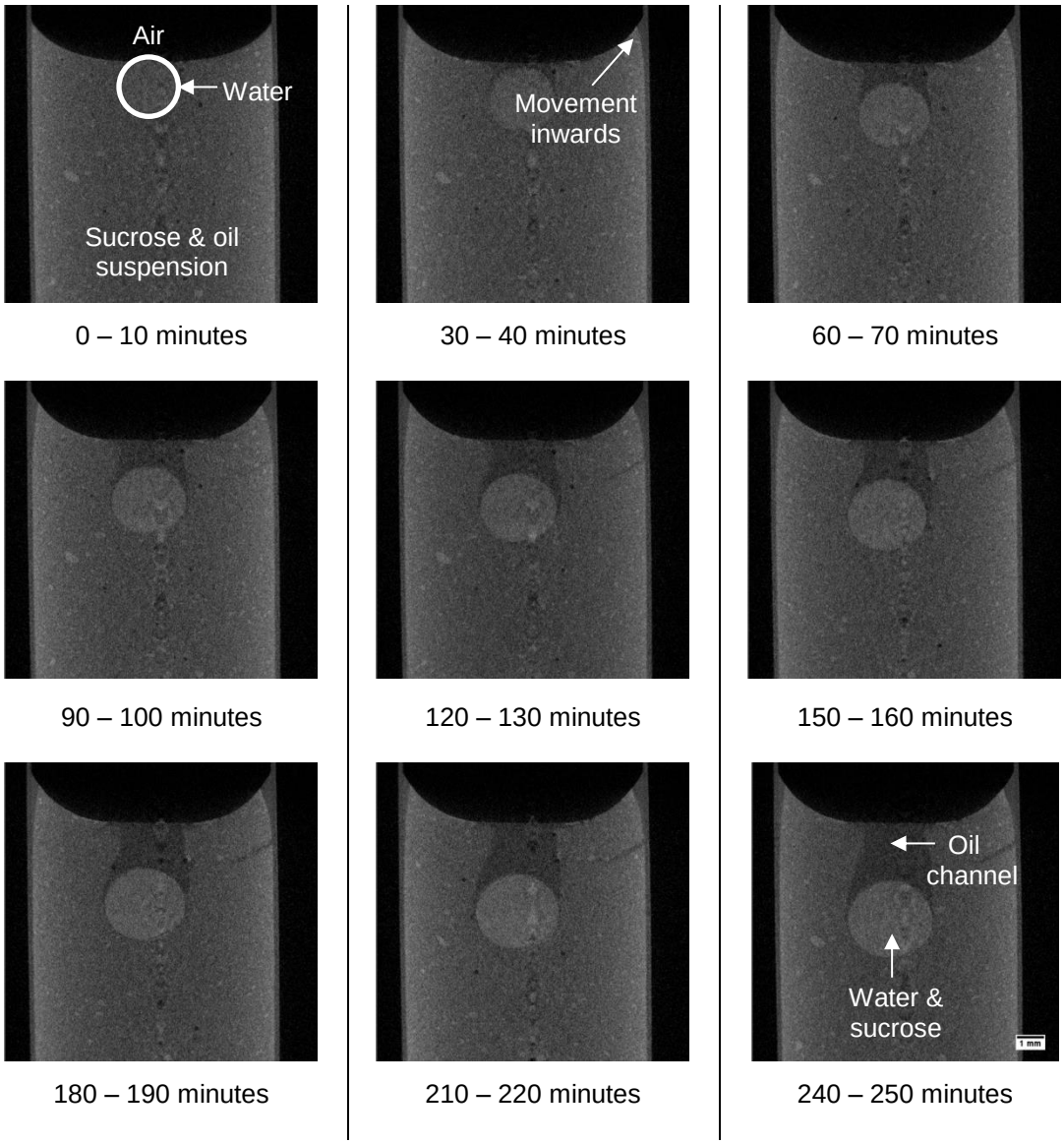

Figure 4-9. Time lapse of images for suspension to which 5 µl water was added. Scale on 240 - 250 minutes image is 1 mm.

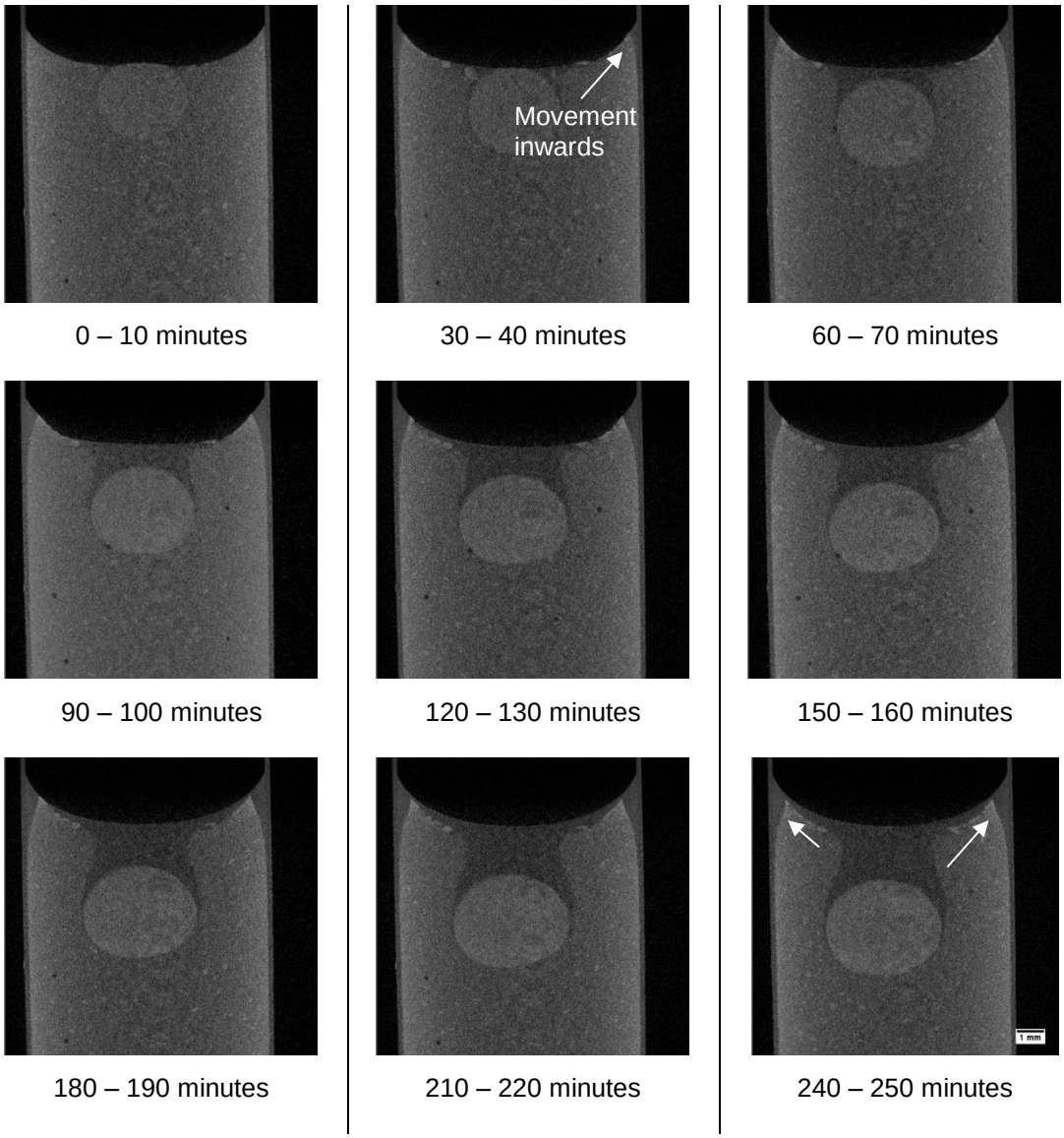

Figure 4-10. Time lapse of images for suspension to which 15 µl water was added. Scale on 240 - 250 minutes image is 1 mm.

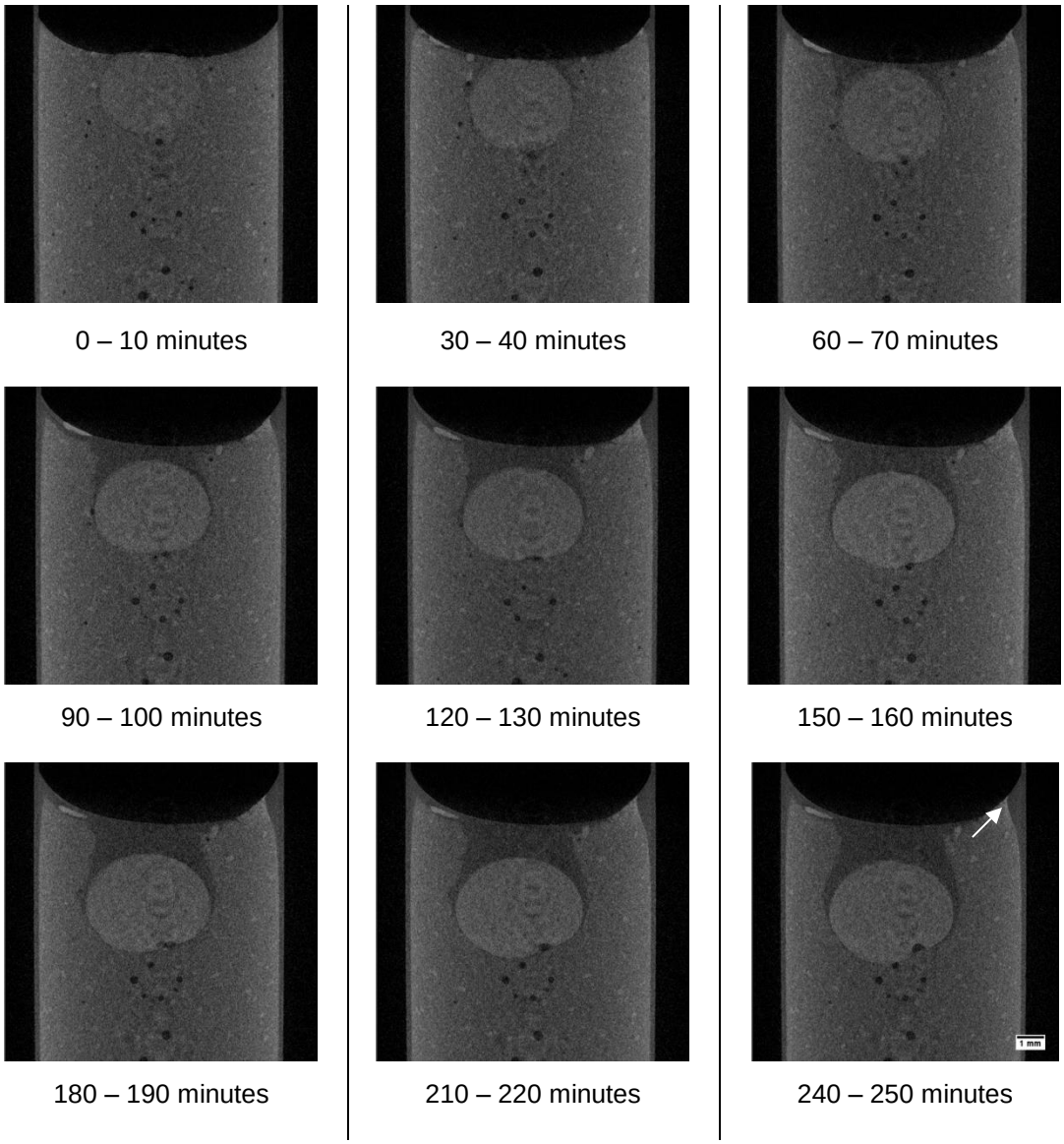

Figure 4-11. Time lapse of images for suspension to which 20 µl water was added. Scale on 240 - 250 minutes image is 1 mm.

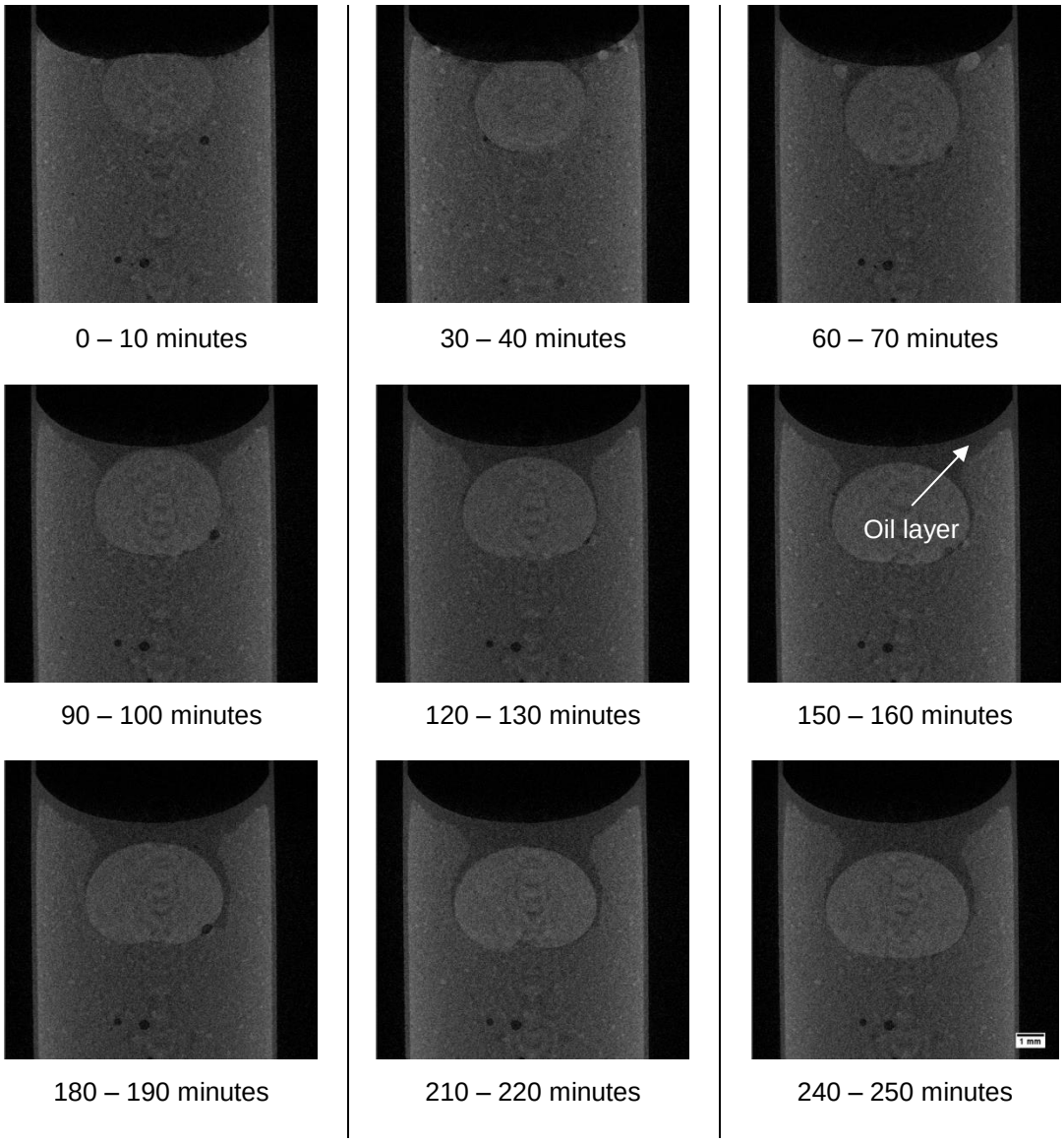

Figure 4-12. Time lapse of images for suspension to which 25 µl water was added. Scale on 240 - 250 minutes image is 1 mm.

The black region above the suspension is air, as has been shown in the image at 0 - 10 minutes in Figure 4-9. The clear progression of the secondary liquid droplets (5 - 25 µl water) into the suspension can be seen in the time lapse of images in Figure 4-9 - Figure 4-12. For the first two images shown in Figure 4-9 - Figure 4-12 (0 - 10 and 30 - 40 minutes) there is very little movement of the secondary liquid. After 60 minutes, some clear movement of the secondary liquid can be seen, which increases as we progress through the time lapse of images. Also, as we progress through the images we can see the size of the droplet is increasing, indicating the movement of sucrose from the bulk suspension into the water droplet. Also, there

is clear change in the shape of the droplet from a spherical body, to a more ellipsoidal shape (with a larger horizontal dimension in comparison to the vertical dimension) with time as can be seen in Figure 4-9 - Figure 4-12. This shows that benchtop X-ray CT can successfully track the macroscale movement of the water droplet into the suspension.

As the water droplet progresses into the suspension, a clear trail can be seen showing the path taken by the droplet. This has been highlighted in the scan taken at 240 - 250 minutes in Figure 4-9. This path left behind is thought to be sunflower oil, as the sucrose which was previously present here, has been taken along with the water droplet as it progresses, leaving only the sunflower oil behind as the oil and water are immiscible with one another. A reference scan of only sunflower oil was conducted and the greyscale value of this was compared to that of the oil channel within Figure 4-9. The mean grey value of sunflower oil from both scans was similar (39.8 for the reference scan, 40.8 from Figure 4-9) indicating a similar composition as the other components within the image had a very different grey value (sucrose and water from reference scans).

It also evident in Figure 4-9 - Figure 4-12 that there is some movement from the top right and left, highlighted in the scan after 30 - 40 minutes in Figure 4-9, which is believed to be due to the water droplet as it progresses into the suspension. This movement continues and is present in all subsequent images in Figure 4-9. The proposed movement of the water droplet into the suspension and sucrose from the bulk suspension can be schematically seen in Figure 4-13. After the water droplet is added, it begins to move into the suspension. During its movement into the suspension, it will take up sucrose from the bulk suspension which moves into the water droplet. In addition to this, there is some movement from the top side (the purple arrows on the left and right of Figure 4-13) for the sucrose particles, which move inwards towards the bulk suspension.

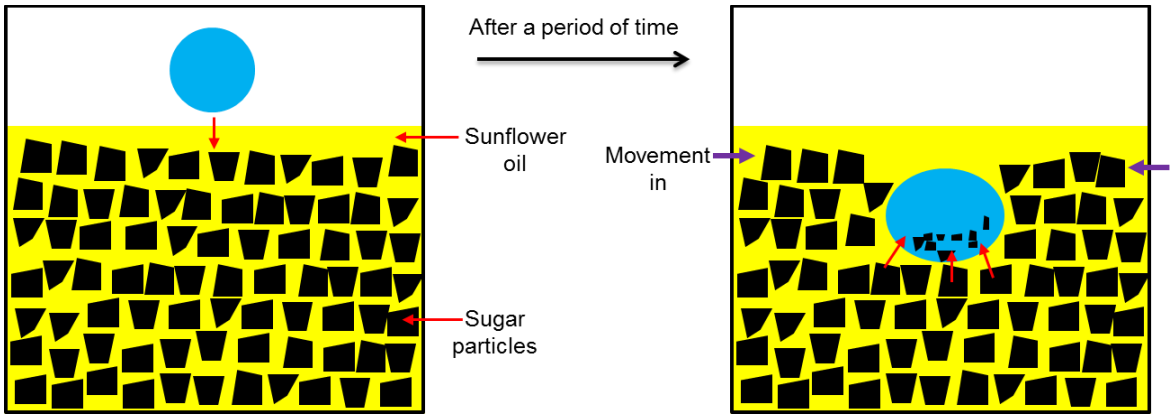

Figure 4-13. Schematic movement of water in suspension.

A similar trend can be seen for the images in Figure 4-10 for 15 µl water as that mentioned for 5 µl water in Figure 4-9. The trend of penetration into the suspension and increase in dimensions of the droplet is the same. One difference which is evident is that there is more of a pull from the top left and right of the suspension of the sucrose, leaving behind just sunflower oil which has been highlighted in Figure 4-10 and as schematically shown in Figure 4-13. The pull from the top left and right is stronger and more evident, as the initial volume of water added is increased as can be seen in the images in Figure 4-9 - Figure 4-12. Also the distance the droplet travels into the suspension is reduced as the volume of the initial water droplet is increased.

4.3.3 Secondary Liquid Droplet Dimensions

The changes in dimensions of the different secondary liquid droplet volume with time from the images from the scans in Section 4.3.2 for the horizontal and vertical diameters were measured. An example of the measured region can be seen in Figure 4-14. The distance measured was for the longest length in both the horizontal and vertical dimension.

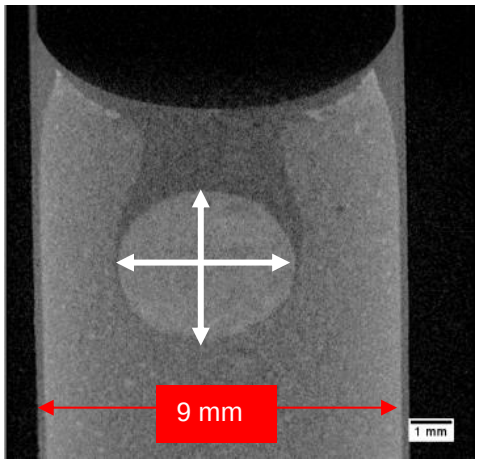

Figure 4-14. Example for measurement of dimensions of secondary liquid.

The measured horizontal and vertical dimensions can be seen in Figure 4-15 and Figure 4-16 respectively. For a sphere with the volumes used (5 – 25 µl), the projected diameters can be seen in Table 4-1, which are similar to the points seen at time 0 in Figure 4-15 and Figure 4-16 for the horizontal and vertical diameters. It can be seen that the droplet is not perfectly spherical as the horizontal and vertical diameters are different, and the difference between the two increases with time and progresses towards a more ellipsoidal shape.

The horizontal diameters for both volumes showed the same trend of increasing indicating axial spreading. For the vertical diameters the same trend of increase is seen, though the vertical diameters is always smaller in comparison to the horizontal diameters as can be seen when comparing Figure 4-15 and Figure 4-16.

Table 4-1. Projected diameters of droplets based on volume of a sphere.

Volume of droplet (µl)	Projected diameter (mm)
5	2.12
15	3.06
20	3.36
25	3.62

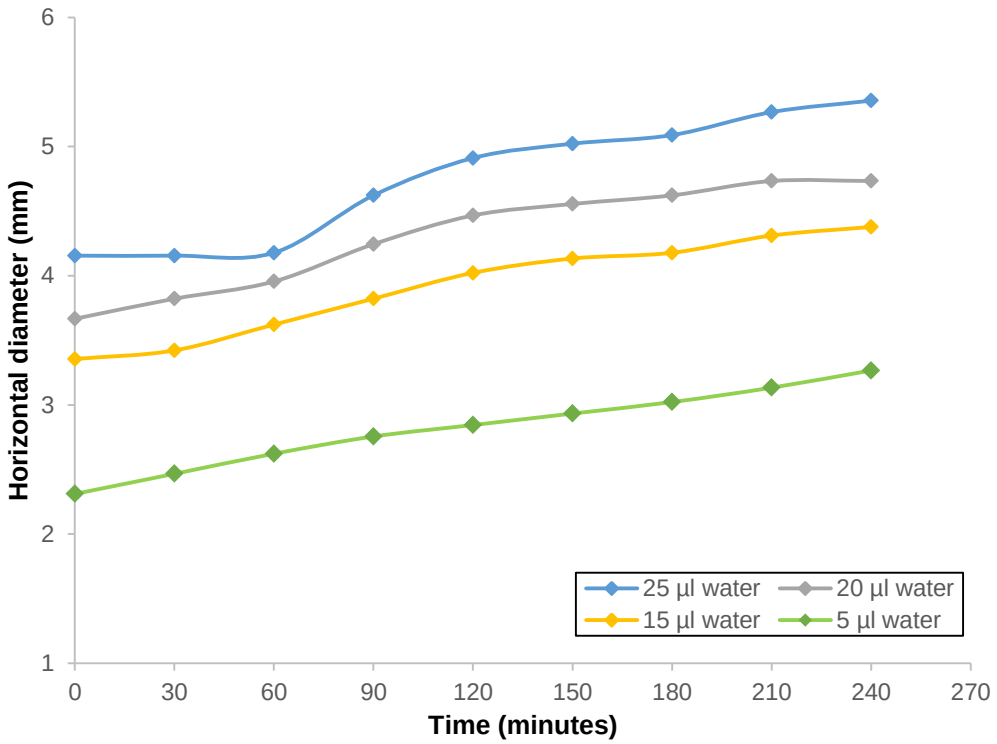

Figure 4-15. Graph of the change in the horizontal diameter for the secondary liquid droplet within the suspension against time (5 µl, 15 µl, 20 µl and 25 µl water droplets).

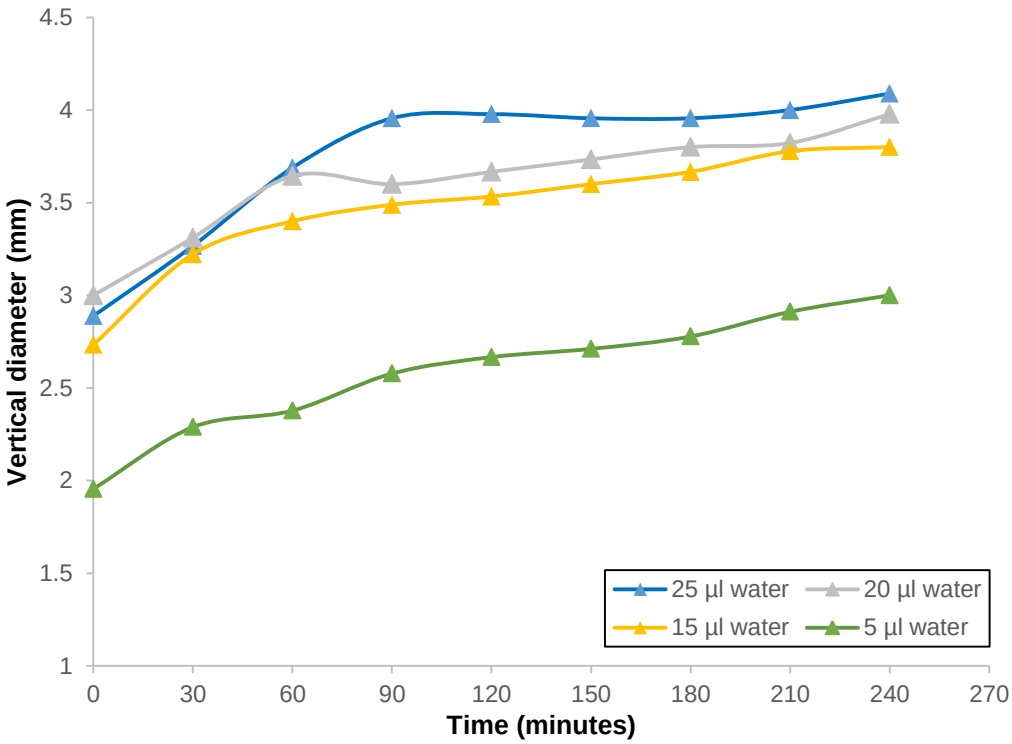

Figure 4-16. Graph of the change in the vertical diameter for the secondary liquid droplet within the suspension against time (5 µl, 15 µl, 20 µl and 25 µl water droplets).

4.3.4 Penetration Distance

The images shown in Section 4.3.2 were used to calculate the penetration distance (from the top of the suspension surface to the top of the droplet) of the various volumes of water droplet into the suspension with time. An example for the distance measured can be seen in Figure 4-17.

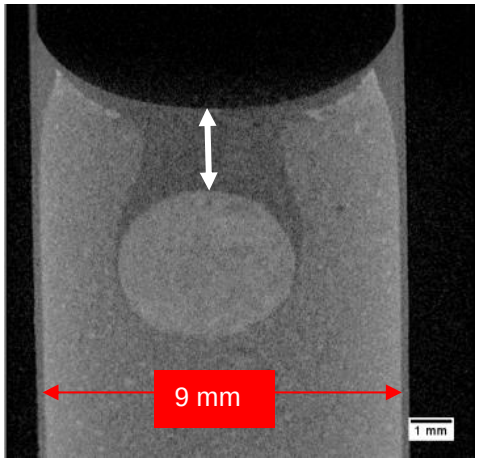

Figure 4-17. Example of penetration distance measured from top of suspension to the top of droplet.

Again, the slice chosen for this was that for which the diameter of the secondary liquid is greatest. The penetration distance with time can be seen in Figure 4-18. It can be seen that the penetration distance with time is quicker for the smaller volume water droplets for the time period studied. For the scan conducted after 30 minutes from addition, there is very little difference between the varying volumes. Once 60 minutes has passed, it can be seen that the 5 µl water droplet has travelled the furthest, followed by the 15 µl water droplet. Up until 90 minutes, the 25 µl water droplet still remains in contact with the surface of the suspension.

When looking at the images from Section 4.3.2 for all the volumes between 0-10 minutes, it can be seen that the water droplet is already completely immersed within the suspension and therefore the capillary action has already taken place. The penetration shown for when a droplet of water is applied to sucrose tablets in Section 4.3.1 has already occurred, though in this system the sucrose is not compressed into a tablet. The movement of the droplet into the suspension is continuing for the droplet, indicating other mechanisms are driving the droplet such as gravity and diffusion.

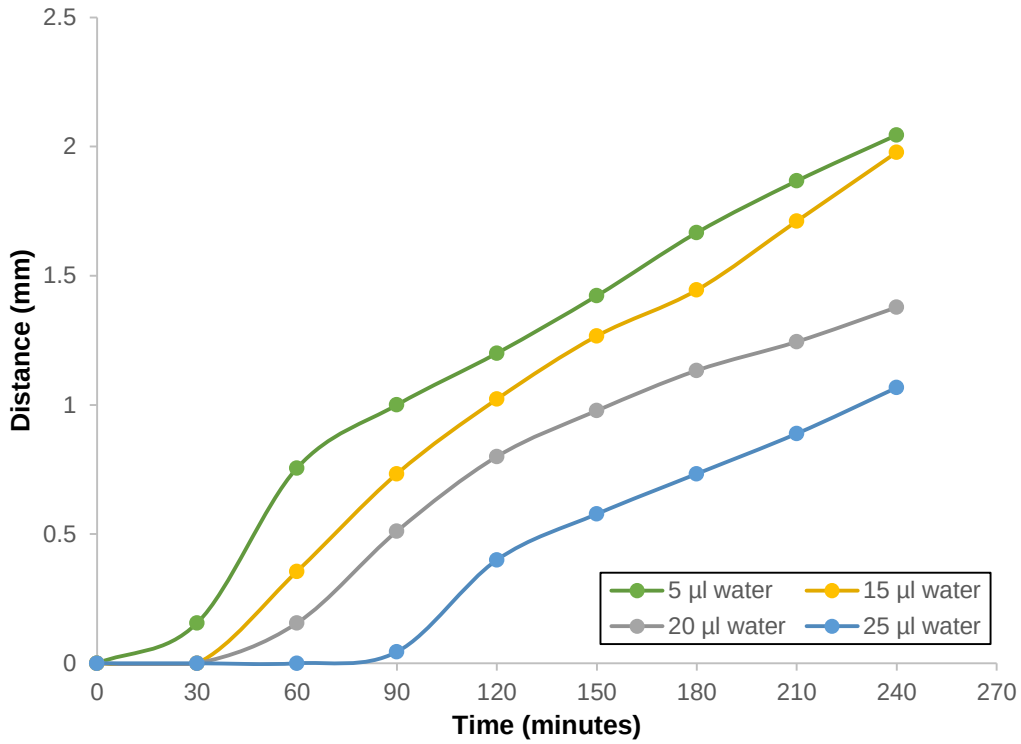

Figure 4-18. Graph of distance penetrated by secondary liquid into suspension plotted against time (5 µl, 15 µl, 20 µl and 25 µl water droplets).

4.3.5 Velocity Profile for Secondary Liquid

The data from Figure 4-18 was used to plot the velocity of the droplet, which can be seen in Figure 4-19. It can be seen for the 4 hour period, in which the X-ray scans were conducted, the velocities of the 5 µl water droplet initially increases for the first 60 minutes, indicating a period of acceleration, followed by a period of deceleration after this. The 15 µl water droplet shows a similar but slower acceleration for the first 90 minutes, followed by a steady state period, after 90 minutes. The reason for this is believed to be due to the surface area to volume ratio of the smaller droplet (5 µl water), which is larger in comparison to the bigger volume droplet (15 µl water) enabling the droplet to penetrate quicker. However, the smaller droplet (5 µl water) has a lower capacity in its ability to take up sucrose in relation to its initial volume, thus will not be able to travel as quickly or as far in comparison to the larger volumes. For the largest volume used (25 µl water), there was no acceleration for the first 90 minutes, followed by a period of acceleration between 90 - 150 minutes, then after 150 minutes showing it has reached a steady state up until 240 minutes. It is believed if further scans had been conducted, this

period of steady state would have continue for a much longer period after the smaller volumes had come to a stop, due to the ability and capacity of the 25 µl water droplet to take up sucrose from the bulk suspension.

For droplets in the range of 5 µl to 25 µl water deposited onto a sample of sunflower oil only, the larger volume water will travel quickest. However, for the case of a suspension of sucrose and sunflower oil, this is not the case. The reason for this is believed to be due to the presence of sucrose and the surface area of contact available between the sucrose and the water droplet. As the water droplet is progressing through the suspension, it can only continue to progress into the suspension by displacing or taking up the sucrose within its path. Thus, the smaller volume droplet, which in this case is the 5 µl droplet, had a higher settling velocity in comparison to the larger volume water droplets.

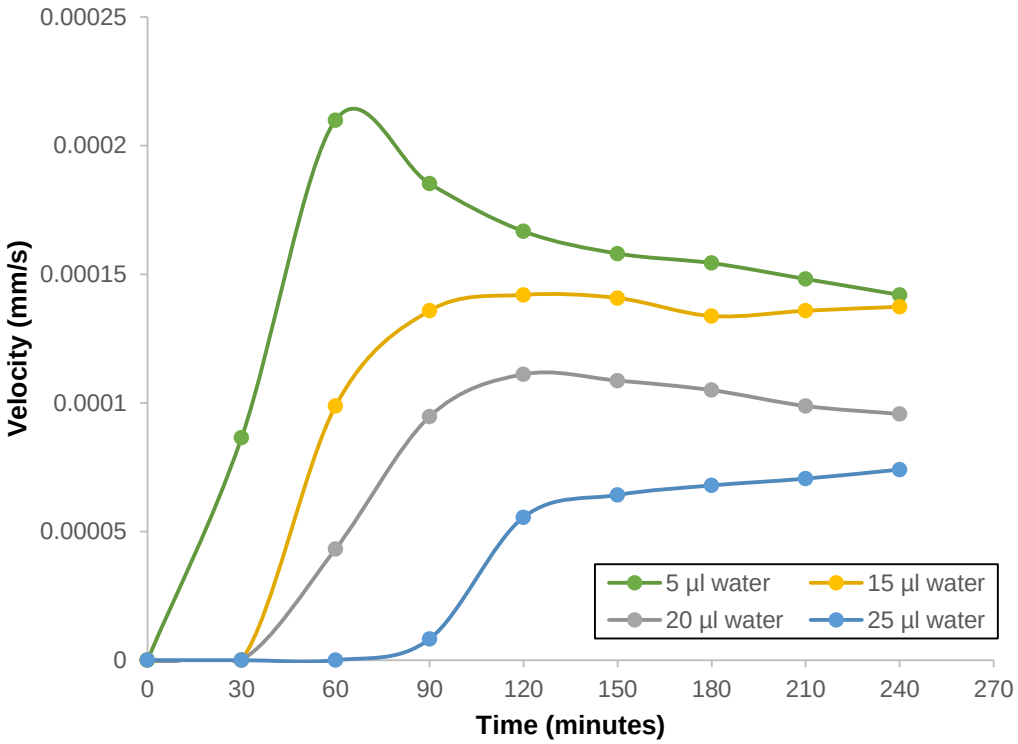

Figure 4-19. Graph of velocity of secondary liquid into suspension plotted against time (5 µl, 15 µl, 20 µl and 25 µl water droplets).

Figure 4-19 would indicate that the droplets do begin to reach a settling velocity for the time period studied. The reason for this has been ascribed to the droplets ability to take up sucrose from the surrounding suspension, which directly

influences the rate at which it progresses into the suspension. In the first 4 hour period monitored, the water droplets are able to continuously take up sucrose, as it has not been saturated yet. Though after a period of time, the droplet becomes saturated and will no longer be able to absorb any further sucrose and therefore not be able to proceed further into the suspension.

Scans were conducted on a sample to which a 5 µl water droplet was added after 24 hours and 52 hours from addition, which can be seen in Figure 4-20. The shape of the secondary liquid has changed significantly from the initial spherical shape, and the dimensions have changed from the initial scan at time 0 indicating significant spreading. The top surface of the secondary droplet has transformed into a flat surface, resembling a semi-circle shape. The flat top shows the secondary droplet as it progressed into its present location, was composed of liquid. This is evident from the flat top, as if it was a solid body, it would not deform into this shape.

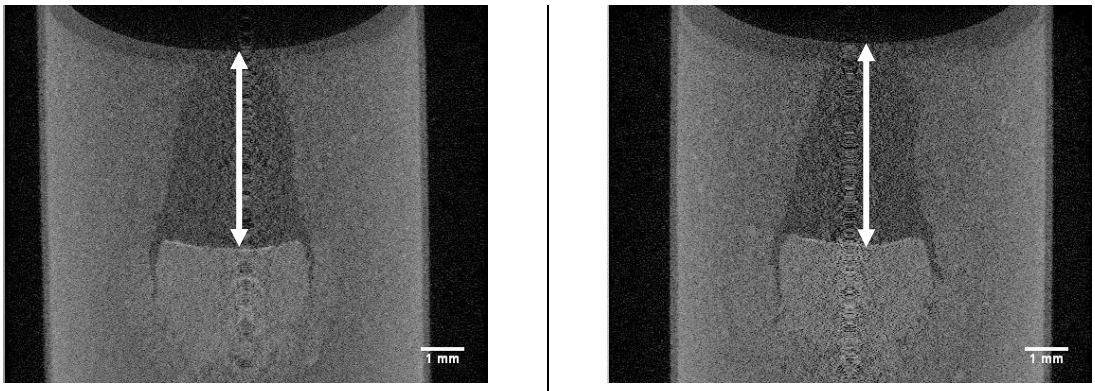

After 24 hours | After 52 hours

Figure 4-20. Long term scans conducted on 5 µl water droplet sample.

Also, the route taken by the secondary liquid to its position after 24 hours can clearly be seen, when looking at the region above the secondary liquid within Figure 4-20. The sucrose particles have settled, creating a small oil layer surface which can be seen in Figure 4-20. This is expected as the sucrose is denser in comparison to the oil, and therefore will naturally settle with time. Also, a clear path the secondary liquid droplet has taken can be seen to its present location within the figure. The path has remained, with the sucrose on both sides remaining and not

collapsing inwards. Similar long term scans were conducted on different volume water droplets, which showed comparable behaviour.

The distance from the surface of the suspension to the top of the droplet in Figure 4-20 measures 4.52 mm, showing the droplet continued to progress even after the 4 hour period shown for the images in Figure 4-9. However, between the images shown in Figure 4-20, there is a time difference of 28 hours. In this 28 hour period the droplet moved from 4.52 mm to 4.54 mm (0.02 mm), showing that although the droplet is still continuing to move, the velocity has retarded dramatically compared to the earlier velocities shown in Figure 4-19. This would indicate that the absorption kinetics between the sucrose particles and the water directly influence the velocity of the droplet. If a water droplet was deposited in a similar homogenous system with a fluid of similar viscosity and density, it would be expected that the water droplet would continue to progress once it had reached its terminal velocity, to the bottom of the sample, which was not the case for the system being studied here. Therefore, other forces must be playing a part as well as the absorption of sucrose into the water droplet.

The sucrose/water mixture from Figure 4-20 after 52 hours was removed and it was found to be solid in composition. This was cleaned with hexane to remove any oil residue, leaving behind only the sucrose/water skeleton network (Killian and Coupland, 2012). This was then scanned under the SEM for which an image can be seen in Figure 4-21. The presence of large sucrose crystals can be seen. A magnified image of this can be seen in Figure 4-22, where it can be seen that the presence of sucrose crystals which are bound with solid bridges. It is believed these bridges formed as water came into contact and dissolved some sucrose, then recrystallized.

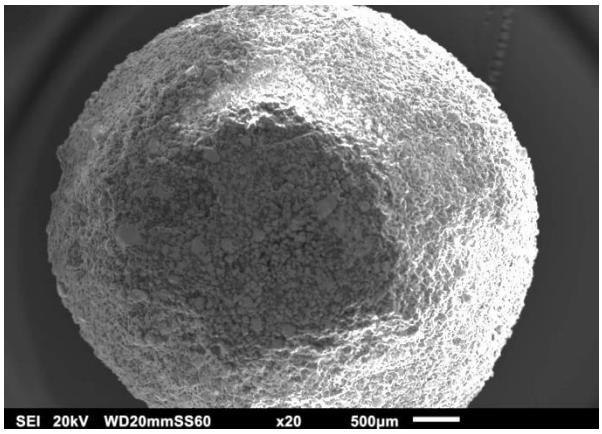

Figure 4-21. SEM image of sucrose/water mixture after removal of oil by hexane.

This agrees with the work carried out by Killian and Coupland (2012) who used model suspensions of soybean oil and sucrose with water addition. The samples with water were able to resist structural changes due to elevated temperature (maintaining shape and structure), due to the matrix network formation of the sucrose and water in comparison to samples without water incorporated. This was ascribed to the liquid bridge formation, which then form a solid structure when water is removed, due to recrystallization resulting from supersaturation, similar to that seen in Figure 4-22.

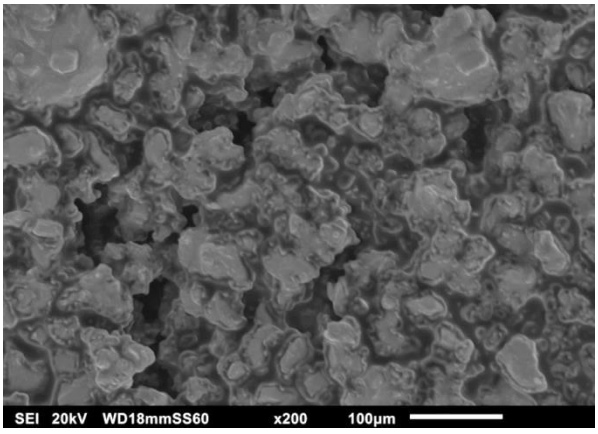

Figure 4-22. Magnified image from central region of Figure 4-21.

As well as this, the review carried out by Stortz and Marangoni (2011) highlighted the significance of water incorporated either directly or indirectly into chocolates to create a heat resistant chocolate. The strength due to the sugar network formed with water present, was one of the main methods exploited in achieving a heat

resistant chocolate. This allowed the product to be able to withstand temperatures experienced nearer the equator.

It should be noted that the suspension composition of 50 % wt. for both the sucrose and sunflower oil was chosen based on the size of the particles, to have sufficient oil to coat all of the particles with the continuous phase and minimise settling and thus a layer of oil on the surface. Should the mass fraction of sucrose be changed to a lower value, it may well be the case that the velocity of the larger droplet would be quicker as now the surface area to volume ratio of contact between the sucrose from the suspension and the water droplet is no longer significant in determining the settling velocity.

4.3.6 Mass Transfer of Sucrose

The change in volume of the different volume water droplets used (5 - 25 µl) with time can be seen in Figure 4-23. As expected the larger volume droplets always remain greater in volume in comparison to the smaller volume droplets.

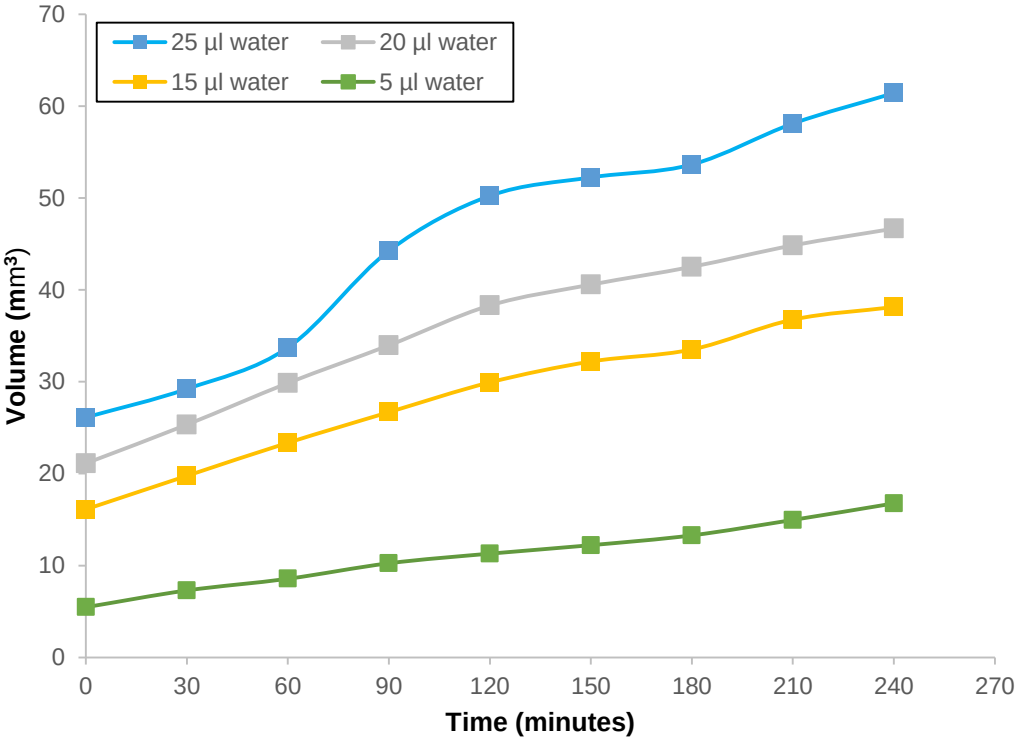

Figure 4-23. Change in volume of secondary liquid droplet within the suspension against time (5 µl, 15 µl, 20 µl and 25 µl water droplets).

Assuming that the increase in volume seen in Figure 4-23, is due solely to the mass transport of sucrose from the bulk suspension into the water droplet, and that there is no diffusion of oil into the droplet or water away from the droplet, it is possible to calculate the change in sucrose concentration within the water droplet over time. For a given volume of water to reach saturation with sucrose would result in a 126% increase in volume (based on 67 % wt. to reach saturation of sucrose) at 25°C (Bucke, 1995). From Figure 4-23, it can be seen the time required for the 5 µl droplet to increase by 126% is approximately 150 minutes (initial volume of 5 mm^3, increase of 6.3 mm^3), whereas, for the 25 µl droplet the same is achieved in approximately 210 minutes (initial volume of 25 mm^3, increase of 31.5 mm^3), requiring an additional 60 minutes to achieve the same increase in volume, thereby, indicating that the larger volume water droplet is taking up sucrose at a slower rate in comparison to the smaller volume water droplet.

The true density of sucrose is 1588 kg/m^3 and at 25°C one can dissolve 2.07 grams of sucrose per gram of water to produce a saturated solution which equates to a 67 % wt. concentration (Bucke, 1995). Using the information that the volume of water is conserved, it is possible to track the increase in the volume of the water droplet as sucrose enters, and correlate this back to the sucrose concentration (by knowing the density) within the droplet with time. This is shown schematically in Figure 4-24. At time 0, before the addition of the water droplet, the volume of the water Vw_1, volume of sunflower oil Vs_1 and the volume of sucrose Vs_1 are known. Then after a period of time, as the water droplet progresses into the suspension, the water droplet volume increases to Vw_2, due to the movement of sucrose from the bulk suspension into the water droplet. The total amount of sucrose within the system is still the same, however, the amount of sucrose within the surrounding bulk suspension Vs_2 is now less than Vs_1 as some has moved into the water droplet. The sunflower oil volume Vo_2 is the same as Vo_1, the location of the oil does not change.

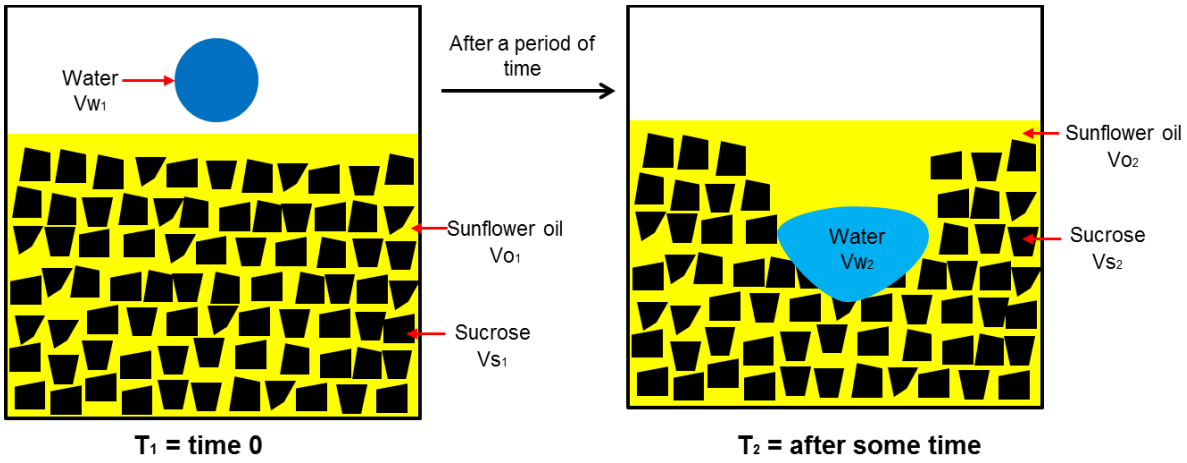

Figure 4-24. Schematic of tracking the change in volume of the water droplet within the system with time.

Now just focusing on the water from Figure 4-24, this can be seen in Figure 4-25. Thus, by tracking the increase in volume of the water droplet with time as sucrose enters, the sucrose concentration of the water droplet with time can be calculated through the density of sucrose which can be seen in Figure 4-26.

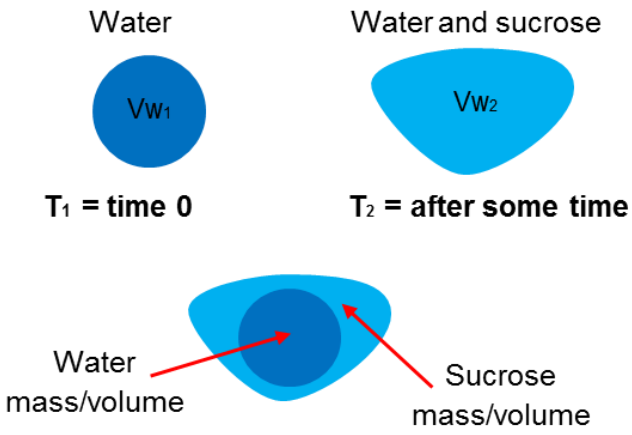

Figure 4-25. Schematic focusing on the change in volume of the water from Figure 4-24.

It can be seen that the sucrose concentration of the droplet goes above the saturation limit of 67 % wt. at 25°C (red dashed line in Figure 4-26), indicating that the droplet must contain both dissolved sucrose and solid sucrose. Also, as the secondary liquid droplet progresses into the suspension, the viscosity and density will change as sucrose dissolves into the droplet, which needs to be considered for the dynamics taking place. This will be explored further in subsequent chapters.

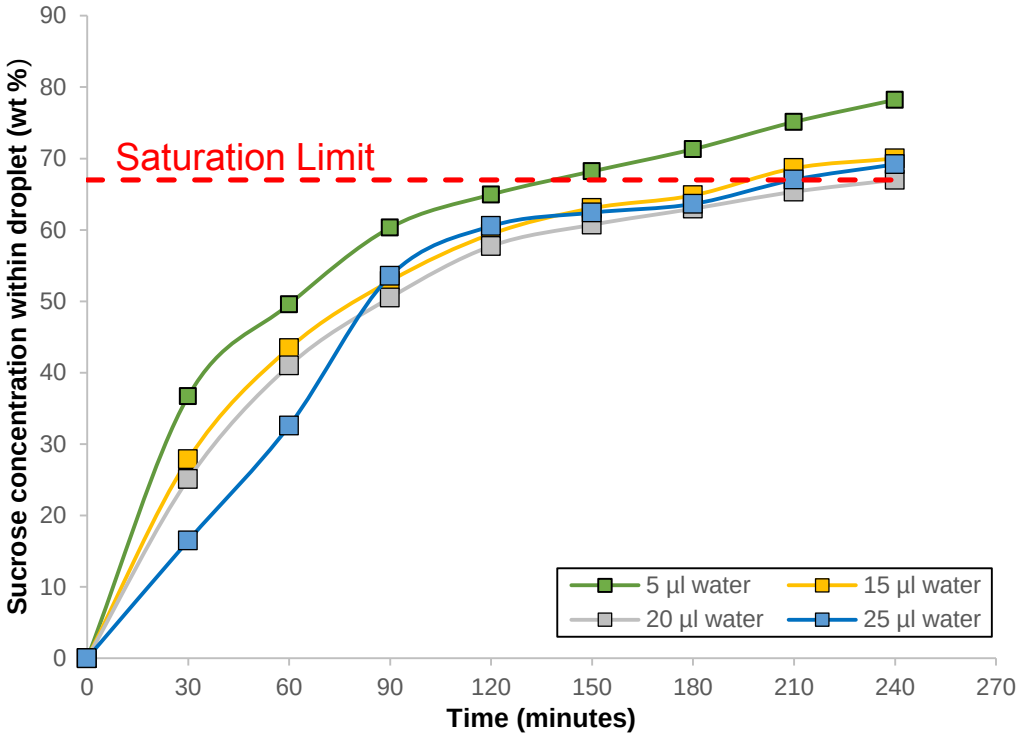

Figure 4-26. Change in sucrose concentration of the secondary liquid droplet against time (5 µl, 15 µl, 20 µl and 25 µl water droplets).

4.3.7 Large Volume of Secondary Liquid

A test was conducted with a much larger volume of water than those presented so far, to see if a similar trend is seen. To contain this larger volume of water, a larger diameter sample holder was needed. The outer diameter of the sample holder was 22 mm and the inner diameter was 18 mm. The scan was conducted at a 34.1 µm resolution, to allow the field of view to be increased to contain the whole sample. Images for scans conducted on a suspension sample to which a volume of 500 µl water was added can be seen in Figure 4-27.

As expected the volume of the droplet at time 0 is substantially larger than those shown earlier in this chapter. After 210 minutes, it can be seen that the droplet has progressed approximately 2 mm into the suspension and increased in overall volume. This trend continues and after 24 hours it can be seen that the water droplet has increased even further in volume and penetrated considerably more. It is interesting that even at this volume of water, the trend is the same as that shown previously for smaller volumes of water, with the creation of an oil channel

(highlighted with the red dashed line in Figure 4-27 after 24 hours). Therefore, the structure which remains may have some remanence of water which created liquid bridges that are strong enough to hold the structure in place. It is believed that the bridges shown in Figure 4-22 may be something similar which is holding the structure in position or the packing arrangement of the sucrose particles which settle after preparation of the sample.

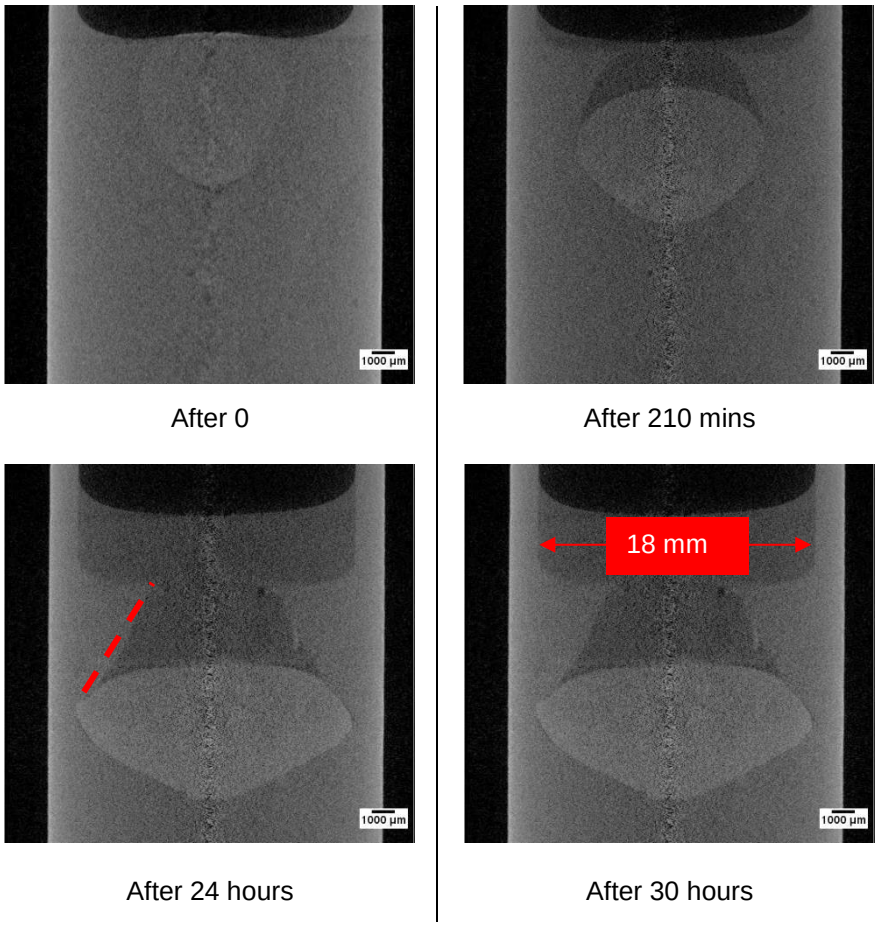

Figure 4-27. Time lapse of images for suspension to which 500 µl water was added. Scale on images is 1 mm.

4.4 Conclusions

In this chapter, the penetration and movement of water when applied to suspensions of sunflower oil and sucrose was investigated on the macroscopic scale. Initial tests were focused on surface penetration (capillary penetration) using optical methods (Figure 4-28). It was shown how the surface penetration was quickest for sunflower oil alone, in comparison to sucrose. For a suspension of sucrose and sunflower oil, for the water to progress it needed to either displace or

absorb the sucrose present to continue its penetration. This initial surface penetration was less than 1 second.

Tests were also conducted on sucrose tablets (dry and immersed in oil), which displayed axial spreading on the surface of the tablet after the primary contact of the water as well as the penetration into the tablet. This penetration time was quickest for the dry sucrose tablet in comparison to the tablet immersed in oil, due to the resistance offered by the oil.

Due to limitations in this optical method in only being able to see the surface penetration of the water, this was then taken further by using a non-invasive method employed by X-ray CT to study further penetration into the sample, after the initial surface penetration, as can be seen schematically in Figure 4-28. Scans were conducted for the movement of different volumes of water (range of 5 - 25 µl) when applied to suspensions for a 4 hour period from the initial addition.

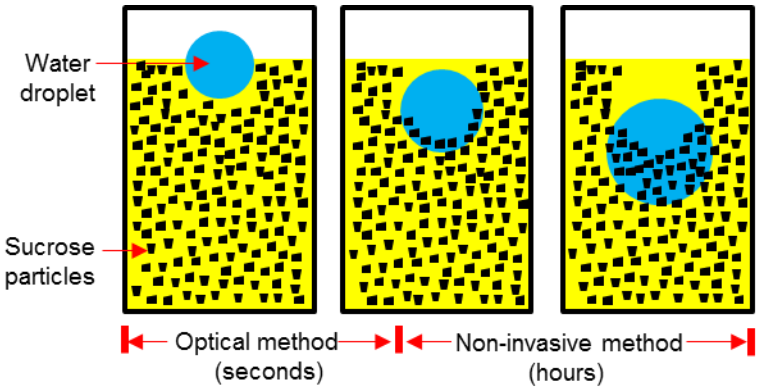

Figure 4-28. Schematic drawing for different techniques employed to track movement of water when applied to a suspension.

Indications from the experiments carried out so far, show an initial fast movement dominated by capillary penetration followed by other mechanisms such as gravity and / or diffusion playing a part as well. Figure 4-29 shows how this may be perceived, though not to scale in terms of time. Also, it is likely some mechanisms occur simultaneously and not in isolation.

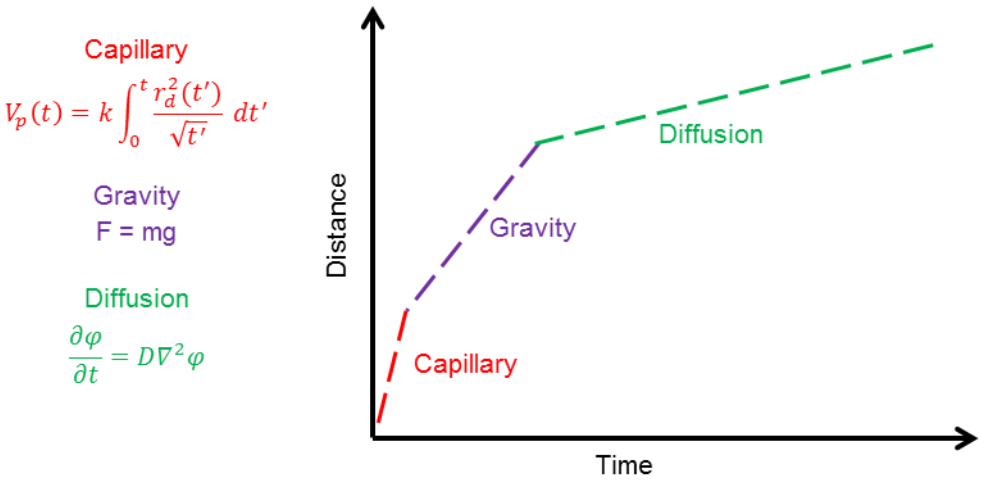

Figure 4-29. Schematic showing how movement dynamics change with time.

Chapter 5 Microscale study on suspensions

5.1 Introduction

It has been shown using qualitative methods it is possible to track the movement of bulk water by monitoring the change in mass with time (Yuan et al., 2009). However, seeing localised mass transfer on the microscale is not possible using this method. High resolution synchrotron X-ray CT was used to help expose the movement of water internally within model suspensions. The work in this chapter progresses on the benchtop X-ray CT results presented in Section 4.3.2.

5.2 Materials & Methods

The suspensions of sucrose and sunflower oil described in depth within Section 3.2.9 were used in this chapter. The secondary liquid used was water of two different volumes (5 µl and 10 µl). The diameter of the sample holder was 9 mm.

The X-ray energy used was 17 keV, with a voxel size of 9 µm. The field of view was set to 18 mm × 12 mm (horizontal × vertical). The total scan duration for each sample was 24 minutes. Full details of the set-up used can be found in Section 3.2.11.2.

5.3 Results & Discussions

5.3.1 High Resolution Scans

Experiments (X-ray CT) were conducted to which water (5 µl and 10 µl water) was applied to the surface of suspensions at the Elettra synchrotron facility in Trieste, Italy, producing high resolution images. The time period studied covered early and intermediate stages of movement after the application of the secondary liquid. The time lapse of images for the 5 µl and 10 µl water droplet added can be seen in Figure 5-1 & Figure 5-2 respectively.

All 2D slices shown in Figure 5-1 & Figure 5-2 were opened in an image stack using ImageJ. For the stack, the maximum interval of grey values was adjusted to enhance the details of the regions of interest and this was then applied to the complete stack of images. Then the stacks of images were saved as individual tiff files, to which the analysis of the grey value was carried out. This ensured all

images were adjusted using the same grey values interval, and the same adjustment was made for all scans of a given sample.

The dark region above the suspension is air, as has been highlighted in the first image in Figure 5-1 and highlighted previously in Figure 4-9. Similar to that seen in Figure 4-9 for the same experiment using the benchtop X-ray system, when looking at the images from Figure 5-1, the 5 µl water droplet is increasing in size as it progresses through the suspension. This is due to the uptake of solid sucrose from the bulk suspension by the droplet which results in a volume increase. The time between scans 1A and 2A is 60 mins, and it can be seen during this time period, the droplet has moved approximately 1 mm into the suspension. Also, the path taken by the water droplet can be seen as a channel of oil is left behind from where the droplet was initially present, to where it is now.

The droplet initially takes a spherical shape which is expected for a water droplet. With time the droplet transforms into a ellipsoidal shape (larger in the horizontal diameter, in comparison to the vertical diameter) as can be seen in the image from scan 6A after 390 mins. After 480 mins in scan 7A, the top portion of the droplet slowly moves towards a flat shape and this continues until the upper portion transforms to a concave shape as can be seen in scan 8A (after 600 mins). The concave shape shows the droplet as it progresses was composed of liquid. This is evident from the top shape, as if it was a solid body it would not deform into this shape. Also, the route taken by the secondary liquid to its position can be seen, when looking at the region above the secondary liquid. After 600 mins, the droplet continues spreading axially (both horizontally and vertically below the droplet), as can be seen in scan 9A (after 1080 mins).

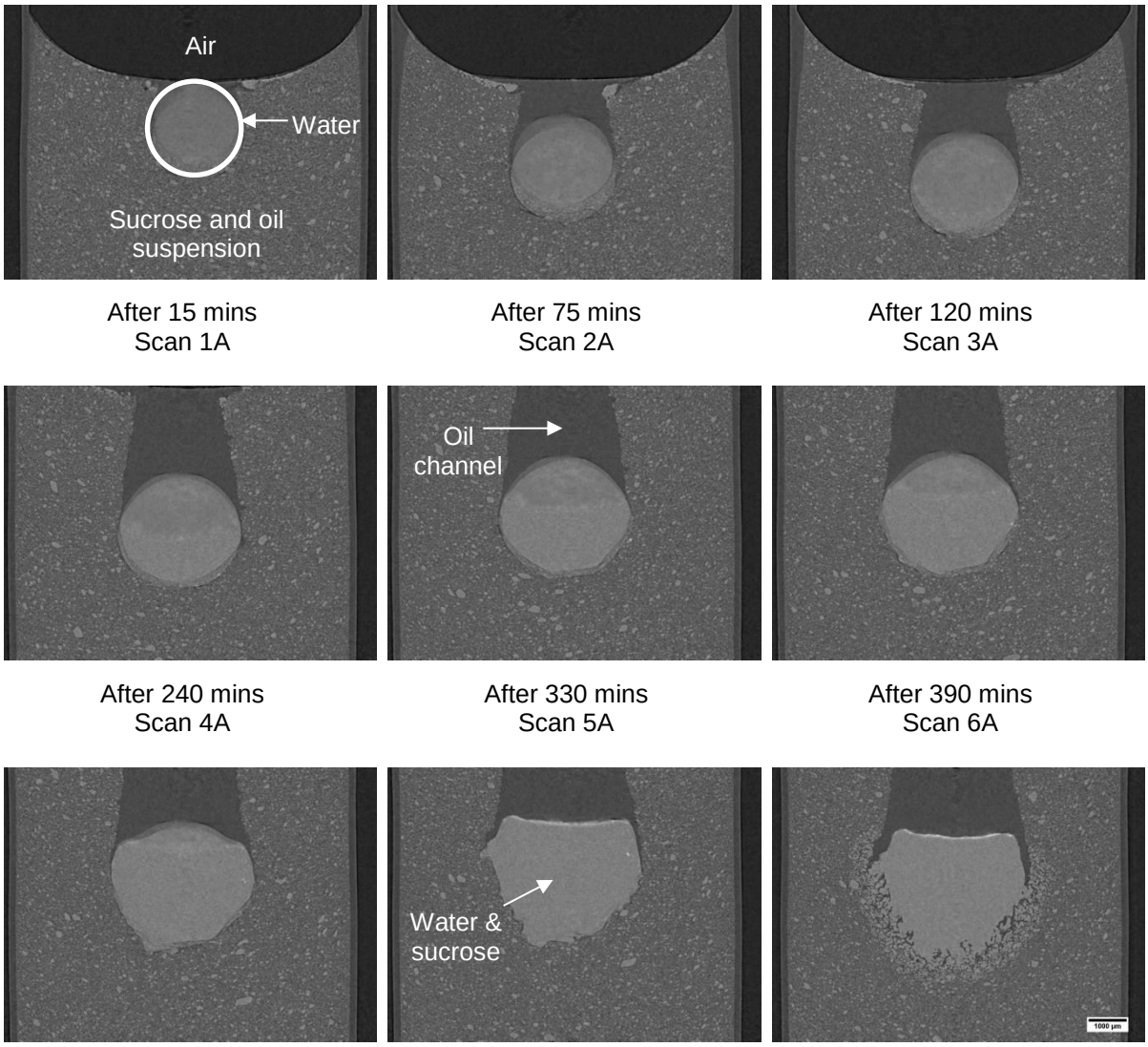

After 15 mins
Scan 1A

After 75 mins
Scan 2A

After 120 mins
Scan 3A

After 240 mins
Scan 4A

After 330 mins
Scan 5A

After 390 mins
Scan 6A

After 480 mins
Scan 7A

After 600 mins
Scan 8A

After 1080 mins
Scan 9A

Figure 5-1. Time lapse of central slice along X-axis (where diameter of water droplet is largest), for 5 µl water droplet. Scale on Scan 9A is 1 mm.

A similar trend can be seen in Figure 5-2 for the time lapse of images for the 10 µl water droplet, in that the size of the droplet increases as it progresses into the suspension as mentioned for Figure 5-1. This as mentioned earlier is believed to be due to the uptake of sucrose from the bulk suspension by the droplet. The droplet is physically bigger than that seen in Figure 5-1, which is expected, as the volume added initially is twice the amount. The trend is the same as that seen in Figure 5-1 for the 10 µl water droplet in Figure 5-2, in that initially the droplet takes

a spherical shape which then slowly transforms to an ellipsoidal shape with time and finally ends with a concave top with more evident axial spreading.

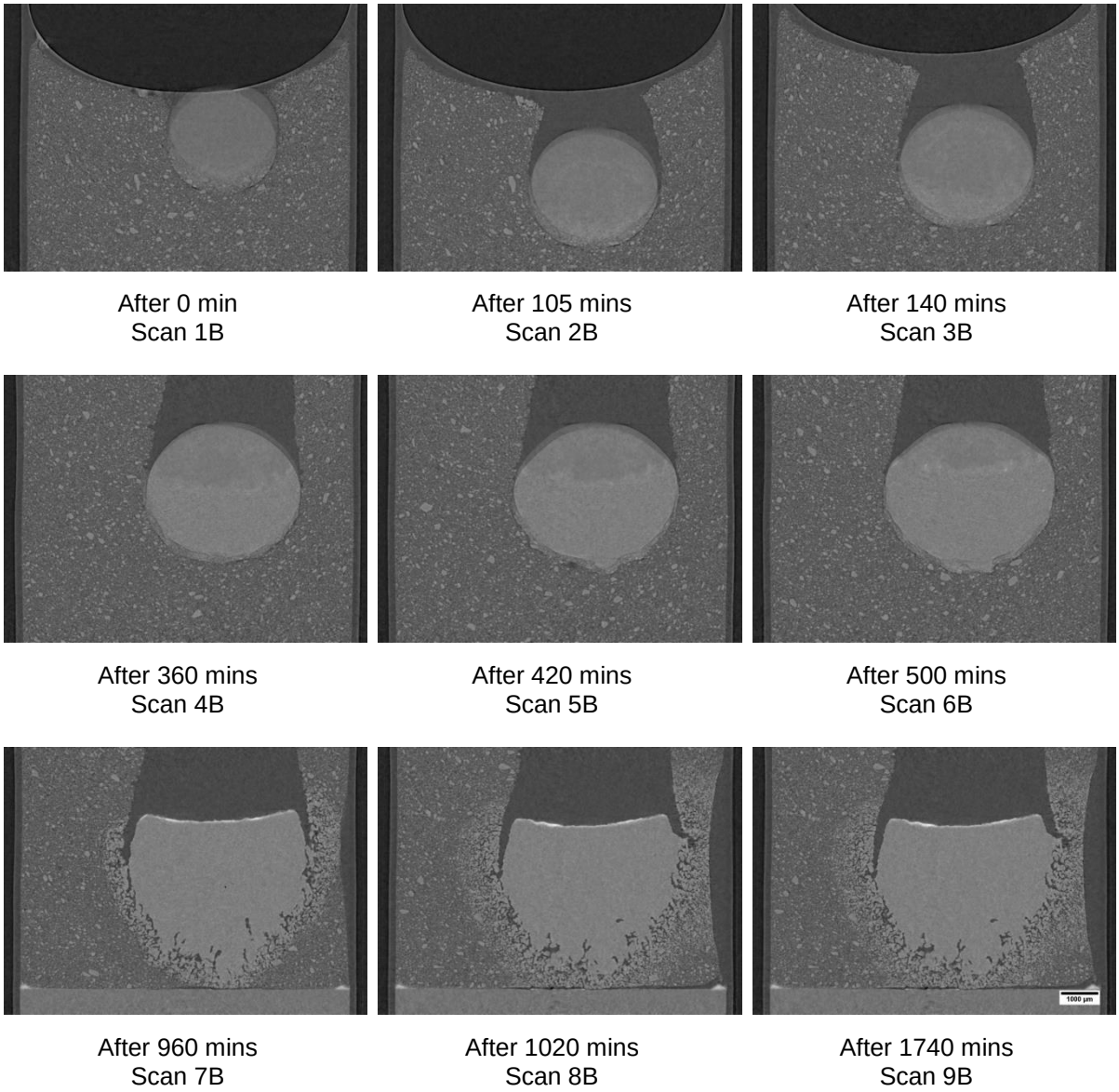

Figure 5-2. Time lapse of central slice along X-axis (where diameter of water droplet is largest), for 10 µl water droplet. Scale on Scan 9B is 1 mm.

During the scan as seen in Figure 5-1 and Figure 5-2, the droplet is moving with time further into the suspension. Therefore, to follow the droplet, the portion of the sample being scanned was changed between scans when needed to ensure the droplet was within the field of view. For example in Figure 5-1, between scan 1A and scan 6A, the portion scanned was changed along the height (y-axis in Figure 3-13) of the sample, to ensure the region of interest which in this case was the

water droplet was in complete view for the portion being scanned. This can schematically be seen in Figure 5-3. Similar changes were made to the scans for the 10 µl water droplet in Figure 5-2, to ensure the droplet movement was tracked.

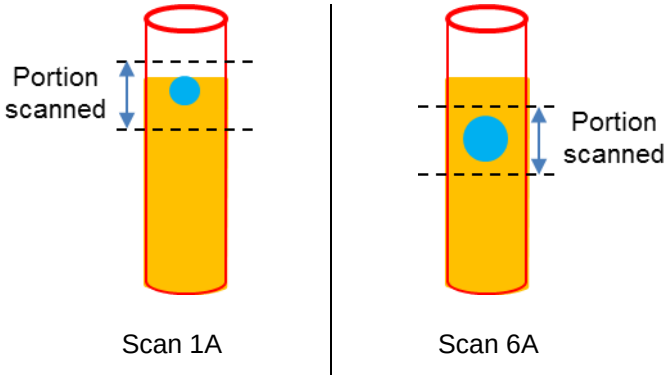

Figure 5-3. Schematic for the change in field of view scanned for samples, to follow progression of secondary liquid.

A larger image of scan 9A from Figure 5-1 can be seen in Figure 5-4, along with a magnified region of the boundary region of the water/sucrose and sucrose/oil mixture. Here it can be seen there is some contracted regions of sucrose, which have displaced the oil which was previously present between them. This is believed to be similar to the formation of the sucrose network being referred to when attempts have been made to create a heat resistance chocolate (Stortz and Marangoni, 2011). The presence of water creates a structure which can maintain its shape and resist elevated temperatures, to assist in shape retention of the product.

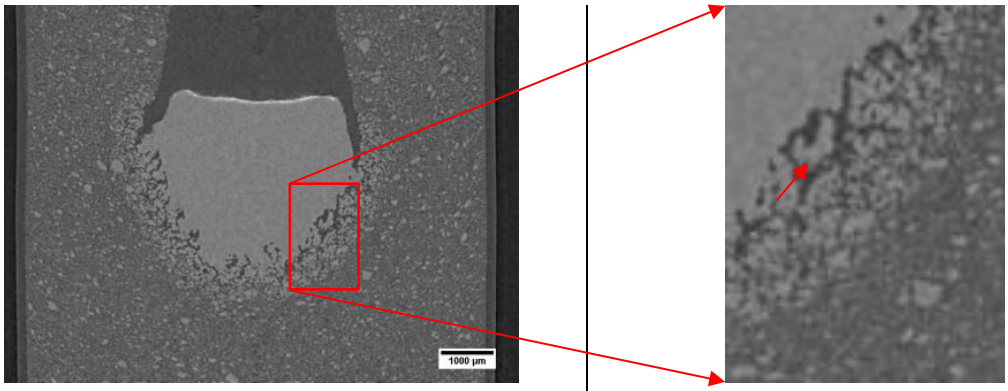

(a) standard image (b) magnfied region

Figure 5-4. Scan 9A from Figure 5-1.

Using the software VGStudio MAX2.0, 3D volume renderings were produced to show the sample along the different planes. Figure 5-5 is a volume rendering for scan 4A from Figure 5-1. It can be seen that the sample has been cut along the X and Y plane, to show the details of the water droplet. Within the droplet, the central region is darker in comparison to the outer portions of the droplet, which is believed to be due to the presence of sucrose within the droplet. The diameter of the water droplet is approximately 3 mm in this image.

Also, it can be seen that large individual sucrose crystals within the bulk suspension can be seen, which was not possible for the scans shown in Section 4.3.2. The reason for this is due to the quality of the detector and camera as well as the X-ray energy source available at synchrotron facilities in comparison to benchtop systems.

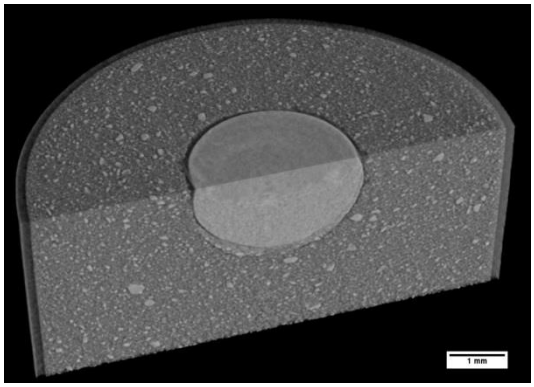

Figure 5-5. Volume rendering of Scan 4A from Figure 5-1, cut along the X and Y plane.

A similar volume rendering was produced for scan 9A which can be seen in Figure 5-6. It can be seen there is a vivid change in shape of the droplet in comparison to scan 4A shown in Figure 5-5. It can be seen that a clear separation has formed between the bulk water/sucrose and the surrounding suspension. In addition, the axial spreading (horizontally and vertically below the droplet) of the secondary liquid can be seen. The oil phase has been masked out, placing emphasis on the sucrose and water/sucrose phase. A crater surface on the top of the water/sucrose mixture is evident, which is believed to be due to the sucrose particles. The water alone is not able to take and deform into such a shape within the liquid state, indicating now the droplet is in a solid or semi-solid state. Also, near the top of the water/sucrose mixture, it can be seen there is a separation between the droplet and the bulk suspension, which was occupied by oil. This indicates both the movement of sucrose into the droplet as well as spreading of water from the droplet into the bulk suspension.

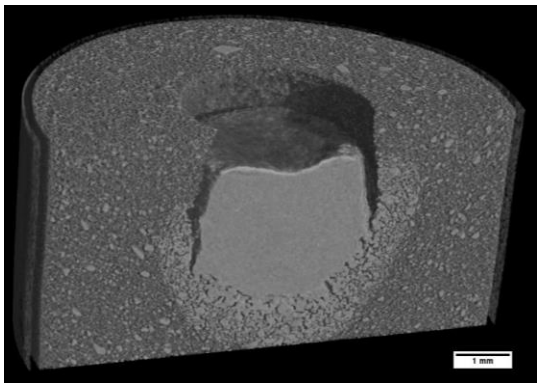

Figure 5-6. Volume rendering of Scan 9A from Figure 5-1, cut along the X and Y plane focusing on the droplet after removing oil phase.

A larger image of scan 9B from Figure 5-2 can be seen in Figure 5-7, along with a magnified region of the boundary region of the water/sucrose and sucrose/oil mixture near the side of the sample holder (cellulose straw). It can clearly be seen that solid sucrose from the bulk suspension, has pulled from the side nearer to the straw towards the bulk water phase, creating a contracted sucrose region. This results in displacing the oil to the side closest to the wall of the sample holder. The strength of the bonding of the sucrose with the water is strong enough to pull the whole sugar structure from the side (as the sucrose exists in a network form).

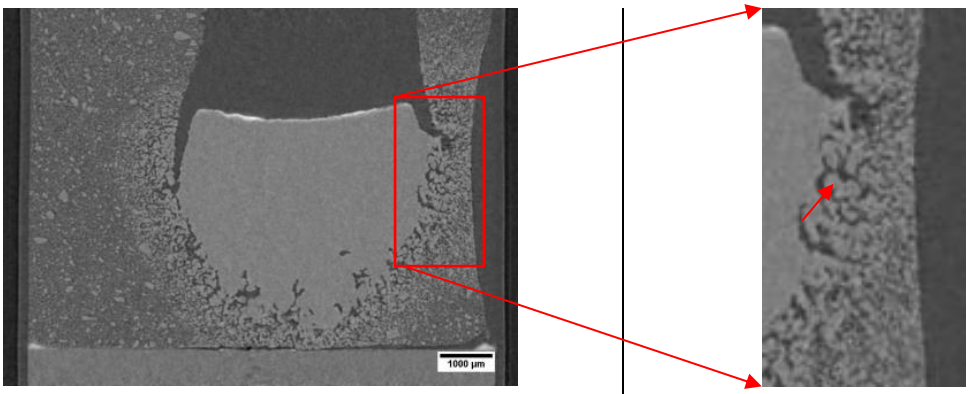

(a) standard image (b) magnfied region

Figure 5-7. Scan 9B from Figure 5-2.

Further volume renderings were produced for scan 9B from Figure 5-2 which can be seen in Figure 5-8. Image (a) shows how far the water has spread along the different planes, similar to that shown in Figure 5-6 for the 5 µl water droplet. The shape is similar to that shown for the 5 µl water droplet as well as a separation of oil layer between the bulk water and the surrounding suspension. In image (b) the oil phase has been masked out, with a volume of interest focusing on the sucrose/water droplet. A similar crater surface on the top of the water/sucrose shown in Figure 5-6 can be seen, which is believed to be due to the sucrose particles. The sucrose/water droplet body shows a consistent greyscale, indicating that the body is uniform in composition throughout.

Also, it can be seen how far the water has spread and reached from the bulk centre. This is highlighted with the red arrow in image (a) of Figure 5-8. Thus, now the water is moving away from the bulk and into the suspension to continue its movement, as the capacity of the droplet to take up any further sucrose is no longer there, due to being fully occupied by sucrose.

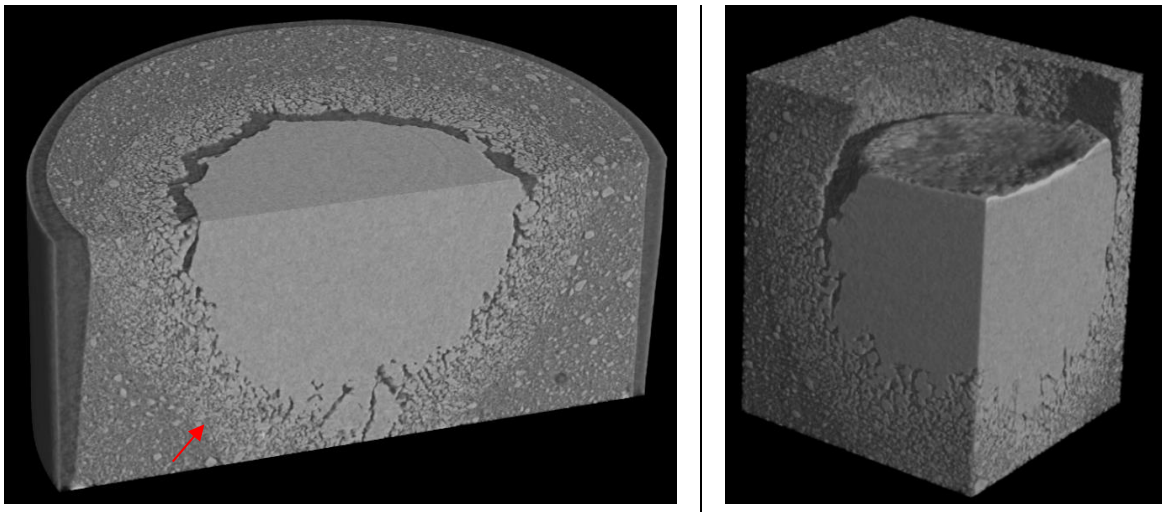

(a) (b)

Figure 5-8. Volume rendering of Scan 9B from Figure 5-2; (a) cut along the X and Y plane focusing on the droplet; (b) cut along the X and Y plane with the removal of the oil phase to highlight the top surface of the sucrose/water droplet.

The images from Figure 5-1 were adjusted using a look up table in image J to better enhance the contrast within the water droplet which can be seen in Figure 5-9. This is achieved by assigning colours to different regions of the grey scale, to better enhance the contrast between the different phases present. For scan 1A in Figure 5-9 it can be seen that the whole droplet is dark blue, indicating it is predominantly water with very little sucrose which is expected after 15 minutes from addition. By scan 3A, the lower portion of the droplet is turning slightly towards a lighter blue colour, as some solid sucrose enters from the lower region of the droplet as it progresses into the suspension. This lower portion of light blue continues to progressively grow from scans 4A to 6A, gradually coming closer to the top of the droplet as time progresses. After 480 mins by scan 7A, nearly the whole droplet is of a fairly uniform colour of both light and dark blue. By scan 8A the droplet is of uniform colour, indicating that the presence and location of sucrose within the water droplet is uniformly distributed. For the final scan 9A, the colour is the droplet is similar to scan 8A, however, there is some change in the region surrounding the droplet towards the bulk suspension, which shows a more concentrated blue colour. This is believed to be due to the movement of the sucrose particles which come closer together due to the presence of water (liquid bridges) between sucrose particles.

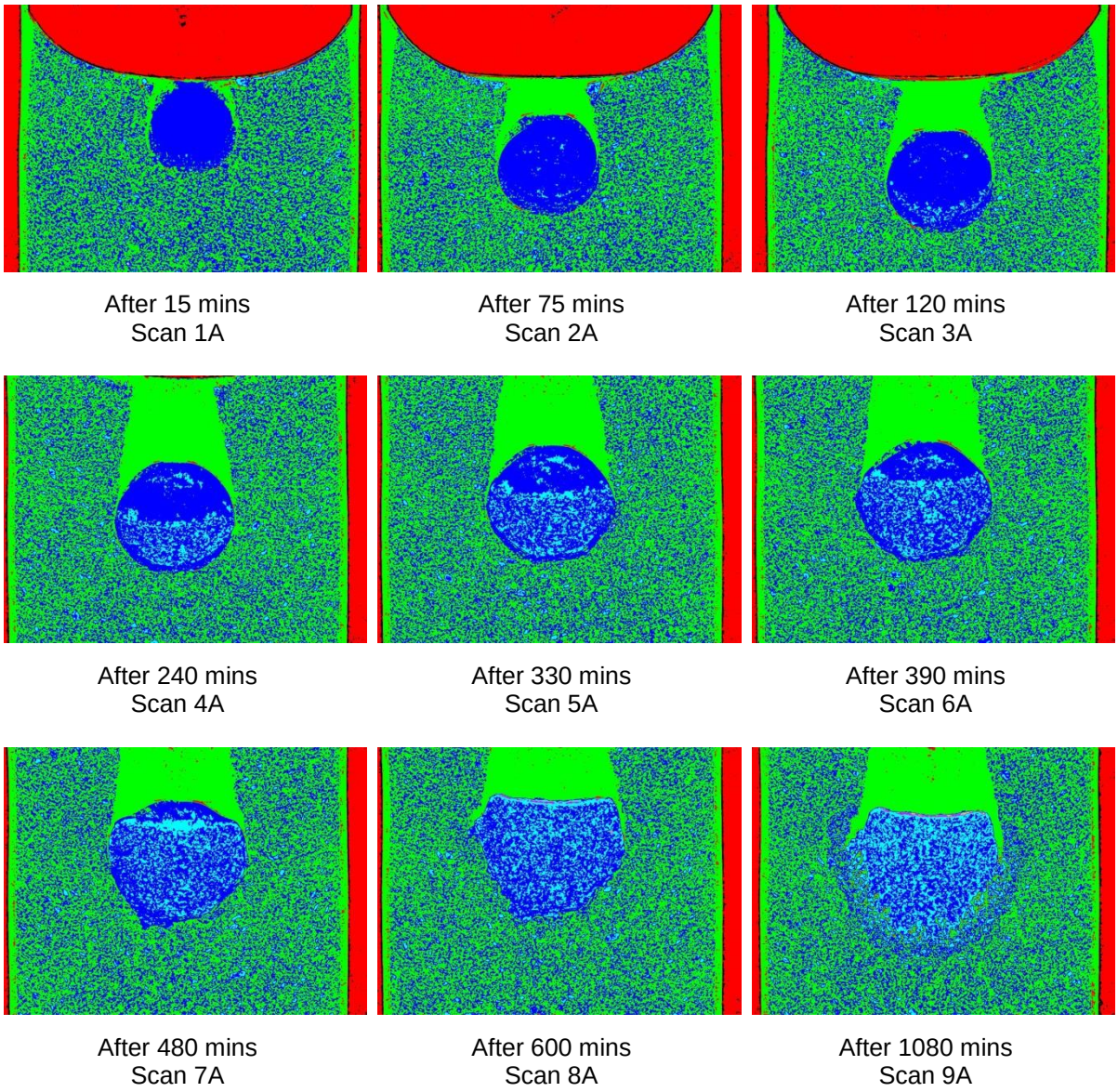

Figure 5-9. Time lapse of central slice along X-axis for 5 µl water droplet. Same images as in Figure 5-1, with adjusted brightness and contrast.

From the images presented in Figure 5-9, it is hypothesised that the sucrose enters into the water droplet from the lower portion of the droplet which results in the volume increase for the droplet seen within the time lapse of images presented. A schematic of this can be seen in Figure 5-10. In stage 1 after the initial addition of the water droplet, the droplet contains no sucrose and is composed solely of water, which corresponds to scan 1A from Figure 5-9. By stage 2, the water droplet has moved a little into the bulk suspension, with some sucrose from the bulk suspension entering into the lower portion of the droplet, which causes a slight

increase in volume of the droplet, while maintaining its spherical shape. Stage 2 corresponds to the period shown in scan 3A from Figure 5-9.

By stage 3, the droplet has moved further into the suspension with additional sucrose entering into the droplet from the bulk suspension, as well as, some of the sucrose which had previously entered in stage 2 dissolving, which results in a further increase in volume of the droplet. In stage 3, the droplet begins to transform from a spherical shape seen in stage 2 to a more ellipsoidal shape as the horizontal diameter becomes larger quicker in comparison to the vertical diameter due to the area of contact of sucrose from the bulk suspension with the droplet. Stage 3 corresponds to scan 4A from Figure 5-9. A magnified image for the droplet from stage 3 can be seen in Figure 5-10, to emphasise the location of the sucrose within the droplet in additon to the change in the shape of the droplet. Then after a long time from the intial addition in stage 4 in Figure 5-10, the droplet has progressed even further into the bulk suspension, with dramatic changes in the shape of the droplet. The droplet is no longer ellipsoidal as that seen in stage 3 and now has changed to a distinct irregular shape due to how sucrose entered into the droplet as it progressed. Also, now the droplet is fully occupied by sucrose which corresponds to scan 8A from Figure 5-9.

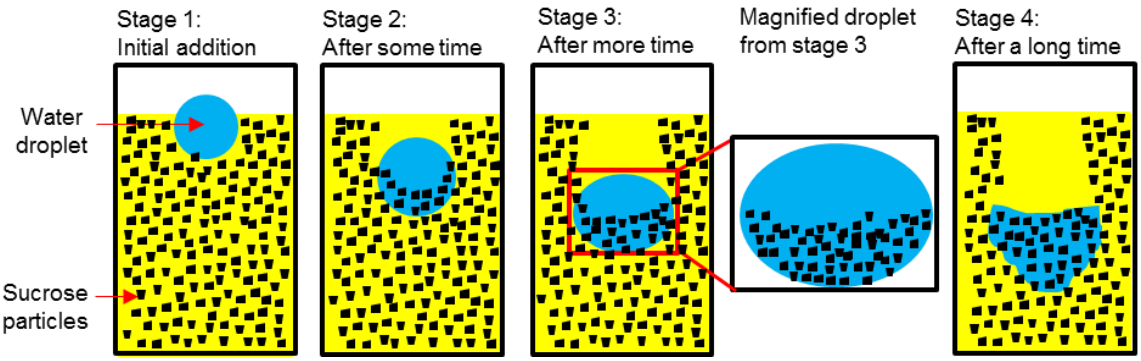

Figure 5-10. Schematic of early stages movement of sucrose from suspension into water droplet.

After stage 4 in Figure 5-10, now the droplet cannot accept any further solid sucrose, as it is fully occupied by sucrose as it can feasibly take. Therefore, now the movement direction is of the water or water sucrose solution mixture away and into the bulk suspension, to come into contact with further solid sucrose within the bulk suspesnion. This is highlighted as stage 5 in Figure 5-11, as further spreading

can be seen in scan 9A from Figure 5-9, which demonstrates the system has not yet reached equilibrium and further transport mechanisms are taking place to drive the movement of the secondary liquid. A magnified image of the droplet from stage 5 can be seen in the right of Figure 5-11, in particualr highlighting the channels of water spreading into the bulk suspesnion which can be seen in scan 9A from Figure 5-9. Thus, the shape of the droplet is changing further with channels on the outer region due to further spreading of the secondary liquid.

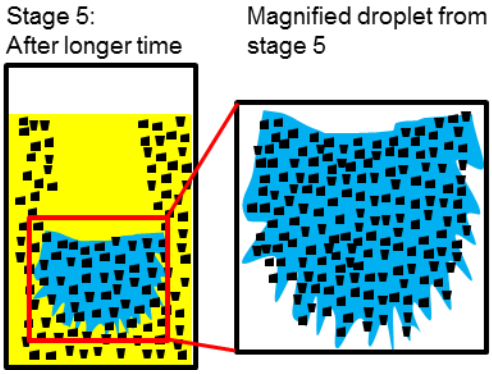

Figure 5-11. Schematic of longer stages movement of water into the bulk suspension.

Similar comparisons can be made for the images for the 10 µl water droplet from Figure 5-2, to correlate to the different stages shown schematically in Figure 5-10 and Figure 5-11. This shows how initially the movement is of the sucrose from the bulk suspension into the water droplet, as long as the water droplet can take up the sucrose. However, after the droplet is fully saturated and occupied by sucrose, the movement is of the water away from the bulk water into the suspension, to allow it to come into contact with further sucrose from the bulk suspension.

5.3.2 Changes in Droplet Greyscale

It can be seen that there is a clear change in the greyscale of the droplet in the time lapse of images shown in Figure 5-1 & Figure 5-2 for the 5 µl and 10 µl water drop respectively, as the droplet progresses through the suspension. Image J was used to track the change in grey value with time for the images shown. The images shown are 16 bit images, with a grey range of 0-65535, where 0 corresponds to black and 65535 to white and in between are shades of grey.

The area for the secondary liquid droplet within the images in Figure 5-1 and Figure 5-2 was used to calculate the greyscale change. The data was normalised, by dividing the number of pixels with a particular grey value, by the total number of pixels. Therefore, the sum of the counts of the total number of pixels for each scan is 1. The reason for this is, as can be seen the droplet is growing in size which results in an increase in area coverage within the image. This in turn results in a larger amount of pixels being occupied by the droplet, for the latter scans as the droplet grows in size. Therefore, the distribution will be focused on and occupied by the later images as they contain more pixels. By normalising the data, all scans will occupy the same area when plotted, showing the trend of the greyscale.

The grey scale distribution for the images from Figure 5-1 for the 5 µl water droplet can be seen in Figure 5-12 and for the 10 µl water droplet from Figure 5-2 can be seen in Figure 5-13. The change in mean grey value for both volume droplets with time can be seen in Figure 5-14.

It can be seen that with time there is a shift from left to right for the grey value for the droplet with time, indicating the droplet is getting brighter as it takes up sucrose from the suspension. This agrees with the images from the suspensions, in that the sucrose particles within the suspension are of a brighter grey value in comparison to the oil and water. Thus, when the droplet takes up sucrose from the suspension, this will lead to a change in the grey value of the droplet towards a higher value (as a higher number corresponds to a lighter grey value).

In Figure 5-12 it can be seen for scan 1A, the range of grey value is 26000 – 33000, with a mean of approximately 28500. After 60 mins from scan 1A to scan

2A, the mean grey value increases to 30200 which results in a significant shift to the right along the grey scale. Scan 3A is similar to scan 2A as the time difference between the scans, is approximately 45 minutes, though there is a small shift to the right with the mean grey value increasing slightly to 30500. By scan 4A after 240 mins, the range of grey values increases with the lower end similar to scan 2A and 3A, while the mean increases considerably to 31500 for scan 4A. For scan 5A after 330 mins, the upper limit of the grey value is similar to scan 4A, though the lower limit has shifted to the right, with the mean increasing slightly to 31800. The mean grey value for scan 6A is 32000 with a similar range of grey values to scan 5A. Scans 7A and 8A have a similar mean grey value of 32200, as the scans were taken close to each other, after 480 mins and 600 mins respectively. Finally, scan 9A has the highest mean grey value of 32500 with a grey scale range of 29000 – 37000 which is considerably higher than the grey scale range for scan 1A (from the images in Figure 5-1) after 1080 mins. This is expected, as this scan was the last to be taken, and will contain the most sucrose within the droplet and therefore have the highest mean grey value.

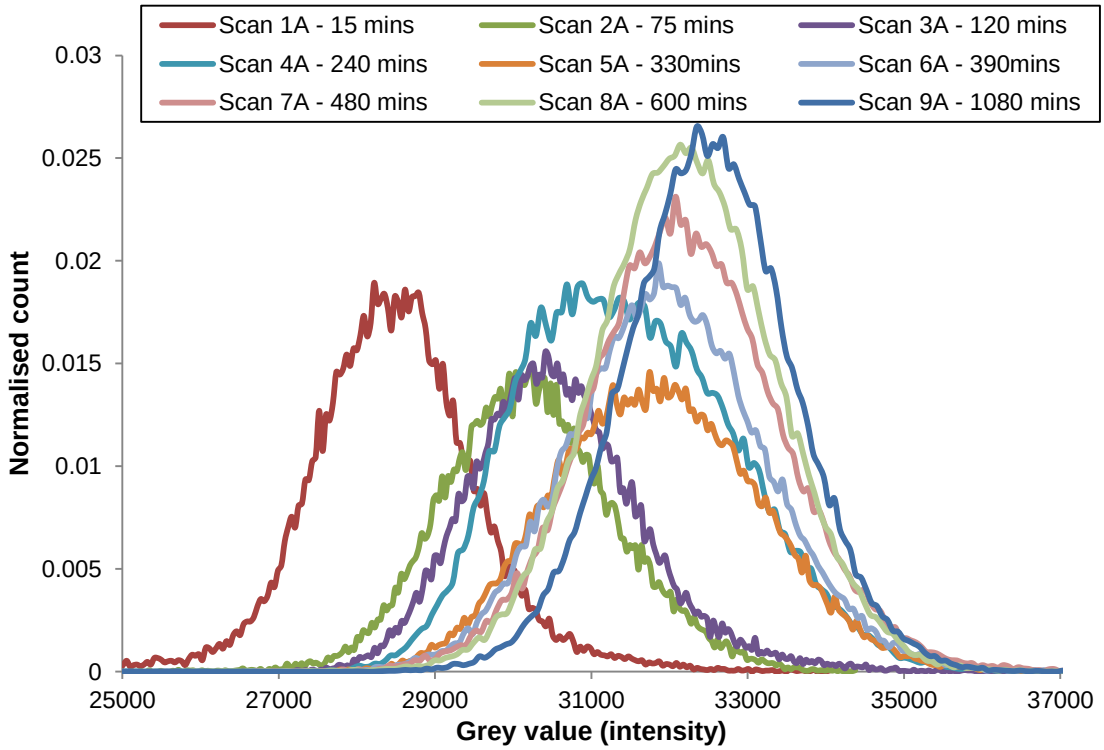

Figure 5-12. Change in grey value for 5 µl droplet from images in Figure 5-1.

A similar change in the grey value range is seen for the 10 µl water droplet for the images from Figure 5-2 as mentioned for the 5 µl water droplet which can be seen in Figure 5-13, in terms of a gradual shift to the right as the droplet takes up sucrose from the bulk suspension. For scan 1B, the grey range is 26000 – 31000, which is slightly narrower in comparison to scan 1A. This is due to the amount of time the water droplet has been present within the sample, which is less for scan 1B in comparison to 1A. By scan 2B there is a very clear shift to the right with an increase in the grey scale range. This shift continues to the right from scan 4B to 7B for consecutive scans. Scan 8B and 9B have a similar range grey value as the after this time period, the droplet is now fully occupied by sucrose and is no longer able to take up any further sucrose from the bulk suspension.

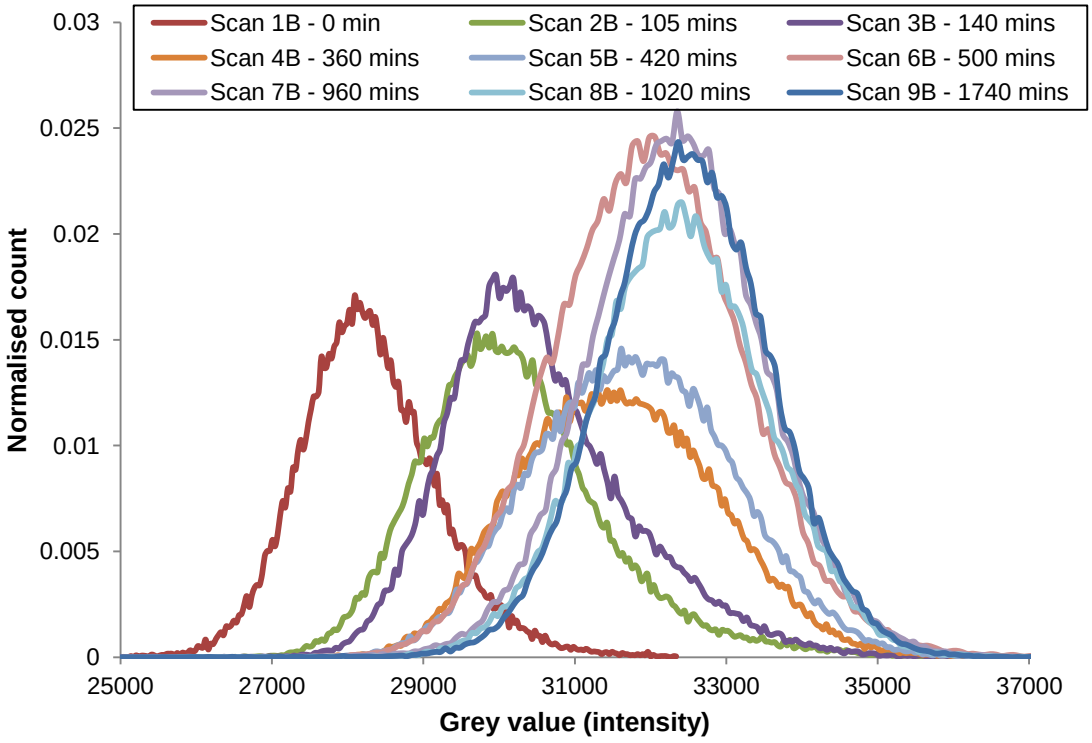

Figure 5-13. Change in grey value for 10 µl droplet from images in Figure 5-2.

The mean grey values for the images from Figure 5-1 and Figure 5-2 can be seen in Figure 5-14. The mean grey value for scan 1B (0 min) from Figure 5-2 is approximately 28300. This is slightly lower than scan 1A (15 mins) from Figure 5-1, which is expected as scan 1B for the 10 µl droplet was taken immediately after addition whereas scan 1 for the 5 µl droplet was started 15 minutes after addition.

Therefore, scan 1B for the 10 µl droplet will contain less sucrose as it has not had the same amount of time within the system to take up sucrose and progress into the suspension. After 105 mins from scan 1B to scan 2B, the mean grey value increases to 30200 which is similar to scan 2A for the 5 µl droplet, though this was only after 75 mins. This indicates the ratio of the sucrose and water within the droplet is similar for both volumes; however, the smaller volume droplet of 5 µl managed to achieve this in a shorter period of time. The reason for this is believed to be due to the surface area to volume ratio of the initial droplets. The surface area to volume ratio for a perfect sphere is $\frac{3}{radius}$. The calculated surface area to volume ratio for a volume of 5 µl and 10 µl can be seen in Table 5-1. Thus, based on the area of contact through which sucrose can come into the suspension in relation to its total volume, the smaller 5 µl droplet can take up sucrose faster in relation to the 10 µl droplet. It can be seen that with time, the shape as well as the surface area of the water droplet changes dramatically, however, this does give an indication of its effect for the earlier stages after addition.

Subsequent scans show a similar trend to that seen for the 5 µl droplet, with a slow shift to the right and the mean grey value increasing with time. Scans 6B to 9B have a similar grey value range and mean grey value. The final scan 9B mean grey value is 32500 which is comparable to that of scan 9A from the images in Figure 5-1 as can be seen from Figure 5-14. This is anticipated as this scan was the last to be conducted, and will contain the most sucrose within the droplet. By this time the droplet has become fully occupied with sucrose and now there is some axial movement of the water into the suspension as shown schematically in Figure 5-11.

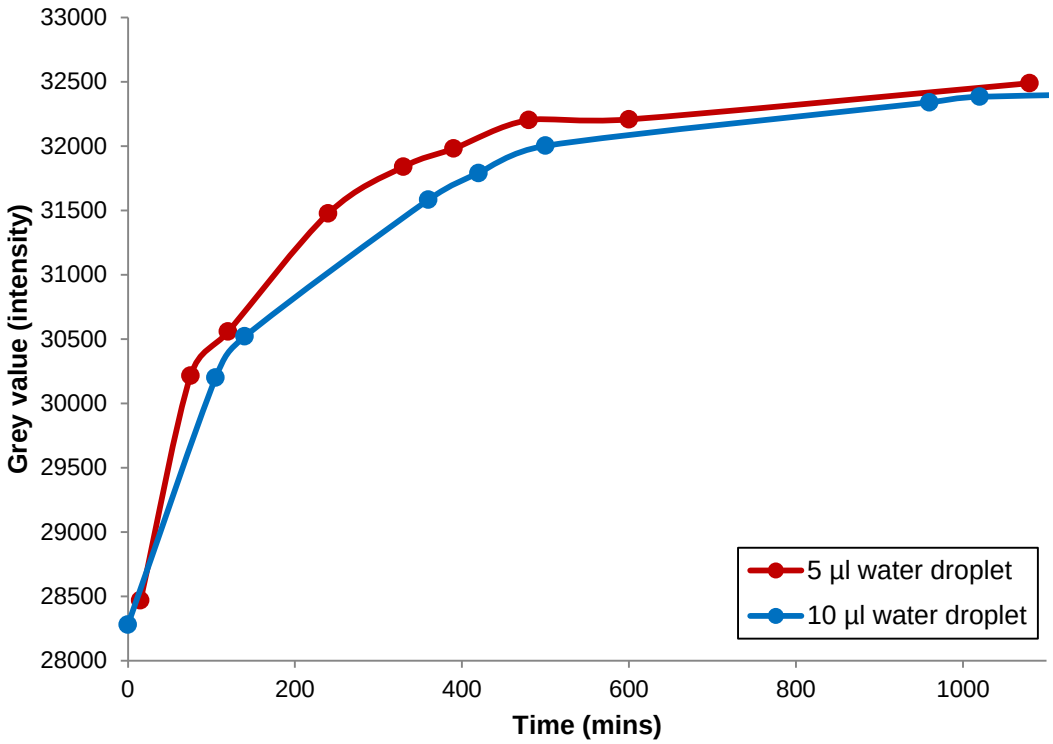

Figure 5-14. Mean grey value for images from Figure 5-1 & Figure 5-2.

Table 5-1. Surface area to volume ratio for droplets.

Volume of droplet (µl)	Surface area to volume ratio (mm^{-1})
5	2.82
10	2.24

5.3.3 Greyscale Changes within Droplet

Figure 5-15 is an enlarged image of scan 5A from Figure 5-9. It can be seen that the top portion of the water droplet has a different grey value in comparison to the bottom portion of the droplet. The reason for this is believed to be as mentioned previously is as the droplet is progressing through the suspension; the lower portion of the droplet is coming into contact with sucrose which is moving into the droplet. The two proposed behaviours mentioned can be seen schematically in Figure 5-16. The black arrow shows the movement of the water down into the suspension, the red arrows show the movement of sucrose from the bulk suspension in the water droplet as it progresses and comes into contact with the lower portion of the water. At the same time as this, the oil which was previously

located between the sucrose particles has been displaced and is shown as the green arrows flowing around the water droplet. The movement of oil around the droplet would explain the dark region on the right and left of the water droplet, which can be seen in magnified image in Figure 5-18 and is highlighted with the white arrows.

Therefore, the lower portion of the water droplet will contain more sucrose in comparison to the top portion of the water droplet. The top portion of the droplet will contain a sucrose solution based on the previous sucrose which entered the droplet, and has now dissolved, and the lower portion containing solid sucrose which has entered as the droplet moves, thus creating a concentration gradient of sucrose within the droplet. As shown in Figure 5-12, as sucrose enters the droplet it causes the grey value to shift to a higher value as it becomes brighter due to the sucrose.

A 90 by 90 square box (8100 pixels) was drawn within the top region of the droplet as can be seen in Figure 5-15, using Image J to see the grey scale distribution. A similar box was drawn within the lower region of the droplet. The blue and red boxes within Figure 5-15 show the regions measured. The distribution of the grey values of these boxes can be seen in Figure 5-17. It can be seen that from the top region to the bottom region there is a shift to the right showing the portion is brighter, which as mentioned previously is believed to be due to the presence of sucrose. The mean grey value of the top region is 31500, whereas for the bottom region it is 32200.

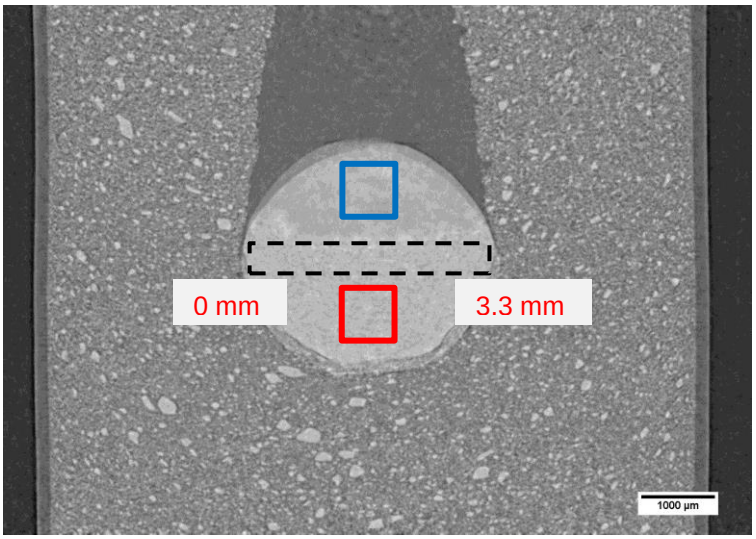

Figure 5-15. Enlarged image of scan 5A from Figure 5-1.

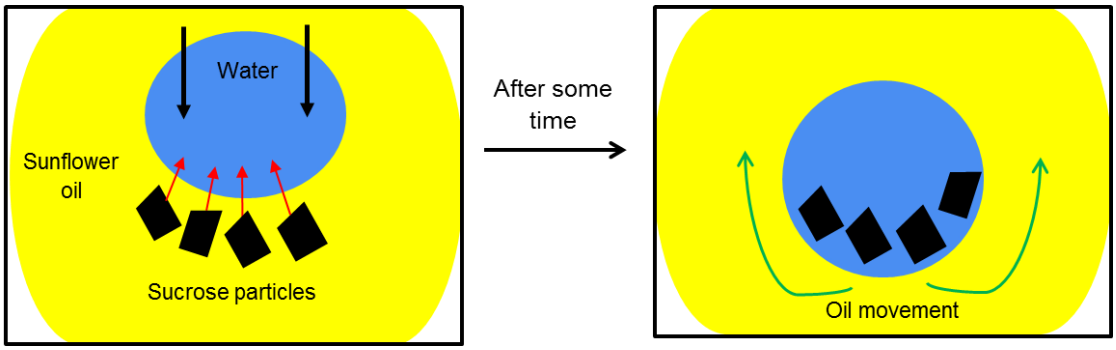

Figure 5-16. Schematic for the movement of water into the suspension, movement of sucrose into the water droplet and movement of oil around the water droplet.

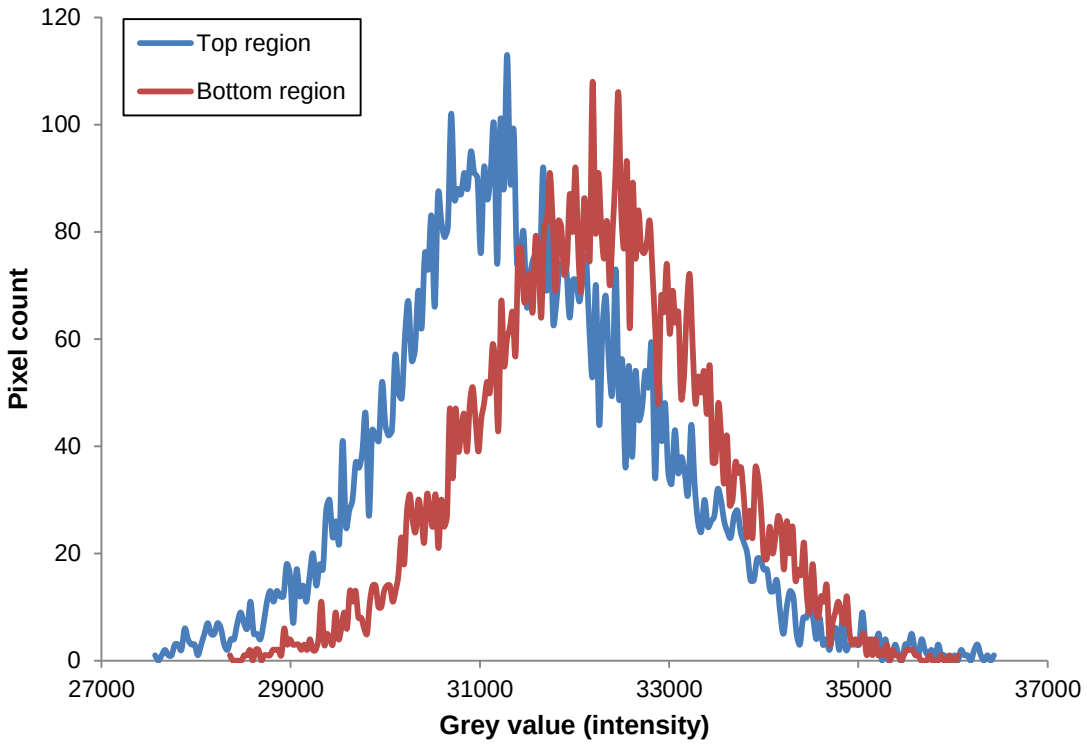

Figure 5-17. Grey value for blue and red box regions from Figure 5-15.

Similar boxes were drawn on scan 5B from Figure 5-2 for the 10 µl, which showed a similar trend. By scans 8A and 8B, the droplet grey value was relatively uniform throughout the droplet, as significant sucrose had entered the droplet to be present throughout the whole droplet. Similar boxes were drawn for scan 8A in Figure 5-18 which can be seen in Figure 5-19. It can be seen in Figure 5-19 the top and bottom region have a similar grey range value with a mean of 32450 and 32200 respectively. This shows even though the average grey value is changing for the whole droplet as shown in Figure 5-12 & Figure 5-13 for the 5 µl and 10 µl water droplet respectively, within the droplet itself there is a grey scale range, corresponding to the presence of sucrose as it enters into the droplet. This shows X-ray CT can successfully be employed to track the movement of sucrose into the droplet as well as the movement of sucrose within the droplet.

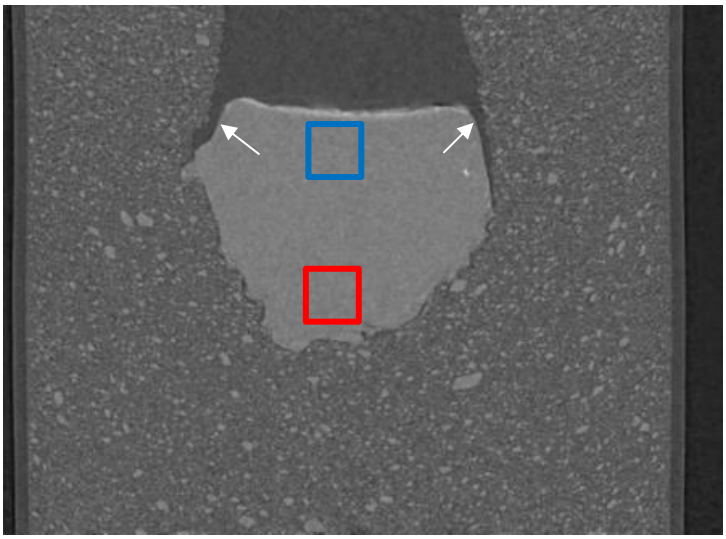

Figure 5-18. Enlarged image of scan 8A from Figure 5-1.

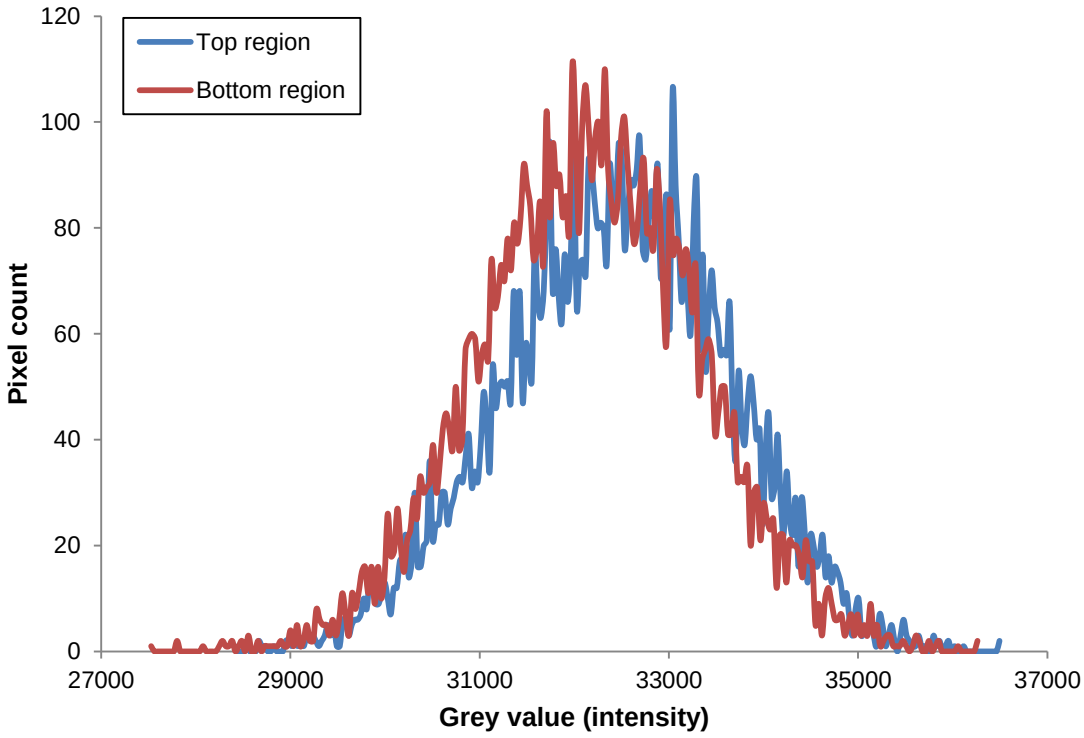

Figure 5-19. Grey value for blue and red box regions from Figure 5-18.

The grey profile of the horizontal black dashed box from Figure 5-15 can be seen in Figure 5-20. It can be seen that the grey value of the suspension of oil and sugar is lower than the water droplet with sucrose. The grey profile of the droplet is fairly consistent in the range of 31500-33000. The diameter of the droplet for Figure 5-15 is 3.3 mm, which was measured using Image J. This shows the droplet has grown

substantially from scan 1A when the droplet diameter was 2.1 mm. This increase in diameter has been ascribed to the large amount of sucrose which has entered the droplet.

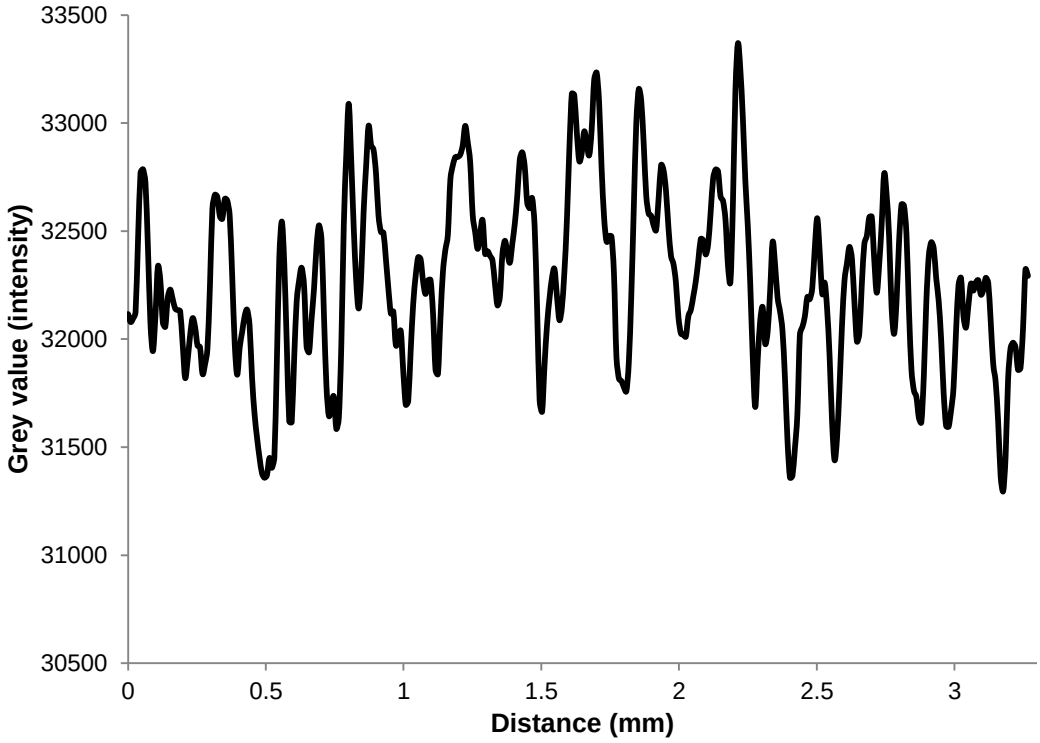

Figure 5-20. Grey value for the horizontal black dashed box from Figure 5-15.

For Figure 5-21, this time the grey value profile from the lower region of the droplet to the upper region of the droplet was measured (vertical dashed purple box, from the bottom to the top) which can be seen in Figure 5-22. It can be seen for the lower portion from 0 – 1.5 mm the grey value is fairly consistent at approximately 32000. At the region of 1.5 mm, it drops to 31000, which is believed to be the location change within the water droplet between the presence of solid sucrose below this region and the absence of solid sucrose above this region.

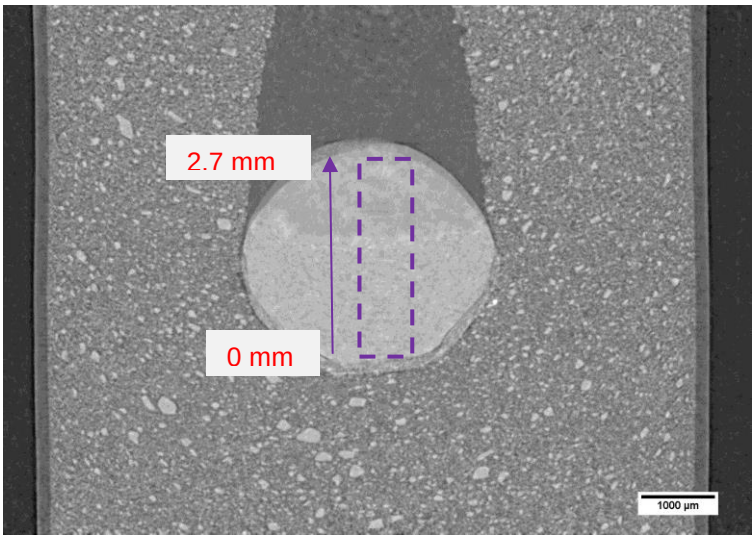

Figure 5-21. Enlarged image of scan 5A from Figure 5-1.

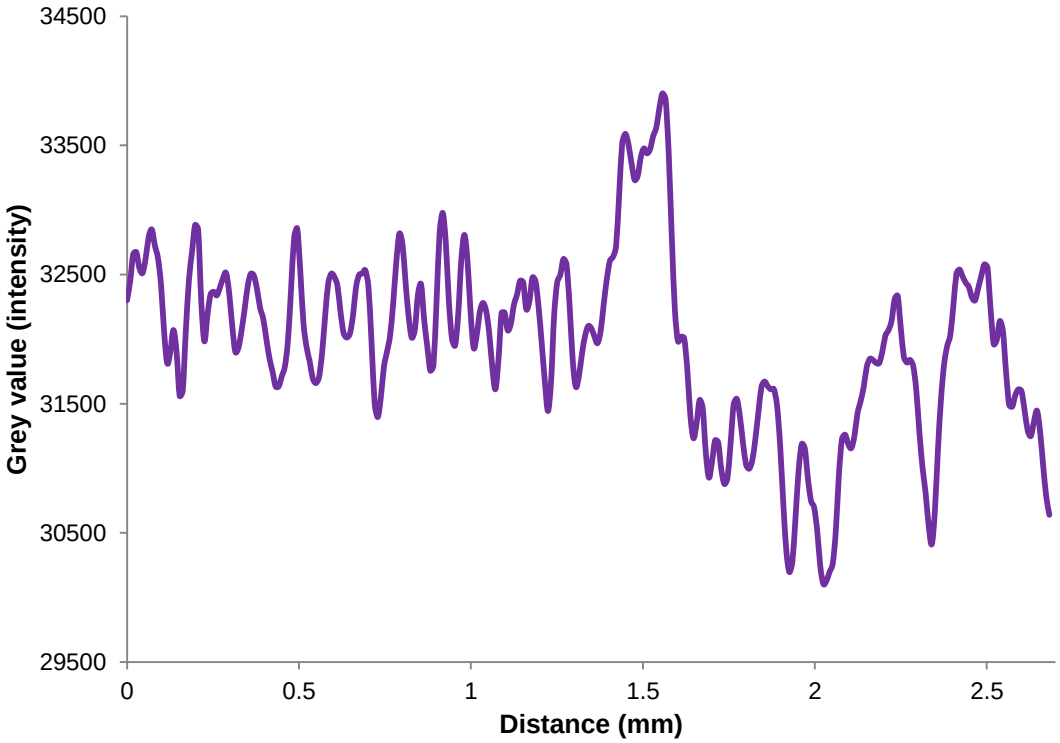

Figure 5-22. Grey value for the vertical dashed purple box from Figure 5-21.

After 120 mins (scan 3A) for the 5 µl water droplet, the volume of the droplet had increased beyond 126% indicating sufficient sucrose is now within the droplet to saturate the droplet, assuming that only sucrose has entered the droplet from the suspension and it is this sucrose which is responsible for the volume increase. For the 10 µl water droplet, it took longer than 120 mins to reach a similar increase in

volume. Even after this volume increase due to sucrose entering the droplet, the droplet continued to grow, indicating more sucrose than that which can be dissolved is entering the droplet and therefore, some of the sucrose within the droplet will be within the solid phase. The volume increase for the smaller 5 µl droplet, at a faster rate is believed to be due to the surface area to volume ratio of the droplet which was mentioned previously.

An enlarged image of scan 9A from Figure 5-1 which was taken after 1080 mins can be seen in Figure 5-23. As mentioned, after the droplet movement into the suspension slows down as the capacity to take any further sucrose from the bulk suspension is not possible, leads to a phase of water now moving out as shown schematically in Figure 5-11 as stage 5, which is believed to be responsible for the further axial spreading of water. This is highlighted in Figure 5-23 with a dashed red line and labelled as water front. Water will continue to move as the system is not in equilibrium due to the water gradient between the different regions present.

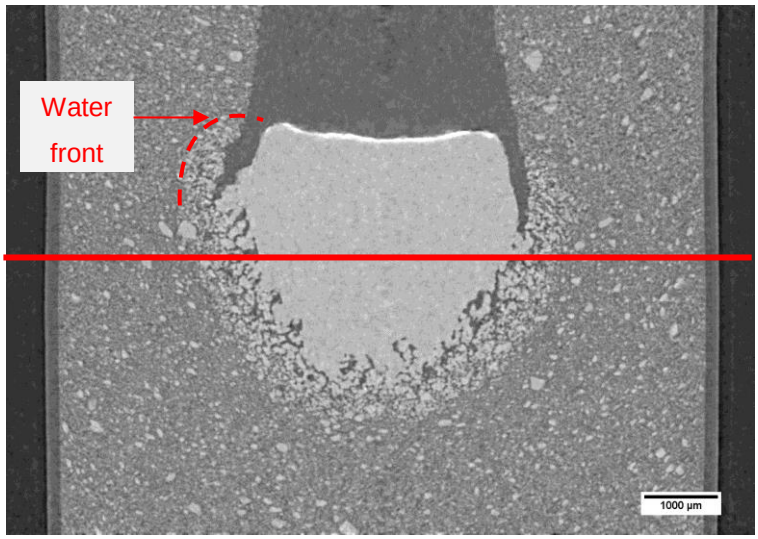

Figure 5-23. Enlarged image of scan 9A from Figure 5-1.

An axial slice along the Y-axis (in relation to Figure 3-13) for the solid red line shown Figure 5-23 can be seen in Figure 5-24. At the centre of the image on the left, the droplet of water and sucrose can be seen in the centre with a layer of oil around it, then some further spreading axially of the water into the surrounding suspension. For the image on the right, the threshold was adjusted to remove the

oil and sample holder, isolating the water and sucrose phase. The larger sucrose crystals within the suspension can be seen, but around the bulk water in the centre, an outer circle can be seen which shows how far the water has spread. There also seems to be a consolidation of sucrose particles which are attracted towards water, due to their hydrophilic nature.

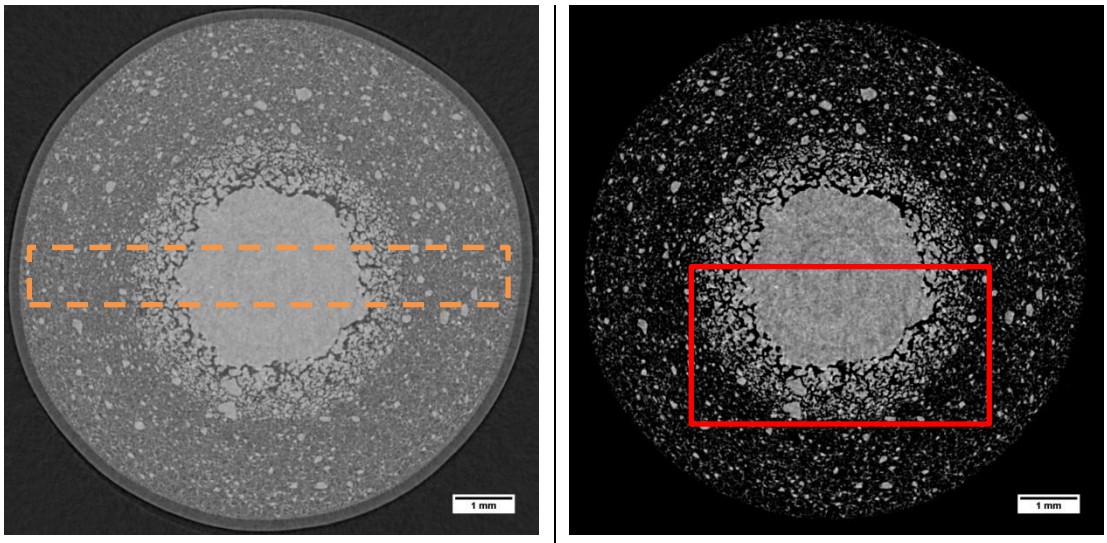

Standard slice | After adjusting threshold

Figure 5-24. Axial slice from Figure 5-23 before and after adjusting threshold.

A plot of the change in the grey value for the vertical dashed region (orange box) from Figure 5-24 can be seen in Figure 5-25. It can be seen how the region of sucrose and sunflower oil (between 0 – 2 mm) has a consistent greyscale value and as you approach the centre of the image (between 2 – 3 mm), there is a sudden sharp increase in the grey value to where the sucrose and water is located (between 3 – 6 mm), and then a sharp decrease back down (between 6 – 7 mm) as the area of sucrose and sunflower oil on the right of the image (between 7 – 9 mm) is approached. This demonstrates the clear changes in the transformation between the different regions, which can be tracked quantitatively due to the high resolution offered by the scans conducted at the synchrotron facility.

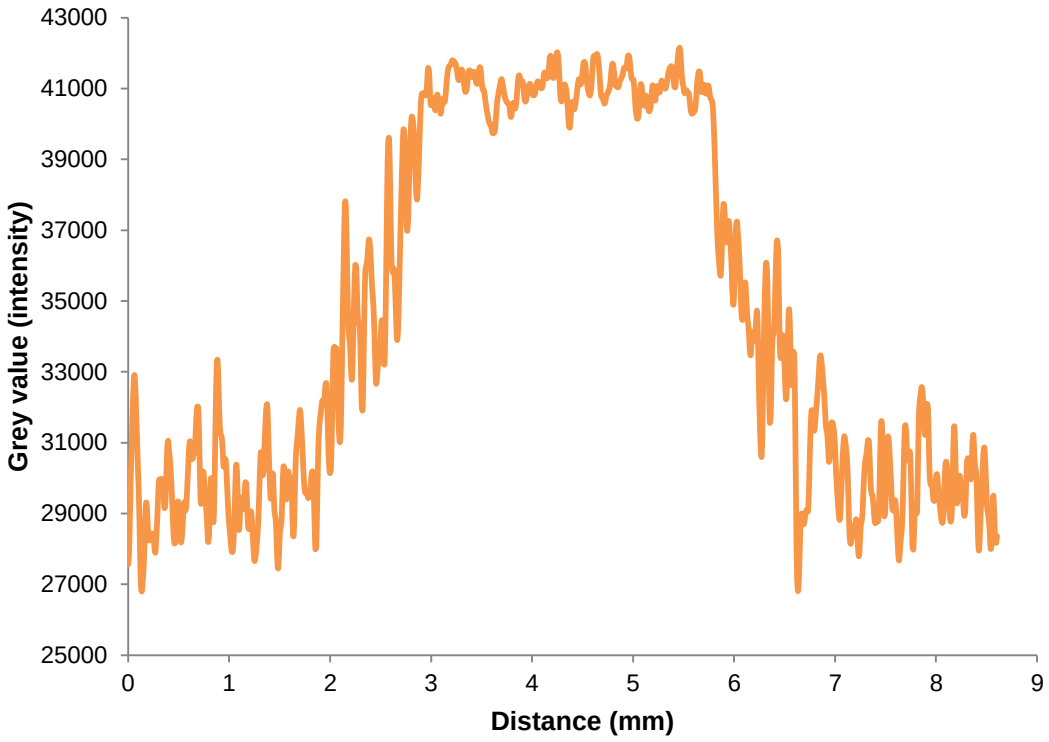

Figure 5-25. Grey value for the vertical dashed orange box from Figure 5-24.

Figure 5-24 demonstrates an axial spread which cannot be attributed to gravitational effects. Thus, this indicates other mechanisms are driving the movement of the water away from the bulk of the water and into the suspension. A magnified image for the red rectangle box from Figure 5-24 can be seen in Figure 5-26. The additional region in which the water has reached has been highlighted by the region present between the two dashed red lines. It can be seen that there is the presence of bridges between sucrose particles, which is believed to be formed by the movement of water away from the bulk in the centre and into the surrounding bulk suspension.

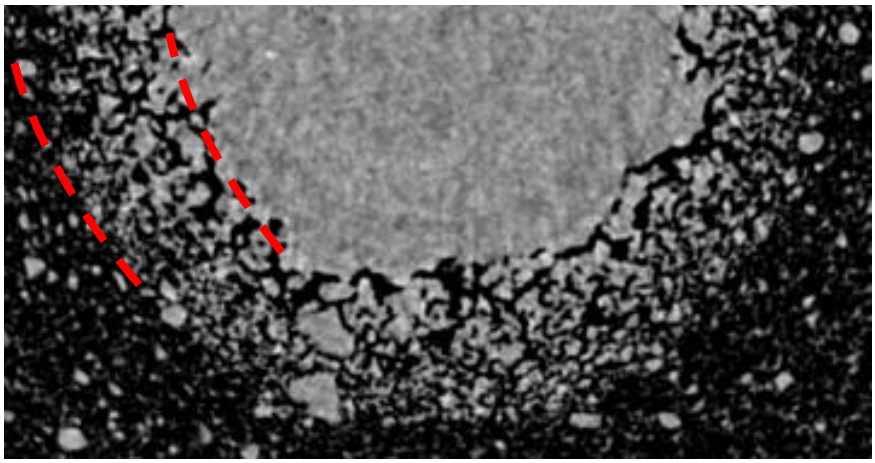

Figure 5-26. Magnified image of red rectangle from image in Figure 5-24.

5.4 Conclusions

In this chapter, it was shown the advantage offered by synchrotron X-ray facilities over benchtop X-ray CT systems (presented in Section 4.3.2), in tracking the movement of water when applied to a suspension of sucrose and sunflower oil. This was mainly due to the significant improvement in image quality, after conducting the scan which allowed the microscopic details including the presence of individual sucrose particles to be seen. This was not possible with conventional benchtop X-ray CT systems.

From these high quality scans, it was possible to identify two movement mechanisms taking place, in sequence (after the completion of one, the start of the next). The first being the movement of sucrose from the bulk suspension into the water droplet as it progresses into the suspension. This continued as long as the water droplet had the capacity (internal volume) to take up sucrose. Once the droplet of water was fully occupied by solid sucrose, this was followed up by the movement of the sucrose solution away and into the bulk suspension to further drive the movement and contact with additional solid sucrose. These different stages were shown schematically to demonstrate the transition from the sucrose moving into the water droplet followed by the water/sucrose away from the bulk.

It was also shown how from the high resolution scans conducted at the synchrotron facility, it was possible to quantitatively track the movement of sucrose by following the change in grey value of the water droplet with time. The presence of sucrose

within the water droplet led to an increase (shift towards the right, from black and towards white) in the grey value. It was also demonstrated, how the surface area to volume ratio plays an important role in the rate of movement of sucrose from the bulk suspension into the water droplet, due to the area of contact present for different water volume droplets.

As well as studying early stages of movement for the water droplet after initial addition, longer term scans were conducted to better understand how the kinetics change with time. The results indicate that though the movement in the vertical direction is driven by the capacity of the water droplet to take up sucrose from the bulk suspension and is not driven by gravity, once the droplet is fully occupied by water, further spreading axially and vertically below the droplet takes place at a substantially slower rate.

Chapter 6 Effect of changing secondary immiscible liquid

6.1 Introduction

In Chapter 4 the macroscale movement of water and in Chapter 5 the microscale movement of water was investigated. As the water droplet progresses into the suspension of sucrose and sunflower oil, it is known to take up sucrose which dissolves into the droplet and changes the liquid properties such as viscosity, density and surface tension.

To further develop on this, the effect of changing the properties of the secondary liquid was investigated, to understand how this changes the dynamics of the kinetics taking place within the system.

6.2 Materials & Methods

Samples were prepared as mentioned in Section 3.2.9 for sucrose and sunflower oil suspensions. The secondary immiscible liquids used were water, sucrose solutions, saturated sucrose solution, saturated fructose solution and glycerol. Viscosity measurements were conducted using the cone and plate geometry using the methodology mentioned in Section 3.2.4.

All X-ray scans presented in this section were conducted at the Canadian Light Source synchrotron facility (Saskatoon, Canada), which offered the opportunity to see the microscopic detail. The diameter of the sample holder used for the X-ray experiments was 5.75 mm, to allow scans to be conducted at a higher pixel resolution in comparison to scans from Chapter 4 and Chapter 5. The X-ray energy used was 25 keV. The effective voxel size used was 6.4 µm. The scan duration was approximately 12 minutes. Full details of the set-up used can be found in Section 3.2.11.2.

6.2.1 Secondary Liquid Characteristics

In this chapter the effect of changing the characteristics of the secondary liquid was evaluated. This was achieved by varying the sucrose concentration of the secondary liquid, the viscosity of the secondary liquid, the density of the secondary

liquid as well as the surface tension. The liquids used to achieve this were distilled water, sucrose solutions (10 % wt., 30 % wt., 40 % wt. and 67 % wt.), saturated fructose solution and glycerol.

6.3 Results & Discussions

6.3.1 Rheological and Wetting Properties

Experiments were conducted to investigate the rheological properties of the secondary immiscible liquids used for this research which can be seen in Figure 6-1. Also the effect of increasing the concentration of sucrose solution upon the viscosity was measured (% relates to mass fraction). The purpose of looking at the effect of increasing the sucrose concentration is that once the water droplet is added to the suspension of sucrose and sunflower oil, it is believed that as the water progresses into the suspension, sucrose particles enter into the droplet and dissolve. This in turn will result in an increase in viscosity of the secondary liquid droplet. Also, this will give an indication if the movement of the secondary liquid is driven due to density differences between the different phases or other factors such as the sucrose solubility within the secondary liquid.

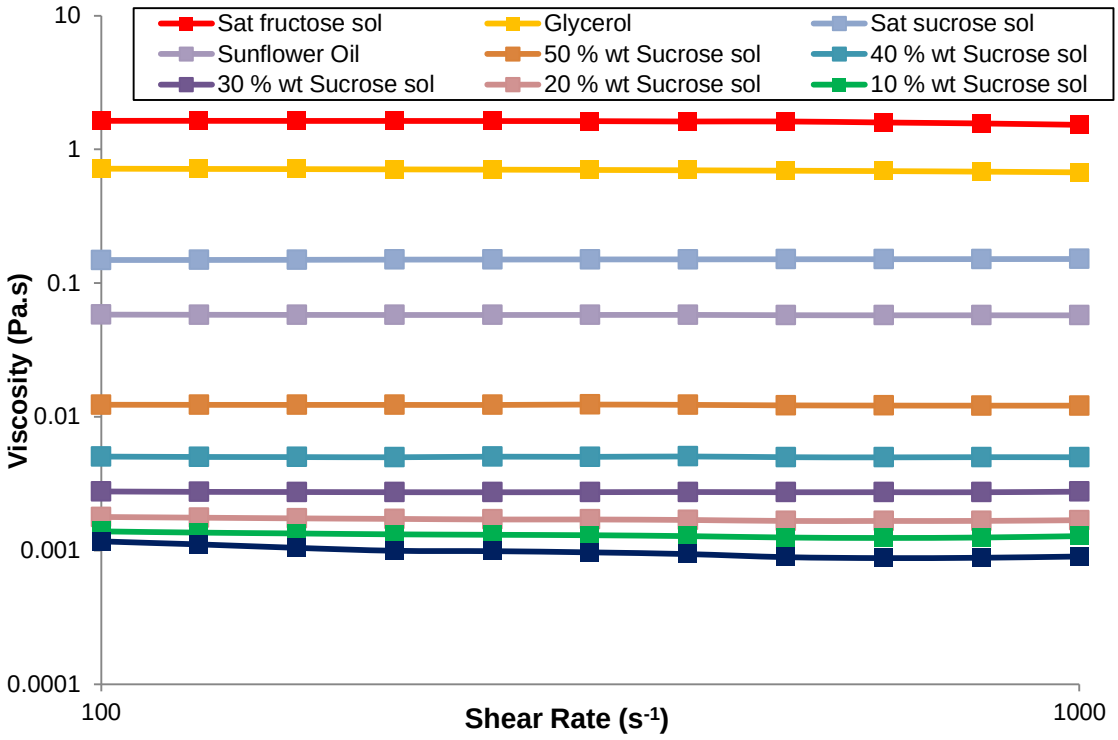

Figure 6-1. Viscosity measurements of different secondary immiscible liquids.

All the liquids showed Newtonian behaviour, as can be seen in Figure 6-1. From the samples measured in Figure 6-1, it can be seen saturated fructose solution has the highest viscosity, which is approximately 1600 times higher than that of water and 10 times more viscous than a saturated sucrose solution. Also the solubility of fructose in water is higher than that of sucrose in water (81 % wt. fructose, 68 % sucrose at 25°C (Bucke, 1995, Danisco, 2003)). Glycerol has a viscosity approximately 700 times higher than that water, however, the solubility of sucrose is substantially lower in comparison to water (7 % wt. at 25°C (Bucke, 1995)).

The relationship between sucrose concentration and viscosity can be seen in Figure 6-2 and Table 6-1. For a 40 % wt. sucrose solution, the increase in viscosity is roughly 5 times more than water. For a further 10 % wt. increase in sucrose to 50 % wt. of sucrose, the viscosity more than doubles in comparison to the viscosity at 40 % wt. If viscosity and density play a key role in the movement of the secondary liquid within the suspension, it can be seen how considerably they change as sucrose is dissolved in water to make solutions (Table 6-1).

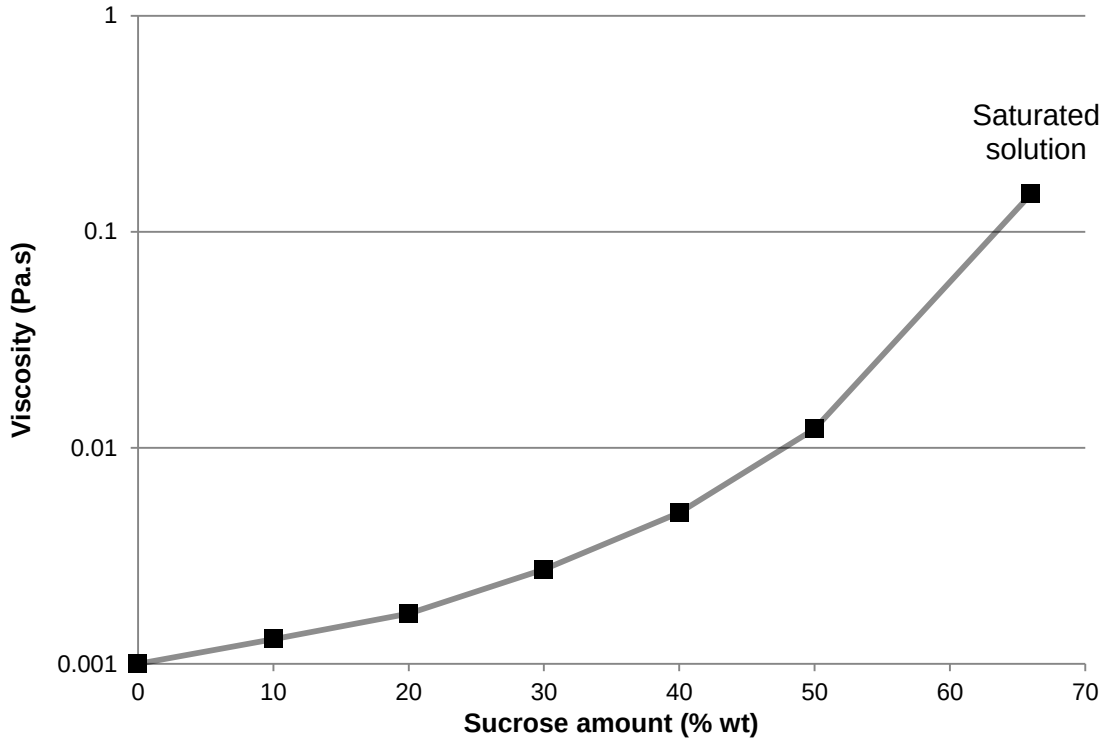

Figure 6-2. Viscosity measurements for different concentration sucrose solutions (from distilled water (0 % wt.) to saturated sucrose solution (67 % wt.) at 25°C, average value for shear rate range between 100 – 1000 s^{-1}).

Table 6-1. Viscosity and density values for water and sucrose solutions.

	Viscosity (mPa s)	Density (kg/m^3)[1]
Distilled water	0.98	1000.00
10 % wt. sucrose solution	1.30	1039.98
20 % wt. sucrose solution	1.71	1082.87
30 % wt. sucrose solution	2.74	1128.98
40 % wt. sucrose solution	5.00	1178.53
50 % wt. sucrose solution	12.2	1231.74
Saturated sucrose solution	150	1337.08

[1] Values from Asadi (2005) at 25°C.

The rheological properties for different mass fractions of sucrose and sunflower oil suspensions were measured using the serrated plate geometry (Section 3.2.4), which can be seen in Figure 6-3. It can be seen that as the mass fraction of the solid sucrose is increased from 50 % wt., to 55 % wt. then 60 % wt. (by reducing

the oil mass fraction), the viscosity increases which is expected. Once a suspension sample is prepared (50 % wt.), it is known that the sucrose particles will settle creating a small layer on the surface of the suspension. It is thought this is the reason for the channel formation once the secondary liquid droplet has penetrated into the sample, is able to maintain its structure. This can also be seen visually in Figure 6-4, as the sample with a higher solid mass fraction does not spread as easily and maintains its shape (even after 72 hours).

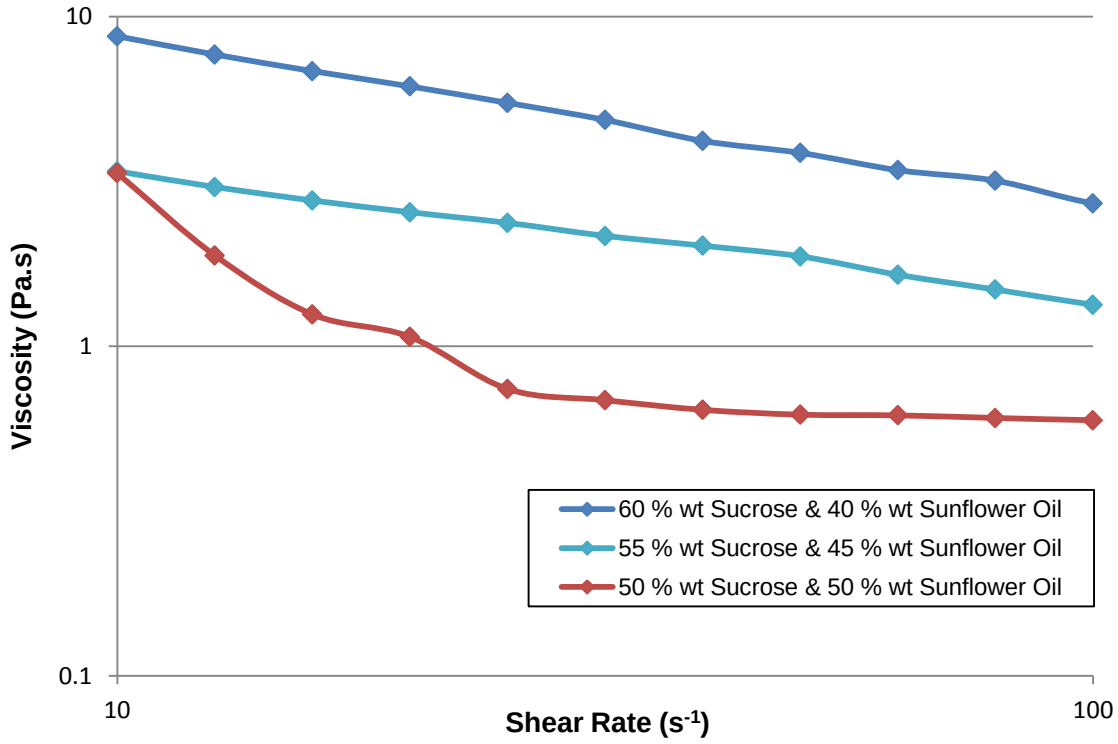

Figure 6-3. Viscosity measurements for different mass fraction of sucrose and sunflower oil suspensions.

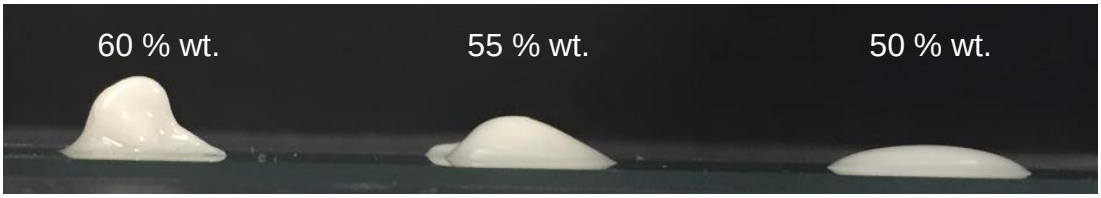

Figure 6-4. Different sucrose solid mass fraction suspensions.

The surface tensions of the secondary liquids in both air and sunflower oil can be seen in Table 6-2. It can be seen that the highest surface tension was recorded for fructose, followed by sucrose, then water and finally glycerol.

Table 6-2. Surface tension measurements for secondary liquids.

	Surface tension (mN/m)	Interfacial tension in sunflower oil (mN/m)[1]
Distilled water	68.84 ± 0.4	26.4 ± 0.1
Saturated sucrose solution	76.12 ± 0.1	25.1 ± 0.2
Saturated fructose solution	90.74 ± 0.2	-
Glycerol	62.51 ± 0.5	17.7 ± 0.5

[1] Values from Negreiros et al. (2015).

The contact angle was measured on large sucrose crystals, as shown in 3.2.3. Measurements were conducted directly on sucrose crystals, and on sucrose crystals which were immersed in oil. A graph showing the measurement of water on the surface of a sucrose crystal can be seen in Figure 6-5. It can be seen that the graph does not reach complete steady state (though does seem to be approaching it), and due to the nature of the system the water will dissolve some sugar from contact surface of the sucrose. This will also in turn affect the viscosity and composition of the liquid, as it is no longer pure water and thus making it difficult to measure the absolute contact angle. The values shown in Table 6-3 are an average of the final 60 readings (1 minute) over the 10 minute period which the readings were taken.

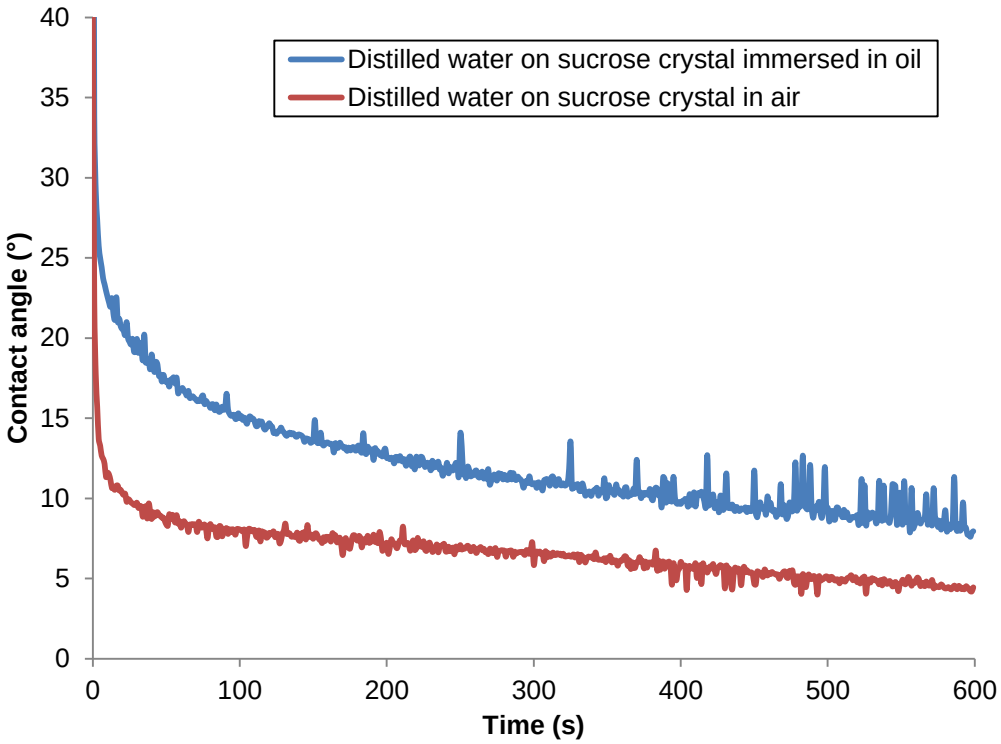

Figure 6-5. Contact angle measurement of distilled water on a sucrose crystal in air or in oil.

From Table 6-3, it can be seen that water had the lowest contact angle value when applied on a dry sucrose crystal and a sucrose crystal covered in oil in comparison to the other secondary liquids used (saturated sucrose solution, saturated fructose solution and glycerol), which is believed to be due to hydrophilic nature of the large sugar crystal. This is followed by glycerol, then fructose and finally the saturated sucrose droplet which has no capacity to dissolve any further sucrose. The effect of the introducing the oil layer on top of the sucrose crystal increased the contact angle value between the secondary liquid and the sucrose crystal.

Table 6-3. Contact angle measurements conducted on large sucrose crystals.

	Contact angle in air (°)	Contact angle in oil (°)
Distilled water	4.59 ± 0.26	8.79 ± 0.91
30 % wt. sucrose solution	7.81 ± 0.18	19.89 ± 0.17
Saturated sucrose solution	34.46 ± 0.07	36.33 ± 0.11
Saturated fructose solution	29.62 ± 0.33	35.14 ± 0.18
Glycerol	14.35 ± 0.24	30.23 ± 0.16

6.3.2 Varying Sucrose Concentration

X-ray scans were conducted on suspensions of sucrose and oil (50 % wt. for both) to which a fixed volume of 5 µl secondary liquid was added to the surface of the suspension. The secondary liquids added were distilled water, 10 % wt. sucrose solution, 30 % wt. sucrose solution, 40 % wt. sucrose solution and a saturated sucrose solution. Water has the greatest affinity and ability to dissolve sucrose, whereas saturated sucrose solution has no affinity to dissolve any further sucrose at 25°C, thus allowing the two extremes in terms of sucrose solubility to be investigated in driving the movement of the secondary liquid within the suspension.

Scans taken after 150 minutes from initial addition can be seen in Figure 6-6 for water, 10 % wt. sucrose solution, 30 % wt. sucrose solution, 40 % wt. sucrose solution and saturated sucrose solution all of the same volume (5µl). The images displayed are along the X-axis in relation to Figure 3-13, for the slice in which the diameter of the secondary liquid droplet is the largest. It can be seen that the water droplet has progressed the furthest into the suspension, followed by the 10 % wt. sucrose solution. The 30 % wt. sucrose solution is still holding onto the surface of the suspension as well as the saturated sucrose solution. For the 40 % wt. sucrose solution, it can be seen that the droplet has moved a small amount into the suspension. Assuming the penetration of the secondary liquid was dominated by the density of the secondary liquid (Table 6-1, due to gravity), the saturated sucrose solution would have penetrated the furthest in comparison to the other 4 secondary liquids mentioned. However, it can be seen this is not the case, though, if viscosity was a key factor, this would agree with the trend displayed so far. For

the saturated sucrose solution, there has been virtually no movement from the surface of the suspension, with the droplet clearly in contact with the oil/air interface.

The volumes of the droplets were measured for the different liquids in Figure 6-6 which can be seen in Figure 6-7. The initial volume of all droplets deposited using the pipette was 5 µl (5 mm^3), and it can be seen after 150 minutes, the water droplet has increased the greatest extent to approximately 8.1 mm^3 indicating it has taken up the greatest amount of sucrose from the bulk suspension, followed by the 10 % wt. sucrose solution with a volume of 7.7 mm^3, then with the 30 % wt. and 40 % wt. sucrose solutions with a volume of 6.1 mm^3 and 5.8 mm^3, respectively.

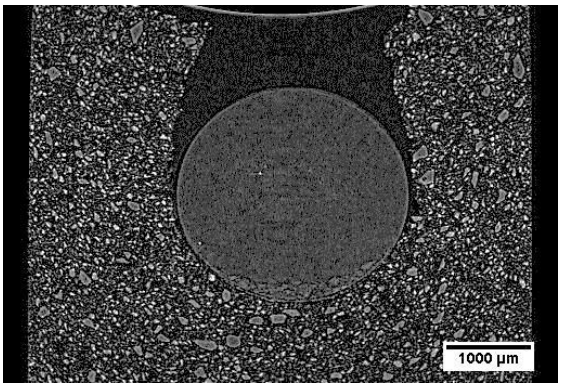

Water

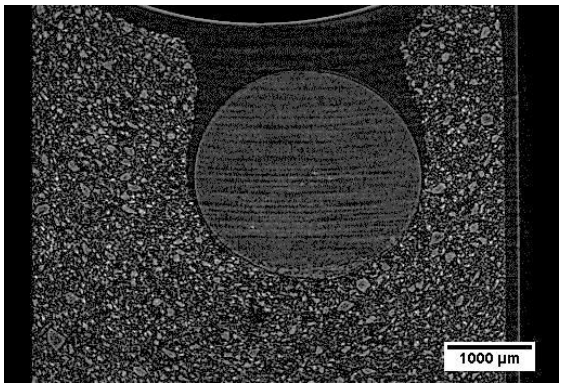

10 % wt. Sucrose Solution

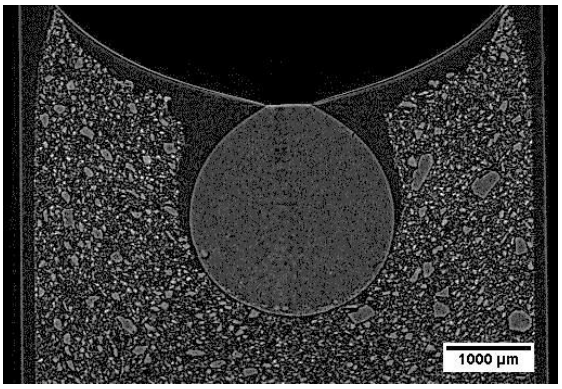

30 % wt. Sucrose Solution

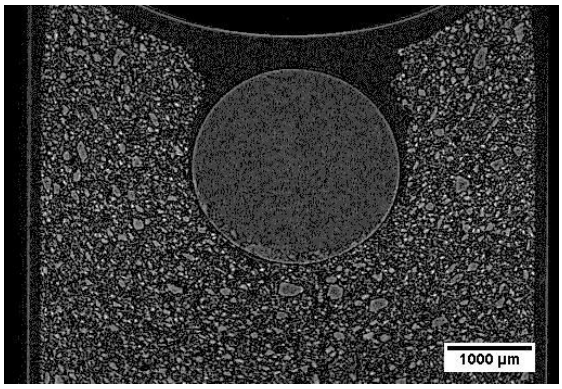

40 % wt. Sucrose Solution

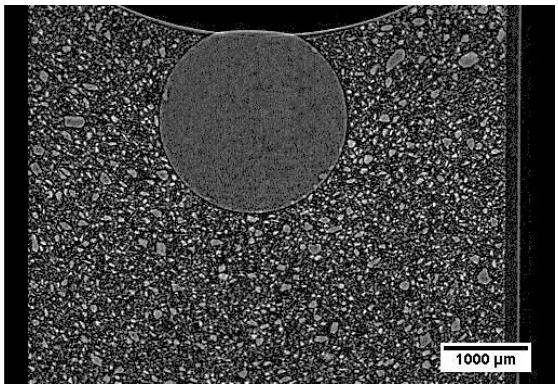

Saturated Sucrose Solution

Figure 6-6. After 150 mins of central slice along X-axis (where diameter of droplet is largest), for 5 µl droplet. Scale on images is 1 mm.

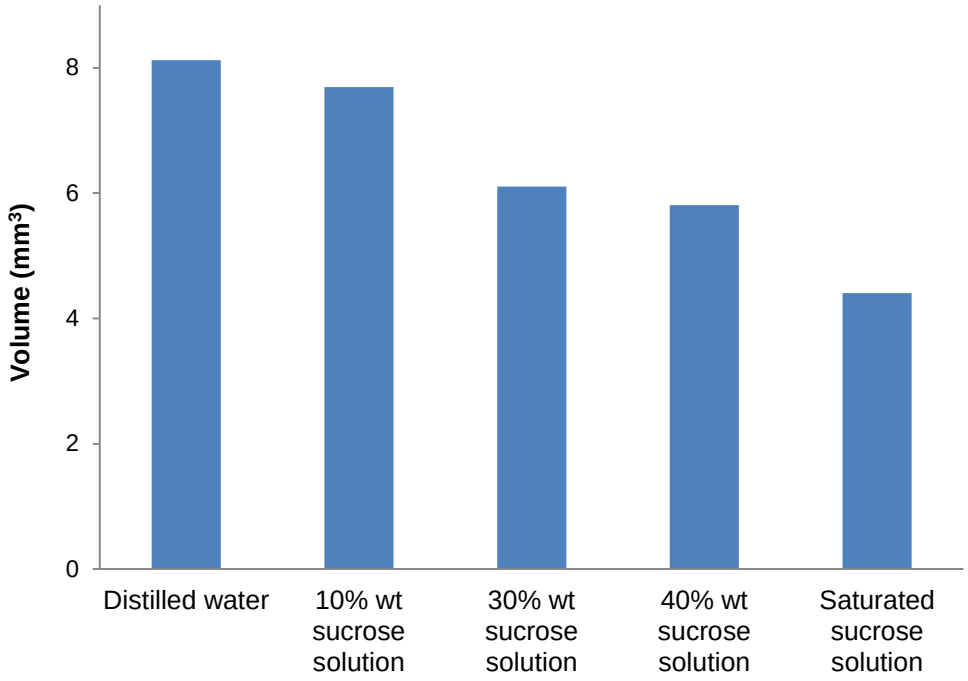

Figure 6-7. Volume of the droplets from the images in Figure 6-6 after 150 minutes.

Further scans were conducted after 300 minutes, for the samples mentioned in Figure 6-6 which can be seen in Figure 6-8. The same trend continues with the water droplet moving the greatest into the suspension and increasing the most in volume, whereas, for the saturated sucrose solution there has been virtually no change in volume or movement into the suspension. There is some settling of the surrounding sucrose particles from the bulk suspension within the image for the saturated sucrose solution which can be seen near the top portion of the suspension. The volume of the secondary liquid droplet from the images in Figure 6-8 can be seen in Figure 6-9. One possible reason for the saturated sucrose solution not moving at all is believed to be due to the droplets inability to take up sucrose, due to already being at the saturation point.

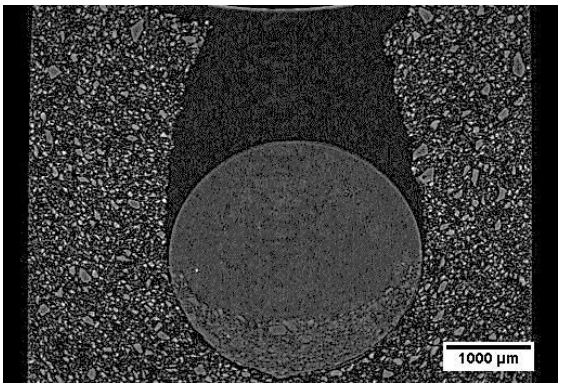

Water

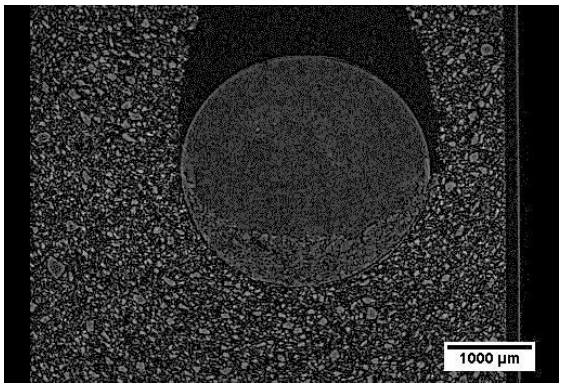

10 % wt. Sucrose Solution

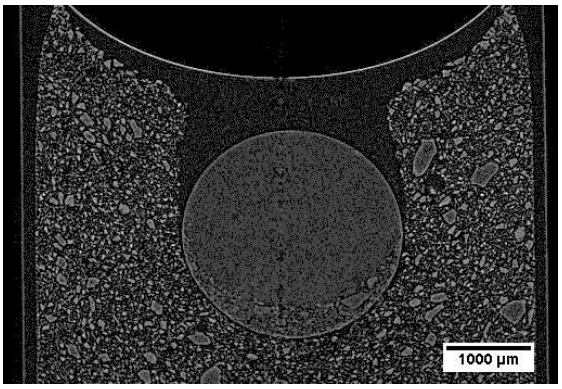

30 % wt. Sucrose Solution

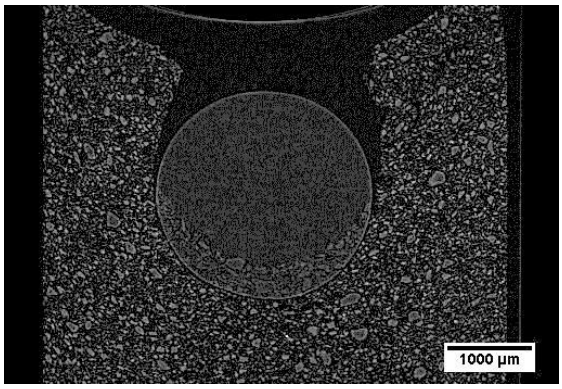

40 % wt. Sucrose Solution

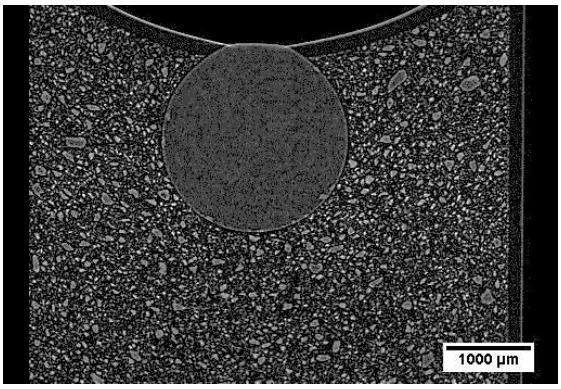

Saturated Sucrose Solution

Figure 6-8. After 300 mins of central slice along X-axis (where diameter of droplet is largest), for 5 µl droplet. Scale on images is 1 mm.

The water droplet has increased in volume from 8.1 mm^3 to 10.4 mm^3, an increase of 2.3 mm^3 after a further 150 minutes (300 minutes in Figure 6-9). The 10 % wt. sucrose solution increased from 7.7 mm^3 to 9.8 mm^3, which is an increase of 2.1 mm^3, whereas in the same period the 40 % wt. sucrose solution increased from 5.8

mm^3 to 6.6 mm^3, an increase of only 0.8 mm^3. Finally, the saturated sucrose solution showed no change in volume.

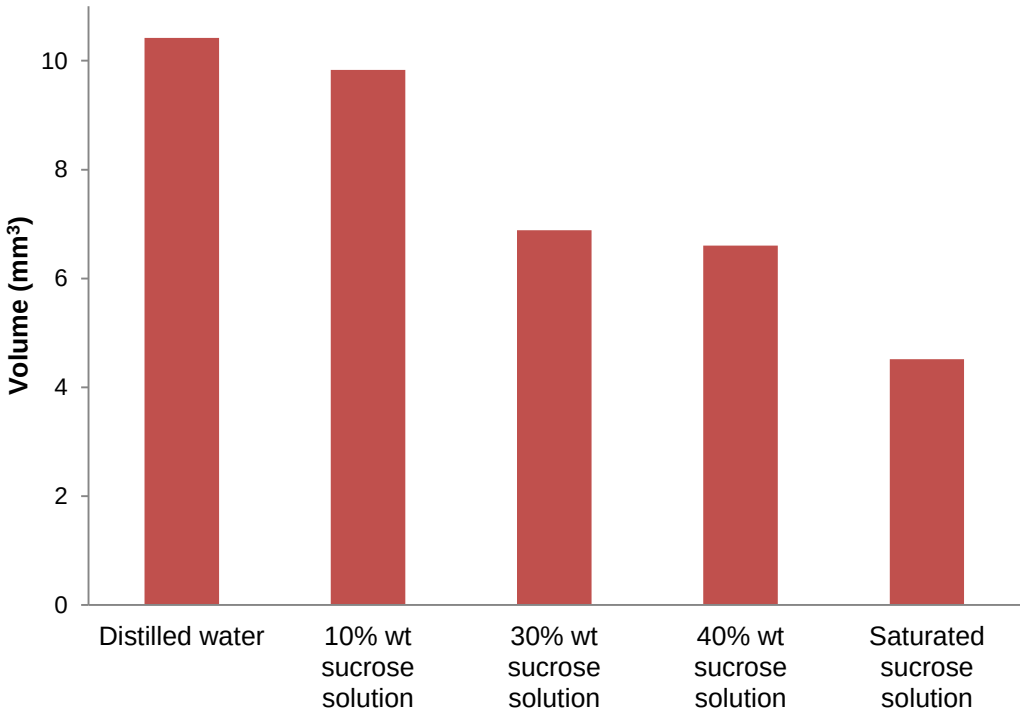

Figure 6-9. Volume of the droplets from the images in Figure 6-8 after 300 minutes.

As mentioned previously in Section 4.3.6, for a fixed volume of water to achieve saturation with sucrose would result in a 126 % increase in volume. Therefore for a 5 µl (5 mm^3) water volume to become saturated with sucrose, the increase would be 6.3 mm^3 to have a total volume of 11.3 mm^3. A scan was conducted after 630 minutes for the 5 µl water sample which can be seen in Figure 6-10. After 630 minutes, the droplet now has a total volume of 18.2 mm^3, which is above the 11.3 mm^3 required to achieve complete saturation with sucrose. A magnified image focusing only on the droplet from Figure 6-10 can be seen in Figure 6-11. The level of where the solid sucrose has entered and reached inside the droplet can be seen and is highlighted by a red dashed line. Also individual large sucrose crystals can be seen. These can only be seen due to the use of the synchrotron facility, which offers substantially improved scan and image quality in comparison to scans conducted on benchtop X-ray CT systems, which were shown in Section 4.3.2.

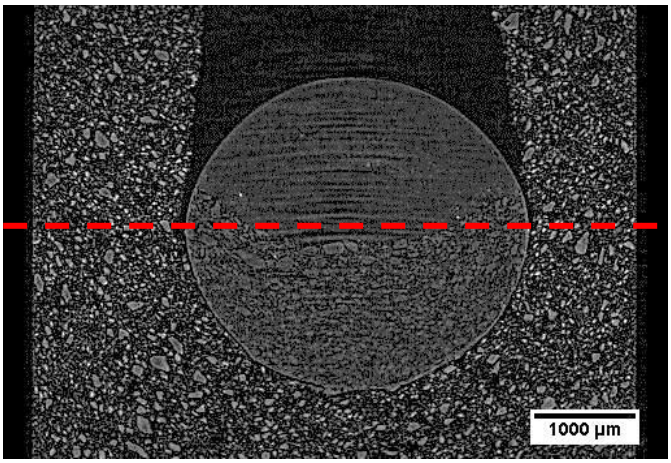

Figure 6-10. After 630 mins of central slice along X-axis (where diameter of water droplet is largest), for 5 µl water droplet.

Also the curved solid red line in Figure 6-11 solid sucrose front within the droplet, agrees with the 3D volume rendering shown in Figure 5-6 & Figure 5-8, once the oil phase was masked out. The top crater is due to the presence of sucrose which initially entered the droplet and continued to progress further into the droplet.

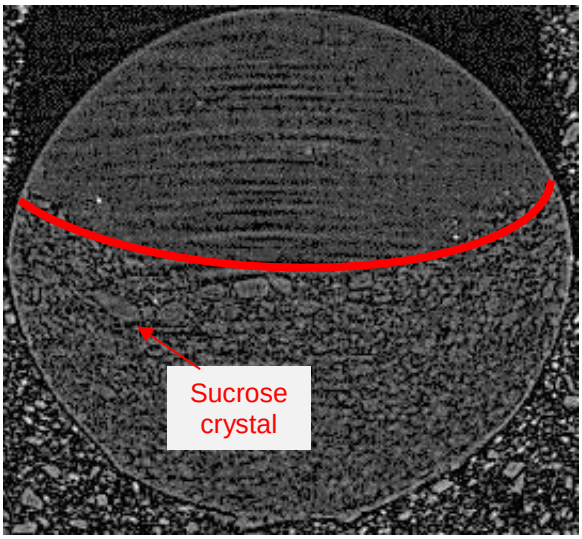

Figure 6-11. Magnified image of the droplet only from Figure 6-10.

The slice for the red dashed line in Figure 6-10 along the Y-axis can be seen in Figure 6-12. It can be seen how solid sucrose crystals are present within both the bulk suspension and the water droplet. The central most region of the secondary liquid droplet is clear, indicating no presence of solid sucrose, and while moving away from the centre of the droplet to the outer region, the presence of solid sucrose can be seen. This is due to the sucrose from the bulk suspension entering

into the droplet at the interface between the two. Therefore the solid sucrose will gradually approach the centre as new solid sucrose enters from the bulk suspension.

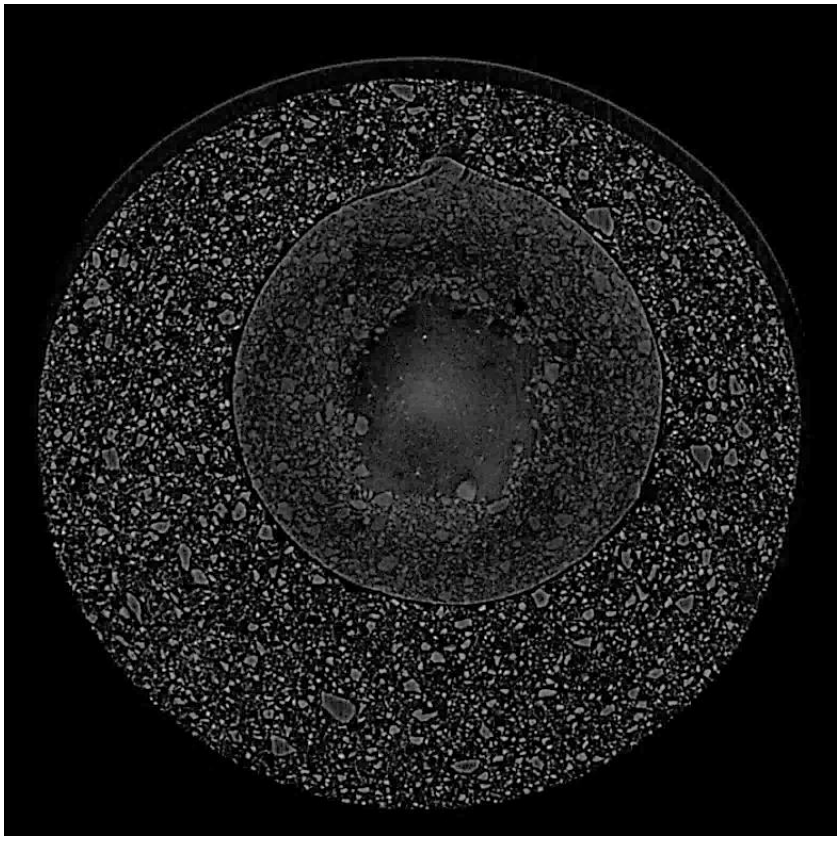

Figure 6-12. Slice along Y-axis from Figure 6-10.

6.3.3 Long Term Experiments

Some long term scans were conducted to better understand how the behaviour and dynamics of the system changes. The hypothesis is that the water secondary liquid droplet is able to penetrate the furthest into the suspension and take up the greatest amount of sucrose in comparison to the sucrose solutions. To verify this, long term scans were conducted on the sample to which water, 40 % wt. sucrose and saturated sucrose solution was added after approximately 40 hours from initial application of the secondary liquid. These images can be seen in Figure 6-13. The water and 40 % wt. sucrose solution droplet now have a similar distinguished shape to each other, which is very different in comparison to the spherical shape which could be seen in Figure 6-8 and Figure 6-6, for the scans taken much earlier

after addition. However, the water droplet is bigger in both the horizontal and vertical dimension in comparison to the 40 % wt. sucrose solution droplet, even though initially the same volume was added. This is believed to be due to the ability of the droplet to dissolve and take up additional sucrose. For the initial sucrose which enters into the droplet will easily dissolve into the liquid state and allow further sucrose to be taken up. Whereas for the 40 % wt. sucrose droplet, this ability is reduced as the droplet is nearer to the saturation limit initially and thus has limited capacity to dissolve further sucrose. Therefore, any sucrose which does enter will most probably remain in the solid state.

The maximum length in the horizontal and vertical dimension of the distinguished shaped droplet from Figure 6-13 for both the water and 40 % wt. sucrose solution were measured (example can be seen with red arrows in image of water in Figure 6-13). For the water droplet, the maximum horizontal dimension and vertical dimension was 3.8 mm and 3 mm respectively, whereas for the 40 % wt. sucrose solution the maximum dimension measured was 3.2 mm and 2.6 mm, respectively. This clearly shows the significant difference in the final volume for the different liquids.

For the saturated sucrose droplet in Figure 6-13, the volume showed an increase of 0.3 mm^3 from Figure 6-8, after approximately 35 hours. It can be seen the droplet has broken from the surface of the oil layer and the surrounding sucrose particles from the bulk suspension have settled. The timescale of movement, for the saturated sucrose solution which has the highest density from the difference solutions used (Table 6-1), shows that gravity is not the dominating mechanism driving the movement.

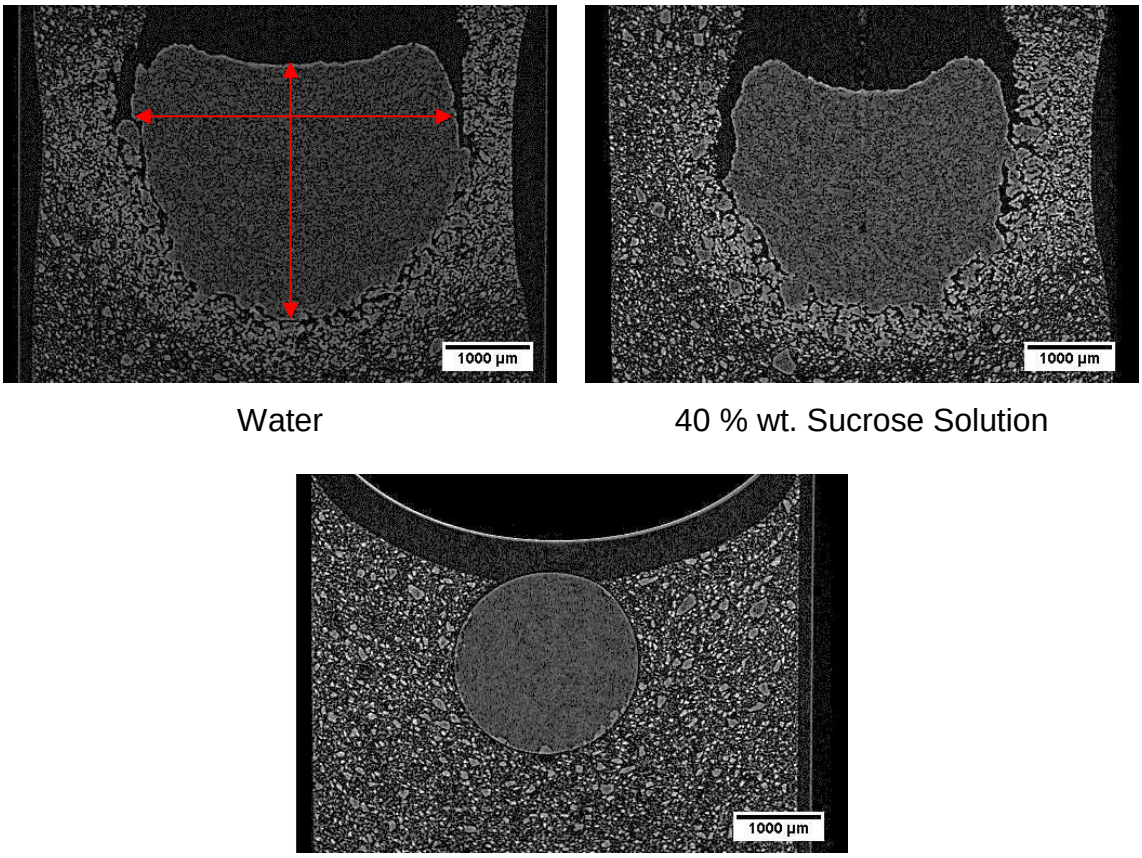

Water

40 % wt. Sucrose Solution

Saturated Sucrose Solution

Figure 6-13. After approximately 40 hours, the central slice along X-axis (where diameter of water droplet is largest), for 5 µl droplet. Scale on images is 1 mm.

A scan was conducted after 102.5 hours for the saturated sucrose sample which can be seen in Figure 6-14. The volume showed an increase of is 0.2 mm^3 from Figure 6-13, after approximately an additional 62 hours. It can be seen some change is occurring, though at a considerably lower speed in comparison to the water and sucrose solutions used.

A slice was taken along the Y-axis, for the red dashed line in Figure 6-14, which can be seen in Figure 6-15. It can be seen that some sucrose crystals are present at the boundary between the saturated sucrose solution and the bulk suspension. It is possible that the increase in volume seen is due to sucrose crystals entering into the droplet from the bulk suspension, or these crystals may have been formed due to the crystallisation of the sucrose droplet near the boundary. It is believed they are more likely due to crystallisation as at the boundary (interface) between the bulk suspension and the saturated sucrose droplet, there is no solid sucrose

crystal present between the two. This would be expected for a sucrose crystal entering from the bulk suspension into the secondary liquid droplet. Also, in Figure 6-14 it can be seen near the top of the saturated sucrose droplet, there is some evidence of solid sucrose being present and at this location there is no contact with the bulk suspension in which sucrose crystals were present.

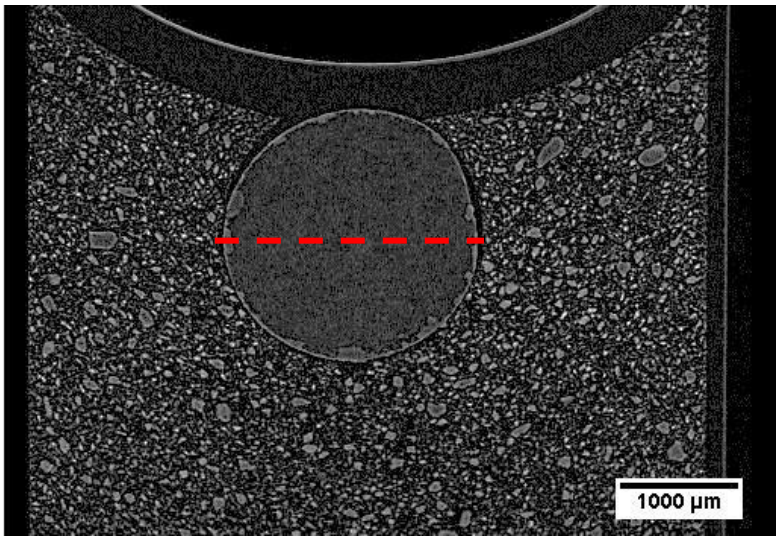

Figure 6-14. After 102.5 hours for 5 µl saturated sucrose droplet.

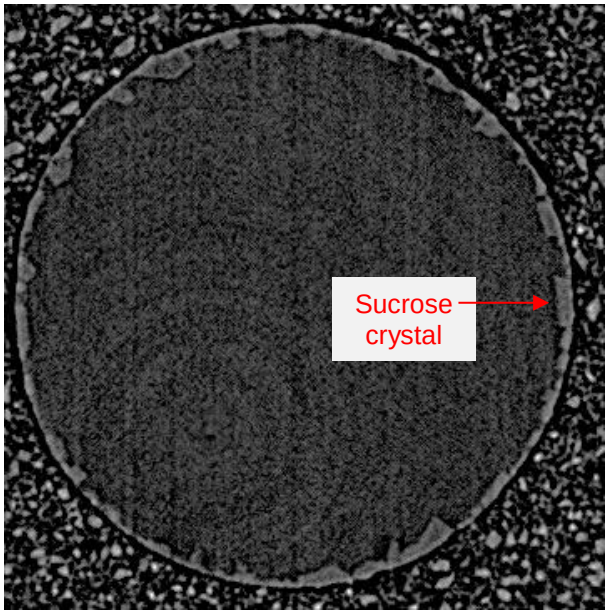

Figure 6-15. Image along Y-axis for 5 µl saturated sucrose droplet after 102.5 hours from Figure 6-14.

6.3.4 Glycerol

Similar scans were conducted on a suspension sample to which a 5 µl glycerol droplet was added to the surface, for which images can be seen in Figure 6-16. Trial scans showed that the behaviour of glycerol is very different in comparison to that of water, in that the movement in significantly slower. Therefore, a plan was engineered to conduct scans after longer periods of storage, which would be required to see any noteworthy change. After 12.5 hours, it can be seen that there is virtually no change to the droplet of glycerol itself, though the surrounding sucrose from the bulk suspension has settled displaying some oil to form a layer on the surface of the suspension (due to density differences and sunflower oil having the lowest density within the suspension). After 22 hours, it can be seen that the droplet is holding onto the oil layer on the surface of the suspension. After 44 hours from the initial droplet of glycerol being added, the surface has completely detached from the surface of the suspension, with further settling of sucrose from the bulk suspension, increasing the layer oil displaced to the surface. In the image after 44 hours, a red arrow is shown to highlight the presence of a large sucrose crystal within the bulk suspension whose movement into the glycerol droplet can be seen after 84 hours in Figure 6-17. Between 44 hours to 84 hours, a noteworthy amount of sucrose has entered the glycerol droplet and occupied the lower region of the droplet. The particular large sucrose crystal from the image taken after 44 hours has been highlighted in Figure 6-17 in the image after 84 hours, showing both its previous location within the bulk suspension which is now a void, as well as its new location within the glycerol droplet.

The density and viscosity of glycerol is lower when compared to that of saturated sucrose solution (Table 6-1). However, as can be seen from the images in Figure 6-16 and comparing those to the images from Section 6.3.3, the behaviour seen is very different, in terms of the movement of the secondary liquid droplet within the suspension both during short and long term storage periods.

The glycerol droplet increased by 0.8 mm^3 in volume within the first 44 hour period from addition (0 – 44 hours). For the next 40 hour period from this (44 – 84 hours)

the droplet increased by 1.9 mm^3, which was a greater increase in volume for a shorter period of time (40 hours as opposed to 44 hours).

When comparing this to the 5 µl water droplet, the water droplet achieved a greater increase in volume in the initial 5 hour period from addition (Figure 6-9), compared to what the glycerol droplet of the same volume achieved in 84 hours. The solubility of sucrose in glycerol is approximately 7%, which is very low in comparison to water which is approximately 67% (Bucke, 1995). Therefore, any sucrose which does enter the glycerol droplet will most likely remain in a solid state. This was confirmed by looking at a slice along the Y-axis from the image after 97 hours in Figure 6-16 (dashed red line) which can be seen in Figure 6-19. A particular large crystal of sucrose has been highlighted to shows its presence within the glycerol droplet. No further scans were conducted after 97 hours.

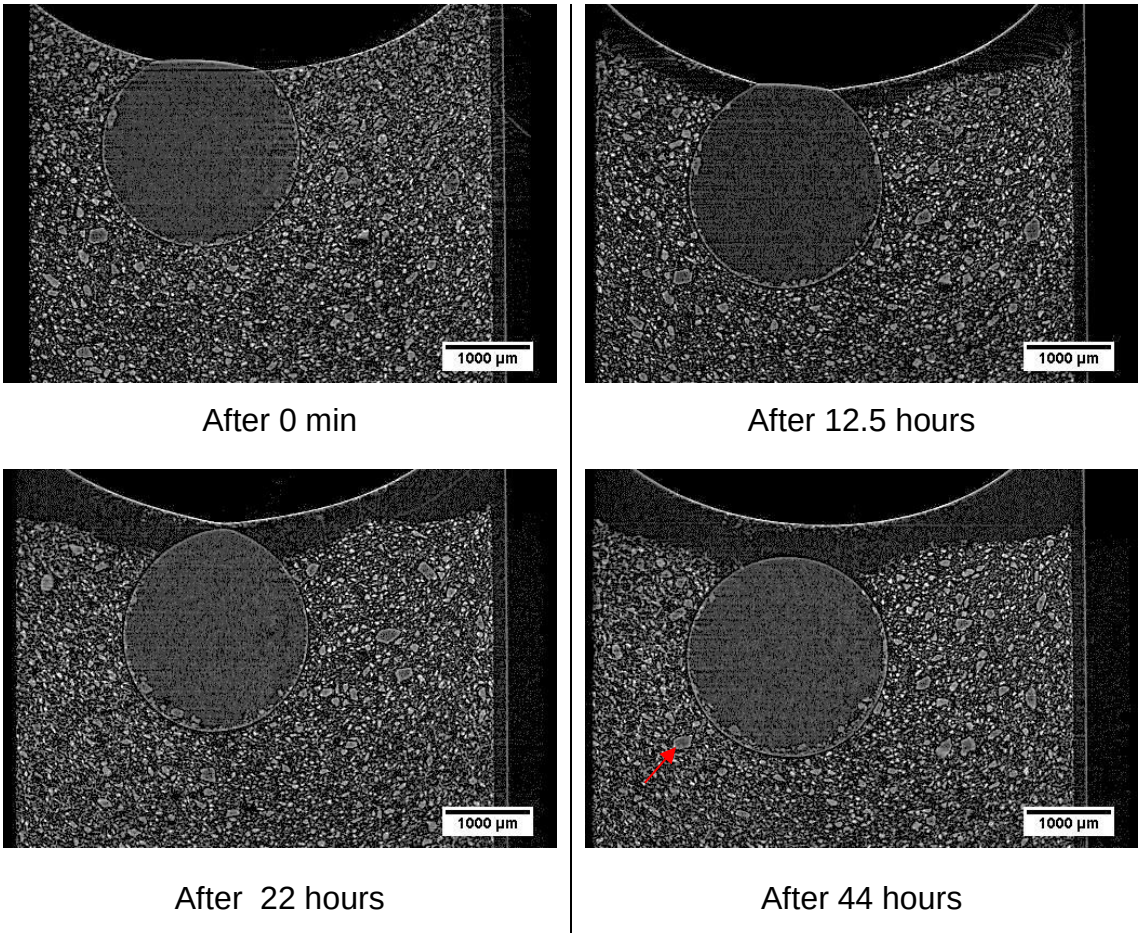

Figure 6-16. Time lapse of central slice along X-axis (where diameter of droplet is largest), for 5 µl glycerol droplet. Scale on images is 1 mm.

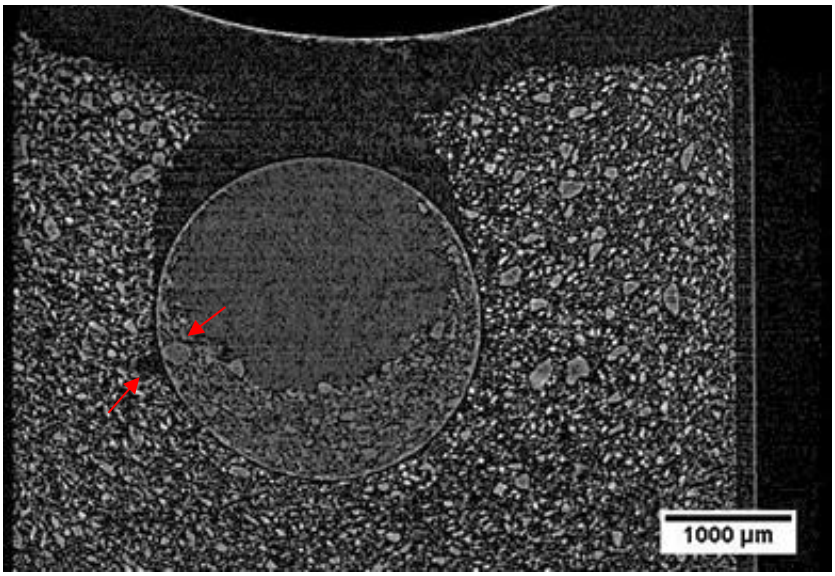

Figure 6-17. After 84 hours for 5 µl glycerol droplet.

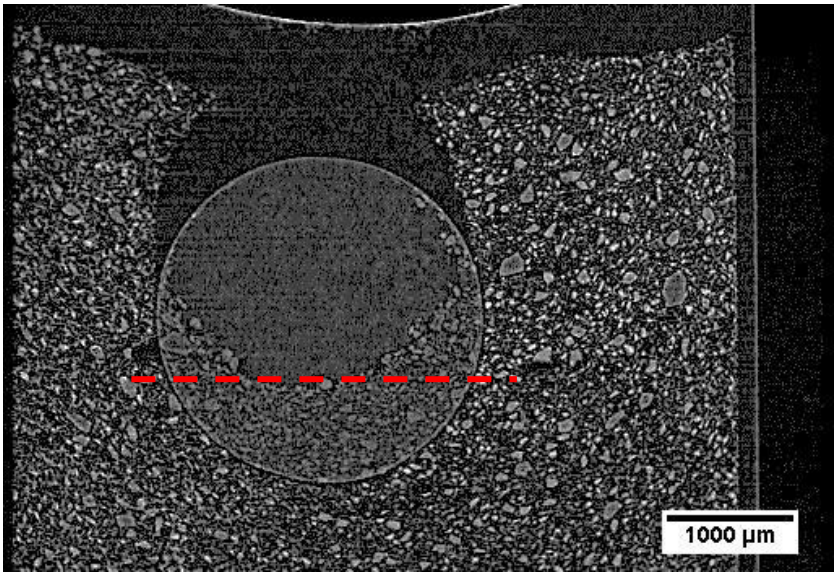

Figure 6-18. After 97 hours for 5 µl glycerol droplet.

Also in Figure 6-19 it appears the packaging arrangement of the sucrose particles is more closer/denser in comparison to the surrounding bulk suspension.

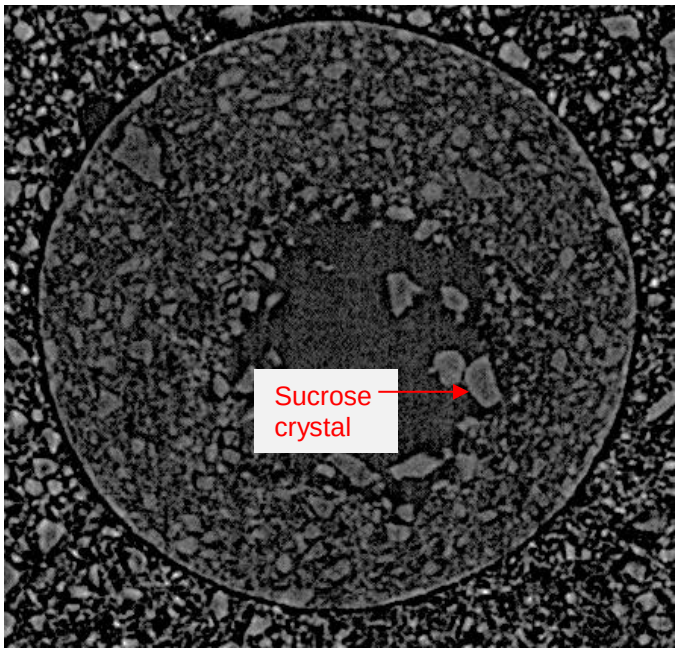

Figure 6-19. Image along Y-axis for 5 µl glycerol droplet after 97 hours from Figure 6-18.

6.3.5 Saturated Fructose Solution

The solubility of sucrose is low in glycerol as shown in Section 6.3.4. Therefore, a saturated fructose solution was chosen as a secondary liquid to see how this would behave when added to a suspension of sucrose and sunflower oil. The reason for this is that a saturated fructose solution still has the capacity to dissolve sucrose. This can be seen in Figure 6-20, which is the three component diagram for a sucrose-fructose–water mixture. Point A (68.2 % wt.) is for a pure saturated sucrose solution and point B (81.5 % wt.) is for a pure saturated fructose solution.

The line A-C signifies a solution saturated with sucrose, to which fructose is being added and line B-C signifies a solution saturated with fructose to which sucrose is being added. Point C in Figure 6-20 is the triple point, for a solution saturated in both fructose and sucrose. The composition of point C is 66 % wt. fructose, 23 % wt. sucrose and 11 % wt. water.

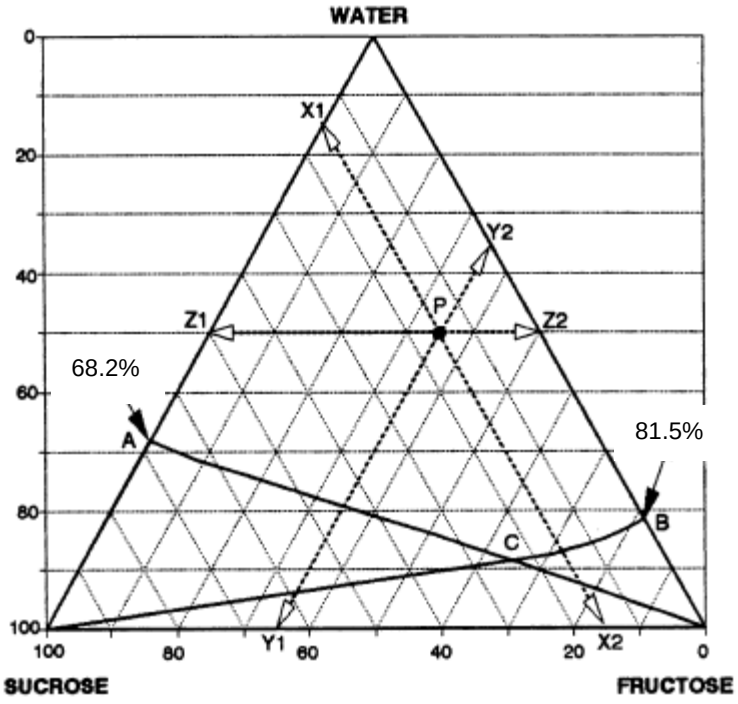

Figure 6-20. Sucrose-fructose-water solution diagram at 30°C (Bucke, 1995). Point A is a saturated sucrose solution (68.2 % wt.) and point B is a saturated fructose solution (81.5 % wt.).

Scans were conducted on a suspension sample to which a 5 µl saturated fructose droplet was added to the surface, for which images can be seen in Figure 6-21. After 48 hours, it can be seen that the droplet has detached from the surface, but remains very close to the top of the suspension and the surrounding sucrose from the bulk suspension has settled creating a layer of oil on the surface. After 83.5 hours (an addition 35.5 hours) there has been very minimal change in the size (volume) of the droplet as well the location of the droplet. This is the same after 97 hours in Figure 6-21. No further scans were conducted after 97 hours.

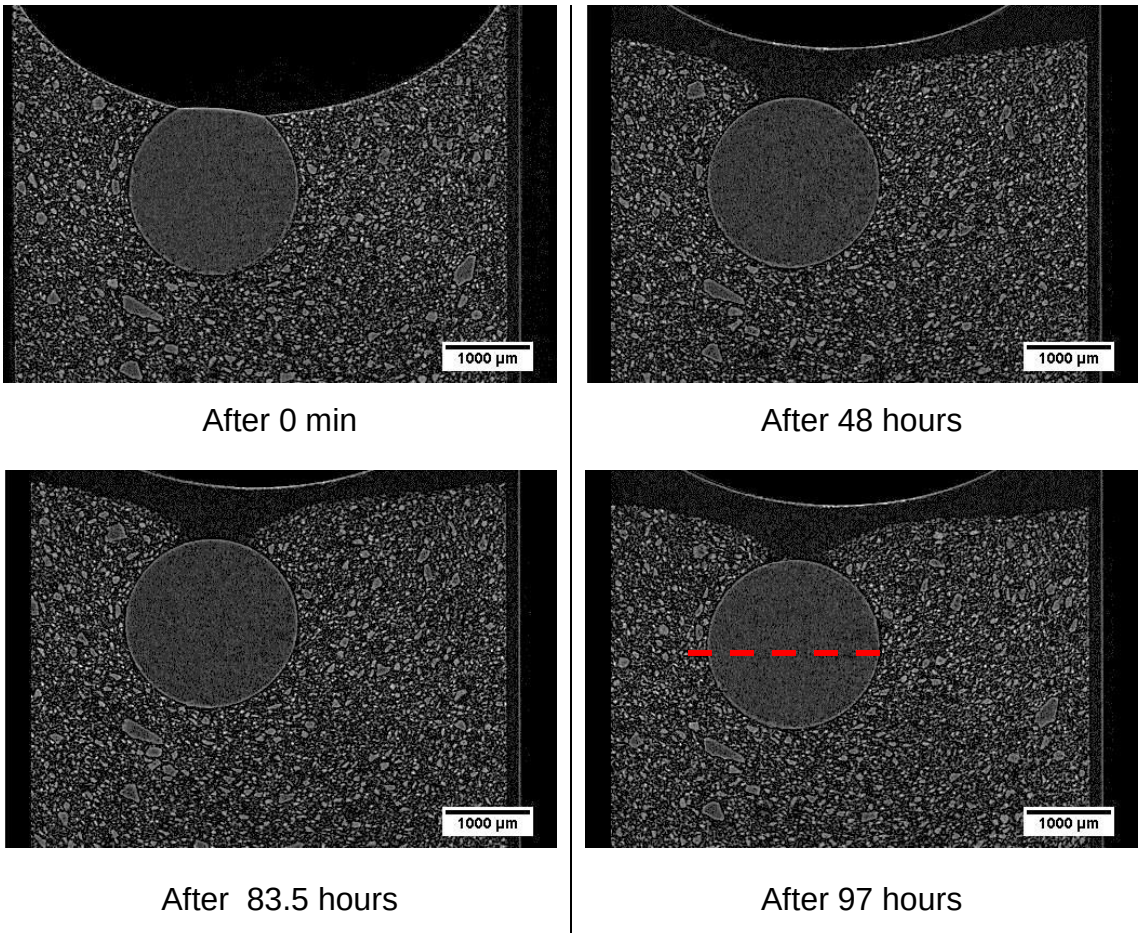

Figure 6-21. Time lapse of central slice along X-axis (where diameter of droplet is largest), for 5 µl saturated fructose droplet. Scale on images is 1 mm.

A slice along the Y-axis for the image after 97 hours in Figure 6-21 (dashed red line) can be seen in Figure 6-22. The boundary is very different to that seen in Figure 6-15 for the saturated sucrose solution droplet, in that at the boundary there is no presence of any solid sucrose crystals. It was expected that sucrose crystals from the bulk suspension would be able to enter the fructose droplet due to its ability to dissolve sucrose; however, this was not the case for the period studied and shows different behaviour from the other secondary liquids studied.

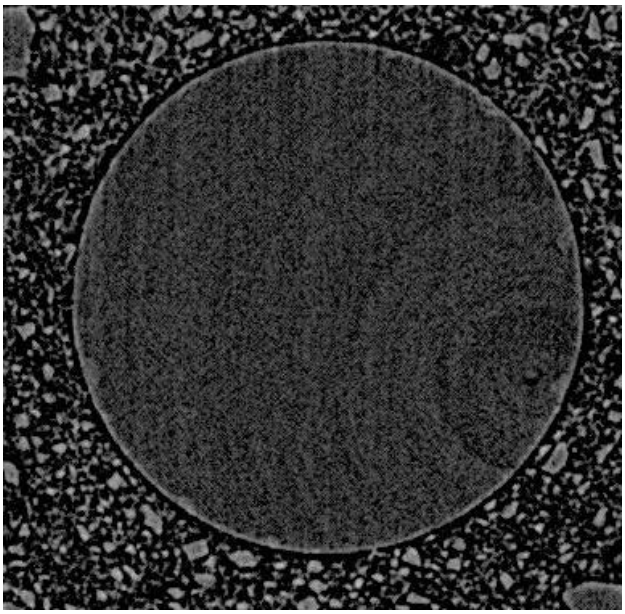

Figure 6-22. Image along Y-axis for 5 µl saturated fructose droplet after 97.5 hours from Figure 6-21.

This may be due to the high viscosity and surface tension of saturated fructose solution, in comparison to the other secondary liquids mentioned. The time required is to see changes comparable to glycerol may be longer and therefore for the time period studied, no visible changes were observed.

6.3.6 Dissolution of Sucrose

The images shown so far in this chapter have shown that high resolutions scans from the X-ray machine in the Canadian synchrotron facility, have the capability to capture the microscale detail of solid sucrose particles within suspension as well as the secondary liquid droplet. Also, for the secondary liquid droplet to progress into the suspension, it needs to either take up or displace the sucrose from the space below to continue its progression into the suspension.

It is hypothesised that for the initial sucrose which enters the water droplet first from the bulk suspension will dissolve. It is easiest to dissolve a soluble material within water initially, and further amounts of this material are added and the saturation level is approached, it becomes more difficult to dissolve and therefore mechanical stirring is required to assist dissolution. To test this hypothesis, experiments were conducted on a 7.5 µl volume water droplet, in particular focusing on the early time period from initial addition. Images from the initial

addition up to 150 minutes after the addition can be seen in Figure 6-23. The same trend as shown previously can be seen when water is added to a suspension, in that the water droplet moves into the bulk suspension and increases in volume with time. Within the first 150 minutes in Figure 6-23, the 7.5 µl (7.5 mm^3) volume water droplet increases in volume by 5 mm^3 and travels a distance of 0.55 mm into the suspension (into the highlighted red rectangle present in the image after 0 min in Figure 6-23). Therefore a region of 0.55 mm below the droplet, which was previously occupied by a mixture of sucrose and sunflower oil is now occupied by the water droplet. The sucrose which was previously situated here has entered into the water droplet, as it can be seen from the images. The location further below the droplet is the same and occupied by sucrose which was present their in the earlier scans.

The location of a large sucrose crystal (approximately 200 µm in diameter) which is present in the image for the first scan and for the scan after 90 minutes in Figure 6-23 is highlighted in the image with a red arrow. It can be seen in the image after 105 minutes in Figure 6-23 the large sucrose crystal has entered into the water droplet (again red arrow showing its location) and is present near the surface of the water droplet and appears smaller in size (due to some dissolution). After 120 minutes this sucrose crystal is no longer present within the water droplet. The stack of images along the X and Y-axis in relation to Figure 3-13 were analysed and no presence of this large sucrose crystal could be for the scans taken after 120 mins and 150 mins. Therefore, this sucrose crystal entered into the droplet and dissolved completely between 90 – 120 minutes from the initial addition of the water droplet. A slice along the Y-axis for the scan after 150 minutes in Figure 6-23 with the red dashed line can be seen in Figure 6-24. It can be seen within this image, there is no presence of large sucrose crystals near the lower region of the droplet. Thus, if any solid sucrose from the bulk suspension had entered into the water droplet, it is no longer present in a solid state and has dissolved into the liquid state.

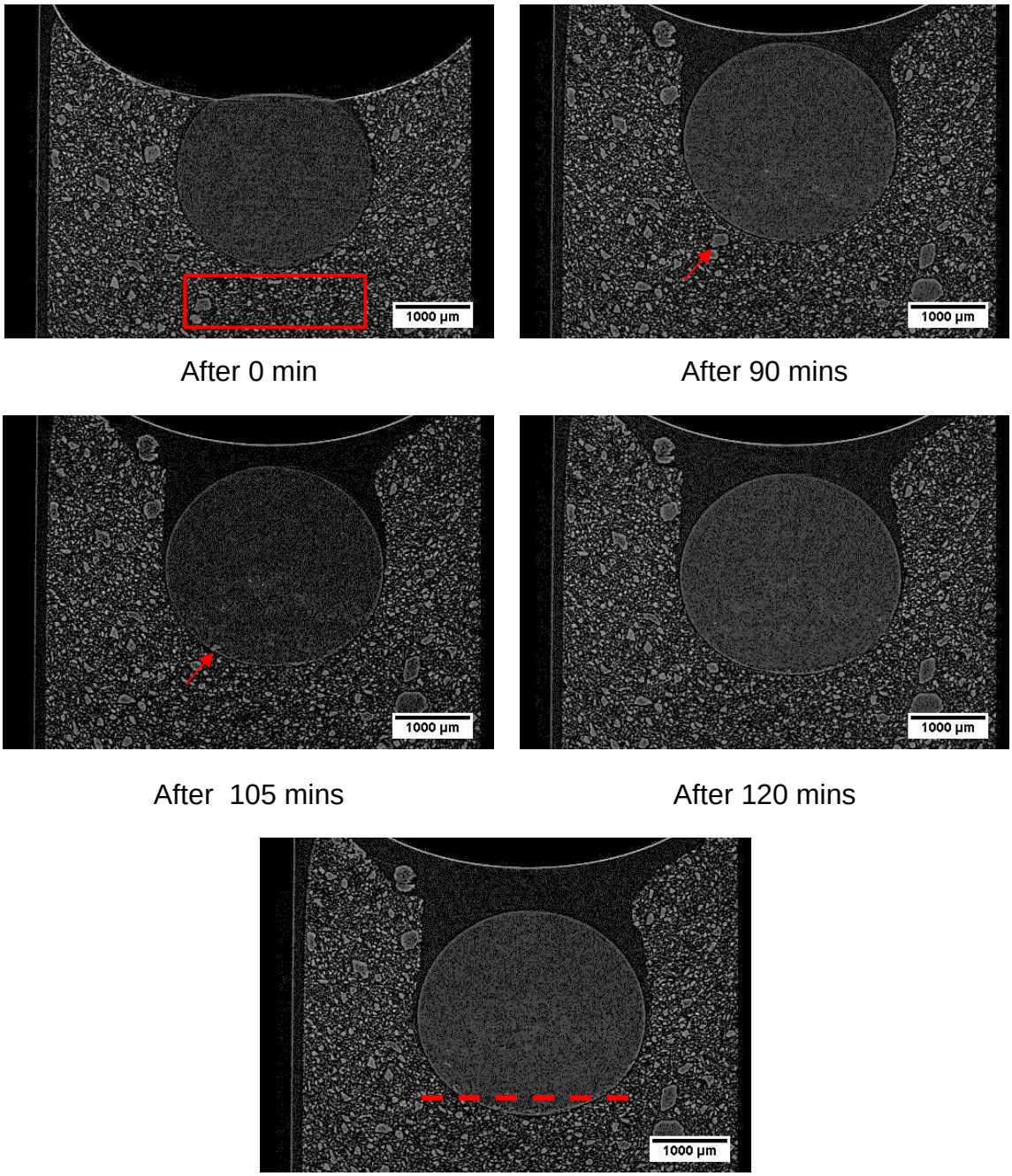

After 0 min

After 90 mins

After 105 mins

After 120 mins

After 150 mins

Figure 6-23. Time lapse of central slice along X-axis (where diameter of droplet is largest), for 7.5 µl water droplet. Scale on images is 1 mm.

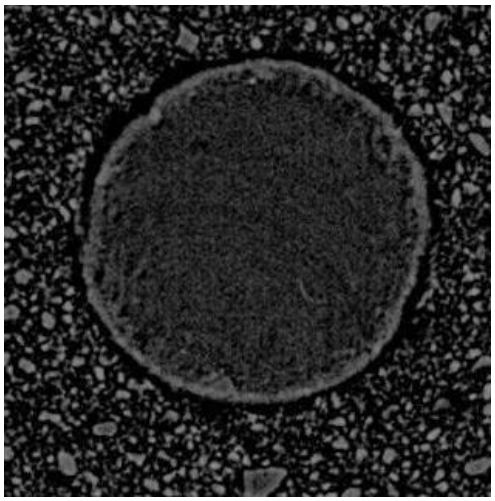

Figure 6-24. Slice along Y-axis from image after 120 minutes from Figure 6-23.

Up until the first 150 minutes from addition in Figure 6-23, the increase in volume of the water droplet seen has been due to solid sucrose entering from the bulk suspension and dissolving. Some scans after a longer period of time from the addition of the 7.5 µl water droplet were conducted which can be seen in Figure 6-25. It can be seen after 330 minutes, that the lower portion of the water droplet is now beginning to fill with solid sucrose, which is different to that seen in the images in Figure 6-23, where there was only an increase in volume of the water droplet with no trace of solid sucrose being present inside the droplet itself. This indicates the rate of dissolution of the sucrose is not the same, which is expected as additional sucrose enters into the water droplet.

The volume of the droplet after 330 mins in Figure 6-25 is 17.1 mm^3 and this increases to 25.6 mm^3 in the image after 750 mins (an increase of 8.5 mm^3) in a period of 420 minutes. After 750 minutes, the 7.5 µl water droplet is approximately half full with solid sucrose. Assuming that the solid sucrose from the bulk suspension only entered into the water droplet and did not dissolve, for a 7.5 µl (7.5 mm^3) water droplet, this would result in a 50 % increase in volume which would be approximately 11 mm^3. However, the actual volume at this stage after 750 minutes when half the droplet is occupied by solid sucrose is more than double the 11 mm^3 volume at 25.6 mm^3. This is believed to be due to the presence of solid sucrose, which entered previously and has now dissolved into the liquid state and thus cannot be seen within the images.

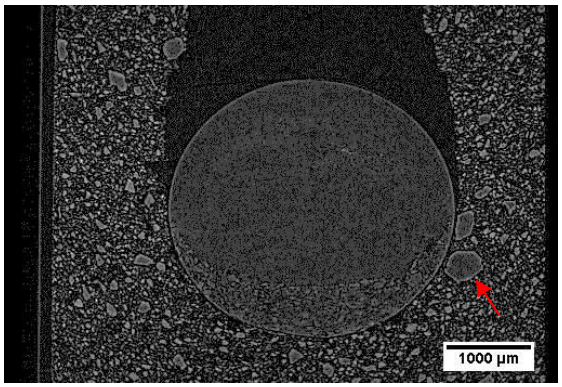

After 330 mins

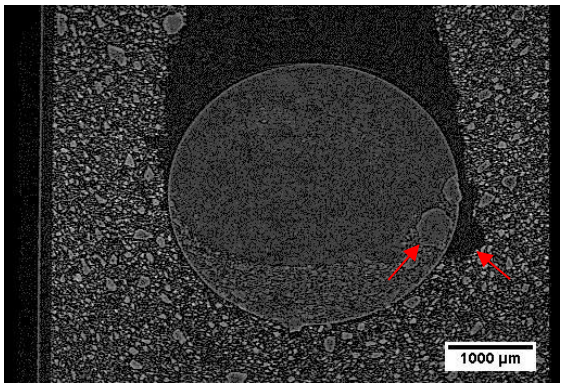

After 360 mins

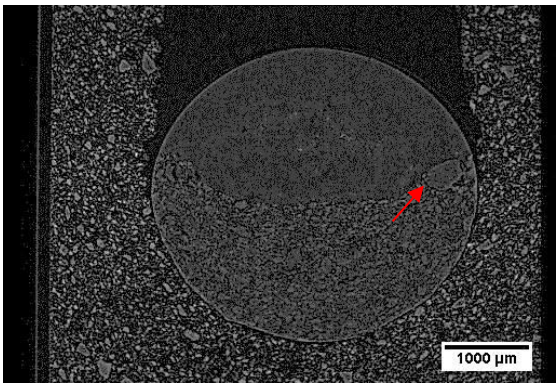

After 750 mins

Figure 6-25. Later scans from sample in Figure 6-23 for 7.5 µl water droplet. Scale on images is 1 mm.

This indicates there are two reasons for the increase in volume seen within the images in Figure 6-23 and Figure 6-25 which can be seen schematically in Figure 6-26. The first is solid sucrose entering into the water droplet and then dissolving into the liquid state which results in a volume increase. The presence of solid sucrose cannot be seen within the water droplet for this period which is highlighted as stage 1 in Figure 6-26. The second is further solid sucrose entering and resulting in a further increase in volume. This time the sucrose remains in the solid state and therefore its presence within the water droplet can be seen which is highlighted as stage 2 in Figure 6-26.

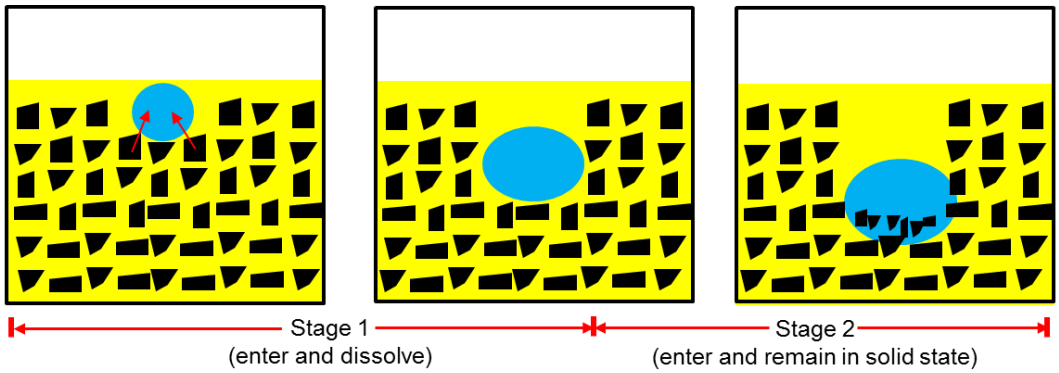

Figure 6-26. Schematic for proposed movement of sucrose from bulk suspension into water droplet during early and late stages.

A particularly larger than normal sucrose crystal can be seen in Figure 6-25 after 330 mins which is highlighted with a red arrow in the bulk suspension. This same large crystal moves into the water droplet between 330 – 360 mins, and for the scan after 360 mins its location within the droplet as well as where it came from within the bulk suspension is highlighted with red arrows. After 750 mins, the same large crystal can be seen within the water droplet, though now its location has changed significantly within the droplet as further solid sucrose from the bulk suspension enters. A slice along the Y-axis in Figure 6-27 highlights the location of this same large sucrose crystal.

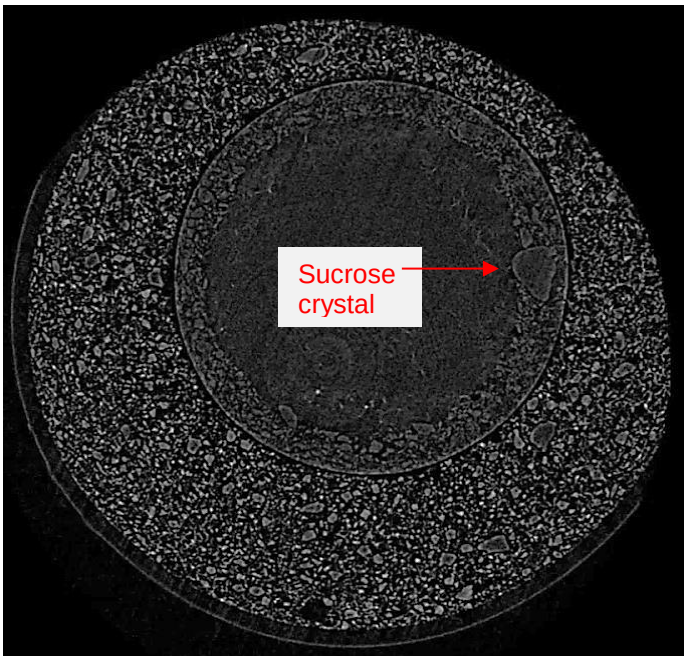

Figure 6-27. Slice along Y-axis from image after 750 minutes in Figure 6-25.

Two further scans were conducted after 24 hours and 34 hours which can be seen in Figure 6-28. After 24 hours, it can be seen that the water droplet is now fully occupied by solid sucrose and has changed dramatically in shape in comparison to the images seen previously. Also, the location of the large crystal shown in Figure 6-25 can be seen (highlighted with a red arrow in Figure 6-28) which has been pushed to the top of the droplet as further sucrose entered into the water droplet from the bulk suspension. Though, now this sucrose crystal appears a little smaller in size which may be due to some dissolution during the period it has been present within the water droplet, though it has not been able to fully dissolve. Once the droplet is full, the movement of water continues as shown in Chapter 5 as the system in not within a state of equilibrium as can be seen in the image after 34 hours.

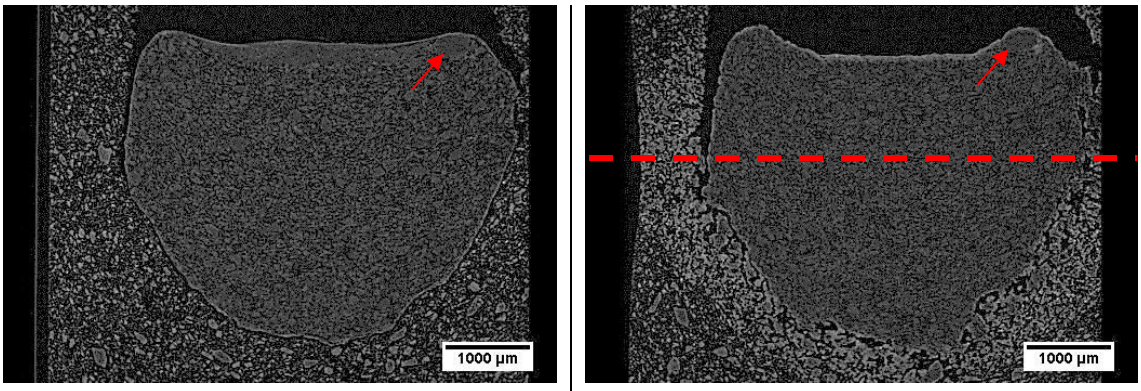

After 24 hours | After 34 hours

Figure 6-28. Long term scans from sample in Figure 6-23 for 7.5 µl water droplet. Scale on images is 1 mm.

A slice along the Y-axis for the red dashed line in Figure 6-28 after 34 hours, can be seen in Figure 6-29. On the right of side of Figure 6-29, is a magnified image for a portion from the slice. It can be seen within this magnified image, that the area away from the bulk water has come together and contract with regions which are belived to be the bridges forming between sucrose particles. This causes the oil to be dipslaced, which was previously present between the sucrose particles. The hypothesised mechanism can be seen schematically in Figure 6-30. This is different to the image shown in Figure 6-27, where the sucrose particles are suspended more spaciously throughout the bulk suspension.

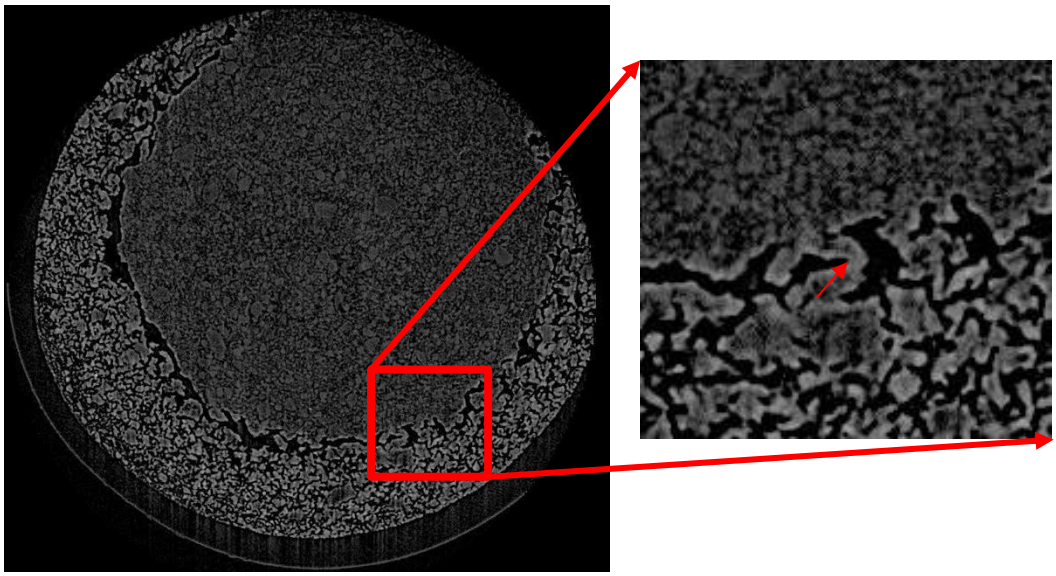

Slice Magnified image

Figure 6-29. Slice along Y-axis for red dashed line in image after 34 hours in Figure 6-28.

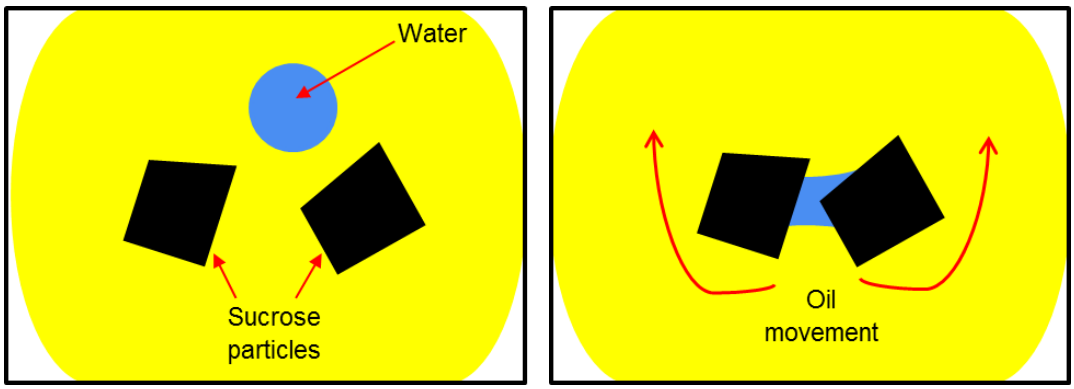

Sucrose suspended Liquid bridge formation

Figure 6-30. Schematic for proposed liquid bridge formation between sucrose particles.

Initially the sucrose particles are suspended within the continuous oil phase. Once the sucrose particles come into contact with the water present, they form a liquid bridge, displacing the oil which was previously present between the particles. The driving force for the formation of the liquid bridge is the interfacial tension and the resistance to this flow is due to the viscosity (Downton et al., 1982). The sucrose particles also partially dissolve into the liquid water bridge causing an increase in viscosity as well as coming closer together. This creates a separation layer, pushing away the oil, which appears separately as a layer on top of the suspension or the side of the suspension.

6.4 Conclusions

In this chapter, the behaviour of different secondary immiscible liquids (water, sucrose solution, saturated sucrose solution, saturated fructose solution and glycerol) on the microscale was investigated when added to a suspension of sucrose and sunflower oil. It was hypothesised that the sucrose solubility plays a key role in the rate of movement of the secondary liquid during the early stages of movement. This was tested by using sucrose solutions from pure water to a saturated sucrose solution. Distilled water exhibited the quickest increase in volume and movement into the bulk suspension, whereas a saturated sucrose solution showed very minimal movement and limited changes in volume even after 100 hours from the initial application of the saturated sucrose droplet. Even though the saturated sucrose solution has a higher density in comparison to distilled water, it was shown that gravity/density differences are not key factors in driving the movement of the secondary liquid within such a system.

For the saturated fructose solution, it showed similar behaviour to saturated sucrose solution (up until 100 hours from initial addition), even though it has the capability to dissolve sucrose (based on the three component diagram sucrose-fructose-water). However, it does have a higher viscosity in comparison to the saturated sucrose solution and substantially higher than water, which may reduce the kinetics of the system dramatically.

Glycerol, which is more viscous and dense in comparison to the saturated sucrose solution, did take up solid sucrose from the bulk suspension. It showed similar behaviour to water, though at a considerably slower speed. It is known that the solubility of sucrose within glycerol is very low (approximately 6%) in comparison to water.

The noteworthy quality of the X-ray machine at Canadian synchrotron facility enabled the presence of solid sucrose within the secondary liquid droplet to be seen and monitored. This proved significant, as two movement mechanisms into the distilled water droplet for the solid sucrose from the bulk suspension were identified. The first during the early stages, being solid sucrose entering and dissolving into the liquid state, which leads to an increase in volume but no trace of

the solid sucrose within the secondary liquid droplet. This is highlighted as stage 1 in the schematic within Figure 6-31 for the initial period from early addition of the secondary liquid, showing there is change in the location of the water droplet and increase in volume of the water droplet (due to the uptake and dissolving of sucrose), though there was no presence of solid sucrose within the water droplet. This is followed by stage 2 after the intermediate to long term periods, where further sucrose from the bulk suspension enters into the water droplet; however, remains in the solid state. Thus, its presence within the water droplet can be seen. This was verified by tracking the changes in the volume of the droplet and the presence of solid sucrose within the droplet with time.

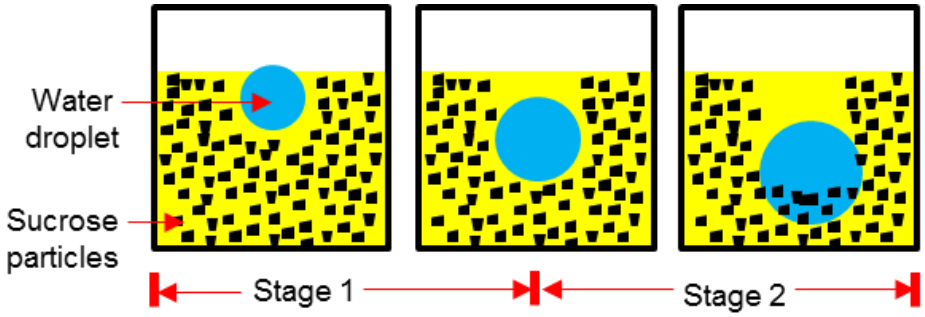

Figure 6-31. Schematic for proposed movement of sucrose from bulk suspension into water droplet during short term and long term periods from initial addition.

Chapter 7 Effect of environmental conditions on suspensions

7.1 Introduction

It is important to ensure appropriate storage conditions (in terms of humidity) of powders to avoid undesired effects such as sticking and agglomeration which can affect flowability and lead to wastage (Stoklosa et al., 2012). For a crystalline material, if the surrounding atmosphere contains a humidity level equal to or higher than the deliquescence point (process by which a material absorbs moisture from the atmosphere and dissolves to form a solution) of the material, it will lead to a substantial increase in mass due to moisture uptake and phase change from solid to liquid as the material dissolves.

Also, within consumer products moisture migration is a key problem for many industries including cosmetic, food and materials. An understanding of the transport mechanisms taking place, is essential to limiting moisture migration, as it is very common that the effects are unfavourable to the product (Marom, 1985).

Furthermore, it has been shown how for binary mixtures of powders, which are very common in food products, the mixture deliquescence point is lower than that of the individual components. An example of this is for sucrose and fructose mixtures. The relative humidity of deliquescence for sucrose and fructose is 85 % and 62 % respectively, however when mixed this lowers to 58 % (Salameh et al., 2006).

7.2 Materials & Methods

The materials are described in detail within Chapter 3. Studies were conducted on sucrose powder as well suspensions of sucrose and sunflower oil as well as fructose and sunflower oil.

X-ray scans were conducted on the Scanco µCT 35. The diameter of the sample holder used for the X-ray experiments was 9 mm. The X-ray energy used was 45 keV. The effective voxel size used was 12 µm. The scan duration was approximately 20 minutes. Full details of the set-up used can be found in Section

3.2.11.1. During the scans, the samples were removed from the storage container and covered with a lid, to seal the sample from the atmosphere of the room. Once the scan was complete, the sample lid was removed and returned to the storage container.

7.3 Results & Discussions

7.3.1 Optical Measurements

A suspension sample of sucrose and sunflower oil (approximately 11 g) was placed in a small plastic petri-dish (90 mm in diameter) within the environmental chamber mentioned in Section 3.2.10, (set to 90 % RH and 25°C). The sample was weighed before being placed into the environmental chamber and after 24 hour intervals for 72 hours. The sample was removed from the environmental chamber and weighed in room conditions and then returned to the environmental chamber. The time required to weigh the sample was less than 1 minute. Photos of the sample were taken at the same time as weight measurements, which can be seen in Figure 7-1 before and after 72 hours of storage.

It can be seen before the sample was placed at 90 % RH, the surface is smooth with no cracks. After 72 hours, the surface begins to show some cracks and has moved in from the side, also separating from the oil (this was confirmed with more than one sample under these conditions). The cracks are believed to have formed due to the compaction and segregation of the sucrose particles away from the bulk continuous oil layer. The change in weight (% increase in relation to the weight of the sample at time 0) of the sample can be seen in Figure 7-2. From Figure 7-2, it can be seen there is a linear trend in the increase in weight of the sample with time.

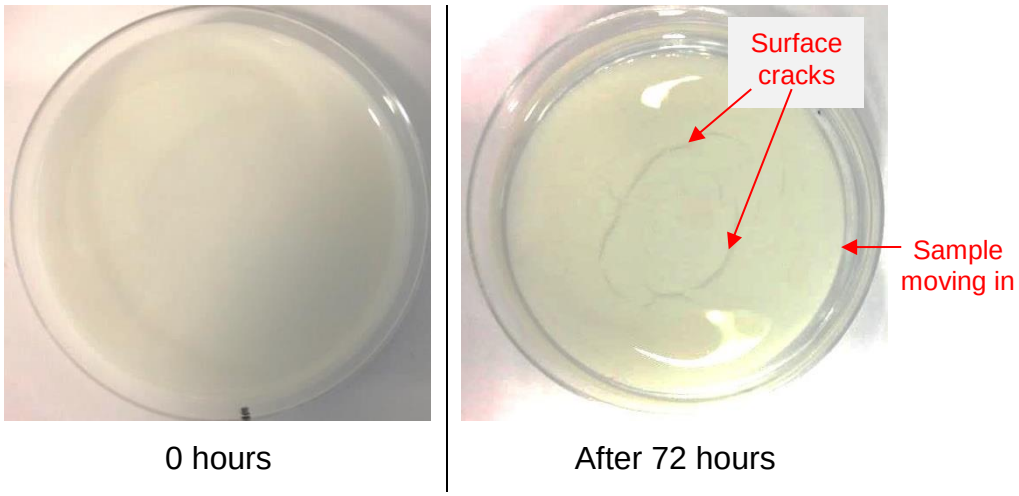

Figure 7-1. Images for sucrose suspension stored at 90 % RH. Petri-dish diameter is 90 mm.

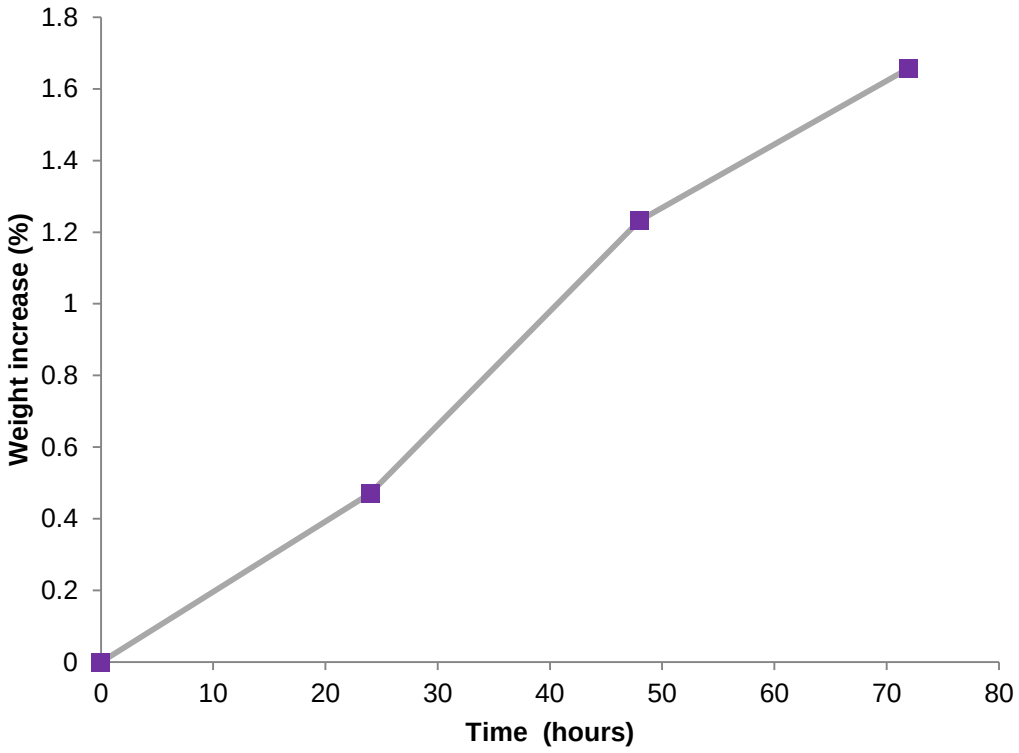

Figure 7-2. Change in sucrose suspension sample weight with time for sample stored at 90% RH.

A reference sample was prepared at the same time, with the top sealed and stored under room conditions. This sample showed no visual changes or mass increase over the same 3 day period.

7.3.2 Online Imaging - Inverted Microscope

The results in Section 7.3.1 show what is occurring to the bulk sample. It does not show how bonding between particles is affected by the conditioning of the sample. To see what is occurring between the particles, experiments were conducted with the inverted microscope and bio-cell set-up mentioned in Section 3.2.10.

The water activity of the sucrose and sunflower oil suspension was measured using rotronic Hygrolab described in Section 3.2.7 and was found to be 0.416 (41.6 % RH.

A sample of sucrose (powder) was spread as a thin layer on a glass slide and placed at 40 % RH, for which images can be seen in Figure 7-3. As mentioned already, the deliquescence point for sucrose is 85% RH (Salameh and Taylor, 2005). Therefore, as a reference to ensure no changes were seen at a condition below this and the flowrate used (40 ml/min) within the bio-cell does not affect the sample, the sample was placed at 40 % RH.

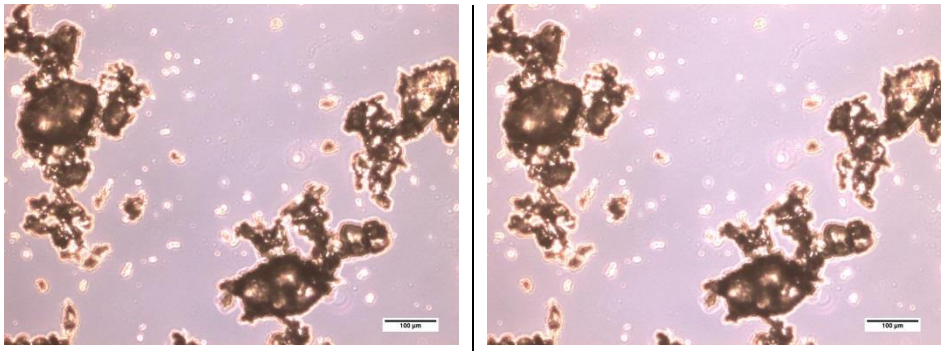

Time 0 | After 4 hours

Figure 7-3. Sucrose powder stored at 40 % RH. Scale on images is 100 µm.

The RH for the same sample shown in Figure 7-3 was then increased to 90 %, for which images can be seen in Figure 7-4. It can be seen after 20 minutes, very clear change can be seen as the sucrose takes up moisture and partially dissolves and contracts together. This is even more evident after 40 minutes (as the small sucrose particles dissolve first), with a large reduction in area of the sucrose. This is due to the hygroscopic nature of sucrose powder, which when subject to high humidity levels, will take up large amount of moisture. Also the presence of sufficient liquid from the surrounding atmosphere, will result in the formation of

liquid bridges between sucrose particles (Downton et al., 1982). This also agrees with the results shown for the bulk suspension sample in Figure 7-2, with the sucrose particles moving in and cracks appearing within the sample.

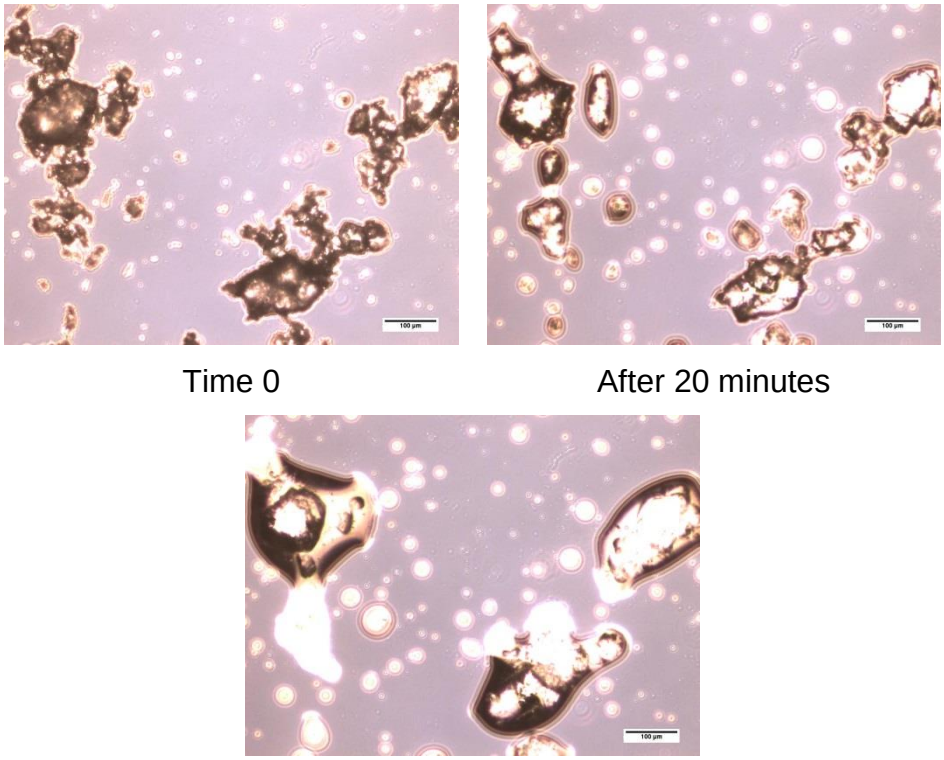

Figure 7-4. Sucrose powder stored at 90 % RH. Scale on images is 100 µm.

Another sample was prepared, this time a suspension of sucrose and sunflower oil. A sample was left to condition at 40 % RH for which images can be seen in Figure 7-5. No change was seen for the sample after 4 hours of conditioning in this environment, which is the same as that seen in Figure 7-3 for sucrose only (powder), due to the conditioning humidity being lower than the deliquescence point of sucrose.

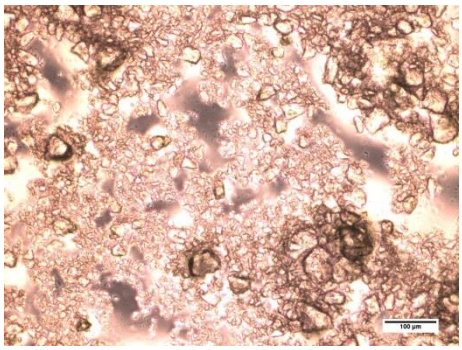

Time 0

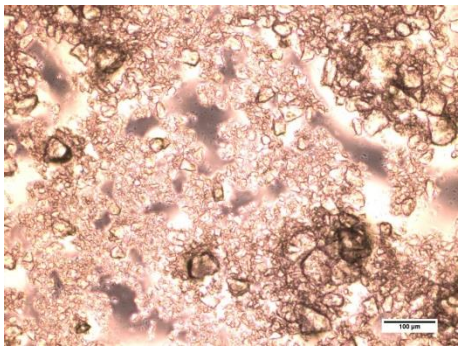

After 4 hours

Figure 7-5. Sucrose suspension stored at 40% RH. Scale on images is 100 µm.

For the same sample in Figure 7-5, the RH was increased to 90 %, for which images can be seen in Figure 7-6. It can be seen, after 10 minutes, the sucrose begins to take up moisture from the surrounding atmosphere and partially dissolve. This continues to be the case, while this condition is maintained as can be seen in the images up until 40 minutes.

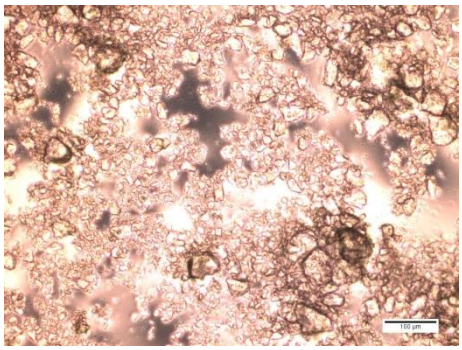

Time 0

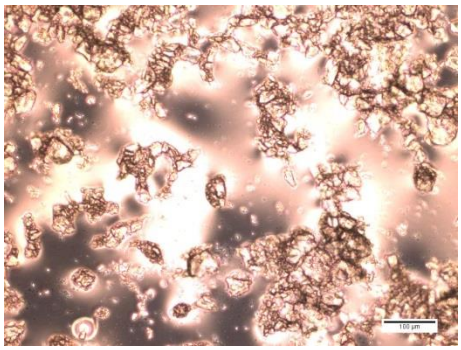

After 10 minutes

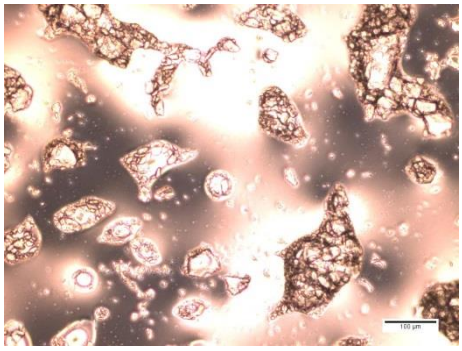

After 20 minutes

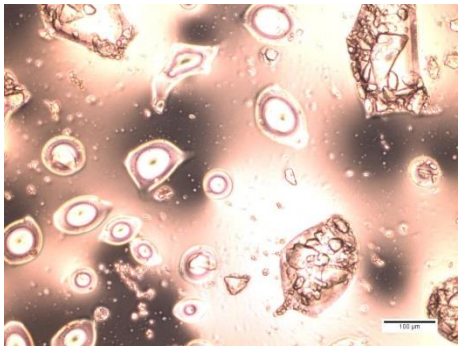

After 40 minutes

Figure 7-6. Sucrose suspension stored at 90% RH. Scale on images is 100 µm.

The moisture sorption isotherm for crystalline sucrose can be seen in Figure 7-7. It can be seen once the relative humidity (proportional to water activity × 100), is increased above the deliquescence point, the moisture uptake is very significant.

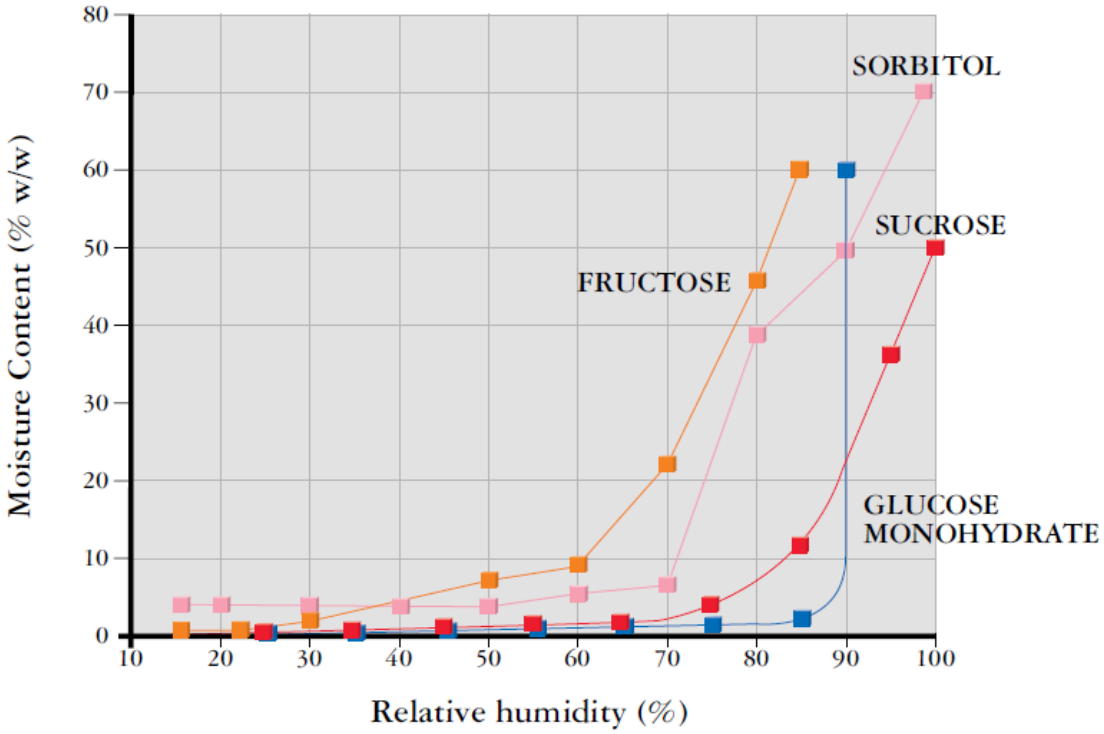

Figure 7-7. Moisture sorption profile for fructose and sucrose (Danisco, 2003).

A suspension sample of fructose, sucrose and sunflower oil (25 % wt., 25 % wt. and 50 % wt. respectively) was stored at 60 % RH which can be seen in Figure 7-8. Similar changes to that seen at 90 % RH for the sucrose suspension in Figure 7-6 was observed, though at a lower humidity. This is believed to be due to the lowering of deliquescence point for binary mixtures, which has been extensively studied. It was shown that this lowering of the deliquescence takes place at the point of contact in binary mixture systems, and also is present in tertiary mixture systems which are common in food based products. Dupas-Langlet et al. (2013) displayed similar results when sodium chloride and sucrose crystals were conditioned, in that the binary mixture deliquescence was lowered in comparison to the individual components.

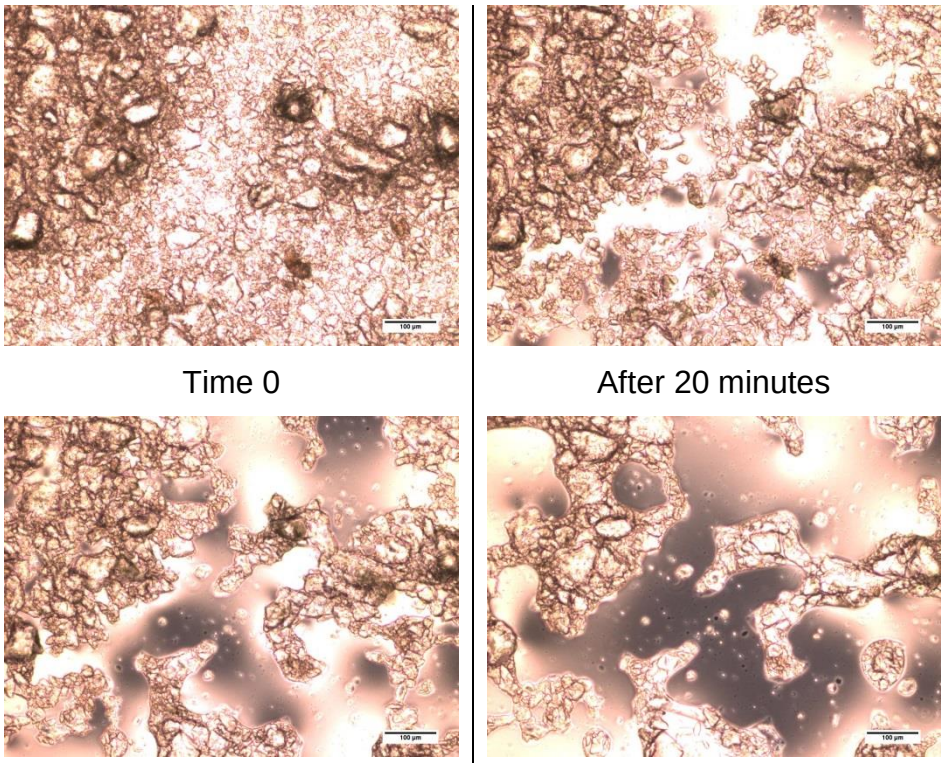

Figure 7-8. Fructose/sucrose suspension stored at 60 % RH. Scale on images is 100 µm.

The moisture sorption curve for fructose and sucrose can be seen in Figure 7-7. It can be seen that at 60 % RH, fructose has a moisture content of 10 % wb, whereas for sucrose there is very little moisture content. At 80 % RH, the difference is even greater as the deliquescence point of sucrose has not been reached yet, however, for fructose the moisture content is 60 % highlighting its extremely hygroscopic nature. This could be used to manipulate and create a sugar network within products which would assist in resisting high temperatures (maintaining structure) for oil based products, similar to that found for sucrose though at less extreme environmental conditions (Killian and Coupland, 2012).

For the samples presented in this section, a single layer (powder or suspension) was used for experimental purposes. This was to allow sufficient light through the sample to the lens, which enabled the sample to be seen optically. It was not possible to use a multi-layer of suspension, as insufficient light would pass through. Therefore, the surface area of contact between the suspension (sucrose) and the surrounding atmosphere being conditioned is abundant (due to the thin layer) and

thus the moisture uptake rate will be rapid. The sorption property of particle has been shown to influence the formation of capillary bridges, in suspensions as was demonstrated by Hoffmann et al. (2014) which is similar to the behaviour seen here for sucrose suspensions. This was ascribed to energetically favourable cluster formation. This highlights the importance of storage conditions, as well as how product consistency can be manipulated for consumer preference.

7.3.3 X-ray CT of Suspensions

7.3.3.1 Sucrose

Suspensions of sucrose and sunflower oil were prepared and placed in sample holders with a 9 mm diameter. These were then scanned initially and intermittently after being stored (Section 3.2.10, the box set-up) at different environmental conditions for different periods of times. Experiments were conducted at 4 different humidity conditions (80 %, 85 %, 87.5 % & 90 % RH).

Figure 7-9 shows the central slice for the sucrose suspension sample (0.5 g sample, approximately 6 mm in height) stored at 80 % RH and 25°C, initially after preparation and then after 18 days of storage under these conditions. It can be seen after 18 days, the only change to the sample, is the settling of sucrose particles near the surface of the suspension due to the density difference between the sucrose and sunflower oil, which is expected to occur. No weight change was recorded for this sample.

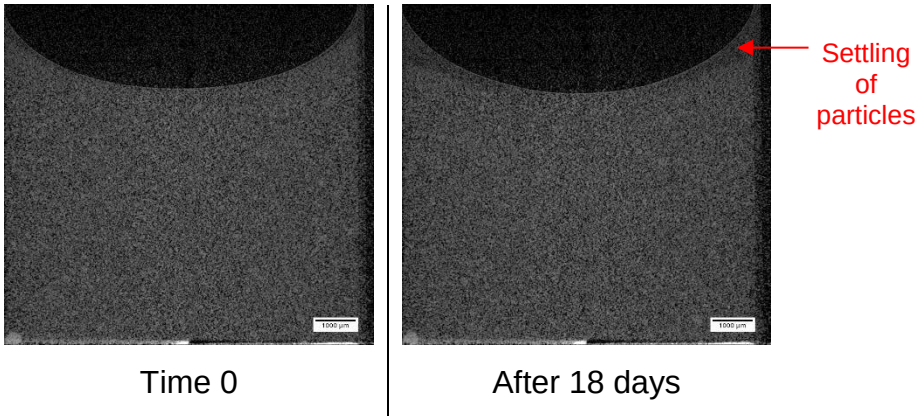

Figure 7-9. Images for sucrose suspensions stored at 80 % RH. Scale on images is 1 mm.

Similar behaviour was observed for a new sample (0.5 g sample, approximately 6 mm in height) stored at 85 % RH and 25°C which can be seen in Figure 7-10, with only settling of the sucrose particles after 15 days storage. This is expected as this humidity level is below the deliquescence point and critical humidity to result in any moisture gain for the sucrose within the suspension. This behaviour is expected, based on the water vapour sorption for sucrose. As sucrose is a crystalline material, for water activities below 0.85 there is very little change in the moisture content. Though for water activities above 0.85 (deliquescence point of sucrose is 0.85), the moisture content changes dramatically as it begins to take up moisture (Yu et al., 2008, Salameh and Taylor, 2005). Therefore for storage at conditions below 0.85, very little change would be expected. The layer of oil on the surface of the suspension does appear slightly more in comparison to the sample in Figure 7-9.

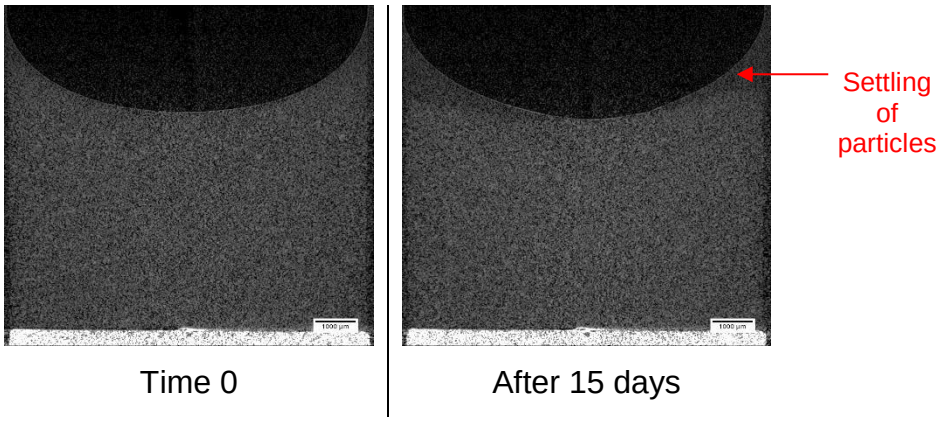

Figure 7-10. Images for sucrose suspensions stored at 85 % RH. Scale on images is 1 mm.

For a new sample (0.7 g sample, approximately 7 mm in height) stored at 87.5 % RH and 25°C, clear changes could be observed to the sample, which can be seen in Figure 7-11. After 3 days at this storage condition, the sucrose particles near the surface of the suspension came closer together, increasing the packing near the top, resulting in a layer of oil forming on the surface of the suspension. There is very clear movement from the sides towards the central region of the suspension which has been highlighted with the red arrows. This layer of oil present at the surface of the suspension continues to increase, as the storage period is prolonged to 6 days, as well as further movement from the side towards the centre, indicating further movement of the sucrose particles. This behaviour corresponds to that seen

when using the inverted microscope for sucrose at 90 % RH in Figure 7-4 in Section 7.3.2. For the suspensions used in Section 7.3.2, the changes observed were markedly quicker, as they were taking place on a single layer suspension. Here, the sample being conditioned is a multi-layered suspension, and the moisture from the surrounding environment requires time to reach further down the bulk suspension. This agrees with the variation in brightness seen within the images in Figure 7-11. For the scan taken after 12 days, the top portion of sucrose within the image appears brighter in comparison to the lower portion. This is believed to be due to the rate at which the sample can gain moisture, and rate at which the moisture can travel within the sample. The increased brightness is due to both the moisture uptake and attraction of sucrose particles together as they pack closer together and force the oil out which then forms on the surface. This change observed in Figure 7-11 is expected, as now the RH condition is above the critical deliquescence point for sucrose.

When comparing this to the results presented in Chapter 4 to Chapter 6, the water was added as a bulk and therefore not completely distributed throughout the bulk suspension. For the sample being studied here, there is no accumulation of the water, as it progresses continuously into the suspension (as a water front), as new moisture is taken up from the atmosphere, due to the water gradient between the two. This can be seen schematically in Figure 7-12, for how the moisture from the environment enters into the bulk suspension, forming bridges between sucrose particles and bringing the particles closer together. This accounts for the side movement seen, which is similar to the behaviour seen in Chapter 4 to Chapter 6 when bulk water was added, causing the sucrose particles near the side of the sample holder (straw) to be pulled in.

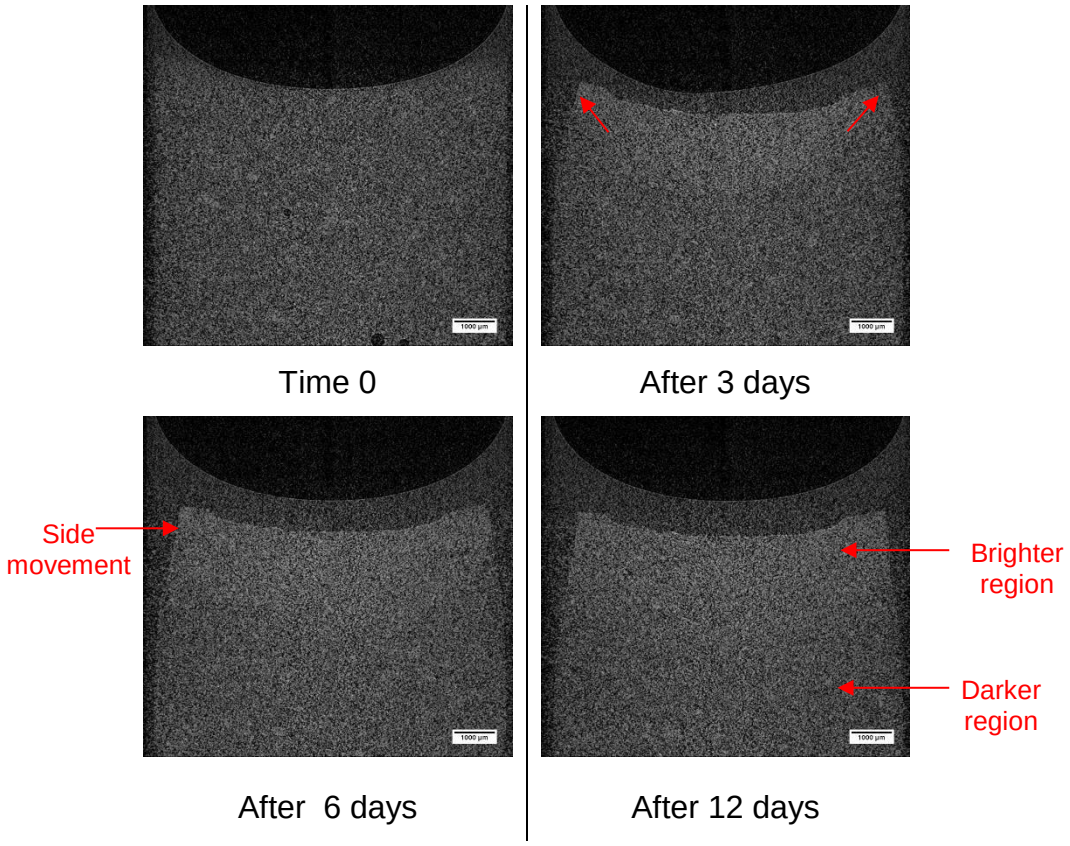

Figure 7-11. Images for sucrose suspensions stored at 87.5 % RH. Scale on images is 1 mm.

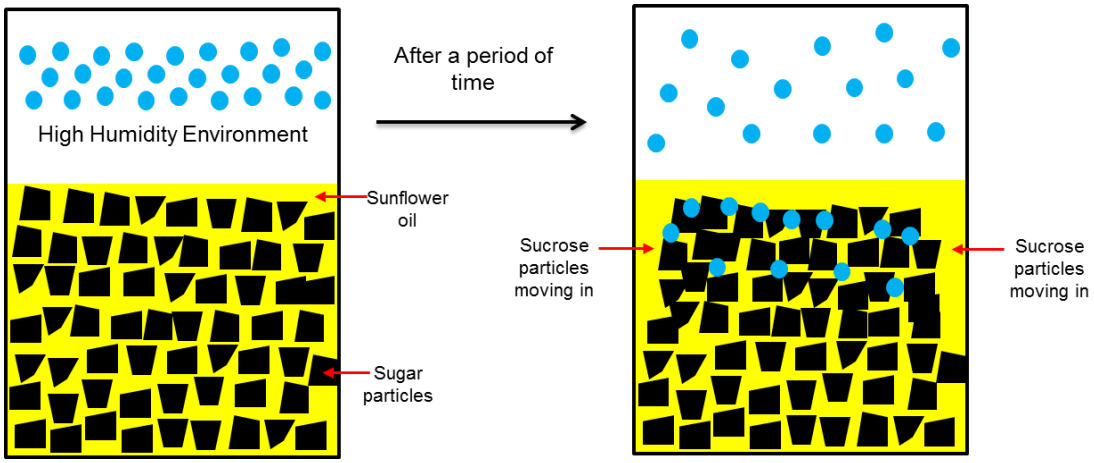

Figure 7-12. Schematic behaviour of water movement seen in Figure 7-11.

When the humidity is increased from 87.5 % RH to 90 % RH, it is expected that the result of the outcome would be similar to that seen at 87.5 % RH, though at a quicker rate. Images from a new a sample (0.4 g sample, approximately 5 mm in height) stored at 90 % RH and 25°C can be seen in Figure 7-13. After 6 hours, clear changes can be seen to be occurring, with the brighter region forming near

the top region of the suspension, as sucrose takes up humidity from the surrounding environment. The area being referred to is highlighted with a red arrow. The change is a more rapid than that seen at 87.5 % RH for the images in Figure 7-11, which is expected due to the higher humidity.

The change seen in Figure 7-13 is slightly different as initially the sucrose holds onto the surface and breaks from the lower portion of the suspension, as can be seen between the images for the scans taken after 2 to 3 days. This region of sucrose, which has an initial uneven top surface, becomes smooth as the storage period is increased further from 3 to 4 days, as well as reducing in volume. This reduction in volume is believed to be due to the uptake of further moisture, which then displaces the oil and causes further packing of the structure (sucrose particles). Then between 6 and 8 days it collapses and falls, which is believed to be due to the weight of the body becoming too much as it continues to take up water. Similar change is seen from the side as sucrose moves towards the centre as that seen for the sample stored at 87.5 % RH.

The reason for the difference is due to the concentration gradient between the sample and the surrounding atmosphere. The sample stored at 87.5 % RH (Figure 7-11), the diffusion rate of moisture from the atmosphere to the sample (sucrose suspension) is slow, as the RH difference between the sample and the atmosphere is low. Thus, the water migrates at a controlled rate into the bulk suspension for the sucrose. The sample stored at 90 % RH (Figure 7-13), the diffusion rate of moisture from the atmosphere is fast and the RH difference between the atmosphere and the bulk suspension is high. Thus, sucrose is able to take moisture and dissolve partially, forming liquid bridges and accumulating, before spreading further into the bulk suspension.

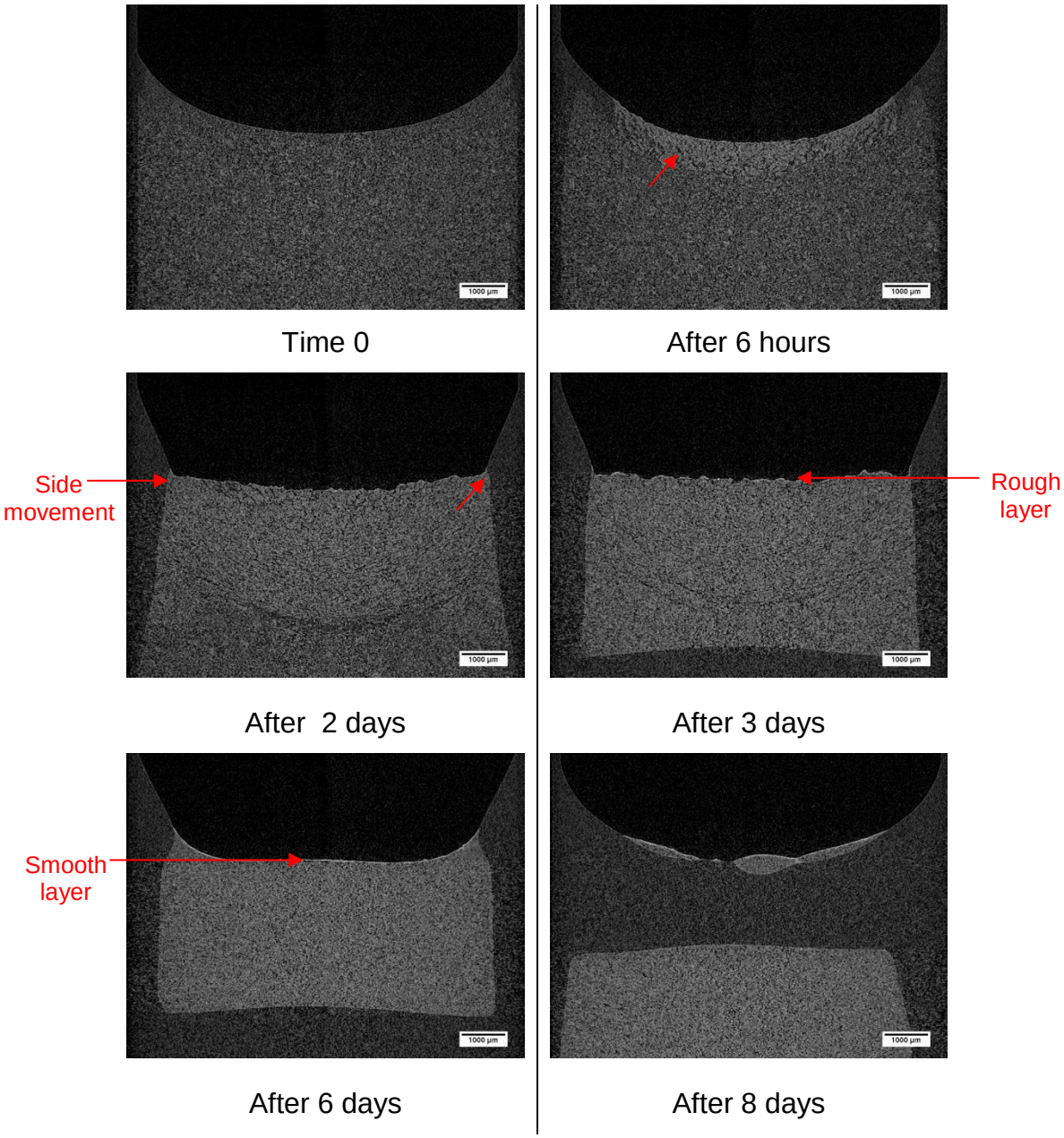

Figure 7-13. Images for sucrose suspensions stored at 90 % RH. Scale on images is 1 mm.

The changes seen for the suspension sample in Figure 7-13 can be schematically seen in Figure 7-14. Stage 1, the sample has just been exposed to an atmosphere of high water content, though no water has entered which corresponds to the scan taken at time 0. Later, for stage 2, the moisture enters into the bulk suspension from the top and side (which are areas of least resistance) and causes a contraction in solid volume (due to closer packing of sucrose), while maintaining contact with the surface/surrounding atmosphere which corresponds to the scan taken after 2 days. After, for stage 3, the bulk sucrose (acting as one body) begins

to float, and takes up further moisture and packs more tightly together which corresponds to the scan taken after 6 days. Finally, for stage 4, the bulk sucrose is has taken up substantial moisture and is now too dense (due to decrease in volume while taking up moisture) to float and, therefore, drops to the bottom of the sample, being covered in a layer of oil. Now, the oil is the limiting factor in any further moisture uptake, as moisture must pass through the oil phase before reaching the sucrose which corresponds to the scan after 8 days.

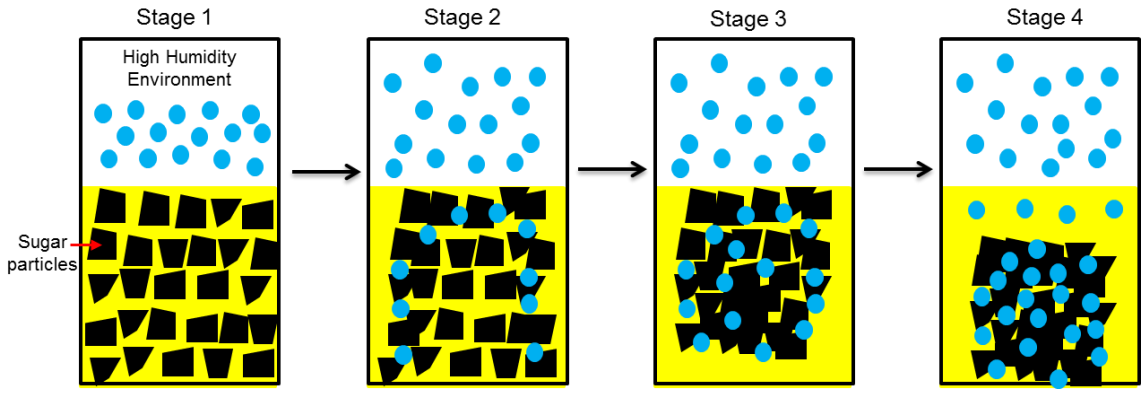

Figure 7-14. Schematic behaviour of water movement seen in Figure 7-13.

The changes seen in Figure 7-11 and Figure 7-13 could help explain the reason for accelerated blooming of chocolates when exposed to humid air or when placed in contact with a water-based filling. Due to the concentration gradient present between surrounding air and the suspension, the sucrose particles will absorb moisture. As the sucrose particles begin to take up the moisture, liquid bridges are formed and this forces the continuous oil phase out from between the particles, as the particle structure contracts. This allows the continuous phase to migrate to the surface and crystallise into a more stable form and hence could explain why blooming is accelerated under the presence of moisture or a water gradient between different domains.

The sucrose suspension sample stored at 90 % RH created a solid body after 8 days storage as can be seen in Figure 7-13. This solid body was removed and washed with hexane to remove residual oil (Killian and Coupland, 2012) and a piece was taken and imaged using the SEM, from which an image can be seen in Figure 7-15. It can be seen that bridges have formed between the sucrose

particles, creating a solid network formation. One particular solid bridge is highlighted with a red arrow, which is believed to have formed after the partial dissolving of sucrose surface from the moisture gain, followed by a liquid bridge formation of this sucrose solution, which then recrystallized.

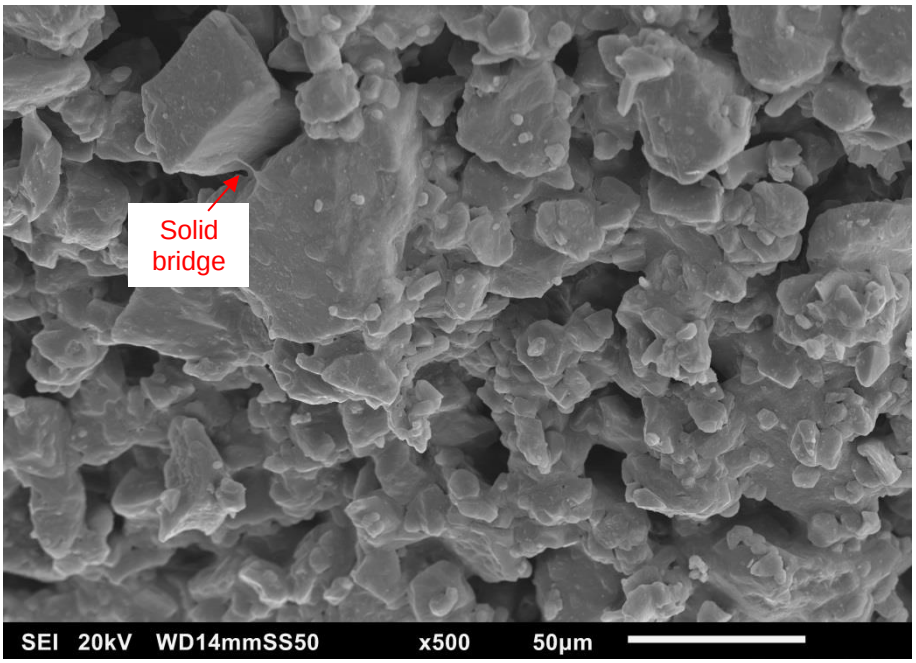

Figure 7-15. SEM image of sucrose/water mixture after removal of oil by hexane for sample from Figure 7-13.

To confirm the changes seen in images from Figure 7-11 and Figure 7-13 were due to environmental storage conditions, a reference sample was prepared which was stored in room conditions with the top sealed at the same time as the sample which was stored at 90 % RH. Similar scans were conducted of this sample, and no visible change could be seen to that sample as can be seen in Figure 7-16. The behaviour was the same as that seen for the sample stored at 80 % and 85 % RH in Figure 7-9 and Figure 7-10 respectively, with only some settling of the sucrose particles within the suspension due to density differences. No change in weight was recorded for this sample.

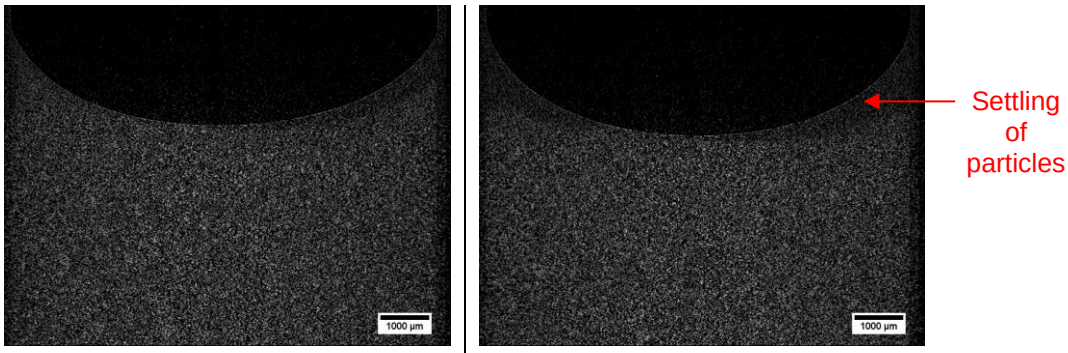

Figure 7-16. Reference sample. Scale on images is 1 mm.

Weight measurements of the samples were taken before each scan which can be seen in Figure 7-17. For the samples stored at 80 % and 85 % RH (Figure 7-9 and Figure 7-10 respectively) no change was recorded for the weight of these samples. For the sample stored at 87.5 % RH (Figure 7-11), after 6 days the weight increased by less than 1 %, whereas for the sample stored at 90 % RH (Figure 7-13) this increased by nearly 8 % by 6 days. After 24 hours at 90 % RH the weight gain for the sucrose suspension was more than that seen for the sample stored at 87.5 % RH for 6 days.

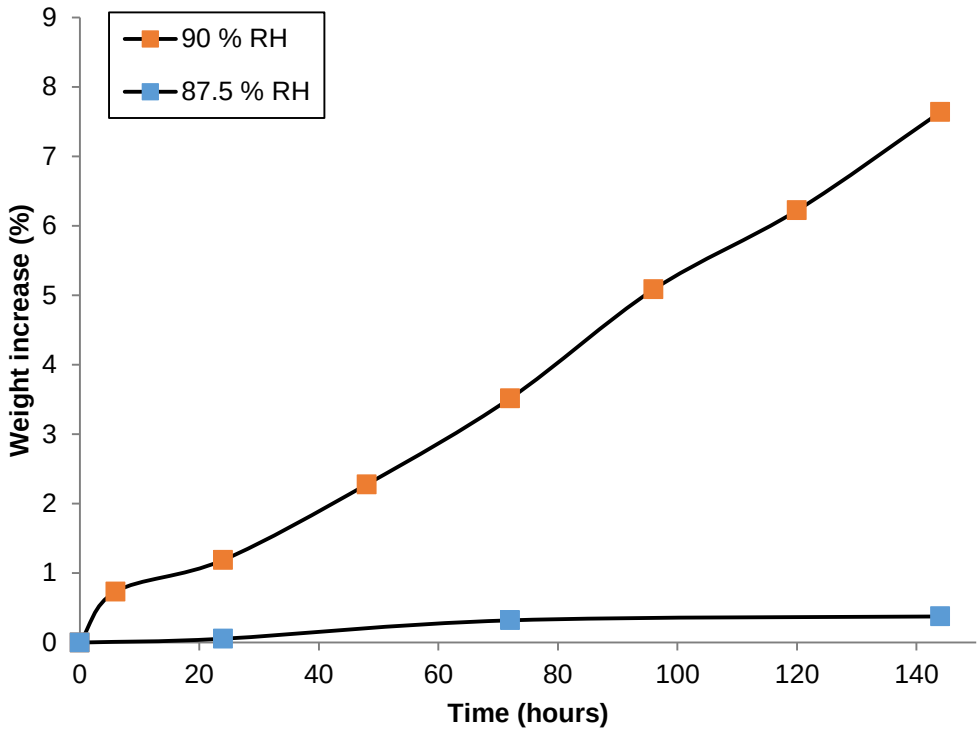

Figure 7-17. Change in weight of sucrose suspensions stored at 87.5 % and 90 % RH from Figure 7-11 and Figure 7-13, respectively.

7.3.3.2 Fructose

Suspensions of fructose and sunflower oil was prepared and placed in sample holders with a 9 mm diameter. These were then scanned initially and intermittently after being stored at different environmental conditions for different periods of times.

Experiments were conducted at different humidity conditions (75 % & 90 % RH) for different samples, with another sample stored in the lab (closed) as a reference sample.

Figure 7-18 shows the central slice from scans taken after different time periods of the sample (0.3 g) storage at 75 % RH for the fructose suspension. It can be seen that after 6 hours change is occurring similar to that seen for the sucrose suspensions at humidity levels of 87.5 % and above in Section 7.3.3. Also, there is an oil layer formation near the top of the suspension, which is believed to have formed as the fructose particles contract inwards and force out the oil. There is likewise movement from the side and contraction of the fructose particles continues as can be seen for the scans conducted after 1 and 3 days of storage at this

condition. This coming together of the fructose particles and reduction in solid volume and separation from the surrounding oil continues, as can be seen for the scans taken after 7 and 13 days.

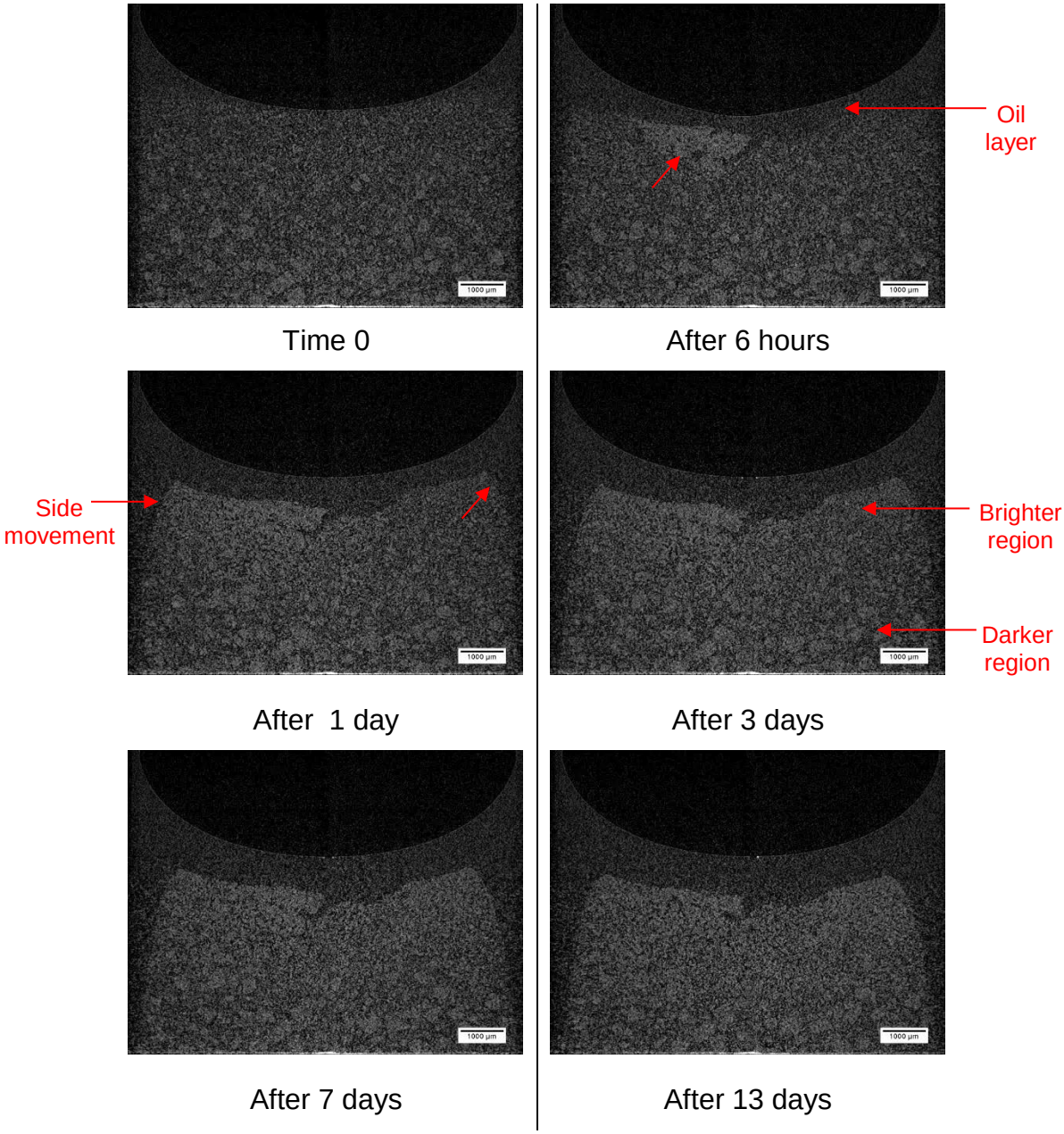

Figure 7-18. Images for fructose suspensions stored at 75 % RH. Scale on images is 1 mm.

For the sample (0.3 g) stored at 90 % RH, similar behaviour is observed to that seen at 75 % RH in Figure 7-18, though at a quicker rate as can be seen in Figure 7-19. In terms of the reduction in volume of the sugar particles, after 1 day being stored at 90 % RH is similar to that which required 13 days at 75 % RH. Also, there

was a separation formed between the fructose particles, with a bulk portion on the right of the image and a smaller portion on the left.

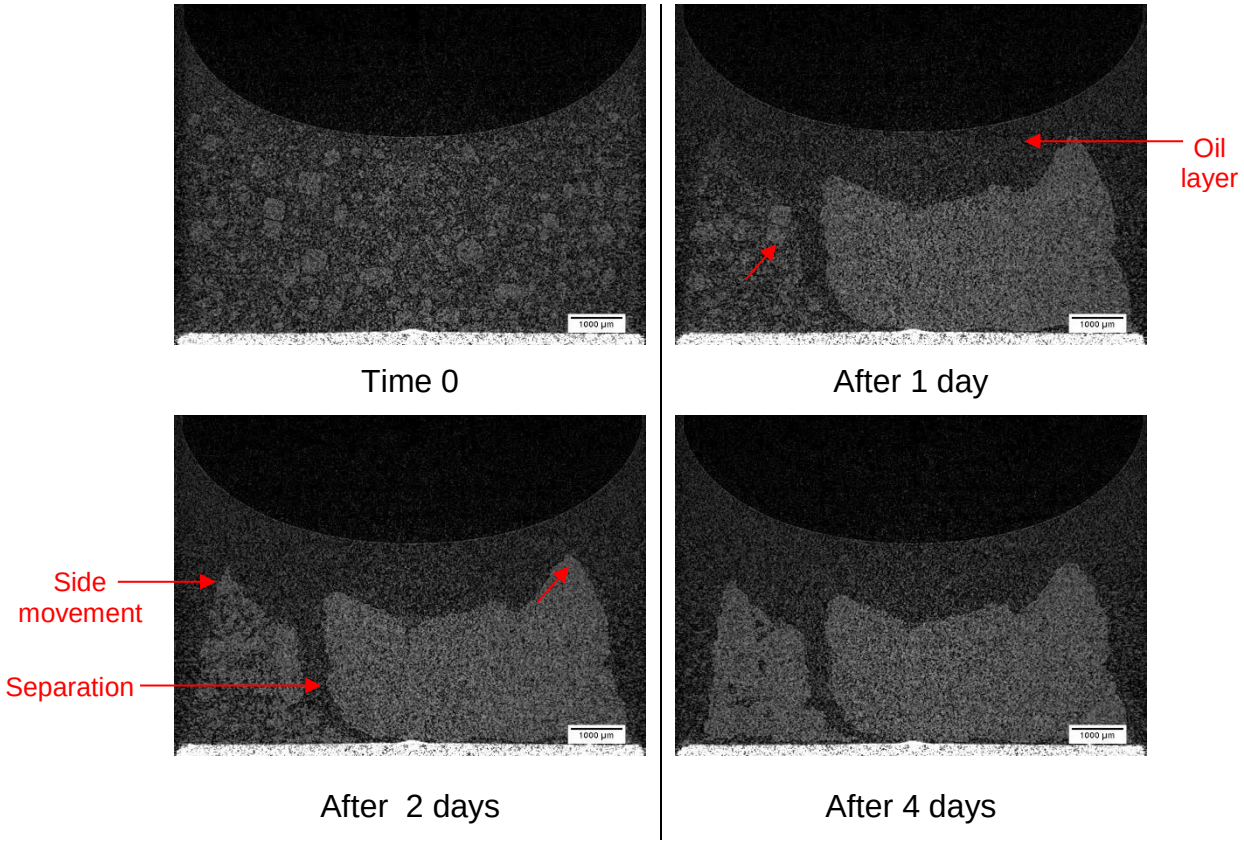

Figure 7-19. Images for fructose suspensions stored at 90 % RH. Scale on images is 1 mm.

Weight measurements of the samples were taken before each scan which can be seen in Figure 7-20, for the samples stored at 75 % and 90 % RH (Figure 7-18 and Figure 7-19 respectively). For the sample stored at 75 % RH (Figure 7-18), over the 13 day period scanned, the weight increased by less than 1 %, whereas for the sample stored at 90 % RH (Figure 7-19) this increased by nearly 2 % in one day, showing a very rapid increase for the first 24 hours, followed then by a much slower uptake of moisture.

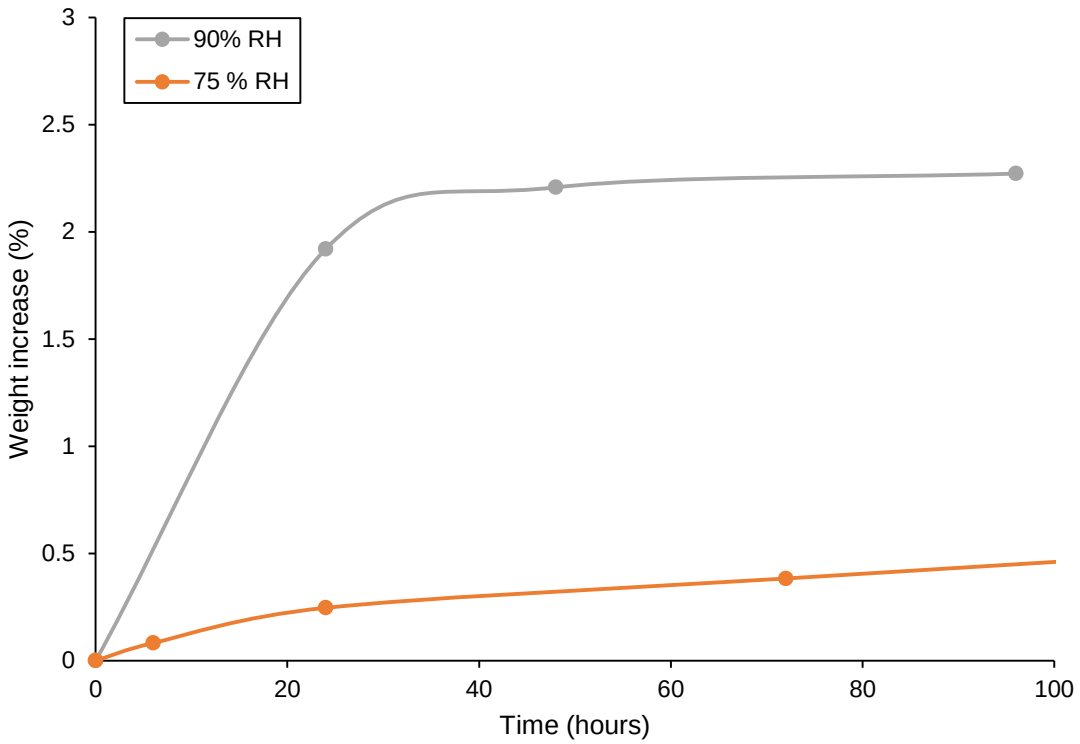

Figure 7-20. Change in weight of sucrose suspensions stored at 75 % and 90 % RH from Figure 7-18 and Figure 7-19, respectively.

To confirm that the changes seen in images from Figure 7-18 and Figure 7-19 for the fructose and sunflower oil suspension were due to environmental storage conditions, and not, for example, due to settling of the suspension, a reference sample was prepared which was stored in room conditions with the top sealed at the same time as those samples. Similar scans were conducted of this sample, some of which can be seen in Figure 7-21. It can be seen that after 10 days, the sample is same as the scan taken initially after preparation, with only some settling of the fructose particles with a small oil layer forming on the surface. This is expected due to the density differences between the liquid and solid and thus naturally settling will occur with time. No change in mass was recorded for this sample.

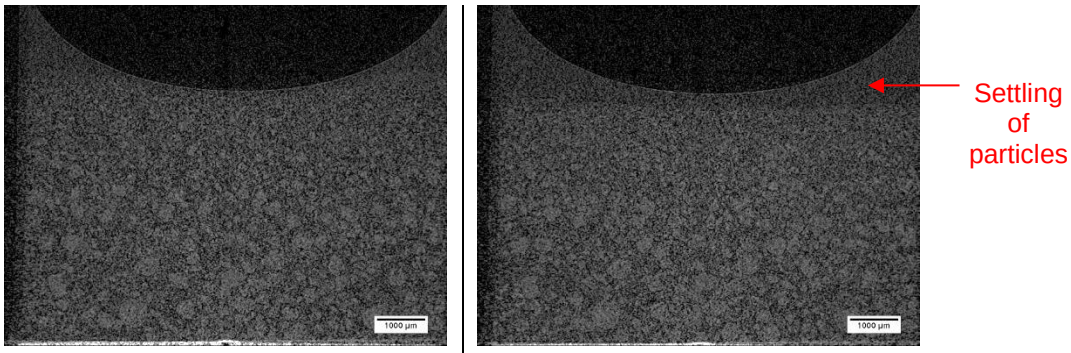

Figure 7-21. Images for reference fructose suspension. Scale on images is 1 mm.

7.3.3.3 Mixtures of Sucrose & Fructose

Experiments were conducted to see the effect of suspensions which contained both sucrose and fructose and comparing these with suspensions of only sucrose and fructose. It is known from the literature that the deliquescence (and sorption isotherm) of binary mixtures is different to individual components. Also, most food products, the composition are a mixture of many components including sugars. Samples were stored at 75 % RH, as it was known for this humidity level, no change will occur for sucrose crystals, whereas for fructose crystals changes would be observed as shown in Sections 7.3.3 and 7.3.3.2 respectively.

To test this, three different samples were prepared. Sample 1 contained sucrose and sunflower oil. Sample 2 contained fructose and sunflower oil. Sample 3 contained sucrose, fructose and sunflower oil. The wt. % of the different components of the 3 samples can be seen in Table 7-1.

Table 7-1. Sample compositions for suspensions, in wt. %.

	Sucrose (%)	Fructose (%)	Sunflower oil (%)	Weight (g)
Sample 1	50	0	50	0.26
Sample 2	0	50	50	0.29
Sample 3	25	25	50	0.31

Figure 7-22 shows the central slice from scans taken after different time periods of storage at 75 % RH and 25°C for the 3 samples mentioned in Table 7-1. For

sample 1 which contained just sucrose and sunflower oil, very limited change was seen in this sample. The sample remained similar after 4 days, when comparing to the scan at time 0, with some settling of sucrose particles near the top of the sample due to density differences. This is expected, based on the moisture sorption curve of sucrose, as it only begins to take up moisture above a water activity of 0.85.

Sample 2 which contains fructose and sunflower oil shows clear changes after 6 hours. This change continues to progress as can be seen in the scans taken after longer durations of storage. The change was similar to that seen in Section 7.3.3.2, with movement from the side initially, followed by a reduction in the volume of the solid area, as it continues to take up water from the environment. This results in a layer of oil which is present on the top of the suspension, as it separates from the particles present. This agrees with the moisture sorption curve for fructose, which begins to take up significant quantities of water above a water activity of 0.5. Therefore, in an environment of 75 % RH would lead to significant water uptake.

Sample 3 which contains sucrose, fructose and sunflower oil shows changes after 6 hours of storage at 75 % RH similar to sample 2, but the change seen is less uniform as can be seen Figure 7-22. A bright region is seen on top which increases in size after 1 day, but in comparison to sample 2 which contains just fructose, the distance the water has reached is less and the movement from the side is less. After 4 days, samples 2 and 3 look very similar, in terms of the reduction in volume of the sugar region, brightness of the solid region and the layer of oil present near the top surface.

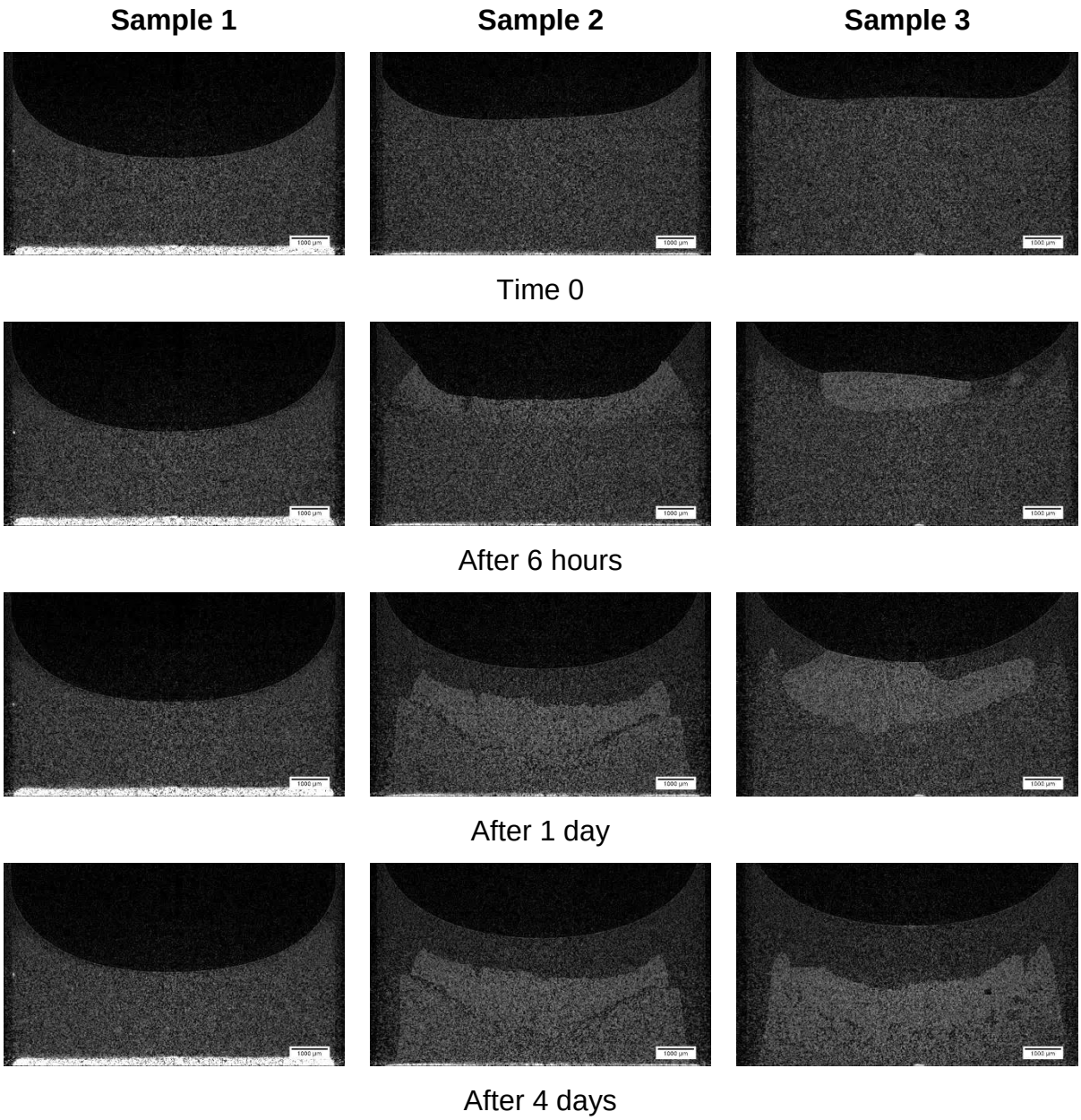

Figure 7-22. Images for the suspensions samples (sample 1 – sucrose and sunflower oil, sample 2 – fructose and sunflower oil, sample 3 – sucrose, fructose and sunflower oil) stored at 75 % RH. Scale on images is 1 mm.

As the samples were removed from the storage chamber for X-ray scans, the weight of the sample were measured at the same time. The change in weight of the samples with time can be seen in Figure 7-23. Sample 1 for the sucrose suspension showed no increase in weight which agrees with the images in Figure 7-22. Samples 2 and 3 showed comparable increase of approximately 1.8 % in weight after 1 day storage at 75 % RH. After 1 day, the weight increase for sample 3 was greater in comparison to sample 2, even though the overall amount of

fructose present in sample 3 is less than sample 2 and the sucrose does not take up any water as seen from sample 1. The reason for this is believed to be due to the effect of binary mixtures (sucrose and fructose). Work in the literature shows the deliquescence point of a binary mixture, is lower than the deliquescence point for individual components. This was seen for mixtures of salts such as HCl and KBr, and mixtures of sucrose and pharmaceutical ingredients such as Thiamine HCl (Salameh and Taylor, 2005). Therefore, in sample 3, the increased weight increase is due to this lowering of the deliquescence point due to the mixture of the sugars sucrose and fructose.

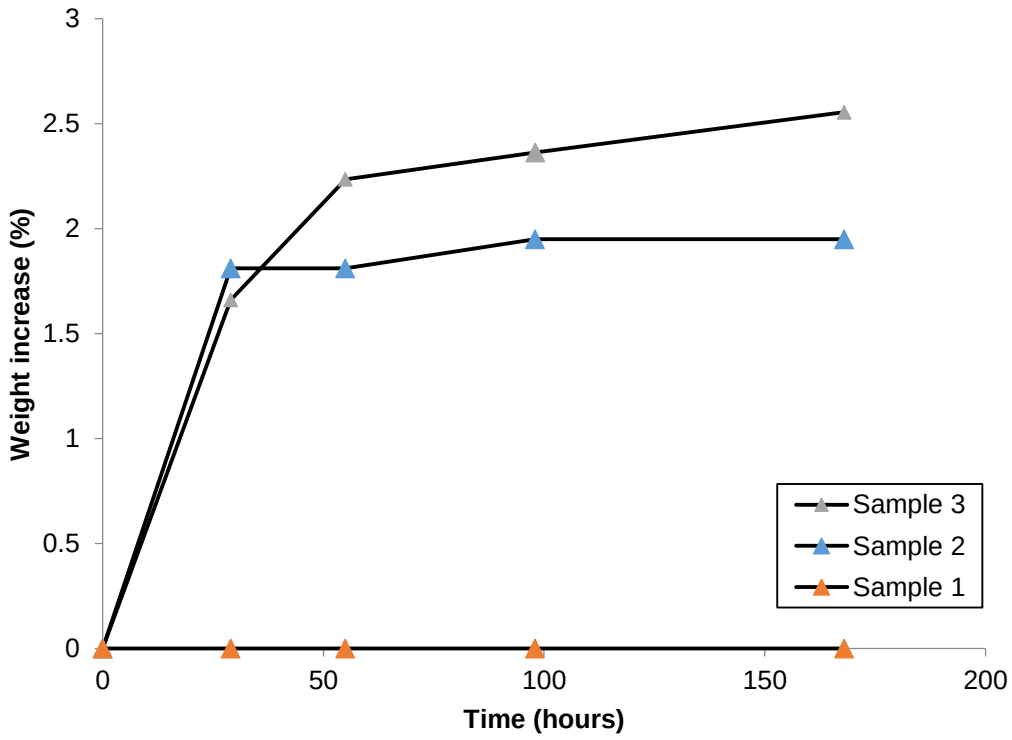

Figure 7-23. Change in sample weight for suspension samples stored at 75% RH for the sample from Figure 7-22.

7.3.3.4 Fructose with a layer of Sucrose Particles

From the results presented in Section 7.3.3.3 for fructose suspensions, it was hypothesised that the moisture sorption properties of sucrose could be used, to reduce or stop the moisture gain from the environment for a fructose suspension. Using the information that sucrose begins to take moisture above a water activity of 0.85 (humidity 85 % RH), therefore by placing a layer of sucrose particles on the

surface of a fructose suspension, should assist in resisting environmental effects provided the humidity level is below 85 % RH.

Therefore to investigate this, suspensions of fructose and sunflower oil were prepared as mentioned previously. Two samples were prepared; sample 1 (0.5 g) contained fructose and sunflower oil and sample 2 (0.55 g total, 0.05 g sucrose) was the same as sample 1, with a layer of sucrose on top. The compositional schematic of both samples can be seen in Figure 7-24.

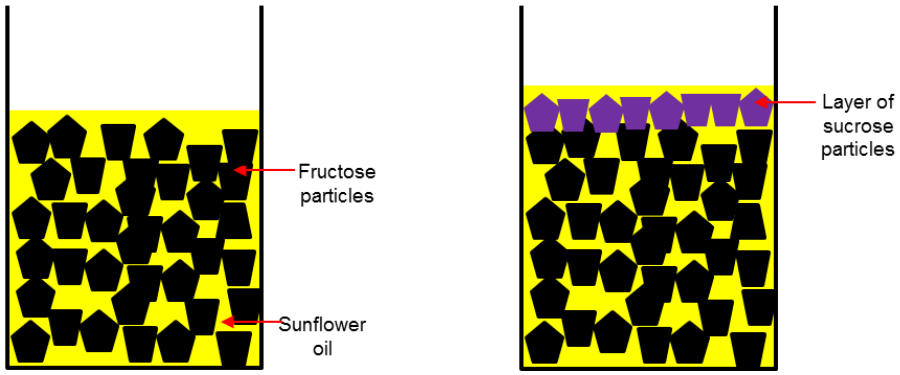

Figure 7-24. Schematic for sample preparation. (a) sample 1: fructose and sunflower oil; (b) sample 2: fructose and sunflower oil with a layer of sucrose on the surface.

Experiments were conducted at humidity level of 75 % RH. The reason for choosing 75 % RH is, after looking at the moisture sorption curve for fructose & sucrose, the moisture content at this water activity is negligible for sucrose whereas for fructose there is a significant uptake of moisture. Therefore, this will allow for the effects of placing the sucrose layer on the surface to be seen.

Figure 7-25 shows the central slice from scans taken after different time periods of storage at 75 % RH for the fructose suspension with and without a layer of sucrose on the surface. Both samples look similar for the scan taken before the start of the experiment at time 0 as expected. Clear changes could be seen after 2 days of storage for sample 1 of just fructose and sunflower oil, such as movement from the side and a layer of oil forming on the surface as shown in Figure 7-18 in Section 7.3.3.2. However, for sample 2, with a layer of sucrose on the surface, very little change is observed after the same storage period of 2 days. This change for

sample 1 continues as can be seen in Figure 7-25 after 10 days, with movement from the side and contraction of the fructose particles. Sample 2 does begin to show some movement from the side in the image after 10 days. It would appear that the moisture has managed to find a path into the suspension, as the lower fructose suspension was not completely sealed, though the layer of sucrose has resisted and slowed down the environmental effects.

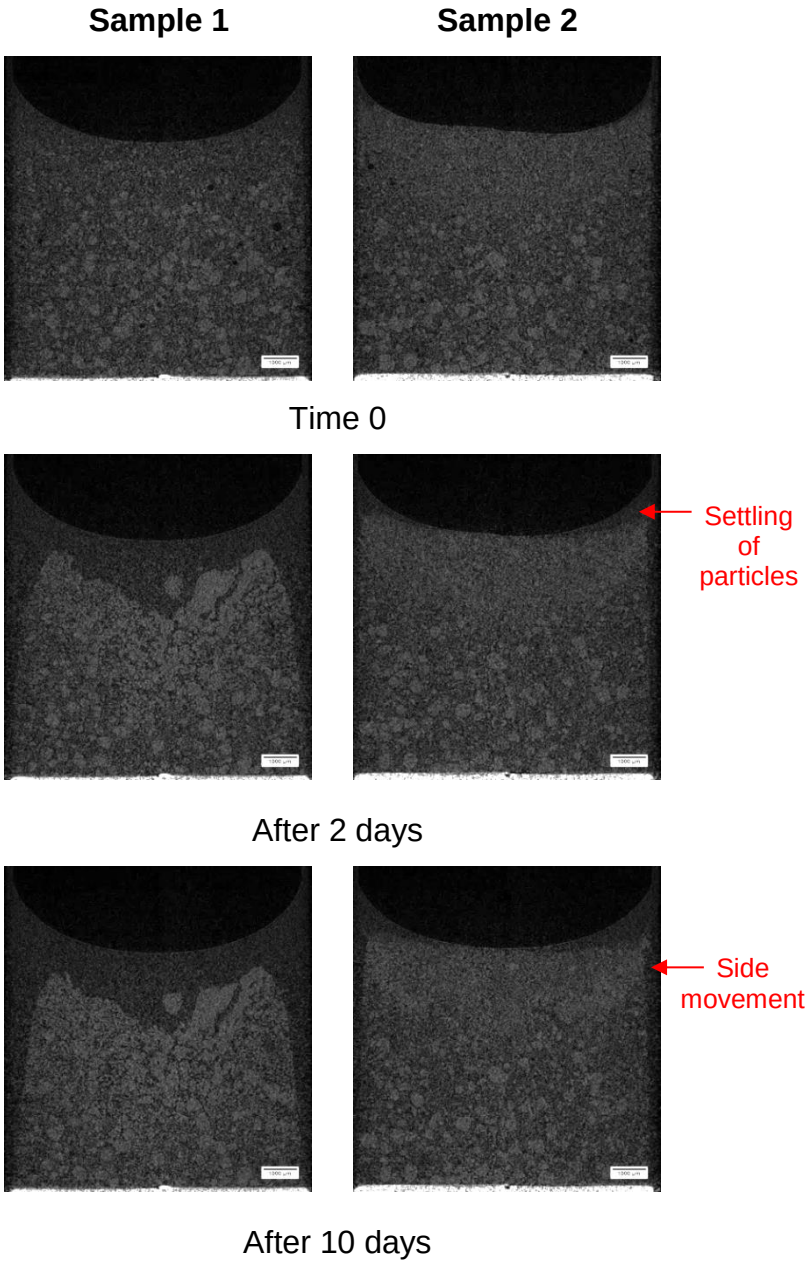

Figure 7-25. Images for the suspensions samples (fructose and sunflower oil, fructose and sunflower oil with sucrose on top) stored at 75 % RH. Scale on images is 1 mm.

It would appear that by positioning a layer of sucrose on the surface of a fructose suspension has helped reduce the environmental effects of storing the sample at 75% RH. This is very different to the behaviour seen when a suspension of sucrose and fructose was mixed and stored at 75 % RH as shown in Figure 7-22. This sample preparation used for sample 2 in Figure 7-25 would only be successful, as long as the environmental condition is below the critical deliquescence point for sucrose which is 85 % RH. If the environmental condition is exceeded above this value, it would no longer act as a barrier mechanism.

7.4 Conclusions

In this chapter, the environmental effect of storing sugar suspensions was studied. An initial approach using optical methods showed that the hygroscopic properties of sugars lead to a substantial moisture uptake once the humidity level exceeds the critical deliquescence point. Once the critical humidity level was exceeded, moisture from the environment would absorb onto the surface and result in liquid bridge formation between solid particles.

This was then taken one step further, in studying suspensions of binary mixtures containing sucrose and fructose. It was shown how the deliquescence of the binary mixture is lower than that of the individual components. This is the case for food based products, which are composed of many ingredients. The behaviour seen using X-ray CT for storing these suspensions above the critical point, was similar to that shown in the previous chapters (Chapter 4, Chapter 5 & Chapter 6) for when the secondary liquid is added as a bulk. The formation of liquid bridges due to the water, as well as a contraction of the solid volume, was due to the hydrophilic properties of the sugar particles. When the moisture migration was due to the environmental conditions, the moisture progressed through the suspension sample continuously due to the moisture gradient between the sample and the surrounding atmosphere, as opposed to the bulk movement seen for when the water was added directly to the suspension sample.

It was found that the information from the moisture sorption isotherm could be used to reduce the environmental effects for suspensions. As the deliquescence point

for sucrose is higher than for fructose, by positioning a layer of sucrose powder on the surface of a fructose suspension, the moisture effect could be reduced (slowed down), in comparison to a fructose suspension without any sucrose on the surface. This information gives insight into potential solutions, of how food products could be prepared to reduce environmental effects to resist spoilage and product degradation.

Chapter 8 Modelling the kinetics of mass transport

Attempts were made to develop models to look at the different stages of penetration for a secondary liquid shown in the experimental chapters. The initial capillary action shown in the experimental data in Section 4.3.1 (water being added to dry sucrose tablets) is modelled first. As well as this, the movement of sucrose from the bulk suspension into the water droplet shown in experimental Section 4.3.2 (for water addition to suspension of sucrose and sunflower oil) was modelled based on the flux of sucrose into the droplet.

8.1 Capillary Action on a Dry Powder Bed

The penetration of water into a dry powder bed (based on a tablet) was modelled based on capillary movement with no oil phase (in air). The model of the penetration of a 5 µl (5×10^{-9} m^3) water droplet, into a dry powder bed was conducted based on approaches used by Denesuk et al. (1993) and Hapgood et al. (2002) using an infinite number of pores. A diagram of how the pores and water penetration is modelled can be seen in Figure 8-1.

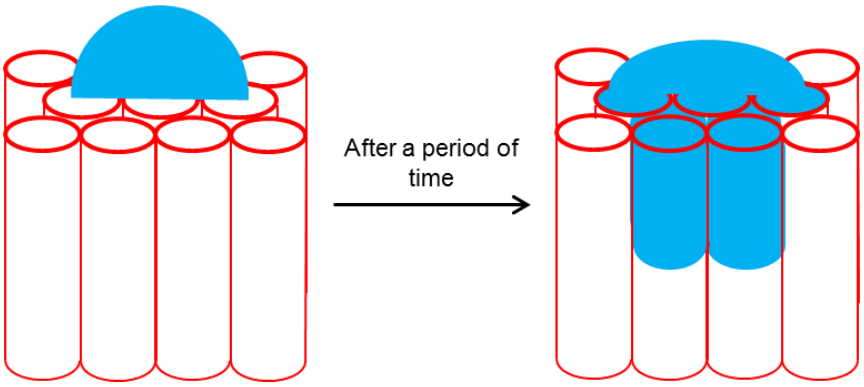

Figure 8-1. Liquid droplet penetrating into a powder bed of infinite pores.

As input parameters, the surface tension and viscosity were taken from the experimental data. The d_{32} was obtained from the particle size distribution and a sphericity of 1 was used as the model is based on spherical shape particles. The spreading radius was taken from Section 4.3.1.2, for the initial contact diameter of the 5 µl water droplet on the dry sucrose tablet bed. R_{pore} (characteristic pore size

of bed) was calculated from Equation 2-5, and κ from Equation 2-9. A dt of 0.01 s was chosen initially. All input parameters used can be seen in Table 8-1. The porosity was calculated from an X-ray scan of a sucrose tablet. The total amount of pixels with a grey value which corresponds to air was divided by the total amount of pixels to find the porosity of the tablet.

Table 8-1. Input parameters for calculating the volume of penetration rate of water into powder bed.

dt^{-1} (s)	0.01
Surface tension (N/m)	0.068
Contact angle (°)	4.59
Viscosity (Pa·s)	0.001
Porosity (%)	12
d_{32} (m)	1.94×10^{-5}
Sphericity	1
Spreading radius of a 5 µl droplet (m)	2.5×10^{-3}
R_{pore} (m)	3.04×10^{-6}
k	1.02×10^{-2}

The information from Table 8-1 was used in Equation 2-8 to plot the volume of liquid penetrated into powder bed against time which can be seen in Figure 8-2. Equation 2-8 is repeated below, which was previously mentioned in Chapter 2.

$$V_p(t) = k \int_0^t \frac{r_d^2(t')}{\sqrt{t'}}\, dt' \qquad \text{Equation 2-8}$$

where:

$$k = \pi\, \varepsilon \sqrt{\frac{\gamma_{LG}\, R_{pore} \cos\theta}{2\mu}} \qquad \text{Equation 2-9}$$

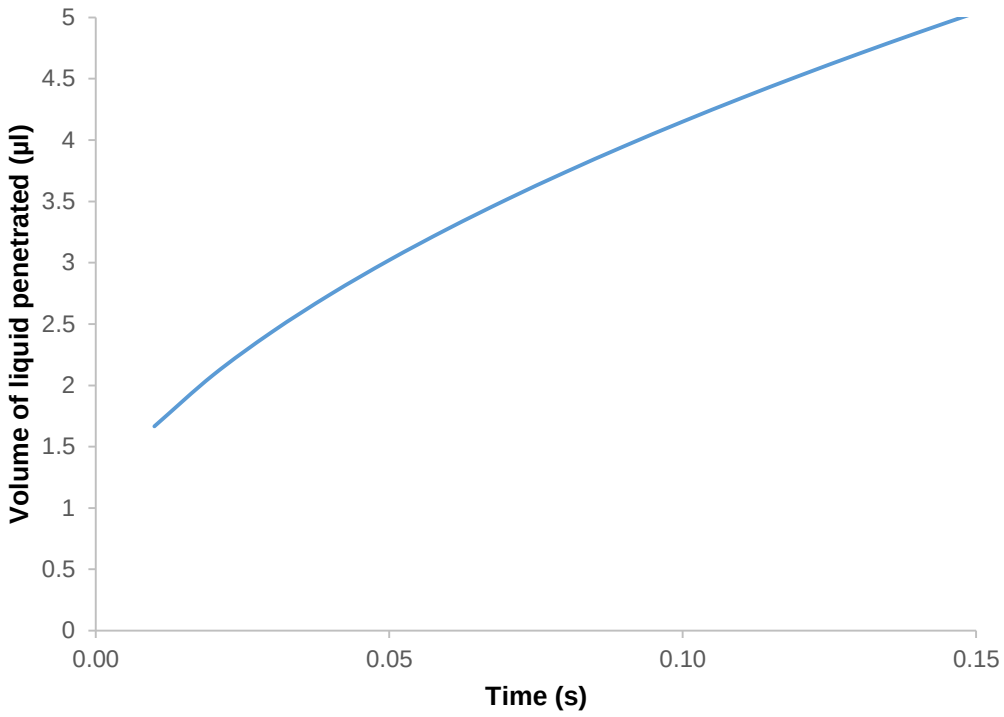

Figure 8-2. Droplet penetration volume against time for water into a dry powder bed.

It can be seen that it takes approximately 0.15 seconds for the complete volume of the 5 µl water droplet to penetrate into a dry powder bed. This was based on the constant drawing area case (CDA) which, as mentioned in Section 2.2.1.1, is the fastest in terms of penetration as the area of contact is maintained. For the slower case of decreasing drawing area (DDA), it would be approximately 9 times this time (≈1.35 seconds). The same model was applied for glycerol and saturated sucrose (changing the viscosity, surface tension and contact angle) and the penetration time was calculated as 122 seconds and 25 seconds respectively for the constant drawing case (quickest penetration time). This highlights the magnitude of difference in penetration based on the liquid properties, something seen in Chapter 6 experimentally for the long term scans for these liquids in comparison to water.

This model was also based on a constant contact radius between the droplet and powder bed which is not completely accurate when looking at Figure 4-5, which showed some axial spreading on the surface after initial impact. However, it does highlight the time scales required for capillary effects for initial penetration when

applied to the surface of a powder. The model was based on a droplet into a dry powder bed surrounded by air. If the tablet and the pores are immersed in oil, this will offer some resistance to the penetration of the secondary liquid when applied to the surface, as shown in the experiments in Section 4.3.1. It is hypothesised that the capillary effect is only dominant when air is in contact with the liquid. Once the liquid droplet is completely immersed in the suspension and surrounded by oil, the capillary effect is no longer dominant, as the capillary pressure is equal throughout the droplet and pushing in all directions equally and, therefore, the net effect is zero.

When the modelled data from Figure 8-2 is compared to the experimental data from Section 4.3.1 using optical methods, it can be seen that the penetration rate is substantially quicker for the experimental data. This may be due to the powder shape and hydrophilic properties, which were not taken into account for this model. This was also highlighted by Nguyen et al. (2009) when mixtures of powders showed varying penetration times in comparison to modelled data.

Also, the movement rate preceding the initial surface penetration is much slower than this, indicating that other mechanisms are now taking place.

8.2 Flux of Sucrose

The initial increase in volume for the early stages of the secondary immiscible liquid water (droplet), as it progresses through the suspension of sucrose and sunflower oil is due to the movement of sucrose from the bulk suspension into the liquid (as shown in the experiments in Chapter 4 - Chapter 6). From the literature it is known that the volume is conserved as the sucrose moves from the bulk suspension to the water and the sucrose dissolves (HirschmÜLler, 2013). The difference between the theoretical volume increase and the actual volume increase is less than 0.35 %, and approaches 0 % when moving towards a saturated sucrose solution.

An attempt was made to fit the experimental data from Chapter 4 to a model based on the flux movement of sucrose from the bulk suspension into the water droplet as it progresses into the suspension.

8.2.1 Model Development

The change in volume of the water droplet with time is a function of the surface area of the droplet and the flux movement of solid sucrose from the bulk suspension into the droplet at the surface of the droplet. This can be written as:

$$\frac{dv}{dt} = a\,J \qquad \text{Equation 8-1}$$

where, v is the volume (m^3) of the droplet (volume of a sphere, $\frac{4}{3}\pi r^3$), t is the time (seconds) of the volume of the water droplet is measured, a is the surface area of the droplet (which initially is a sphere and can be written as $4\pi r^2$ or πd^2 where r is the radius (m) of the sphere and d is the diameter (m) of the sphere) and J is the flux movement of sucrose from the bulk suspension into the water droplet (m^3/m^2s),

Equation 8-1 can be rewritten in terms of the diameter of the water droplet:

$$\frac{3}{6}\pi d^2\,\frac{dd}{dt} = \pi d^2\;J \qquad \text{Equation 8-2}$$

Taking the integral of both sides from d_0 at time 0 and d after a period of time, Equation 8-2 cancels down to:

$$\int_{d_0}^{d} \mathrm{d}d = 2\,J \int_{0}^{t} \mathrm{d}t \qquad \text{Equation 8-3}$$

When Equation 8-3 is integrated with the boundary conditions, it becomes:

$$d = d_0 + 2\,Jt \qquad \text{Equation 8-4}$$

Equation 8-1 can be rewritten using Equation 8-4 as:

$$\frac{dv}{dt} = a\,J = \pi J(d_0 + 2Jt)^2 \qquad \text{Equation 8-5}$$

This can be written and integrated with the following boundary conditions:

$$\int_{v_0}^{v} \mathrm{d}v = \int_{0}^{t} \pi J(d_0 + 2Jt)^2\,dt \qquad \text{Equation 8-6}$$

A substitution is required to simplify the integration in Equation 8-6. As $d_0 + 2Jt$ is constant, this can be expressed as:

$$u = d_0 + 2Jt$$ Equation 8-7

Differentiating Equation 8-7 with respect to t becomes:

$$\frac{du}{dt} = 2J$$ Equation 8-8

Equation 8-8 can be rearranged and expressed as:

$$\frac{dt}{du} = \frac{1}{2}J$$ Equation 8-9

Equation 8-9 can be substituted into Equation 8-6 and can be expressed as:

$$v = v_0 + \int_0^t \pi J \mathrm{u}^2 \, du \quad \left[\frac{dt}{du} = \frac{1}{2}J\right]$$ Equation 8-10

The integration of Equation 8-10 becomes:

$$v = v_0 + \frac{\pi}{2}\left[\frac{u^3}{3}\right] = v_0 + \frac{\pi}{2}\left[\frac{(d_0 + 2Jt)^3}{3}\right]_0^t$$ Equation 8-11

The change in volume of the water droplet as solid sucrose moves into the droplet can be expressed as:

$$c = \frac{v - v_0}{v}$$ Equation 8-12

where v_0 (m^3) is the volume of the water droplet initially when added to the suspension and v (m^3) is the new volume of the water droplet, after a period of time within the suspension. Equation 8-12 can be rewritten as:

$$\frac{1}{c} = \frac{v}{v - v_0}$$ Equation 8-13

Equation 8-13 can be substituted into Equation 8-11 and can be expressed as:

$$\frac{1}{c} = \frac{v_0 + \frac{\pi}{6}\left[(d_0 + 2Jt)^3 - {d_0}^3\right]}{\frac{\pi}{6}\left[(d_0 + 2Jt)^3 - {d_0}^3\right]}$$ Equation 8-14

Equation 8-14 can be written as:

$$\frac{1}{c} = \frac{v_0}{\frac{\pi}{6}\left[(d_0 + 2Jt)^3 - {d_0}^3\right]} + 1 \qquad \text{Equation 8-15}$$

Equation 8-15 can be rearranged as:

$$\left[\frac{1}{c} - 1\right]^{-1} = \frac{\pi}{6v_0}\left[(d_0 + 2Jt)^3 - {d_0}^3\right] \qquad \text{Equation 8-16}$$

The expression of the initial volume of the water droplet v_0 (m^3), expressed in terms of the diameter d_0 (m) of the droplet:

$$d_0 = \left[v_0 \frac{6}{\pi}\right]^{1/3} \qquad \text{Equation 8-17}$$

Equation 8-17 can be substituted into Equation 8-16 and can be expressed as:

$$\left[\frac{1}{c} - 1\right]^{-1} = \frac{\pi}{6v_0}\left[(d_0 + 2Jt)^3 - v_0 \frac{6}{\pi}\right] \qquad \text{Equation 8-18}$$

Equation 8-18 can be rearranged and expressed as:

$$\left[\frac{1}{c} - 1\right]^{-1} = \frac{1}{v_0}\left[\frac{\pi}{6}(d_0 + 2Jt)^3 - v_0\right] \qquad \text{Equation 8-19}$$

Equation 8-19 can be written as:

$$\frac{1}{\frac{1}{c} - 1} = \frac{\frac{\pi}{6}(d_0 + 2Jt)^3}{v_0} - 1 \qquad \text{Equation 8-20}$$

Equation 8-20 can be rearranged to:

$$\frac{c}{1 - c} + 1 = \frac{\frac{\pi}{6}(d_0 + 2Jt)^3}{v_0} \qquad \text{Equation 8-21}$$

Equation 8-17 can be substituted into Equation 8-21 and can be expressed as:

$$\frac{c}{1 - c} + 1 = \frac{\frac{\pi}{6}\left[\left(v_0 \frac{6}{\pi}\right)^{1/3} + 2Jt\right]^3}{v_0} \qquad \text{Equation 8-22}$$

Equation 8-22 can be expressed as:

$$\frac{c}{1-c}+1=\frac{[(v_0)^{1/3}+\left(\frac{\pi}{6}\right)^{1/3}2Jt]^3}{v_0}$$ Equation 8-23

Equation 8-23 cancels down to:

$$\frac{c}{1-c}+1=[1+\left(\frac{\pi}{6v_0}\right)^{1/3}2Jt]^3$$ Equation 8-24

Equation 8-24 can be rearranged to:

$$\left[\frac{c}{1-c}+1\right]^{1/3}=1+\frac{2Jt}{d_0}$$ Equation 8-25

Equation 8-25 is the final derived equation for a linear fit.

Equation 8-25 was rearranged to make c the subject, which becomes:

$$c=1-\frac{1}{\left(1+\frac{2Jt}{d_0}\right)^3}$$ Equation 8-26

Equation 8-26 is the final derived equation for a non-linear fit.

8.2.2 Model Implementation

Experimental data from Section 4.3.3 was used to track the change in volume/diameter of the water droplet with time, an example of which can be seen in Figure 8-3. For the first scan conducted on the sample, this is the image used to calculate the value of d_0/v_0, which is the diameter/volume of the droplet after initial addition. Then, all subsequent scans are used to calculate the new value for d/v, which is the diameter/volume of the water droplet with time, as it increases in size and takes solid sucrose from the bulk suspension.

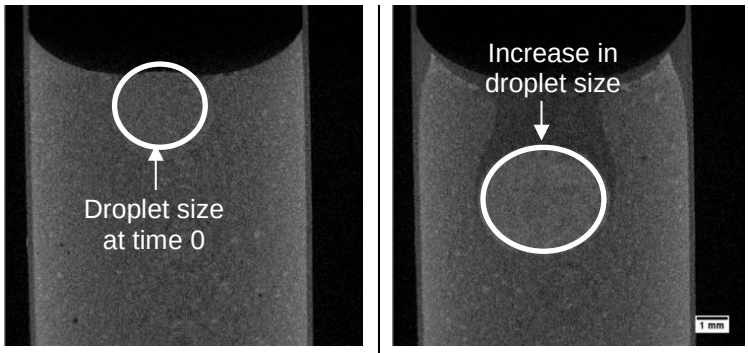

Figure 8-3. Example of volume change for model.

Equation 8-25 was used to plot the left hand side of $y = [\frac{c}{1-c} + 1]^{1/3}$ against t, which can be seen in Figure 8-4 for the experimental data of the water droplet in Section 4.3.2 (5 µl - 25 µl in volume), which was added to the surface of the sucrose and sunflower oil suspension. The y intercept was set to 1, to find the equation of the experimental data. The gradient from the equation was used to calculate the value of the flux J as d_0 is known.

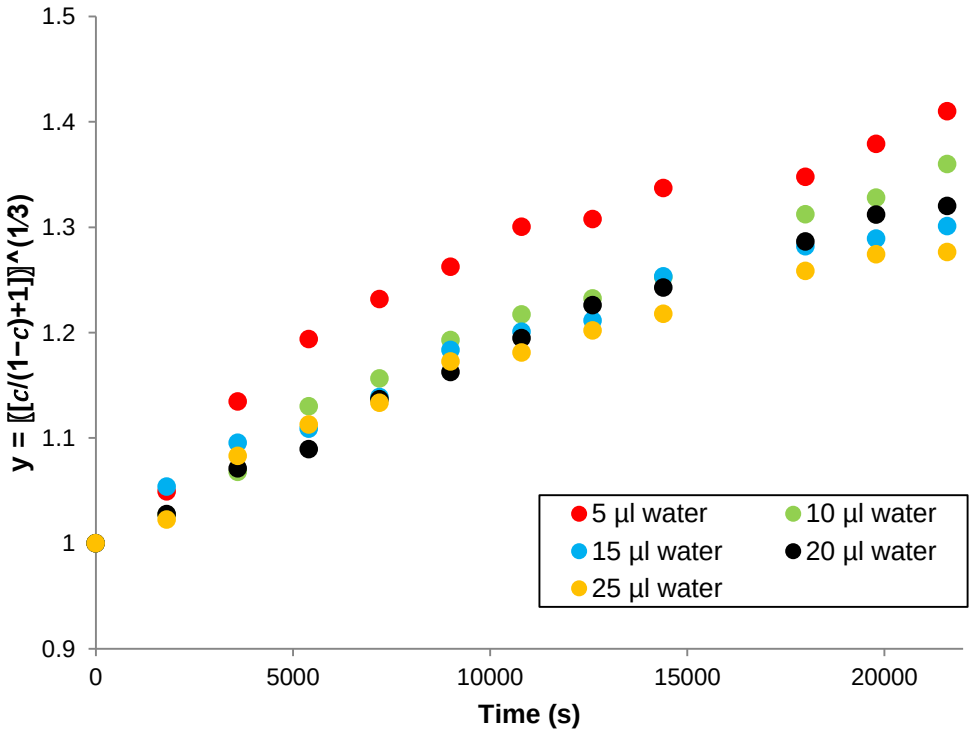

Figure 8-4. Plot of Equation 8-25, looking at change in volume of sucrose in droplet with time.

A similar approach was done with Equation 8-26 with a plot of c against t, which can be seen in Figure 8-5. The experimental data was then used to find the value of the unknown flux J based on Equation 8-26, using Mathematica. The Mathematica code used can be seen in the Appendix II. The values for J for both Equation 8-25 and Equation 8-26 can be seen in Table 8-2.

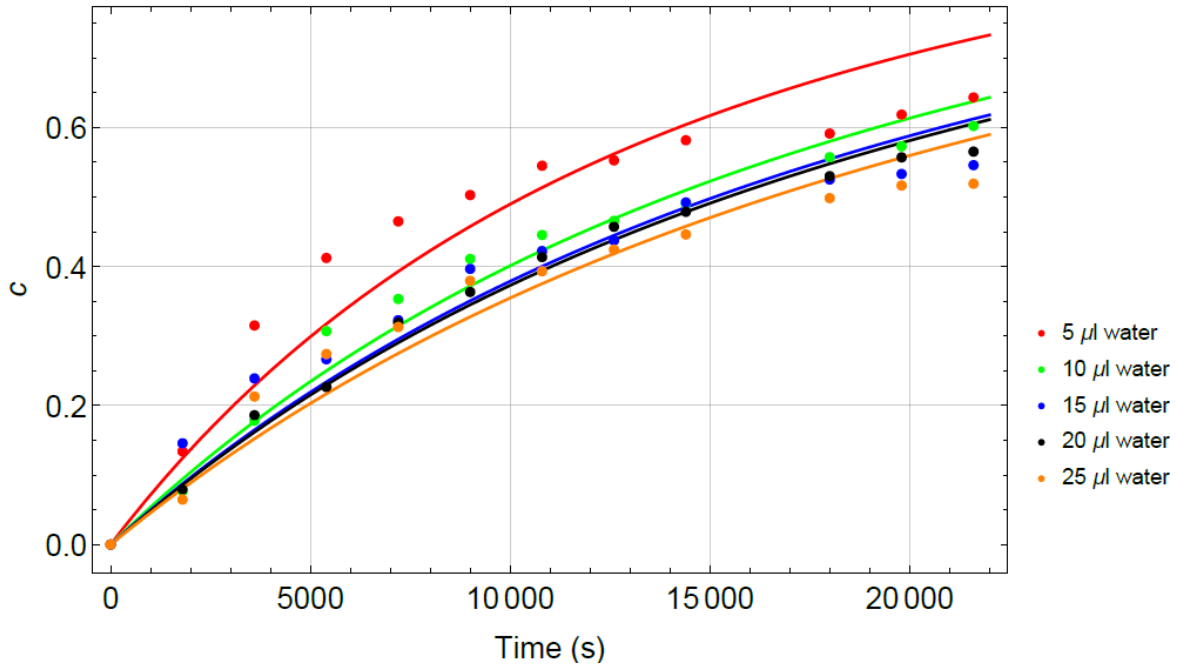

Figure 8-5. Plot of Equation 8-26 showing change in volume of sucrose in droplet with time.

Table 8-2. Calculated values of flux J using linear and non-linear fit.

	Linear J $\left(\frac{m^3}{m^2 s}\right)$	Non-linear J $\left(\frac{m^3}{m^2 s}\right)$	d_0 (m)
5 µl droplet	2.334 x 10^{-8}	2.689 x 10^{-8}	0.00214
10 µl droplet	2.444 x 10^{-8}	2.572 x 10^{-8}	0.00276
15 µl droplet	2.452 x 10^{-8}	2.640 x 10^{-8}	0.00307
20 µl droplet	2.744 x 10^{-8}	2.845 x 10^{-8}	0.00338
25 µl droplet	2.762 x 10^{-8}	2.948 x 10^{-8}	0.00375

The calculated fluxes using both the linear and non-linear fit were plotted against the diameter of the water droplet, at time 0, after initial addition which can be seen in Figure 8-6.

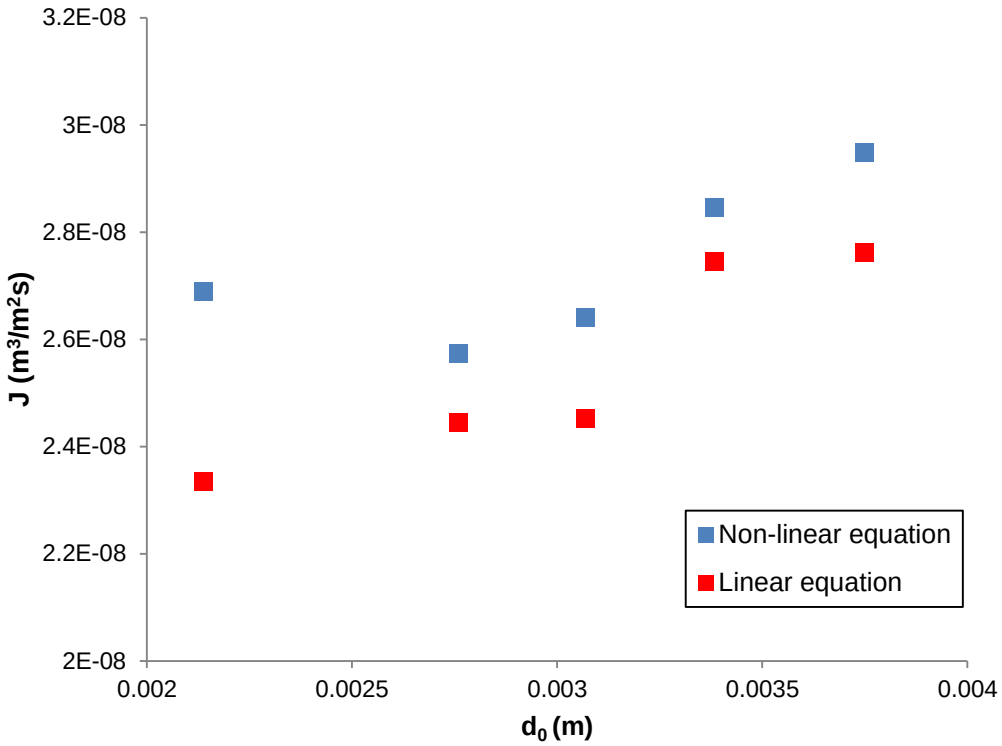

Figure 8-6. Plot of calculated fluxes using linear and non-linear fit against initial diameter of droplet.

It can be seen that there appears to be a linear tend between the diameter and the calculated fluxes, using the linear and non-linear equations. Also, it should be noted that the model is only valid for early time periods from the initial addition of the water droplet, while the droplet has the capacity to take up sucrose from the bulk suspension. After longer periods from initial addition, it is known that the rate of uptake for solid sucrose slows down, as the capacity to take up any further sucrose is reduced. This will therefore reduce the flux rate. Also, as shown experimentally, the sucrose uptake rate is different for different liquids; therefore, liquid properties need to be incorporated into the model. This is suggested as future work, to develop upon the model presented in this section.

8.3 Conclusions

The penetration behaviour of a secondary immiscible liquid, from the experiments conducted in Chapter 4 - Chapter 6 was modelled. Initial surface penetration for the secondary immiscible liquid on a suspension was ascribed to capillary effects, which occurs in seconds to minutes. It was shown how water penetrates very rapidly in comparison to saturated sucrose solution or glycerol, due to its lower viscosity and contact angle on solid sucrose particles. Penetration times for secondary liquids are fastest when applied to dry sucrose tablet, due to the little resistance offered by the air present in the pores. Once the sucrose tablet is immersed in oil, to fill the pores with this continuous hydrophobic phase, the penetration time is increased several fold due to the resistance offered by the oil, highlighting the role of the continuous hydrophobic phase in slowing down the kinetics, as presented from the experimental data.

Once the droplet is fully immersed within the suspension, it is believed now the movement is driven by the flux movement of solid sucrose from the bulk suspension into the secondary liquid droplet, as the capillary effects are no longer present. The flux is greater for water as a secondary liquid in comparison to sucrose solutions or glycerol, due to its lower viscosity and contact angle as well as capacity to dissolve sucrose. Also, the flux in relation to the surface area for different volume of water droplets is higher for smaller volume droplets. This is due to the surface area to volume ratio of the initial water droplet. Though this is only for the earlier periods (hours) from initial addition. Once the water droplet is saturated, this then leads to additional mechanisms driving the movement of the secondary liquid into the bulk suspension.

Chapter 9 Conclusions & Future Work

In the present work, the behaviour and interactions of a secondary immiscible liquid and model suspensions of sugar (hydrophilic in nature) and sunflower oil (hydrophobic in nature) was studied. The secondary liquid was either added directly as a bulk to the suspension (droplet addition) or the suspension was exposed to an environment (exposure to relative humidity, RH) in which the secondary liquid was present in high concentration.

The secondary immiscible liquids used ranged from water, sugar solutions, saturated sugar solutions and glycerol. The behaviour observed, varied greatly depending on the secondary liquid. Efforts were also made to model early stage capillary action as well as the flux movement of sucrose from the bulk into the secondary liquid.

9.1 Direct Addition of Droplet to Suspensions

9.1.1 Optical Approach

Initial surface penetration based on capillary action was studied using optical methods to look at the macroscale detail. This was conducted first on tablets of sucrose, followed by tablets immersed in sunflower oil. It was shown how the sunflower oil, offers resistance and thus slows down the kinetics and penetration of the secondary liquid. The fastest penetration was seen for water and the slowest for a saturated sucrose solution. The results from glycerol fall in between the results from the other two liquids.

9.1.2 Non-invasive Approach

This was followed up by using two different X-ray CT systems to track the movement of the secondary liquid within the bulk suspension, once the droplet enters and displaces sucrose and sunflower oil from the suspension. The macroscale movement of the liquid was tracked using conventional benchtop systems. The microscale detail between individual sucrose particles and the liquid bridge formation was tracked using synchrotron facilities, which offered high resolution scans and the ability to see details on the micron scale.

Two movement mechanisms were identified, once the immiscible liquid (water) was added and completely immersed within the bulk suspension.

i. Firstly, the solid sucrose from the bulk suspension moves into the water droplet (against gravity), as the droplet progresses into the suspension. Initial solid sucrose which enters into the droplet (during approximately the first 150 minutes) dissolves. This is due to the large difference in concentration gradient between the water initially and its ability to dissolve sucrose. Subsequent solid sucrose which enters into the droplet remains in the solid state, until the droplet is fully occupied by solid sucrose.
ii. Secondly, once the droplet is saturated with sucrose, now the movement is of the secondary liquid (water/sucrose solution) away into the bulk suspension to create liquid bridges with further solid sucrose particles. As the system is not in equilibrium and the affinity between the secondary liquid and sucrose is high, the driving force is there for a network formation between solid sucrose particles and the secondary liquid within the surrounding bulk suspension. The network formation brings sucrose particles closer together, displacing the sunflower oil which was previously present between solid sucrose particles.

It was also shown how the surface area to volume ratio plays a key role in driving the flux of solid sucrose from the bulk suspension into the secondary liquid droplet, which also affects the displacement rate.

The driving force for the penetration of the secondary liquid was found to be the ability and affinity of the secondary liquid droplet to take up sucrose and not gravity. This was confirmed by comparing the two secondary liquids: water and saturated sucrose solution. Water (which can dissolve sucrose up to 67 % wt. at 25°C) has the greatest ability to take up and dissolve sucrose, whereas saturated sucrose solution has no capacity to take up and dissolve further sucrose, although, water is lower in density in comparison to saturated sucrose solution. Therefore, if gravity had been the dominating transport mechanism, the saturated sucrose solution would have penetrated more quickly in comparison to water. The

experimental results showed water to penetrate quicker and further in comparison to saturated sucrose solution, which virtually did not penetrate for the time period studied.

Glycerol (which has a lower solubility of sucrose in comparison to water, ≈ 7 % wt.) showed similar behaviour to water, though at a substantially slower rate, even though it has a higher density in comparison to water.

9.2 Environmental Exposure of Suspensions

When suspension samples were stored in environmental conditions, in which the humidity was above the critical deliquescence point, the movement of moisture and the changes as a result of this could be seen. The compaction of the solid volume could give some insight into how blooming, which is a major issue for chocolate could be explained and the importance of correct storage conditions. The moisture migration proceeded through the sample as a uniform water front (across cross section of sample), due to the water activity gradient between the sample and the surrounding atmosphere. This was in contrast to the bulk movement seen from the direct addition of water to the suspension sample.

Similar experiments were conducted on binary suspensions of sucrose and fructose. It was seen how binary mixtures leads to the lowering of the deliquescence point, which makes samples more susceptible to moisture gain and environmental effects. This affects most food based products, whose composition consists of numerous ingredients. Information from the sorption profile of sucrose could be used to retard moisture migration in fructose suspensions which are more hygroscopic at lower RH conditions, by positioning a layer of sucrose particles on the surface of the fructose suspension.

9.3 Model of Kinetics

Results from the droplet experiments conducted in Chapter 4 - Chapter 6 were modelled based on capillary action of the secondary liquid during the surface penetration, followed by flux movement of sucrose from the bulk suspension into the secondary liquid. The capillary effects occurred on the time scale of seconds to minutes, with water penetrating the quickest, followed by glycerol and finally

saturated sucrose solution. The viscosity and contact angle between the secondary liquid and sucrose particles were the key parameters in driving the penetration rate.

After complete immersion of the droplet into the suspension, the movement was now believed to be driven by the flux movement of solid sucrose from the bulk suspension into the secondary liquid droplet. Provided that the secondary liquid droplet had the capacity to take up further solid sucrose, this would drive the penetration of the secondary liquid.

9.4 Future Work

Based on the results acquired and the conclusions drawn from these within this study, recommendations for how this work can be continued and taken further are suggested.

Extensive work was carried out on varying volumes of secondary liquid, to understand how the behaviour in terms of system dynamics is affected. It would be interesting to test the effect of delivering volumes in more than one droplet, as opposed to one large volume. A preliminary test for depositing two volumes of 10 µl water onto a suspension can be seen in Figure 9-1. It can be seen initially the droplets take their own paths and behave independently, however after a certain period of time they coalesce and combine into one body and continue the progression together. Based on the results presented, related to how the surface area to volume ratio affects the flux of sucrose into the droplet, increasing this by dividing the total volume over several droplets may allow equilibrium and the kinetics taking place to be achieved at a quicker rate.

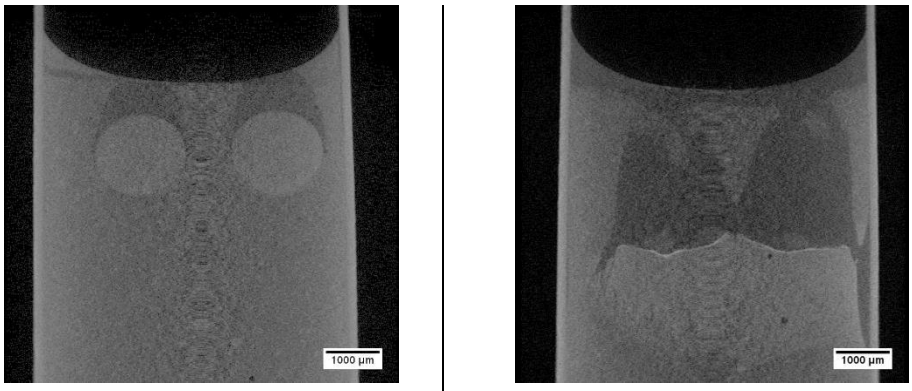

After 120 minutes | After 21 hours

Figure 9-1. Time lapse of central scans for suspension (2 × 10 µl water). Scale on images is 1 mm.

Also, the effect of directly mixing the secondary liquid into the suspension to see how the network formation kinetics is altered would be interesting. A preliminary test for sucrose suspension, with the addition of 1 % wt. water can be seen in Figure 9-2. Some clusters of water/sucrose can be seen and are highlighted with red arrows. How the water redistributes with time would give more insight into the driving force for the network formation. It is anticipated as the secondary liquid is more evenly distributed throughout the system, the kinetics would be slower.

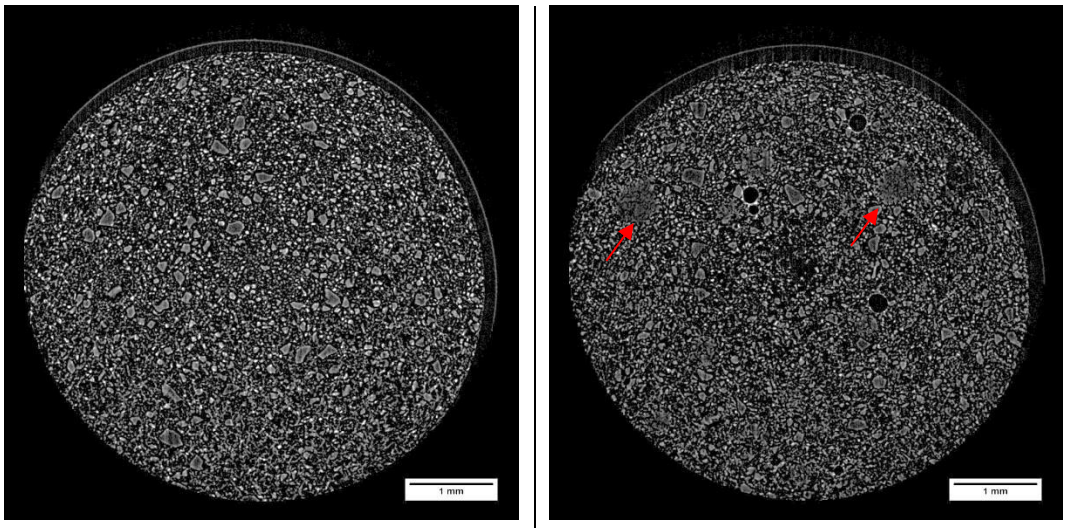

Reference sample – no water | 1 % wt. water mixed

Figure 9-2. Effect of mixing water directly into suspension sample. Scale on images is 1 mm.

In the current work presented the effects of adding emulsifiers such as lecithin into stabilising the system were not investigated. It is hypothesised the surfactant would make the network formation less likely to occur due to the decrease in surface tension.

Furthermore, it would be interesting to look at the effect of exposing samples to low RH either after mixing or exposure to high RH, to see the kinetics during drying and the liquid bridge formation, over a range of temperatures.

Preliminary work also was conducted on modelling the penetration behaviour both during short and long term. For short term penetration, the movement was modelled based on capillary action on a dry powder bed. This needs to be developed to incorporate the oil phase, which offers a level of resistance to the penetration. It could be assumed that the pressure drop of the water as it penetrates into the powder bed covered in oil is given by the Hagen-Poiseuille equation for both the water and oil phase. Therefore the pressure drop for water and oil can be written as:

$$\Delta P = \frac{8\mu_{\mathrm{w}} L_{\mathrm{w}} Q}{\pi r^4} = \frac{8\mu_{\mathrm{w}} L_{\mathrm{w}} \pi r^2 \left(\frac{dL_{\mathrm{w}}}{dt}\right)}{\pi r^4} \qquad \text{Equation 9-1}$$

where μ_w is the viscosity of water, L_w is the distance the water has travelled, Q is the volumetric flow rate and r is the radius of the pore.

As both liquids are incompressible, the velocities of both (Equation 9-2) can be assumed to be the same as water moves and displaces the oil phase, which can schematically be seen in Figure 9-3. Though this is only an assumption and further work would be required for verification.

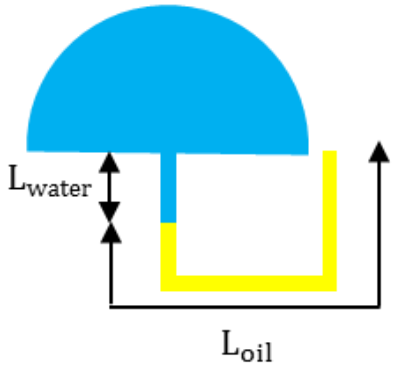

Figure 9-3. Schematic for theoretical displacement of oil phase by water.

$$\frac{dL_{\text{water}}}{dt} = \frac{dL_{\text{oil}}}{dt} \qquad \text{Equation 9-2}$$

where L_{water} is the distance the water has travelled and L_{oil} is the distance the oil has travelled.

Finally, models based on diffusion for the long term kinetics seen would accommodate the current study well, to conclude all the transport mechanisms identified.

List of Tables

References

AGUILERA, J. M., MICHEL, M. & MAYOR, G. 2004. Fat Migration in Chocolate: Diffusion or Capillary Flow in a Particulate Solid?—A Hypothesis Paper. *Journal of Food Science,* 69**,** 167-174.

ALTAN, A., LAVENSON, D. M., MCCARTHY, M. J. & MCCARTHY, K. L. 2011. Oil Migration in Chocolate and Almond Product Confectionery Systems. *Journal of Food Science,* 76**,** E489-E494.

ALTHAUS, T. O., PALZER, S., NIEDERREITER, G., CHISHOLM, H. & BOVET, N. 2013. *Chocolate product with tropicalised shell*. WO2013083641 A1.

ALTIMIRAS, P., PYLE, L. & BOUCHON, P. 2007. Structure–fat migration relationships during storage of cocoa butter model bars: Bloom development and possible mechanisms. *Journal of Food Engineering,* 80**,** 600-610.

ASADI, M. 2005. Tables. *Beet-Sugar Handbook.* John Wiley & Sons, Inc.

ASTM-E96 2016. Standard Test Methods for Water Vapor Transmission of Materials. Philadelphia: ASTM International.

BARUCHEL, J., BUFFIÈRE, J.-Y., MAIRE, E., MERLE, P. & PEIX, G. 2000. *X-ray tomography in Material Science, General Principles,* Paris, Hermes Science Publications.

BECKETT, S. 2009. *The Science of Chocolate,* Cambridge, Royal Society of Chemistry.

BECKETT, S. T. 2011. *Industrial Chocolate Manufacture and Use,* West Sussex, John Wiley & Sons Ltd.

BUCKE, C. 1995. *Sucrose, properties and applications,* London, Chapman & Hall.

CHARLES-WILLIAMS, H. R., WENGELER, R., FLORE, K., FEISE, H., HOUNSLOW, M. J. & SALMAN, A. D. 2011. Granule nucleation and growth:

Competing drop spreading and infiltration processes. *Powder Technology,* 206**,** 63-71.

DADKHAH, M., PEGLOW, M. & TSOTSAS, E. 2012. Characterization of the internal morphology of agglomerates produced in a spray fluidized bed by X-ray tomography. *Powder Technology,* 228**,** 349-358.

DAHLENBORG, H., MILLQVIST-FUREBY, A. & BERGENSTÅHL, B. 2015. Effect of particle size in chocolate shell on oil migration and fat bloom development. *Journal of Food Engineering,* 146**,** 172-181.

DANISCO 2003. Fructose Technical Properties.

DENESUK, M., SMITH, G. L., ZELINSKI, B. J. J., KREIDL, N. J. & UHLMANN, D. R. 1993. Capillary Penetration of Liquid Droplets into Porous Materials. *Journal of Colloid and Interface Science,* 158**,** 114-120.

DOWNTON, G. E., FLORES-LUNA, J. L. & KING, C. J. 1982. Mechanism of stickiness in hygroscopic, amorphous powders. *Industrial & Engineering Chemistry Fundamentals,* 21**,** 447-451.

DUPAS-LANGLET, M., BENALI, M., PEZRON, I., SALEH, K. & METLAS-KOMUNJER, L. 2013. Deliquescence lowering in mixtures of NaCl and sucrose powders elucidated by modeling the water activity of corresponding solutions. *Journal of Food Engineering,* 115**,** 391-397.

EDMONDSON, P. T., GRAMMATIKA, M., FRYER, P. J. & HANDY, B. 2005. Modelling of Heat Transfer, Mass Transfer and Flavour Development in Chocolate Crumb. *Food and Bioproducts Processing,* 83**,** 89-98.

GALET, L., PATRY, S. & DODDS, J. 2010. Determination of the wettability of powders by the Washburn capillary rise method with bed preparation by a centrifugal packing technique. *Journal of Colloid and Interface Science,* 346**,** 470-475.

GHOSH, V., DUDA, J. L., ZIEGLER, G. R. & ANANTHESWARAN, R. C. 2004. Diffusion of Moisture through Chocolate-flavoured Confectionery Coatings. *Food and Bioproducts Processing,* 82**,** 35-43.

GHOSH, V., ZIEGLER, G. R. & ANANTHESWARAN, R. C. 2002. Fat, moisture, and ethanol migration through chocolates and confectionary coatings. *Critical Reviews in Food Science and Nutrition,* 42**,** 583-626.

GHOSH, V., ZIEGLER, G. R. & ANANTHESWARAN, R. C. 2005. Moisture migration through chocolate-flavored confectionery coatings. *Journal of Food Engineering,* 66**,** 177-186.

GOMES, D. J. C., DE SOUZA, N. C. & SILVA, J. R. 2013. Using a monocular optical microscope to assemble a wetting contact angle analyser. *Measurement,* 46**,** 3623-3627.

GUIHENEUF, T. M., COUZENS, P. J., WILLE, H.-J. & HALL, L. D. 1997. Visualisation of Liquid Triacylglycerol Migration in Chocolate by Magnetic Resonance Imaging. *Journal of the Science of Food and Agriculture,* 73**,** 265-273.

GUILLARD, V., BROYART, B., BONAZZI, C., GUILBERT, S. & GONTARD, N. 2003a. Evolution of Moisture Distribution During Storage in a Composite Food Modelling and Simulation. *Journal of Food Science,* 68**,** 958-966.

GUILLARD, V., BROYART, B., BONAZZI, C., GUILBERT, S. & GONTARD, N. 2003b. Modelling of Moisture Transfer in a Composite Food: Dynamic Water Properties in an Intermediate aw Porous Product in Contact with High aw Filling. *Chemical Engineering Research and Design,* 81**,** 1090-1098.

GUILLARD, V., BROYART, B., GUILBERT, S., BONAZZI, C. & GONTARD, N. 2004. Moisture diffusivity and transfer modelling in dry biscuit. *Journal of Food Engineering,* 64**,** 81-87.

HAPGOOD, K. P., LITSTER, J. D., BIGGS, S. R. & HOWES, T. 2002. Drop Penetration into Porous Powder Beds. *Journal of Colloid and Interface Science,* 253**,** 353-366.

HERREMANS, E., MELADO-HERREROS, A., DEFRAEYE, T., VERLINDEN, B., HERTOG, M., VERBOVEN, P., VAL, J., FERNÁNDEZ-VALLE, M. E., BONGAERS, E., ESTRADE, P., WEVERS, M., BARREIRO, P. & NICOLAÏ, B. M. 2014. Comparison of X-ray CT and MRI of watercore disorder of different apple cultivars. *Postharvest Biology and Technology,* 87**,** 42-50.

HIRSCHMÜLLER, H. 2013. Chapter 2 - Physical Properties of Sucrose A2 - HONIG, PIETER. *Principles of Sugar Technology.* S-Hertogenbosch: Elsevier.

HOFFMANN, S., KOOS, E. & WILLENBACHER, N. 2014. Using capillary bridges to tune stability and flow behavior of food suspensions. *Food Hydrocolloids,* 40**,** 44-52.

JOHANSSON, D. & BERGENSTÅHL, B. 1992. The influence of food emulsifiers on fat and sugar dispersions in oils. II. Rheology, colloidal forces. *Journal of the American Oil Chemists Society,* 69**,** 718-727.

KILLIAN, L. & COUPLAND, J. 2012. Manufacture and Application of Water-in-Oil Emulsions to Induce the Aggregation of Sucrose Crystals in Oil: A Model for Melt-resistant Chocolate. *Food Biophysics,* 7**,** 124-131.

KOOS, E., JOHANNSMEIER, J., SCHWEBLER, L. & WILLENBACHER, N. 2012. Tuning suspension rheology using capillary forces. *Soft Matter,* 8**,** 6620.

KOOS, E. & WILLENBACHER, N. 2011. Capillary Forces in Suspension Rheology. *Science,* 331**,** 897-900.

LAITY, P. R., MANTLE, M. D., GLADDEN, L. F. & CAMERON, R. E. 2010. Magnetic resonance imaging and X-ray microtomography studies of a gel-forming tablet formulation. *European Journal of Pharmaceutics and Biopharmaceutics,* 74**,** 109-119.

LAM, C. N. C., WU, R., LI, D., HAIR, M. L. & NEUMANN, A. W. 2002. Study of the advancing and receding contact angles: liquid sorption as a cause of contact angle hysteresis. *Advances in Colloid and Interface Science,* 96**,** 169-191.

LAVERSE, J., MASTROMATTEO, M., FRISULLO, P. & DEL NOBILE, M. A. 2012. X-ray microtomography to study the microstructure of mayonnaise. *Journal of Food Engineering,* 108**,** 225-231.

LAZGHAB, M., SALEH, K., PEZRON, I., GUIGON, P. & KOMUNJER, L. 2005. Wettability assessment of finely divided solids. *Powder Technology,* 157**,** 79-91.

LEE, W. L., MCCARTHY, M. J. & MCCARTHY, K. L. 2010. Oil Migration in 2-Component Confectionery Systems. *Journal of Food Science,* 75**,** E83-E89.

LIM, K. S. & BARIGOU, M. 2004. X-ray micro-computed tomography of cellular food products. *Food Research International,* 37**,** 1001-1012.

MAROM, G. 1985. The Role of Water Transport in Composite Materials. *In:* COMYN, J. (ed.) *Polymer Permeability.* Dordrecht: Springer Netherlands.

MARQUES, L. C. & APPOLONI, C. R. 2015. Quantification of fluids injection in a glass-bead matrix using X-ray microtomography. *Micron,* 74**,** 35-43.

MCCARTHY, K. L. & MCCARTHY, M. J. 2008. Oil Migration in Chocolate–Peanut Butter Paste Confectionery as a Function of Chocolate Formulation. *Journal of Food Science,* 73**,** E266-E273.

MCCULFOR, J., HIMES, P. & ANKLAM, M. R. 2011. The effects of capillary forces on the flow properties of glass particle suspensions in mineral oil. *AIChE Journal,* 57**,** 2334-2340.

MIQUEL, M. E., CARLI, S., COUZENS, P. J., WILLE, H.-J. & HALL, L. D. 2001. Kinetics of the migration of lipids in composite chocolate measured by magnetic resonance imaging. *Food Research International,* 34**,** 773-781.

MIQUEL, M. E. & HALL, L. D. 2002. Measurement by MRI of storage changes in commercial chocolate confectionery products. *Food Research International,* 35**,** 993-998.

MORILLON, V., DEBEAUFORT, F., CAPELLE, M., BLOND, G. & VOILLEY, A. 1999. Influence of the Physical State of Water on the Barrier Properties of Hydrophilic and Hydrophobic Films. *Journal of Agricultural and Food Chemistry,* 48**,** 11-16.

MOTWANI, T., HANSELMANN, W. & ANANTHESWARAN, R. C. 2011. Diffusion, counter-diffusion and lipid phase changes occurring during oil migration in model confectionery systems. *Journal of Food Engineering,* 104**,** 186-195.

NEGREIROS, A. A., ALTHAUS, T. O., NIEDERREITER, G., PALZER, S., HOUNSLOW, M. J. & SALMAN, A. D. 2015. Microscale study of particle agglomeration in oil-based food suspensions: The effect of binding liquid. *Powder Technology,* 270, Part B**,** 528-536.

NGUYEN, T., SHEN, W. & HAPGOOD, K. 2009. Drop penetration time in heterogeneous powder beds. *Chemical Engineering Science,* 64**,** 5210-5221.

O'BRIEN, R. D. 2004. *Fats and oils: Formulating and processing for applications,* Florida, CRC Press LLC.

PERRY, R. A. G., D. 1997 *Perry's Chemical Engineers' Handbook,* New York, McGraw-Hill Professional Publishing.

REID, D. S. 2008. Water Activity: Fundamentals and Relationships. *Water Activity in Foods.* Oxford: Blackwell Publishing Ltd.

REINKE, S. K., WILDE, F., KOZHAR, S., BECKMANN, F., VIEIRA, J., HEINRICH, S. & PALZER, S. 2016. Synchrotron X-Ray microtomography reveals interior microstructure of multicomponent food materials such as chocolate. *Journal of Food Engineering,* 174**,** 37-46.

RUMSEY, T. R. & MCCARTHY, K. L. 2012. Modeling oil migration in two-layer chocolate–almond confectionery products. *Journal of Food Engineering,* 111**,** 149-155.

SALAMEH, A. K., MAUER, L. J. & TAYLOR, L. S. 2006. Deliquescence Lowering in Food Ingredient Mixtures. *Journal of Food Science,* 71**,** E10-E16.

SALAMEH, A. K. & TAYLOR, L. S. 2005. Deliquescence in Binary Mixtures. *Pharmaceutical Research,* 22**,** 318-324.

SMITH, K. W., CAIN, F. W. & TALBOT, G. 2007. Effect of nut oil migration on polymorphic transformation in a model system. *Food Chemistry,* 102**,** 656-663.

STOCK, S. R. 2009. *MicroComputed Tomography: Methodology and Applications,* Florida, Boca Raton: CRC Press.

STOKLOSA, A. M., LIPASEK, R. A., TAYLOR, L. S. & MAUER, L. J. 2012. Effects of storage conditions, formulation, and particle size on moisture sorption and flowability of powders: A study of deliquescent ingredient blends. *Food Research International,* 49**,** 783-791.

STORTZ, T. A. & MARANGONI, A. G. 2011. Heat resistant chocolate. *Trends in Food Science & Technology,* 22**,** 201-214.

SVANBERG, L., LORÉN, N. & AHRNÉ, L. 2012. Chocolate Swelling during Storage Caused by Fat or Moisture Migration. *Journal of Food Science,* 77**,** E328-E334.

VAN DUYNHOVEN, J. P. M., GOUDAPPEL, G.-J. W., WEGLARZ, W. P., WINDT, C. W., CABRER, P. R., MOHORIC, A. & VAN AS, H. 2009. Noninvasive Assessment of Moisture Migration in Food Products by MRI. *Magnetic Resonance Microscopy.* Weinheim: Wiley-VCH Verlag GmbH & Co. KGaA.

WHITEHOUSE, A. S. 2013. *Tropicalizing agent*. WO 2013045523 A1.

WOLLGARTEN, S., YUCE, C., KOOS, E. & WILLENBACHER, N. 2016. Tailoring flow behavior and texture of water based cocoa suspensions. *Food Hydrocolloids,* 52**,** 167-174.

YU, X., KAPPES, S. M., BELLO-PEREZ, L. A. & SCHMIDT, S. J. 2008. Investigating the Moisture Sorption Behavior of Amorphous Sucrose Using a Dynamic Humidity Generating Instrument. *Journal of Food Science,* 73**,** E25-E35.

YUAN, Q., HANSELMANN, W. & ANANTHESWARAN, R. C. 2009. Characterization of vapor-induced and liquid-induced moisture migration through fractionated palm kernel (PKO) based multiphase systems. *Journal of Food Engineering,* 95**,** 460-470.

YUAN, Q., HANSELMANN, W. & ANANTHESWARAN, R. C. 2012. Moisture and sucrose transfer in fractionated palm kernel (PKO) based films immersed in liquid solutions. *Journal of Food Engineering,* 108**,** 13-21.

YUCEL, U. & COUPLAND, J. 2011. Ultrasonic Attenuation Measurements of the Mixing, Agglomeration, and Sedimentation of Sucrose Crystals Suspended in Oil. *Journal of the American Oil Chemists' Society,* 88**,** 33-38.

ZIEGLER, G. 2009. 10 - Product design and shelf-life issues: oil migration and fat bloom A2 - Talbot, Geoff. *Science and Technology of Enrobed and Filled Chocolate, Confectionery and Bakery Products.* Cambridge: Woodhead Publishing.

Appendix I

Penetration of water onto a dry sucrose tablet using X-ray CT

A scan was conducted on a dry sucrose tablet (powder bed, 5 g, 6250 N, 30 mm diameter), before and after the penetration of 5 µl water which can be seen in Figure I-1. The diameter of the initial contact area (approximately 5 mm), along with the penetration and spreading of the water within the tablet can be seen and has been highlighted with the red arrow.

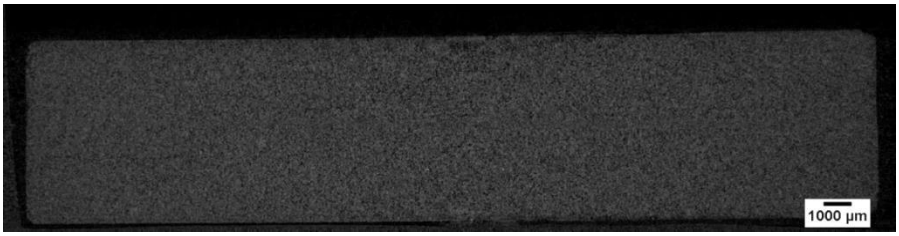

Before addition of 5 µl water

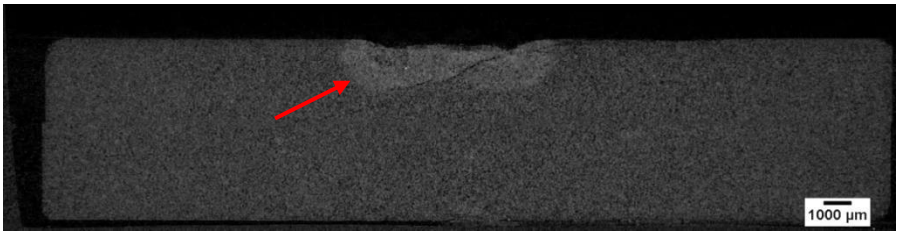

After addition of 5 µl water

Figure I-1. Scan of dry sucrose tablet, before and after addition of 5 µl water.

Shadow Effect

For the first 3 images shown in Figure 5-1, for scans taken up to 2 hours after the initial addition of the water droplet, there is a shadow effect around the droplet. The reason for this is the movement of the droplet during the duration of the scan (the scan duration for the samples scanned here were longer than those in Section 4.3.2). Therefore, the water droplet location for the earlier projections is different, when compared to the later projections. Consequently, when the projections are reconstructed, this leads to the shadow effect being present, in the final reconstructed images. Ideally, when scanning samples using X-ray CT, they should remain completely still without any movement as projections are taken as the sample is rotated. However, for the system being studied in this case, it is not

possible to achieve this. For this reason, efforts were taken with preliminary scans to produce a sufficiently quick scan to capture the dynamics of the system with satisfactory resolution. For the later scans between 4-8 hours after the addition of the water 5 µl water droplet, the shadow effect is less, indicating the droplet movement is now slower. This is expected as the droplet continues to take up sucrose from the bulk suspension at a slower rate. As the water droplet movement is slower, it is expected the change in location between projections of the droplet during a scan will be reduced, and therefore the shadow effect in the final reconstructed image will be less evident. For the final 2 scans taken after 10 and 18 hours in Figure 5-1, there is no shadow as now the speed of the droplet movement has significantly decreased. Though, it can be seen that between 10 and 18 hours, the water movement is still occurring, though now very different to that seen initially from the earlier scans.

For scans 1B-3B shown in Figure 5-2 for scans taken up to 2.5 hours, again there is a shadow effect around the water droplet. Though, the shadow effect is less than those seen for the images in Figure 5-1 for the water 5 µl water droplet for the similar time period after initial addition. This indicates that the droplet is moving slower, which is believed to be due to the surface area to volume ratio of the 10 µl droplet, which is smaller in comparison to that of the 5 µl water droplet. As the ratio of surface area to volume is smaller, the rate at which the larger droplet can take up sucrose and increase in size is reduced, thereby reducing the shadow effect. For the final three scans (scans 7B-9B) taken after 16 hours from the initial addition of the 10 µl water droplet, there is no shadow around the droplet, indicating no significant movement during the scan. Though it can be seen from these images, there is movement from the right region next to the droplet as the sucrose is pulled towards the droplet, leaving a void of sunflower oil near the wall of the cellulose sample holder. The reason for this is believed to be initially the droplet was not added perfectly to the centre as can be seen from scan 1B in Figure 5-2, when compared to scan 1A in Figure 5-1. As the droplet moved into the suspension and was larger in volume compared to the 5 µl droplet, by scan 6B it was very close to one side of the sample holder. Thus by scan 7B, the attraction towards the droplet

for the sucrose particles from the bulk suspension is strong, resulting in the sucrose particles moving towards the droplet. This was not the case for the sucrose particles within the suspension to the left in scans 7B-9B. It can be seen for this section; no major movement towards the droplet is seen. For this reason, attempts were made to avoid the water droplet coming into contact with the cellulose sample holder, to ensure no external influence upon the movement of the droplet.

Appendix II

Mathematica code for Non-linear model fit of experimental data.